Summer 8-15-2015

Structure and Function of Cytochrome Containing Electron Transport Chain Proteins from Anoxygenic Photosynthetic Bacteria

Erica Lois-Wunderlich Majumder
Washington University in St. Louis

WASHINGTON UNIVERSITY IN ST. LOUIS

Department of Chemistry

Dissertation Examination Committee:
Robert E. Blankenship, Chair
Michael Gross
Dewey Holten
Robert Kranz
Liviu Mirica

Structure and Function of Cytochrome Containing Electron Transport Chain Proteins from Anoxygenic Photosynthetic Bacteria

by

Erica Lois-Wunderlich Majumder

A dissertation presented to the
Graduate School of Arts & Sciences
of Washington University in
partial fulfillment of the
requirements for the degree
of Doctor of Philosophy

August 2015
St. Louis, Missouri

Table of Contents

List of Figures

List of Tables

List of Abbreviations

ACIII	Alternative Complex III
ACIII'	Alternative Complex III lacking ActE and ActG
Bchl	Bacteriochlorophyll
CEF	Cyclic Electron Flow
CFX	*Chloroflexus aurantiacus*
DHCC	diheme cytochrome *c*
cyt	cytochrome
ETC	Electron Transport Chain
FAP	Filamentous Anoxygenic Phototroph
GSB	Green Sulfur Bacteria
HDX-MS	hydrogen deuterium exchange mass spectrometry
HM	homology modeling
LEF	Linear Electron Flow
LH	Light Harvesting antenna Complex
OEC	Oxygen Evolving Complex
PB	Purple Bacteria
PSI	Photosystem I
PSII	Photosystem II
Q_i	Quinone reduction site
Q_O	Quinone oxidation site
RC	Reaction Center
RC-LH1	Type II Reaction Center Core Complex with Light Harvesting Type 1 Antenna
RFX	*Roseiflexus castenholzii*
TFA	trifluoroacetic acid

Acknowledgments

I wish to thank and acknowledge my family, friends and colleagues who have been instrumental to my success in graduate school. First, to my mentor, Dr. Blankenship, thank for the continual guidance, advice and academic freedom to pursue interesting research questions. Secondly, to all the members of the Blankenship Lab who have spent hours helping me with experiments and wrestle with ideas- I appreciate your friendship and support. I would also like to thank my friends and family who keep me sane, motivated and inspired to make a difference in the world. I must especially thank my parents Chris and Cindy Wunderlich for their unwavering support these past twenty-seven years. I'd like to thank my brother Kurt for always making me laugh and always having my back. I also need to thank my in-laws, Somajyoti and Nandita Majumder for their love and support from afar. Finally, to my husband Kinjal Majumder- thank you for never doubting me, challenging me to be better, editing my papers, cooking dinner and the million things you do to support and love me.

I would also like to acknowledge the Olin Fellowship for Women for the funding throughout my degree, but also the emotional support and enduring friendships gained. I must also thank the PEO for providing the funding for the PEO Scholar Award that supported me this final year. I offer special thanks to the Washington University Departments of Chemistry and Biology and the Photosynthetic Antenna Research Center for invaluable assistance and collaboration during my research endeavors.

Erica Wunderlich Majumder

Washington University in St. Louis

May 2015

ABSTRACT OF THE DISSERTATION

Structure and function of cytochrome containing electron transport chain proteins from anoxygenic photosynthetic bacteria

by

Erica Lois-Wunderlich Majumder

Doctor of Philosophy in Chemistry

Washington University in St. Louis, 2015

Professor Robert E. Blankenship, Chair

This dissertation examines the structure and function of photosynthetic proteins that contain *c*-type heme cofactors that function in the electron transport chains of anaerobic phototrophic bacteria. The diversity and range of these cytochromes proteins was explored. Then, individual proteins were studied in detail. The diheme cytochrome *c* from *Heliobacteria modesticaldum* was studied using hydrogen deuterium exchange mass spectrometry and homology modeling. A structural model of the protein and a mechanism for the cytochrome *bc* complex was proposed. Next, the monoheme cytochrome c subunit from the Alternative Complex III from the Filamentous Anoxygenic Phototrophs was studied using biochemistry and found to be a necessary subunit for enzyme activity. The structure of the Alternative Complex III was then studied with homology modeling and the interaction of the complex with its soluble electron acceptor auracyanin was studied. Next, the structure of the LHRC was studied using Electron Microscopy and the supramolecular organization of the complex was studied with Atomic Force Microscopy. The relationship between the Alternative Complex III and the LHRC was also explored. A model of the FAP photosynthetic membrane was proposed. Several individual cytochromes were analyzed to understand their structure, function and mechanisms.

Chapter 1: Diversity of Photosynthetic Cytochrome Proteins

Excerpts from this chapter have been accepted for publication as a book chapter in the Advances in Photosynthesis and Respiration series: Majumder, E.L.W. & Blankenship, R.E. Diversity of Photosynthetic Cytochrome Proteins. *Cytochrome Proteins in Photosynthesis and Respiration*. Eds. Cramer, W. & Kallas, T. Advances in Photosynthesis and Respiration. Accepted, Springer (2014).

1.1 Introduction

The photosynthetic process, in both anoxygenic and oxygenic phototrophs, is the major producer of available energy on Earth. Photosynthesis converts sunlight into stable chemical energy through a series of excitation energy transfer, electron transfer and enzymatic steps [1]. Proteins in the cells perform these functions, and the activity is often centered on the metal atom housed in the proteins. A major class of electron transport metalloproteins ubiquitous across the tree of life is cytochrome proteins. Cytochrome proteins contain at least one heme molecule and move electrons via redox reactions. Phototrophic organisms use cytochromes as subunits in membrane protein complexes and as free soluble proteins to transfer electrons around the cell [2].

Phototrophs belong to taxa from the smallest bacteria up through the giant redwood trees. The first photosynthetic organisms were bacteria. Bacterial phyla that contain phototrophic representatives include: Green Sulfur Bacteria, Purple Bacteria, Heliobacteria, Chloroacidobacteria, Cyanobacteria, Filamentous Anoxygenic Phototrophs and Gemmatimonadetes [1,3]. All of these except cyanobacteria carry out anoxygenic (non-oxygen-evolving) photosynthesis. Cyanobacteria developed the ability to perform oxygenic photosynthesis, and the cyanobacteria were the source of the chloroplast of photosynthetic eukaryotes by endosymbiosis [4]. Eukaryotic phototrophs range from algae to plants of all sorts. Cytochromes persisted in the evolutionary jump from anoxygenic to oxygenic photosynthesis because, in order to accommodate the new surroundings, the organisms incorporated different types of cytochromes into the photosynthetic machinery including both *b* and *c* type cytochromes [5]. (Figure 1.1). Table 1 summarizes all of the cytochromes discussed in this chapter. This chapter will focus on the cytochrome proteins from anoxygenic phototrophs.

Table 1.1 Representative Cytochromes in Photosynthesis

Cyto-chrome	Other names	Major organism Family/ies	Location in cell & attachment	Complex or Shuttle	Function	Special features
c_z	PscC, c_{551}	GSB	Periplasm, n complex	T1 RC	Re-reduce special pair	Interacts with c_{555} & c_{556}
c_{553}	PetJ	Helio	Periplasm, soluble/complex, anchor	T1 RC	*bc* to RC	Anchor tail, direct reduces special pair
c_{554}	Tetraheme cyt *c*, RC cyt *c*	PB, FAP	Periplasm, in complex	T2 RC	Re-reduce special pair	Surprise in crystal structure, uphill energy transfer
Cyt *b* anoxy	b_H & b_L, b_p & b_n, b_O & b_i	all	Integral membrane	*bc*	Q cycle	Helio version is PsbE precursor
c_1		PB & mitochondria	Periplasm, in complex	bc_1	Rieske to soluble acceptor	Interacts with far moving Rieske
DHCC	diheme	Helio	Periplasm, in complex	*bc*	Rieske to soluble acceptor	has two hemes
c_{556}		GSB	Periplasm, in complex	*bc*	Rieske to soluble acceptor	Can directly interact with cz
ActA	pentaheme	FAP	Periplasm, in complex	ACIII	FeS to soluble acceptor	has five hemes
ActE	monoheme	FAP	Periplasm, in complex	ACIII	FeS to soluble acceptor	Two copies of the subunit
c_2		PB	Periplasm, soluble	shuttle	*bc* to RC	Rapid kinetics
c_y		PB	Periplasm, soluble, anchor	shuttle	*bc* to RC	Alt c_2, anchor tail
c_4		PB	Periplasm, soluble	shuttle	*bc* to RC	Alt c_2
c_8		PB	Periplasm, soluble	shuttle	*bc* to RC	Alt c_2
c'	CycP	Anoxygenic	Soluble	De-nitrification	Binds NO & CO	Sequence similarities to c_{556}
c_{555}	CycA	GSB	Periplasm, soluble	shuttle	*bc* to RC	Can be reduced by sulfur metabolism
Cyto-chrome	**Other names**	**Major organism Family/ies**	**Location in cell & attachment**	**Complex or Shuttle**	**Function**	**Special features**
b_{559}	PSII cyt *b*, PSBE&F	oxygenic	Integral membrane	PSII	unknown	α & β with heme bridged, 4 potentials
V	PsbV, cyt c_{550}	Cyano, red algae	Lumen, in complex	PSII	Ion gating	Near OEC
V2	PsbV2	Cyano, red algae	Lumen, in complex	PSII	Replace V under stress	Alt to PsbV, His/Cys axial ligation

Cyt *b* oxy	b_H & b_L, b_p & b_n, b_O & b_i	Oxygenic	Integral membrane	b_6f	Q cycle	Has pigments
c_i	c_n, c_x	Oxygenic	Integral membrane	b_6f	Q cycle	Surprise in crystal structure
Cyt *f*		Oxygenic	Lumen, in complex	b_6f	Rieske to soluble acceptor	Beta barrel, unique structure, unknown evolution
c_6	PetJ, Cyt c_{553}	oxygenic	Lumen, soluble	shuttle	*bc* to RC	
c_{6a}		Green algae & plants	Lumen, soluble	shuttle	*bc* to RC, forms disulfide bridges?	Alt c_6, di-thio cyt
c_{6b}	Pet J1	cyano	Lumen, soluble	shuttle	*bc* to RC	Alt c_6
c_{6c}	Pet J2	cyano	Lumen, soluble	shuttle	*bc* to RC	Alt c_6
c_M		cyano	Lumen, soluble, anchor	shuttle	*bc* to RC & donation to COX	Alt c_6

1.2 Cytochromes in Anoxygenic Photosynthetic Electron Transport Chains

The earliest forms of bacterial photosynthesis emerged before the presence of oxygen in the Earth's atmosphere. These pioneering organisms found a way to use solar energy to drive cellular processes without oxygen as an electron source [6]. Anoxygenic phototrophs continue to thrive today in extreme or niche environments such as the under-layers of microbial mats, sulfur springs or deep sea hydrothermal vents [7] because they utilize a variety of electron sources and electron shuttles [8,9]. This variety of electron donors and acceptors is seen in Figure 1.1A. The basic components of a photosynthetic electron transport chain, whether anoxygenic or oxygenic, are a light harvesting antenna, a pigment-protein reaction center, a proton pumping complex, intermembrane electron shuttles and soluble electron carriers. As explored throughout this chapter, cytochromes form key subunits of the reaction center and proton pumping complexes.

They are also the most common form of soluble electron carrier used. Intermembrane carriers are quinols or other small molecules. Anoxygenic phototrophs rely on a diverse collection of cytochromes to survive in their challenging environments.

1.2.1 Cytochromes in type I and II reaction centers

The Reaction Center (RC) is the pigment-protein complex to which excitation energy is transferred to drive charge separation, thereby converting solar energy into redox free energy. The primary charge separation process is carried out by pigments, known as the special pair, and does not involve cytochromes in the primary process. Cytochromes, however, function in RCs to reduce the pigments after the primary electron transfer [10]. RCs are classified into type I and type II as determined by their final electron acceptors, and the iron sulfur clusters or quinones that they carry, respectively, but are thought to all have a common ancestor [11]. The cytochromes associated with type I and type II RCs in anoxygenic phototrophs are found on the periplasmic side of the RC and have the function of special pair re-reduction.

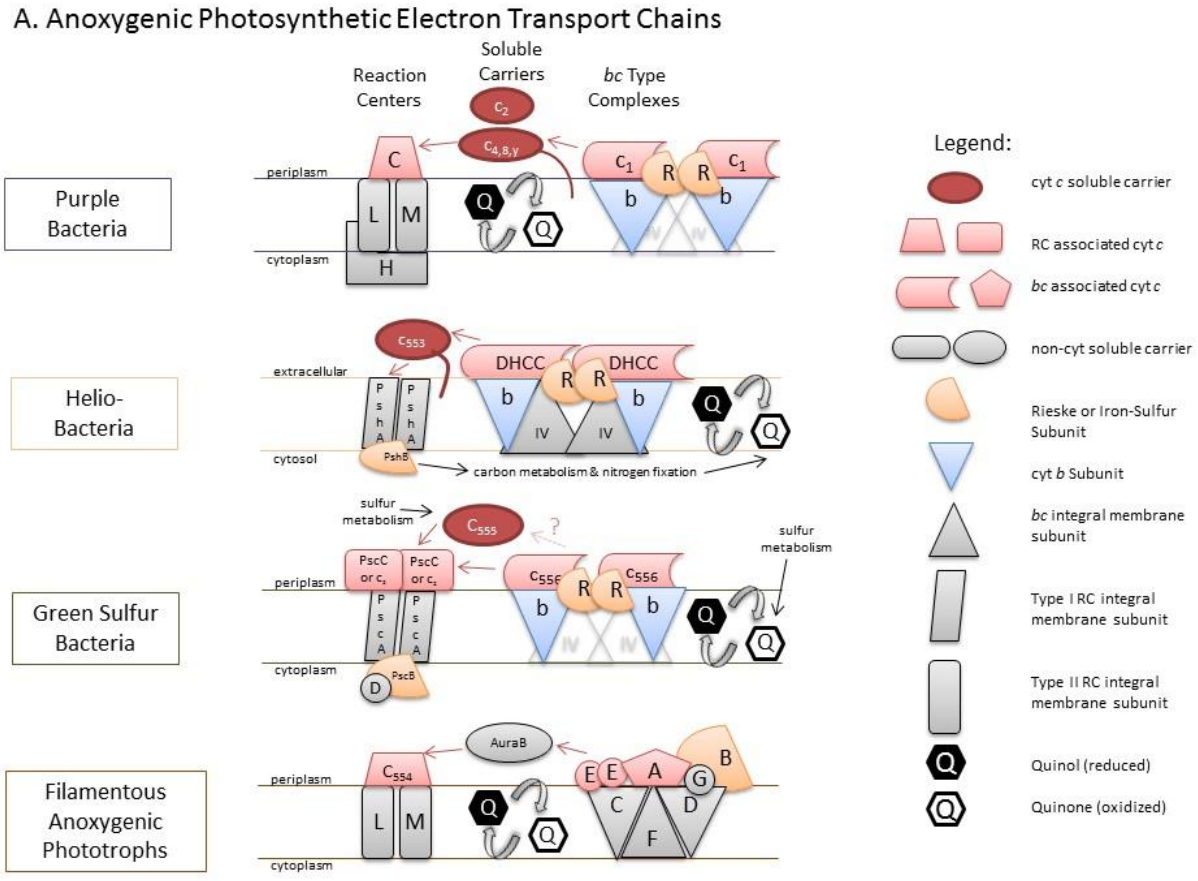

Figure 1.1 Photosynthetic Electron Transport Chains Schematics of electron transport chains in representative families of A) anoxygenic photosynthetic organisms. Legend is included in part A. Arrows represent the flow of electrons. Cytochrome and FeS subunits are in color and labeled with their common name, see table 1 for full names.

Cytochromes in Type I Reaction Centers

Prokaryotic anoxygenic type I photosynthetic Reaction Centers are found in Green Sulfur Bacteria (GSB), Chloroacidobacteria and Heliobacteria [12]. Type I RC's exist as homodimers and are more primitive than their oxygenic counterparts, appearing early in the evolution of photosynthesis [13]. Light energy striking the special pair pigments, P800 or P840, causes charge separation and subsequent electron transfer through the RC iron-sulfur clusters, designated Fe-S_x, Fe-S_A, and Fe-S_B, to a soluble carrier, typically a member of the ferredoxin family, small

iron-sulfur cluster proteins. The *c*-type monoheme cytochrome c_z of Green Sulfur Bacteria and c_{553} of Heliobacteria function in the periplasm to re-reduce the special pair bacteriochlorophylls after charge separation has occurred [12,14]. While performing the same basic function, the differences of these two monoheme *c*-type cytochromes represent the diversity of anoxygenic type I RC associated cytochromes.

For GSB, the RC associated cytochrome is c_z, also known as PscC or by its absorption peak c_{551}. Formal identification of c_z spanned several decades from initial observation in the 1970's by membrane flash kinetics to more sophisticated techniques in the 1990's [15–18]. Cyt c_z is held in place with three N-terminal helices that anchor the cytochrome to the RC complex. This three helix structure on the N-terminus is unique among cytochromes and was assigned its own class, V, of cytochrome protein structures [12]. Cytochrome c_z reduced the special pair pigments on the 40 μs timescale [14]. The anchoring allows for the rapid re-reduction of the special pair by keeping the cytochrome in an ideal place for electron transfer rather than letting the dynamics be diffusion controlled.

Besides the unique structure of the three helix anchor on the N-terminus, the *cyt* c_z C-terminus domain also contained structural surprises. The soluble C-terminal portion of cyt c_z has been overexpressed, characterized, crystallized, and its structure solved [20]. Despite the low amino acid sequence similarity, this domain of cyt c_z surprisingly showed structural similarity to class I cytochromes [19,20]. Class I cytochromes are *c*-type low spin hemes with heme attachment near the N-terminus histidine and a sixth coordinating axial ligand, methionine. The unique structure may contribute to its second proposed role of accepting electrons.

In addition to special pair reduction, cyt c_z has been implicated in direct electron transfer from the cyt bc_1 complex. It was shown to enhance the 150 μs time-scale of electron transfer between the RC and the cyt bc_1 complex by interacting directly with the periplasmic subunit of the bc_1 complex, cytochrome c_{556} [14]. In other bacterial cyclic electron transport chains, an additional free soluble electron carrier would shuttle electrons from the bc_1 to the RC. However, in GSB, no such additional carrier has been observed. One possibility to fill this functional role was the GSB soluble carrier cyt $c_{555,}$ also known as CycA when involved in sulfur metabolism, but it was unable to shuttle electrons between c_{556} and the c_z. This implied that the two peripheral cytochrome subunits of the RC and bc_1 complex may directly contact each other to move electrons without an intermediate [14,21]. Although CycA, cyt $c_{555,}$ was not shown to shuttle between RC and bc_1, in the GSB *Chlorobium tepidum,* cyt c_{555} donated electrons to cyt c_z on the same timescale as cyt c_{556} [21,22]. This finding does not detract from the direct electron transfer between RC and bc_1 hypothesis. Cyt c_z of the GSB type I RC's is a unique cytochrome structurally and in choice of reaction partners.

Apart from cyt c_z, another type I RC cytochrome has been characterized, cyt c_{553} (PetJ) in Heliobacteria. Unlike GSB, Heliobacteria are gram-positive, lacking a periplasmic space and restricting mobile cytochromes to the cytoplasmic space. Cytochrome c_{553} is therefore found in the cytoplasm and thought to be linked to the membrane via the terminal cysteine residue forming covalent bonds with lipid fatty acids [12].When the full Heliobacterial RC complex was purified, cyt c_{553} was integrated as a subunit [23]. The subunit was also expressed and characterized. It displayed with similar function and a redox potential, + 217 mV, to the native RC preparation [24].

Functionally, Heliobacterial cyt c_{553} donates electrons to the RC special pair, P800, with an electron transfer donation rate about 5 x 10^3 s^{-1}, similar to that of cyt c_z [21]. This rate is ten times larger than in purple bacteria, which have type II RCs and are discussed in the next section [12]. The tenfold rate enhancement of type I to type II suggests that the hemes and special pairs of the type I RC's are better aligned for efficient electron transfer. Also like GSB, cyt c_{553} can shuttle electrons directly from the cyt bc_1 complex to the RC [12,25]. Periplasm type I RC cytochromes transfer electrons to re-reduce the RC special pair. Cyt c_z and c_{553} are doing the same job at about the same rate with different structures and attachments showing how organisms can use a variety of cytochromes conditioned to their habitat. Cyt c_z and c_{553} of prokaryotic type I RC's demonstrate the similarity and differences amongst this large family of proteins and reflect the diverse environments in which the proteins function.

Cytochromes in Type II Reaction Centers

Type II Reaction Center protein complexes have been characterized more extensively than their type I counterparts due to enhanced stability and relative ease of purification. Type II RCs typically have a Light Harvesting (LH) subunit attached to or surrounding the Reaction Center complexes, unlike type I's that only have the charge separation and electron transfer subunits [26]. Type II RC cytochromes are usually involved in cyclic rather than linear electron transfer in prokaryotes [1]. The special pair, P870 will receive the excitation energy from light and completes charge separation by quickly passing the electro to bacteriochlorophyll and bacteriopheophytin pigments. The electron is passed through two quinones, from Q_A to Q_B and then to another quinone that will carry the electron through the membrane. The special pair is re-reduced by a cytochrome so that the process can start again.

Anoxygenic Type II RCs, as exemplified by Purple Bacteria (PB), contain three integral membrane subunits: L, M, H and, in many cases, a fourth periplasmic cytochrome subunit. As in the type I RC's, they utilize a cytochrome to re-reduce the special pair of pigments responsible for charge separation [27]. Many of the purple bacteria contain a tightly bound tetraheme cytochrome that reduces the RC special pair after photo-induced electron transfer [28]. However, some purple bacterial RCs do not have a bound cytochrome *c* subunit. Instead, they depend on a soluble cytochrome c_2 that is discussed below or another soluble electron transfer protein [29,30].

The tetraheme cytochrome *c* RC subunit in Purple Bacteria is a periplasmic subunit with four hemes responsible for accepting electrons from a soluble carrier and re-reducing the RC special pair. It belongs to class III of cytochrome proteins, which are defined by their multihemes with low redox potentials [31]. Early biochemical work on PB RC's had focused on *Rhodobacter sphaeroides* or *Rhodobacter capsulatus*, which do not have the tetraheme cytochrome subunit [27,32]. Thus, it had been thought that the PB RC's lacked an attached cytochrome. Additionally, the RC cyt *c* subunit can remain firmly attached during purification, but it is sometimes lost, which made it difficult to detect or characterize. However, an important advance in the knowledge and understanding of the PB RC, and in particular the cytochrome subunit, was the crystal structure of the RC of *Blastochloris viridis,* (formerly known as *Rhodopseudomonas viridis*) (Figure 1.2A) [30]. This was the first photosynthetic RC crystallized and revealed a surprise, the tetra-heme cytochrome *c*. The discovery and characterization of the tetraheme cytochrome in the *Bl. viridis* structure altered the perception not only of PB RC's, but of all cytochrome donors of reaction center complexes. The discovery spurred questions such as: Why are there four hemes? Does each heme have a distinct redox potential? and How do electrons flow through the hemes?

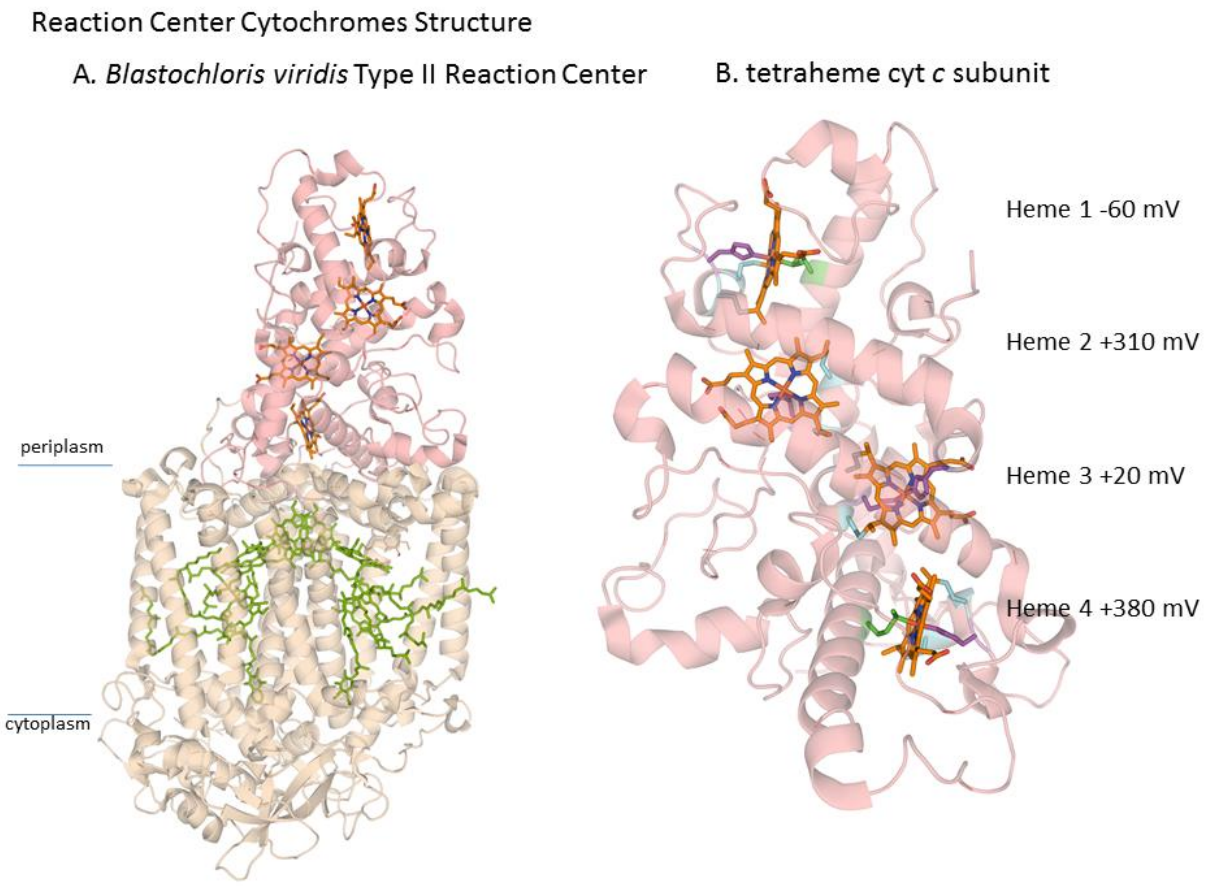

Figure 1.2 Crystal Structures of Photosynthetic Reaction Center Cytochromes A) *Blastochloris viridis* RC (PDBID 3T6D). The tetraheme subunit is in red and the integral membrane subunits are in tan. Heme cofactors are orange and special pair pigments are green. B) The tetraheme subunit alone. Chain is in red and hemes are in orange. Heme binding amino acid side chains are shown as cysteine in cyan, histidine in purple and methionine in green.

This tetraheme subunit, known as cyt c_{554} or RC cyt *c*, accepts electrons from a periplasmic soluble electron donor, and transfers an electron to the special pair of pigments to re-reduce the pair after charge separation has occurred [34,35] Cyt c_{554} is analogous to cyt c_z in type I RC's, but has four hemes and no transmembrane anchor helix. The crystal structure revealed a bound tetraheme cytochrome *c* subunit with a roughly vertically stacked heme alignment (Figure 1.2B) that had not previously been observed in any cytochrome protein [33]. This arrangement was postulated to direct the flow of electron transfer and was confirmed with the assignment of the

redox potentials. The redox potentials are heme 1 at -60 mV, heme 2 at +310 mV, heme 3 at +20 mV, and heme 4 at +380 mV in *Bl. viridis* [36]. The subunit has two low potential and two high potential hemes [37]. The function of each heme and order of electron transfer within this subunit corresponds to the redox potential. A Low Potential-High Potential-Low Potential-High Potential-Special Pair electron flow pathway was established [36].

Another unique feature of cyt c_{554} is the ability of the subunit to move electrons uphill against the redox potential gradient. Overall in cyclic electron transport, the distal heme of the tetraheme cytochrome has a much lower redox potential (-60 mV) than donor, cyt c_2 (+345 mV), yet donates within 60 μs to the electron acceptor special pair, as characterized in *Bl. viridis* [1]. Somehow, the tetraheme subunit is able to overcome this energy barrier; likely from an overall downhill thermodynamics of the electron transfer from cyt c_2 to the RC.

Attached tetraheme cytochromes are not only found in PB, but are also observed in other anoxygenic photosynthetic prokaryotic families such as the Filamentous Anyoxygenic Phototrophs (FAPs) [38]. Many FAPs differ from PBs by growing in warmer environments, being filaments versus rods and having different light harvesting antenna [39]. Their RCs also lack the H subunit but are still type II RC's [40]. FAPs are represented by the closely related *Chloroflexus aurantiacus* (CFX) and *Roseiflexus castenholzii* (RFX), but differ in that CFX has a large peripheral light harvesting complex, the chlorosome, and RFX does not [41,42]. Additionally, the tetraheme cytochrome *c* subunit of RFX stays firmly attached to the RC during purification but that of CFX does not [43]. Despite the loss during purification, the CFX subunit was characterized, and re-reduction of the RC cyt c_{554} was observed *in vitro* [43]. Likewise, the intact RFX RC complex has been purified and characterized [38]. The re-reduction of the RC special pair by the tetraheme cyt *c* kinetics in RFX were similar to that of CFX [44]. The structure of the FAP RC's

has not been determined, but a high sequence similarity between the FAP and PB RCs suggests that structure would be similar (Gardiner, Roszak, & Majumder, unpublished data).

In addition to promoting uphill electron transfer, the presence of an attached cytochrome *c* subunit has been shown to increase the photocurrent detected for a Light Harvesting Reaction Center (LHRC) complex versus an LHRC with no cyt *c* subunit during *in vitro* photochemical cell assays (Friebe & Majumder, unpublished data). This increase in photocurrent is attributed to the attached cytochrome *c* subunit because then the electron donor binding is not the rate limiting step and the assay is not dependent on diffusion and binding of the carrier cyt *c*. The tetraheme cyt *c* enhances function of the RC by contributing to the reaction rate and overcoming an energy barrier. The tetraheme cyt *c* of PB and FAPs adds to the structural and functional diversity of anoxygenic photosynthetic RC cytochromes.

1.2.2 Cytochromes in *bc* complexes

After RCs complete charge separation, electrons move through the cyclic or noncyclic electron transport chain. The electron movement generates a proton-motive force that ultimately drives ATP synthase forming chemical energy such as ATP [45]. In the RC, two electrons and two protons are donated to a quinone, reducing the quinone to quinol. The reduced quinol diffuses through the membrane to the second large complex of the anoxygenic cyclic electron transport chain, the cytochrome *bc* complex [46]. This complex oxidizes the quinol, sending the electrons through the *bc* complex via a process known as the Q-cycle and simultaneously translocates protons to the positive side of the membrane periplasmic or P side [47]. The proton translocation against the electrochemical gradient contributes to the proton motive force. The electrons, after

going through the Q-cycle are loaded onto a soluble carrier, typically a cytochrome [48] which is discussed in the next section.

The cytochrome *bc* complexes are named for the their major cofactors, *b* and *c*-type hemes. A few key differences distinguish *b* and *c* type hemes: *c* type hemes are covalently linked to the protein via thioether bonds while *b* type hemes have vinyl groups in those positions. In typical cytochrome *bc* complexes the *b* and *c* heme cofactors are localized in different subunits. The *b* subunit is usually involved in quinone redox reactions and the *c* subunit in electron transfer with soluble carriers. The proton pumping ability of cyt *bc*-type complexes makes them well suited to electron transport chains for cellular respiration. Cyt *bc* complexes are consequently found in phototrophic and non-phototrophic taxa of prokaryotes including proteobacteria and the in mitochondria of eukaryotes including humans [47]. The cyt *bc* complexes of anoxygenic photosynthetic prokaryotes discussed in this section are small and simple compared to their eukaryotic counterparts [49]. However, despite being present on nearly the whole tree of life, the fundamental catalytic components of this protein complex have relatively few forms compared to the variety of species and electron transport chains in which they exist [50]. This section explores the canonical cyt bc_1 complex, the *bc* complex of Heliobacteria, and the novel functional replacement the Alternative Complex III (ACIII).

Cytochrome bc_1 complex

The proton pumping complex used in most anoxygenic phototrophic bacteria is the cytochrome bc_1 complex, which functions to preserve energy within the cell through the Q cycle [51]. [47]. The establishment of the Q cycle mechanism has been the focus of effort in *bc* complexes in recent years and relied heavily on understanding the cytochrome subunits. Typical cyt bc_1

complexes have a cytochrome *b* subunit, a cytochrome c_1 subunit and a Rieske iron-sulfur cluster subunit (Figure 1.3A) [52]. The cytochrome *b* and Rieske protein subunits start the reactions in the Q cycle by providing the sites for quinol oxidation.

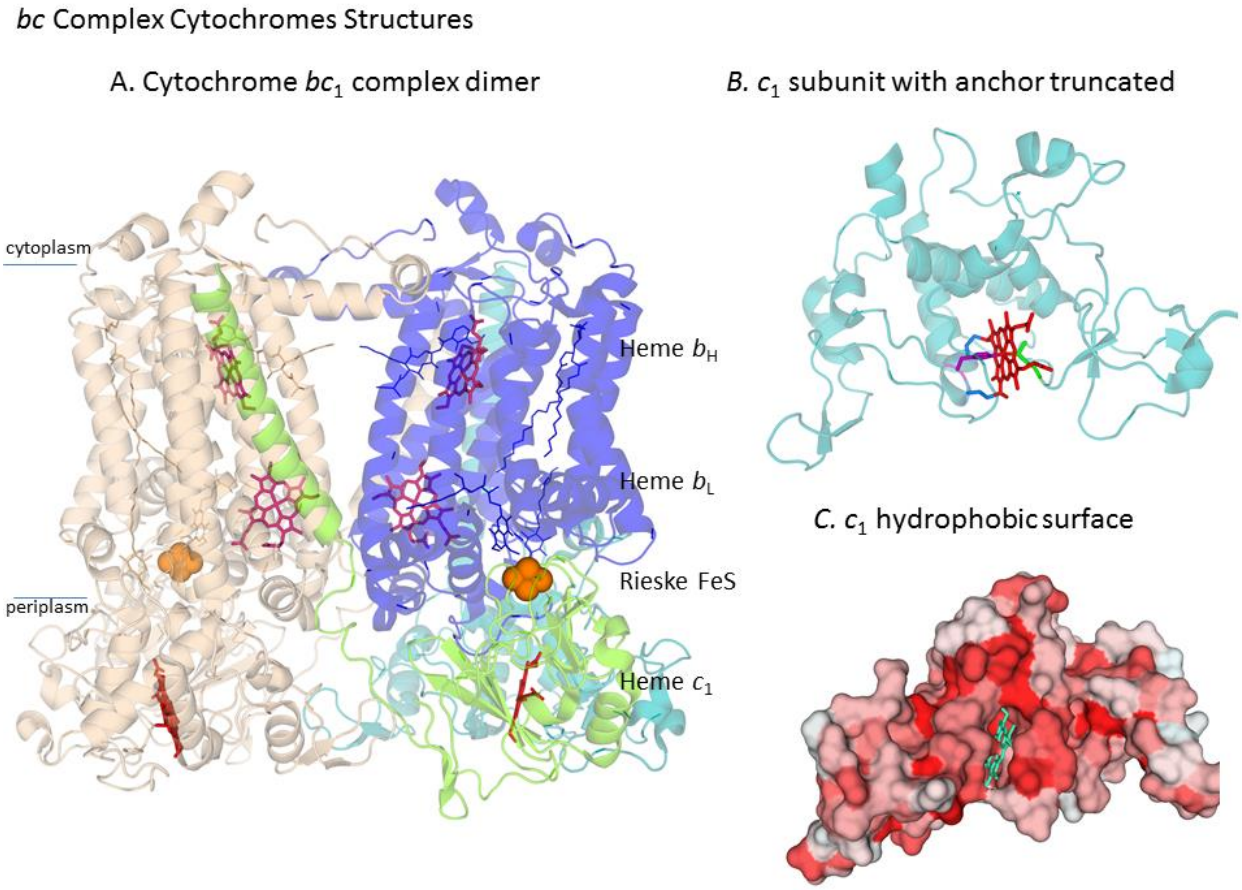

Figure 1.3 Crystal Structures of Photosynthetic *bc* Complex Cytochromes A) Cytochrome bc_1 complex from *Rhodobacter sphaeroides* (PBDID 2QJK). The complex is shown as the biological dimer with one half color-coded. The cytochrome *b* subunit is in blue, the cytochrome c_1 subunit is in teal and the Rieske subunit is in green. *b*-type hemes are pink, *c*-type hemes are red and FeS is in orange. The chains of the second half of the dimer are in tan. B) The cytochrome c_1 subunit alone with anchor helix truncated. Chain is in teal and heme is in red. Heme binding amino acid side chains are shown as cysteine in cyan, histidine in purple and methionine in green. C) Hydrophobic surface of the cytochrome c_1 subunit. The darker the red, the more hydrophobic the area is. Heme is shown in cyan and shown in same orientation as 3B.

The cyt *b* subunit of the cytochrome bc_1 complex has two *b*-type hemes in a classical *b*-type fold with the heme plane parallel to the helix bundle axis [53]. They belong to the cyt *b* family of proteins defined by their two *b*-type hemes and presence in *bc* complexes [50]. The subunit has an elongated structure that spans the membrane with about eight transmembrane helices. It is also predicted to be the precursor of the PSII RC cyt b_{559} discussed in later sections [54]. The two *b* hemes within the subunit are named b_L and b_H for their respective low and high redox potential. They can also be called b_p and b_n, corresponding to b_L and b_H, in reference to their locations near the positive and negative sides of the membrane. The hemes are the major cofactors near to the Q_o and Q_i sites, also known as Q_p and Q_n in the same fashion as the hemes, where quinol is oxidized and quinone is reduced, respectively, during the Q cycle [55]. Heme b_L is found near the Qo site to match the redox potential needs of quinol oxidation, and heme b_H is found near the Q_i site because of the redox potential needed to reduce quinone. The specific chemistry at each of these sites and the mechanism of electron transfer through each heme is part of the Q cycle.

To start the Q cycle, the Q_o site facilitates bifurcated electron transfer. Here we give only a brief description. Two electrons and two protons are extracted from the quinol sequentially [56]. One electron moves onto the Rieske subunit and the other to heme b_L. The now reduced lower potential heme passes its electrons down the energy gradient to heme b_H. In the Q_i site a quinone is bound and receives the electron from b_H generating a semiquinone radical [57]. Another quinol binds to the Q_o site and the process repeats generating a reduced quinol in the Q_i that then diffuses into the membrane.

After a quinol is oxidized at the Q_o site, the second arm of the bifurcation event loads one electron onto the Rieske Fe-S subunit, which moves almost 20 angstroms to dock with the

cytochrome c_1 on the periplasmic face of the bc_1 complex [49,58]. The cytochrome c_1 subunit has a typical cytochrome *c* fold around the monoheme and is anchored to the membrane with a C-terminal helix (Figure 1.3B). It belongs to class I cytochrome *c*'s. Cyt c_1 transfers electrons to a soluble cytochrome c_2 or sometimes interacts with a different soluble cytochromes c_8 or c_y (Figure 1.1A). The cyt c_1 subunit has a hydrophobic surface with positive and negative patches complementary to the soluble acceptor cyt c_2 (Figures 1.3C & 1.4B). The complementary electrostatic surfaces permits c_1 to bind transiently but tightly with the soluble acceptor. Cyt c_2 or the other soluble carriers, as discussed in the next section, serve to re-reduce the RC, thereby completing the Q-cycle [59]. Unlike the cyt *b* subunit of *bc* complexes, which are conserved across nature, there is more variation in the cyt c_1 subunits.

Cytochrome *bc* complexes

Heliobacteria are strictly anaerobic phototrophs that belong to the Firmicutes family, which are gram positive bacteria and to the class of Clostridia which are anaerobic [60]. For photosynthetic machinery, they employ Type I Reaction Centers and a cyt *bc* complex that is comparatively simple or smaller than the previously discussed complexes [61]. From the cyt *bc* complex, the *b* subunit in Heliobacteria is the postulated evolutionary precursor for both cyt b_6f and cyt bc_1 cyt *b* subunits [62]. The deviation from the conventional pattern is in the periplasmic cytochrome subunit. Instead of a monoheme cytochrome *c*, heliobacteria have a diheme cytochrome *c*. This protein is predicted to have resulted from a gene duplication event and subsequent fusion [63].

Unlike other DHCCs, in the heliobacterial DHCC, both hemes have equal reduction potentials [64]. Recent work predicts a structure and mechanism for this complex using homology

modeling in combination with Hydrogen Deuterium Exchange Mass spectrometry [65]. In the absence of a crystal structure, the modelled protein has two similar *c*-type cytochrome domains with an N-terminal helix anchor. In the predicted mechanism, the electron arrives at DHCC via the iron-sulfur cluster. The N-terminal heme would accept the electron from the iron-sulfur cluster. The electron would then pass to the heme of the C-terminal domain. The C-terminal domain is more flexible and solvent accessible and therefore should donate the electron to the soluble electron carrier. This mechanism involving both hemes in the DHCC subunit would allow the complex to store electrons or be able to turn over even if the soluble carrier has not retuned yet [65].

As in Heliobacteria, the complex in Green Sulfur bacteria is also called a *bc* complex because it is also an alternative to cyt c_1. GSB have a cytochrome c_{556} that is structurally much like cyt $c_{1,}$ but differs in that c_{556} is predicted to directly donate to the RC cyt c_z without a soluble intermediate [14]. There is diversity in the structure and mechanism of anoxygenic photosynthetic cyt *bc* complexes.

Alternative Complex III

Some anoxygenic phototrophs contain novel integral membrane cytochrome complexes that do not fit into either the bc_1 or b_6f category. They fulfill the same functional role as a major enzyme of the electron transport chain of organism but do not share sequence homology or an evolutionary relationship with the conventional *bc* complexes.

An unconventional cytochrome complex that stands in contrast to the cytochrome *bc* complex protein family, belonging instead to the molybdopterin oxidoreductase family, is the Alternative Complex III (ACIII) [66–68]. ACIII complexes are found in several families of non-

phototrophic bacteria and in photosynthetic prokaryotes, in the Filamentous Anoxygenic Phototrophs (FAPs) family [69]. ACIII is predicted to have the function of the *bc* complex, but does not resemble the typical complex, having more homology to polysulfide reductase [68]. It has seven subunits, two of which contain *c*-type hemes and does not contain *b*-type cytochromes.

The two heme subunits of ACIII that have been characterized in the photosynthetic prokaryote *Chloroflexus aurantiacus* are ActA and ActE. ActA has five hemes, and ActE is a monoheme subunit with two copies present in the full complex. ActA and ActE are both found in the periplasm. The 5 hemes in ActA have 3 redox potentials of -228 mV (3 hemes), -110 mV (1 heme) and +94 mV (1 heme). ActE has a redox potential of +390mV [70]. ActA is predicted to donate electrons to ActE, and ActE is thought to be the final electron acceptor within the complex, much like cyt c_1 in the *bc* complexes. ActE has been shown to be necessary for oxido-reductase function [71]. Furthermore, it is thought to be a dimer [70]. A homologous protein to ActE has not been identified in the Protein DataBank, and therefore suggests that ActE does not have the typical cytochrome *c* fold. The amino acid sequence of ActA, however, aligns with other multiheme proteins such as the *Escherichia coli* hexaheme nitrite reductase, but shows differences that arise from the presence of a N-terminal trans-membrane helix in ActA [68].

Overall, ACIII contains seven hemes to carry out a one-electron process. Other proteins with mutlihemes carry out chemistry that requires more electrons, which poses the question of the mechanism of ACIII [72,73]. There is no evidence for a Q-cycle-like mechanism in ACIII. A Q_o site has been identified by inhibitor assays by a HQNO fluorescence assay, but there is no Q_i site nor *b*-type hemes [74]. The mechanism of ACIII is expected to be quite different from that of typical cyt *bc* complexes. In mechanism and subunit composition, ACIII is a novel member of the photosynthetic cytochromes.

1.2.3 Soluble cytochromes in anoxygenic cyclic electron transport

Soluble cytochromes are the mobile components of photosynthetic electron transport chains, shuttling electrons between the large membrane proteins. All known soluble cytochromes in photosynthesis are monoheme *c*-type cytochromes, most with the usual *c*-type cytochrome protein fold and are located in the periplasm [12]. Examples of other non-cytochrome soluble electron carriers are two small blue copper proteins: plastocyanin in oxygenic photosynthetic organisms and auracyanin in the FAPs [75]. While some soluble cytochromes are restricted by an anchoring tail that attaches these cytochromes to the membrane surface, other soluble cytochromes are neither attached nor associated with the membrane [24,76]. Regardless of membrane attachment, soluble cytochromes proteins are promiscuous binders allowing them to bind two different protein complexes transiently [77,78].

A canonical soluble anoxygenic cytochrome is cyt c_2, which shuttles electrons from the cyt bc_1 complex to the RC in Purple Bacteria [76,79]. This protein belongs to the class I *c*-type cytochromes having histidine and methionine as axial ligands and the heme attachment near the N-terminus of the protein [80]. The crystal structures of cyt c_2 from several purple bacterial species have been solved (Figure 1.4A). The solved cyt c_2 structures all contain an alpha-helical *c*-type cytochrome fold. The heme is buried except for one exposed edge surrounded by positively charged lysine residues (Figure 1.4B) [81]. This feature defines the binding site to the RC and cyt bc_1 which have corresponding regions consisting of complementary negatively charged residues on their surface [1]. This electrostatic interaction allows for tight but transient binding since c_2 must deliver electrons quickly to the two different partners. The flash-induced kinetics for c_2 donation to the RC special pair are multiphasic, representing each step in the electron transfer

process: first the diffusion of the reduced c_2 and binding to the RC is seen in the slower kinetic phase and secondly, the fast phase, ~1 μs, reflects the rapid oxidation of a bound c_2 [82,83].

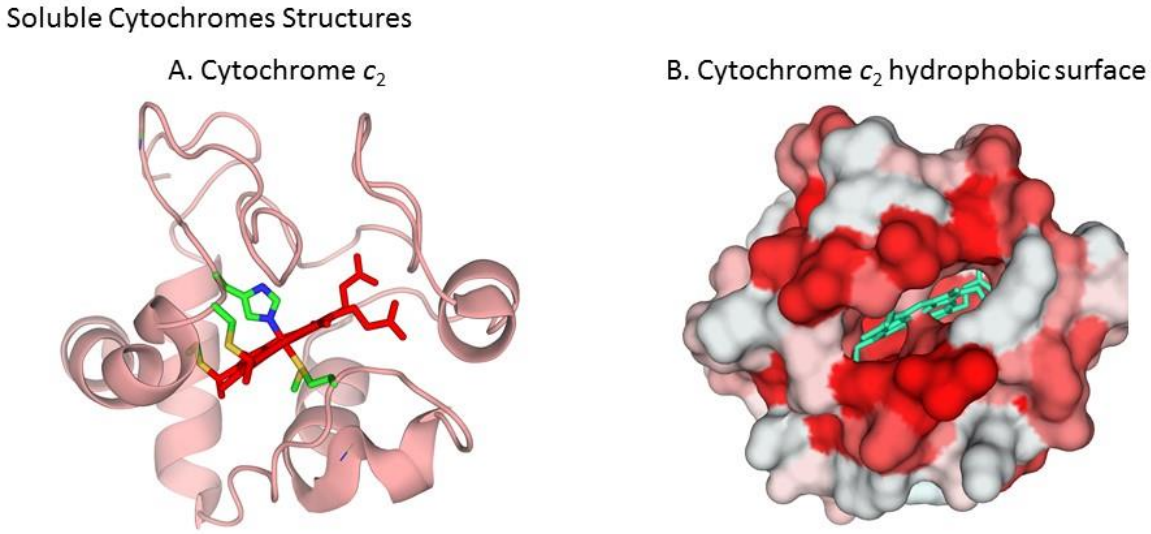

Figure 1.4 Crystal Structures of Photosynthetic Soluble Cytochromes A) Cytochrome c_2 from *Blastochloris viridis* (PDBID 1IO3) that interacts with the RC in Figure 1.2A. Chain is light brown, heme is in red, and the heme binding amino acid side chains are colored by element. B) Hydrophobic surface of the cytochrome c_2. The darker the red, the more hydrophobic the area is. Heme is shown in cyan and shown in same orientation as 4A.

In Purple Bacteria, cytochromes c_y, c_8, c_4, and a HiPIP (High-Potential Iron-Sulfur Protein) have been implicated as alternatives to cyt c_2, the donor to the RC. Cytochromes c_4 and c_8 are also *c*-type soluble cytochromes [84]. The ability of cyt c_8 to donate to the RC in several PB species was established in the 1970's [85–87]. It has also been observed to function during autotrophic growth [84]. The origin of c_8 may be in the nitrite reduction pathway [88]. Cyt c_y is unique as one of the few anchored soluble cytochromes, also found in PB [89]. The membrane anchor is a tail that attaches to a membrane lipid moiety. It therefore has a pendulum type motion in shuttling electrons between the large integral membrane complexes. The electron transfer rates in c_2-less mutants that only use c_y still showed efficient photosynthetic growth suggesting that c_y

is functional replacement for c_2 [77,89,90]. The alternative donors provide PB the flexibility to survive in changing conditions such as light intensity and nutrient concentration.

Another unique class of cytochromes found in phototrophic and aerobic bacteria is cytochrome *c*'[91]. They are soluble *c*-type cytochromes whose function is not well understood. They are designated as c-type because of the covalent bonds from the heme to cysteines but differ in most other ways. Cytochrome *c*' has the heme in a high spin environment, but does not have typical ligands or a *c*-type cytochrome fold and is thus pentacoordinate [92]. This class of alternative cyt *c* proteins has their heme binding sites near the C-terminal end of the protein, which similar to c_{556} from GSB, but has other structure features of cyt c_1 [91]. A study of cyt c' in PB *Rhodobacter sphaeroides* showed that cyt c' is expressed most during photosynthetic denitrification growth and binds NO and CO [93,94]. Further work will reveal the function of cyt *c*'.

The story of soluble cytochromes in other anoxygenic species is not as straightforward. Green Sulfur Bacteria were originally thought to use a soluble cyt c_{555}, but it is now known that there are other sources of electrons from sulfur metabolism that enter the photosynthetic cyclic electron transport chain, but they that are not well characterized [95]. As seen in Figure 1.1A, cyt c_{555} can take electrons from sulfur metabolism and potentially donate them to c_z of the RC. As discussed above, heliobacteria are now believed to have no soluble cytochromes as part of their CET chain and rely solely on membrane-bound cytochromes [1]. The Filamentous Anoxygenic Phototrophs, as mentioned above, rely on the small blue copper protein auracyanin to shuttle electrons between ACIII and the RC (Figure 1.1A) [68]. Whether typical or atypical, many cytochromes are key components in the photosynthetic electron transport chain of anoxygenic bacteria. These cytochromes persisted in their same basic forms during the evolutionary transition to oxygenic photosynthesis.

1.3 Conclusions

From large membrane protein complexes to small soluble proteins, cytochromes play crucial roles in electron transport chains, accomplishing the major processes of energy conversion and oxygen production on the planet. Most that have been studied are *b* or *c*-type cytochromes, but significant variations exist despite overall similarity in functions. Photosynthetic organisms take advantage of the diversity of cytochromes to adapt to different environments and metabolic needs. Humans can take advantage of the processes and mechanisms carried out by cytochromes to grow more crops or to design biomimetic solar panels or fuel cells. This thesis will continue to explore the structure and function of cytochrome proteins from the FAP's and heliobacteria.

References

(1) Blankenship, R. E. (2014) Molecular mechanisms of photosynthesis. Blackwell Science, Oxford, UK.

(2) Cramer, W., and Whitmarsh, J. (1977) Photosynthetic cytochromes. *Annu. Rev. Plant Physiol.*

(3) Zeng, Y., Feng, F., Medová, H., Dean, J., and Koblížek, M. (2014) Functional type 2 photosynthetic reaction centers found in the rare bacterial phylum Gemmatimonadetes. *Proc. Natl. Acad. Sci. U. S. A. 111*, 7795–800.

(4) Margulis, L. (1992) Symbiosis in Cell Evolution 2nd ed. W.H. Freeman, San Fransico.

(5) Moore, G. R., and Pettigrew, G. W. (1990) Cytochromes c: evolutionary, structural, and physicochemical aspects, p 478. Springer-Verlag.

(6) Blankenship, R. E. (2010) Early Evolution of Photosynthesis. *Plant Physiol. 154*, 434–438.

(7) Lau, M. C. Y., and Pointing, S. B. (2009) Vertical partitioning and expression of primary metabolic genes in a thermophilic microbial mat. *Extremophiles 13*, 533–40.

(8) Meyer, T. E., and Donohue, T. J. (1995) Cytochromes, Iron-Sulfur, and Copper Proteins Mediating Electron Transfer from the Cyt bc 1 Complex to Photosynthetic Reaction Center Complexes, in *Anoxygenic Photosynthetic Bacteria* (Blankenship, R. E., Madigan, M. T., and Bauer, C. E., Eds.), pp 725–745. Springer.

(9) Ritchie, R. J., and Runcie, J. W. (2012) Photosynthetic Electron Transport in an Anoxygenic Photosynthetic Bacterium Afifella (Rhodopseudomonas) marina measured using PAM Fluorometry. *Photochem. Photobiol.*

(10) Parson, W. W. (1968) The role of P870 in bacterial photosynthesis. *Biochim. Biophys. Acta 153*, 248–59.

(11) Hohmann-Marriott, M. F., and Blankenship, R. E. (2011) Evolution of photosynthesis. *Annu. Rev. Plant Biol. 62*, 515–48.

(12) Azai, C., Tsukatani, Y., Itoh, S., and Oh-oka, H. (2010) C-type cytochromes in the photosynthetic electron transfer pathways in green sulfur bacteria and heliobacteria. *Photosynth. Res. 104*, 189–199.

(13) Williamson, A., Conlan, B., Hillier, W., and Wydrzynski, T. (2011) The evolution of Photosystem II: insights into the past and future. *Photosynth. Res. 107*, 71–86.

(14) Oh-oka, H., Iwaki, M., and Itoh, S. (1998) Membrane-bound cytochrome cz couples quinol oxidoreductase to the P840 reaction center complex in isolated membranes of the green sulfur bacterium Chlorobium tepidum. *Biochemistry 37*, 12293–300.

(15) Fowler, C. F., Nugent, N. A., and Fuller, R. C. (1971) The isolation and characterization of a photochemically active complex from Chloropseudomonas ethylica. *Proc. Natl. Acad. Sci. U. S. A. 68*, 2278–82.

(16) Prince, R. C., and Olson, J. M. (1976) Some thermodynamic and kinetic properties of the primary photochemical reactants in a complex from a green photosynthetic bacterium. *Biochim. Biophys. Acta 423*, 357–62.

(17) Oh-oka, H., Kamei, S., Matsubara, H., Iwaki, M., and Itoh, S. (1995) Two molecules of cytochrome c function as the electron donors to P840 in the reaction center complex isolated from a green sulfur bacterium, Chlorobium tepidum. *FEBS Lett. 365*, 30–4.

(18) Okkels, J. S., Kjaer, B., Hansson, O., Svendsen, I., Møller, B. L., and Scheller, H. V. (1992) A membrane-bound monoheme cytochrome c551 of a novel type is the immediate electron donor to P840 of the Chlorobium vibrioforme photosynthetic reaction center complex. *J. Biol. Chem. 267*, 21139–45.

(19) Higuchi, M., Hirano, Y., Kimura, Y., Oh-oka, H., Miki, K., and Wang, Z.-Y. (2009) Overexpression, characterization, and crystallization of the functional domain of cytochrome c(z) from Chlorobium tepidum. *Photosynth. Res. 102*, 77–84.

(20) Hirano, Y., Higuchi, M., Azai, C., Oh-Oka, H., Miki, K., and Wang, Z.-Y. (2010) Crystal structure of the electron carrier domain of the reaction center cytochrome c(z) subunit from green photosynthetic bacterium Chlorobium tepidum. *J. Mol. Biol. 397*, 1175–87.

(21) Tsukatani, Y., Azai, C., Kondo, T., Itoh, S., and Oh-Oka, H. (2008) Parallel electron donation pathways to cytochrome c(z) in the type I homodimeric photosynthetic reaction center complex of Chlorobium tepidum. *Biochim. Biophys. Acta 1777*, 1211–7.

(22) Azai, C., Tsukatani, Y., and Miyamoto, R. (2008) Bifurcated Electron Donations from Quinol Oxidoreductase and Soluble CycA to Cytochrome cz of the Photosynthetic Reaction Center Complex in the Green Sulfur. *… . Energy from Sun*.

(23) Sarrou, I., Khan, Z., Cowgill, J., Lin, S., Brune, D., Romberger, S., Golbeck, J. H., and Redding, K. E. (2012) Purification of the photosynthetic reaction center from Heliobacterium modesticaldum. *Photosynth. Res. 111*, 291–302.

(24) Kashey, T. S., Cowgill, J. B., McConnell, M. D., Flores, M., and Redding, K. E. (2014) Expression and characterization of cytochrome c 553 from Heliobacterium modesticaldum. *Photosynth. Res.*

(25) Sattley, W. M., and Blankenship, R. E. (2010) Insights into heliobacterial photosynthesis and physiology from the genome of Heliobacterium modesticaldum. *Photosynth. Res. 104*, 113–22.

(26) Westerhuis, W. H. J. (1996) Consequences for the Organization of Reaction Center-Light Harvesting Antenna 1 (LH1) Core Complexes of Rhodobacter sphaeroides Arising from Deletion of Amino Acid Residues from the C Terminus of the LH1 alpha Polypeptide. *J. Biol. Chem. 271*, 3285–3292.

(27) Allen, J. P., Feher, G., Yeates, T. O., Komiya, H., and Rees, D. C. (1987) Structure of the reaction center from Rhodobacter sphaeroides R-26: the protein subunits. *Proc. Natl. Acad. Sci. U. S. A. 84*, 6162–6.

(28) Jones, M. R. (2009) Structural Plasticity of Reaction Centers from Purple Bacteria, in *The Purple Phototrophic Bacteria* (Hunter, C. N., Daldal, F., Thurnauer, M. C., and Beatty, J. T., Eds.), pp 295–321. Springer, Dordrecht.

(29) Axelrod, H. L., and Okamura, M. Y. (2005) The structure and function of the cytochrome c2: reaction center electron transfer complex from Rhodobacter sphaeroides. *Photosynth. Res. 85*, 101–14.

(30) Ortega, J. M., Drepper, F., and Mathis, P. (1999) Electron transfer between cytochrome c2 and the tetraheme cytochrome c in Rhodopseudomonas viridis. *Photosynth. Res. 59*, 147–157.

(31) Coutinho, I. B., and Xavier, A. V. (1994) Inorganic Microbial Sulfur Metabolism. *Methods Enzymol.*, pp 119–140. Elsevier.

(32) Bauer, C. E., Young, D. A., and Marrs, B. L. (1988) Analysis of the Rhodobacter capsulatus puf operon. Location of the oxygen-regulated promoter region and the identification of an additional puf-encoded gene. *J. Biol. Chem. 263*, 4820–7.

(33) Deisenhofer, J., Epp, O., Miki, K., Huber, R., and Michel, H. (1985) Structure of the protein subunits in the photosynthetic reaction centre of Rhodopseudomonas viridis at 3Å resolution. *Nature 318*, 618–624.

(34) Hara, M. (1998) Redox properties of an H-subunit-depleted photosynthetic reaction center from Rhodopseudomonas viridis. *Biochim. Biophys. Acta - Bioenerg. 1363*, 199–208.

(35) Roszak, A. W., Moulisová, V., Reksodipuro, A. D. P., Gardiner, A. T., Fujii, R., Hashimoto, H., Isaacs, N. W., and Cogdell, R. J. (2012) New insights into the structure of the reaction centre from Blastochloris viridis: evolution in the laboratory. *Biochem. J. 442*, 27–37.

(36) Dracheva, S. M., Drachev, L. A., Konstantinov, A. A., Semenov AYu, Skulachev, V. P., Arutjunjan, A. M., Shuvalov, V. A., and Zaberezhnaya, S. M. (1988) Electrogenic steps in the redox reactions catalyzed by photosynthetic reaction-centre complex from Rhodopseudomonas viridis. *Eur. J. Biochem. 171*, 253–64.

(37) Nogi, T., Hirano, Y., and Miki, K. (2005) Structural and functional studies on the tetraheme cytochrome subunit and its electron donor proteins: the possible docking mechanisms during the electron transfer reaction. *Photosynth. Res. 85*, 87–99.

(38) Collins, A. M., Qian, P., Tang, Q., Bocian, D. F., Hunter, C. N., and Blankenship, R. E. (2010) Light-harvesting antenna system from the phototrophic bacterium Roseiflexus castenholzii. *Biochemistry 49*, 7524–31.

(39) Tang, K.-H., Barry, K., Chertkov, O., Dalin, E., Han, C. S., Hauser, L. J., Honchak, B. M., Karbach, L. E., Land, M. L., Lapidus, A., Larimer, F. W., Mikhailova, N., Pitluck, S., Pierson, B. K., and Blankenship, R. E. (2011) Complete Genome Sequence of the Filamentous Anoxygenic Phototrophic Bacterium Chloroflexus aurantiacus. *BMC Genomics 12*, 334.

(40) Collins, A. M., Xin, Y., and Blankenship, R. E. (2009) Pigment organization in the photosynthetic apparatus of Roseiflexus castenholzii. *Biochim. Biophys. Acta 1787*, 1050–6.

(41) Yamada, M., Zhang, H., Hanada, S., Nagashima, K. V. P., Shimada, K., and Matsuura, K. (2005) Structural and spectroscopic properties of a reaction center complex from the chlorosome-lacking filamentous anoxygenic phototrophic bacterium Roseiflexus castenholzii. *J. Bacteriol. 187*, 1702–9.

(42) Cao, L., Bryant, D. A., Schepmoes, A. A., Vogl, K., Smith, R. D., Lipton, M. S., and Callister, S. J. (2012) Comparison of Chloroflexus aurantiacus strain J-10-fl proteomes of cells grown chemoheterotrophically and photoheterotrophically. *Photosynth. Res. 110*, 153–168.

(43) Meyer, T. E., Tollin, G., Cusanovich, M. A., Freeman, J. C., and Blankenship, R. E. (1989) In vitro kinetics of reduction of cytochrome c554 isolated from the reaction center of the green phototrophic bacterium, Chloroflexus aurantiacus. *Arch. Biochem. Biophys. 272*, 254–61.

(44) Xin, Y., Pan, J., Collins, A. M., Lin, S., and Blankenship, R. E. (2011) Excitation energy transfer and trapping dynamics in the core complex of the filamentous photosynthetic bacterium Roseiflexus castenholzii. *Photosynth. Res.* 1–8.

(45) Crofts, A. R., Hong, S., Wilson, C., Burton, R., Victoria, D., Harrison, C., and Schulten, K. (2013) The mechanism of ubihydroquinone oxidation at the Q(o)-site of the cytochrome bc(1) complex. *Biochim. Biophys. Acta null*.

(46) Hunte, C. (2003) Protonmotive pathways and mechanisms in the cytochrome bc1 complex. *FEBS Lett. 545*, 39–46.

(47) Cape, J. L., Bowman, M. K., and Kramer, D. M. (2006) Understanding the cytochrome bc complexes by what they don't do. The Q-cycle at 30. *Trends Plant Sci. 11*, 46–55.

(48) Kramer, D., Wolfgang, N., and Cooley, J. W. (2009) The Cytochrome bc 1 and Related bc Complexes: The Rieske/Cytochrome b Complex as the Functional Core of a Central Electron/Proton Transfer Complex, in *The Purple Phototrophic Bacteria* (Hunter, C. N., Daldal, F., Thurnauer, M. C., and Beatty, J. T., Eds.), pp 451–473. Springer, Dordrecht.

(49) Esser, L., Elberry, M., Zhou, F., Yu, C.-A., Yu, L., and Xia, D. (2008) Inhibitor-complexed structures of the cytochrome bc1 from the photosynthetic bacterium Rhodobacter sphaeroides. *J. Biol. Chem. 283*, 2846–57.

(50) Berry, E. A., Guergova-Kuras, M., Huang, L. S., and Crofts, A. R. (2000) Structure and function of cytochrome bc complexes. *Annu. Rev. Biochem. 69*, 1005–75.

(51) Trumpower, B. L. (1990) Cytochrome bc1 complexes of microorganisms. *Microbiol. Mol. Biol. Rev. 54*, 101–129.

(52) Khalfaoui-Hassani, B., Lanciano, P., Lee, D.-W., Darrouzet, E., and Daldal, F. (2012) Recent advances in cytochrome bc(1): inter monomer electronic communication? *FEBS Lett. 586*, 617–21.

(53) Berry, E. A., De Bari, H., and Huang, L.-S. (2013) Unanswered Questions about the Structure of Cytochrome bc1 Complexes. *Biochim. Biophys. Acta - Bioenerg. null*.

(54) Shinopoulos, K. E., and Brudvig, G. W. (2012) Cytochrome b_{559} and cyclic electron transfer within photosystem II. *Biochim. Biophys. Acta 1817*, 66–75.

(55) Czapla, M., Cieluch, E., Borek, A., Sarewicz, M., and Osyczka, A. (2013) Catalytically-relevant electron transfer between two hemes bL in the hybrid cytochrome bc1-like complex

containing a fusion of Rhodobacter sphaeroides and capsulatus cytochromes b. *Biochim. Biophys. Acta null*.

(56) Crofts, A. R., Hong, S., Wilson, C., Burton, R., Victoria, D., Harrison, C., and Schulten, K. (2013) The mechanism of ubihydroquinone oxidation at the Qo-site of the cytochrome bc1 complex. *Biochim. Biophys. Acta - Bioenerg. 1827*, 1362–1377.

(57) Cooley, J. W. (2010) A structural model for across membrane coupling between the Qo and Qi active sites of cytochrome bc1. *Biochim. Biophys. Acta 1797*, 1842–8.

(58) Osyczka, A., and Cooley, J. W. (2013) Protein conformational changes involved in the cytochrome bc1 complex catalytic cycle. *Biochim. Biophys. Acta - Bioenerg. 1827*, 1340–1345.

(59) Sanders, C., Turkarslan, S., Onder, O., Frawley, E. R., Kranz, R. G., Koch, H. G., and Daldal, F. (2009) Biogenesis of c-type Cytochromes and Cytochrome Complexes, in *The Purple Phototrophic Bacteria* (Hunter, C. N., Daldal, F., Thurnauer, M. C., and Beatty, J. T., Eds.), pp 407–423. Springer, Dordrecht.

(60) Heinnickel, M., and Golbeck, J. H. (2007) Heliobacterial photosynthesis. *Photosynth. Res. 92*, 35–53.

(61) Redding, K. E., Sarrou, I., Rappaport, F., Santabarbara, S., Lin, S., and Reifschneider, K. T. (2013) Modulation of the fluorescence yield in heliobacterial cells by induction of charge recombination in the photosynthetic reaction center. *Photosynth. Res.*

(62) Dibrova, D. V, Cherepanov, D. A., Galperin, M. Y., Skulachev, V. P., and Mulkidjanian, A. Y. (2013) Evolution of cytochrome bc complexes: from membrane-anchored dehydrogenases of ancient bacteria to triggers of apoptosis in vertebrates. *Biochim. Biophys. Acta 1827*, 1407–27.

(63) Baymann, F., and Nitschke, W. (2010) Heliobacterial Rieske/cytb complex. *Photosynth. Res. 104*, 177–87.

(64) Yue, H., Kang, Y., Zhang, H., Gao, X., and Blankenship, R. E. (2012) Expression and characterization of the diheme cytochrome c subunit of the cytochrome bc complex in Heliobacterium modesticaldum. *Arch. Biochem. Biophys. 517*, 131–137.

(65) Zhang, Y., Majumder, E. L.-W., Yue, H., Blankenship, R. E., and Gross, M. L. (2014) Structural analysis of diheme cytochrome C by hydrogen-deuterium exchange mass spectrometry and homology modeling. *Biochemistry 53*, 5619–30.

(66) Yanyushin, M. F., del Rosario, M. C., Bruno, D. C., and Blankenship, R. E. (2005) New class of bacterial membrane oxidoreductases. *Biochemistry 44*, 10037–10045.

(67) Gao, X., Xin, Y., and Blankenship, R. E. (2009) Enzymatic activity of the alternative complex III as a menaquinol:auracyanin oxidoreductase in the electron transfer chain of Chloroflexus aurantiacus. *FEBS Lett. 583*, 3275–9.

(68) Majumder, E. L. W., King, J. D., and Blankenship, R. E. (2013) Alternative Complex III from phototrophic bacteria and its electron acceptor auracyanin. *Biochim. Biophys. Acta - Bioenerg. 1827*, 1383–1391.

(69) Refojo, P. N., Ribeiro, M. A., Calisto, F., Teixeira, M., and Pereira, M. M. (2013) Structural composition of alternative complex III: Variations on the same theme. *Biochim. Biophys. Acta - Bioenerg. 1827*, 1378–1382.

(70) Gao, X., Xin, Y., Bell, P. D., Wen, J., and Blankenship, R. E. (2010) Structural Analysis of Alternative Complex III in the Photosynthetic Electron Transfer Chain of Chloroflexus aurantiacus. *Biochemistry 49*, 6670–6679.

(71) Gao, X., Majumder, E. W., Kang, Y., Yue, H., and Blankenship, R. E. (2013) Functional analysis and expression of the mono-heme containing cytochrome c subunit of alternative complex III in Chloroflexus aurantiacus. *Arch. Biochem. Biophys. 535*, 197–204.

(72) Clarke, T. A., Cole, J. A., Richardson, D. J., and Hemmings, A. M. (2007) The crystal structure of the pentahaem c-type cytochrome NrfB and characterization of its solution-state interaction with the pentahaem nitrite reductase NrfA. *Biochem. J.* 19–30.

(73) Clarke, T. A., Dennison, V., Seward, H. E., Burlat, B., Cole, J. A., Hemmings, A. M., and Richardson, D. J. (2004) Purification and spectropotentiometric characterization of Escherichia coli NrfB, a decaheme homodimer that transfers electrons to the decaheme periplasmic nitrite reductase complex. *J. Biol. Chem. 279*, 41333–9.

(74) Refojo, P. N., Teixeira, M., and Pereira, M. M. (2010) The alternative complex III of Rhodothermus marinus and its structural and functional association with caa(3) oxygen reductase. *Biochim. Biophys. Acta-Bioenergetics 1797*, 1477–1482.

(75) King, J. D., McIntosh, C. L., Halsey, C. M., Lada, B. M., Niedzwiedzki, D. M., Cooley, J. W., and Blankenship, R. E. (2013) Metalloproteins diversified: the auracyanins are a family of cupredoxins that stretch the spectral and redox limits of blue copper proteins. *Biochemistry 52*, 8267–75.

(76) Dutton, P. L., Petty, K. M., Bonner, H. S., and Morse, S. D. (1975) Cytochrome c2 and reaction center of Rhodospeudomonas spheroides Ga. membranes. Extinction coefficients, content, half-reduction potentials, kinetics and electric field alterations. *Biochim. Biophys. Acta - Bioenerg. 387*, 536–556.

(77) Myllykallio, H., Drepper, F., Mathis, P., and Daldal, F. (1998) Membrane-anchored cytochrome cy mediated microsecond time range electron transfer from the cytochrome bc1 complex to the reaction center in Rhodobacter capsulatus. *Biochemistry 37*, 5501–10.

(78) Bernroitner, M., Tangl, D., Lucini, C., Furtmüller, P. G., Peschek, G. A., and Obinger, C. (2009) Cyanobacterial cytochrome c(M): probing its role as electron donor for Cu(A) of cytochrome c oxidase. *Biochim. Biophys. Acta 1787*, 135–43.

(79) Sponholtz, D. L., Brautigan, D. L., Loach, P. A., and Margoliash, E. (1976) Preparation of cytochrome c2 from Rhodospirillum rubrum. *Anal. Biochem. 72*, 255–260.

(80) Lin, X., Williams, J. C., Allen, J. P., and Mathis, P. (1994) Relationship between rate and free energy difference for electron transfer from cytochrome c2 to the reaction center in Rhodobacter sphaeroides. *Biochemistry 33*, 13517–13523.

(81) Axelrod, H., Miyashita, O., and Okamura, M. (2009) Structure and Function of the Cytochrome c 2:Reaction Center Complex from Rhodobacter sphaeroides, in *The Purple Phototrophic Bacteria* (Hunter, C. N., Daldal, F., Thurnauer, M. C., and Beatty, J. T., Eds.), pp 323–336. Springer Netherlands, Dordrecht.

(82) Gong, X.-M., Paddock, M. L., and Okamura, M. Y. (2003) Interactions between cytochrome c2 and photosynthetic reaction center from Rhodobacter sphaeroides: changes in binding affinity and electron transfer rate due to mutation of interfacial hydrophobic residues are strongly correlated. *Biochemistry 42*, 14492–500.

(83) Daldal, F., Mandaci, S., Winterstein, C., Myllykallio, H., Duyck, K., and Zannoni, D. (2001) Mobile cytochrome c2 and membrane-anchored cytochrome cy are both efficient electron donors to the cbb3- and aa3-type cytochrome c oxidases during respiratory growth of Rhodobacter sphaeroides. *J. Bacteriol. 183*, 2013–24.

(84) Verméglio, A., Li, J., Schoepp-Cothenet, B., Pratt, N., and Knaff, D. B. (2002) The Role of High-Potential Iron Protein and Cytochrome c 8 as Alternative Electron Donors to the Reaction Center of Chromatium vinosum †. *Biochemistry 41*, 8868–8875.

(85) Tatsuhiko, Y. (1970) Solubilization, purification and properties of particulate hydrogenase from Desulfovibrio vulgaris. *J. Biochem.*

(86) Hochkoeppler, A., Ciurli, S., Kofod, P., Venturoli, G., and Zannoni, D. (1997) On the role of cytochrome c8 in photosynthetic electron transfer of the purple non-sulfur bacterium Rhodoferax fermentans. *Photosynth. Res. 53*, 13–21.

(87) Samyn, B., and Smet, L. (1996) A High-Potential Soluble Cytochrome C-551 from the Purple Phototrophic Bacterium Chromatium vinosum is Homologous to Cytochrome C8 from Denitrifying. *Eur. J.* ….

(88) Nagashima, S., Shimada, K., Verméglio, A., and Nagashima, K. V. P. (2011) The cytochrome c_8 involved in the nitrite reduction pathway acts also as electron donor to the photosynthetic reaction center in Rubrivivax gelatinosus. *Biochim. Biophys. Acta 1807*, 189–96.

(89) Hochkoeppler, A., Jenney, F. J., Lang, S., Zannoni, D., and Daldal, F. (1995) Membrane-associated cytochrome cy of Rhodobacter capsulatus is an electron carrier from the cytochrome bc1 complex to the cytochrome c oxidase during respiration. *J. Bacteriol. 177*, 608–613.

(90) Jenney, F. E., Prince, R. C., and Daldal, F. (1994) Roles of the Soluble Cytochrome c2 and Membrane-Associated Cytochrome cy of Rhodobacter capsulatus in Photosynthetic Electron Transfer. *Biochemistry 33*, 2496–2502.

(91) Ambler, R. P., Bartsch, R. G., Daniel, M., Kamen, M. D., McLellan, L., Meyer, T. E., and Van Beeumen, J. (1981) Amino acid sequences of bacterial cytochromes c' and c-556. *Proc. Natl. Acad. Sci. U. S. A. 78*, 6854–7.

(92) Weber, P. C., Bartsch, R. G., Cusanovich, M. A., Hamlin, R. C., Howard, A., Jordan, S. R., Kamen, M. D., Meyer, T. E., Weatherford, D. W., Nguyen huu Xuong, and Salemme, F. R. (1980) Structure of cytochrome c': a dimeric, high-spin haem protein. *Nature 286*, 302–4.

(93) Choi, P. S., Grigoryants, V. M., Abruña, H. D., Scholes, C. P., and Shapleigh, J. P. (2005) Regulation and function of cytochrome c' in Rhodobacter sphaeroides 2.4.3. *J. Bacteriol. 187*, 4077–85.

(94) Russell, H. J., Hardman, S. J. O., Heyes, D. J., Hough, M. A., Greetham, G. M., Towrie, M., Hay, S., and Scrutton, N. S. (2013) Modulation of ligand-heme reactivity by binding pocket residues demonstrated in cytochrome c' over the femtosecond-second temporal range. *FEBS J. 280*, 6070–82.

(95) Sakurai, H., Kusumoto, N., and Inoue, K. (1996) Function of the Reaction Center of Green Sulfur Bacteria. *Photochem. Photobiol. 64*, 5–13.

Chapter 2: Functional analysis and expression of the mono-heme containing cytochrome c subunit of the Alternative Complex III in *Chloroflexus aurantiacus*

Portions of this chapter have been previously published as: Gao, X., Majumder, E. W., Kang, Y., Yue, H. & Blankenship, R. E. Functional analysis and expression of the mono-heme containing cytochrome c subunit of alternative complex III in *Chloroflexus aurantiacus*. Archives of Biochemistry and Biophysics 535, 197–204 (2013). Used with permission of authors.

2.1 Introduction

Chloroflexus aurantiacus (*C. aurantiacus*) is a thermophilic green bacterium belonging to the filamentous anoxygenic phototrophs (FAPs), one of the six phyla of bacteria that possess chlorophyll-based photosynthesis[1,2]. FAPs, formerly named green non-sulfur bacteria or green gliding bacteria[3], occupy a much earlier branching position in the species tree of bacteria compared to the other five phyla of phototrophs based on 16S rRNA analysis[4]. As the first described representative of FAPs, *C. aurantiacus* has been the most extensively studied FAP. *C. aurantiacus* has unique antenna complexes, reaction center composition, secondary electron transport pathway and carbon fixation pathways, making it an important system to investigate the wide range of photosynthetic reactions in evolutionarily diverse organisms.

The unique characteristic of the photosynthetic electron transfer pathway in *C. aurantiacus* is its surprising lack of a cytochrome bc_1 complex or related cytochrome b_6f complex, which were previously believed to be a constant fixture in all photosynthetic systems[5-9]. It also lacks a soluble cytochrome similar to cytochrome c_2, which functions as a soluble electron transfer component in many phototrophs[10-11]. A soluble, yet membrane-associated copper protein known as auracyanin has been proposed to serve the function of cytochrome c_2 in *C. aurantiacus*[12-16]. In addition, a reaction-center-associated tetraheme cytochrome *c*-554 reoxidizes auracyanin and transports electrons to the reaction center complex[17]. A quinol:auracyanin oxidoreductase, which fulfills the functional role of the missing cytochrome bc_1 complex, is predicted to be present to complete the cyclic electron transfer chain in *C. aurantiacus*.

A multisubunit cytochrome complex has been isolated and identified as the quinol:auracyanin oxidoreductase. Along with cytochrome *c*-554, it contains essentially all the

heme-containing proteins in the membrane of *C. aurantiacus*[10]. Furthermore, gene distribution analysis revealed that the pattern of genes coding for this particular protein complex in several different bacteria from diverse taxa usually coincides with the absence of the genes coding for the cytochrome bc_1 complex[11]. Based on this biochemical and genomic evidence, this novel protein complex was proposed to be the functional replacement of the cytochrome bc_1 complex to link quinol oxidation and auracyanin reduction. This protein complex, now named Alternative Complex III (ACIII)[18-22], was shown to function as a quinol:auracyanin oxidoreductase by enzyme kinetic analysis[23]. A preliminary structural model of the ACIII complex has also been built based on a series of biochemical experiments[24]. The putative operon coding for the ACIII complex expressed during photosynthetic growth in *C. aurantiacus* is composed of seven genes, and the corresponding protein subunits have been initially represented as s1 to s7 from the largest to the smallest mass on SDS-PAGE. A new nomenclature for each subunit based on the gene sequence of ACIII has been proposed[25] The genes are now named *actA* through *actG*, based on their order in the operon. Protein subunits are named ActB, C, F, A, E, D and G (replacing the former names of s1 to s7). ACIII contains a single copy of each of the subunits except for ActE, the monoheme containing subunit, which is present in two copies[20]. While much of ACIII is embedded in the membrane, the domains containing prosthetic groups are attached to the membrane and are predicted to be located primarily in the periplasm.

Although genomic analysis as well as functional and structural studies of the ACIII complex suggest that ACIII might substitute for the role of cytochrome bc_1 complex in *C. aurantiacus*, on the basis of genome arrangement and our previous structural investigation, the organization of ACIII was revealed to be entirely different from that of the cytochrome bc_1 or b_6f complex.

In this chapter, we begin to unravel the contribution of individual subunits to the electron transfer process in ACIII. We report the expression and analysis of the monoheme containing subunit ActE in *E. coli*. The midpoint potential of this recombinant cytochrome was determined by potentiometric titration. We also present a biochemical method for removing two of the subunits while leaving the rest of the complex associated and then reconstituting the denatured complex with the recombinant ActE. The activity of the partial and reconstituted complexes were tested and compared with intact ACIII. The results indicate that ActE is essential for menaquinone:auracyanin oxidoreductase activity and may be the final point of electron transfer in ACIII that donates electrons to auracyanin.

2.2 Materials and Methods

2.2.1 Expression and isolation of the monoheme containing subunit ActE from *E. coli*

Bacterial strains and growth conditions

E. coli strain DH5α [26] was used for subcloning, the host for the recombinant plasmid, and the BL21 (DE3) strain [27] was used for expression of recombinant subunit ActE. Both *E. coli* strains were grown aerobically with shaking at 260 rpm in Luria-Bertani broth (LB, Difco) or on LB agar plates with appropriate antibiotics at 37 °C. Concentration of antibiotics (Sigma-Aldrich) were carbenicillin 50 μg ml^{-1}, kanamycin 25 μg ml^{-1} and gentamicin 25 μg ml^{-1}.

Generation of an expression construct for the actE gene

The gene encoding subunit ActE was amplified by polymerase chain reaction (PCR) from *C. aurantiacus* genomic DNA using a Veriti 96 well Thermal Cycler (Applied Biosystems) and

the purified product was cloned into pTEV5 plasmid[28] with modification to yield a construct (pTEV5-ActE) in which the entire coding region of the gene was fused to an *E. coli* PelB signal sequence[29] at the N-terminus and a 6xHis tag at the C-terminus. The cloning procedures, *in vitro* homologous recombination, were carried out generally as described in Li et al.[30]. DNA sequencing was conducted at the Washington University School of Medicine Protein and Nucleic Acid Chemistry Laboratory.

Expression of the recombinant monoheme cytochrome ActE

BL21 (DE3)-Ccm competent cells were cotransformed with pTEV5-ActE containing the subunit ActE gene and pSysI, kindly provided by Prof. Robert Kranz. Plasmid pSysI encodes the complete ccmA-H gene cluster from *E. coli*, which is required for the incorporation of the heme cofactor in the expressed *c*-type cytochrome[30]. Cells harboring both plasmids were selected for their ability to grow on LB agar plate containing carbenicillin 50 μg ml^{-1}, kanamycin 25 μg ml^{-1} and gentamicin 25 μg ml^{-1}. Rich media cultures were performed with LB culture medium supplemented with the same antibiotics. The *E. coli* cultures were incubated with shaking at 37 ^{o} C to an OD_{600} of around 1.0, then induced with 1 mM isopropyl-β-D-thiogalactopyranoside (IPTG) for 4-6 hrs. Cells were harvested at 12000 g for 15min.

Preparation of membrane and soluble fractions

E. coli cells were thawed and resuspended in buffer A (20 mM Tris-HCl pH 8.0) to a concentration of 1 g of wet cells per 5 ml of buffer, treated with 0.1 mg/ml egg white lysozyme (Sigma-Aldrich), 1 mM EDTA-free protease inhibitor cocktail for 30 min on ice. The cells were then broken by sonication at 50% duty, 80% output on a Branson 450 sonicator at 4 °C.

Unbroken cells and the cell debris were separated from the extract by centrifugation at 12000xg for 20 min at 4 °C. The supernatant was then ultracentrifuged at 200000xg for 2 h. Both the supernatant and pellet were collected and stored for further purification.

Recombinant protein purification

The recombinant subunit ActE fractions detected in the resulting pellet, containing the cytoplasmic membrane, and in the supernatant, containing all the soluble proteins in both cytoplasm and periplasm, were both further purified by similar steps except for using detergent-containing buffers for membrane protein purification and detergent-free buffers for the soluble fractions. The membrane pellet was resolubilized with 1% dodecyl maltoside (DDM) in buffer A at 4 °C by shaking continuously. The membrane part was then loaded onto a 1ml gravity-fed cobalt column (Talon resin, Clontech) that had been equilibrated with 0.1% DDM, 200 mM NaCl in buffer A at 4 °C, washed twice with 10 column volumes of equilibration buffer, and eluted with a step gradient of 0-50 mM imidazole in equilibration buffer. The fractions containing the reddish-brown protein were combined, diluted with three times the volume with 0.1% DDM in buffer A and then loaded onto a 5ml QSHP ion exchange column. Crude recombinant subunit ActE protein was obtained with a linear gradient of NaCl from 100-500 mM in 10 column volumes. A final purification step was performed on a Superose 12 (16/60) gel filtration column in buffer A with 0.1% DDM and 100 mM NaCl using concentrated crude subunit ActE fractions. The protein in the soluble fractions was also purified by similar steps except for the change of buffer to a non-detergent buffer.

Electrophoresis and heme quantification

Coomassie-stained tricine SDS-PAGE (12.5% T/3% C) was performed on both purified soluble subunit ActE and membrane-bound subunit ActE. Western blotting and heme staining were carried out using the SuperSignal Femto chemiluminescent substrate (Pierce)[32]. The specific reactivity against 6xHis tag by western blotting was probed using anti-polyHistidine antibody (Sigma-Aldrich) at the dilution of 1:5000. The concentration of ACIII complex was determined by the bicinchoninic acid protein assay (BCA assay) (Pierce). The amount of heme was quantified by pyridine hemochrome analysis using the extinction coefficients of 23.97 $mM^{-1}cm^{-1}$ for *c*-type heme[33]. *UV-Vis* spectra of reduced and oxidized subunit ActE were recorded using a Perkin Elmer Lambda 950 UV-Vis spectrophotometer.

In-gel protein digestion and MALDI-TOF analysis

Coomassie-stained bands of both of the subunit ActE (soluble and membrane-bound) on SDS-PAGE gel were excised, in-gel digested with trypsin, and extracted from the gel as described previously[24]. MALDI-TOF analyses were used to determine protein identities by peptide mass fingerprinting. Analysis was performed using an ABI 4700 MALDI-TOF mass spectrometer (Applied Biosystems, USA). Peptide mass value searches were performed against the National Center for Biotechnology Information (NCBI) sequence (NCBInr) database using MASCOT Peptide Mass Fingerprint database search software (www.matrixscience.com).

2.2.2 Potentiometric titration

Anaerobic potentiometric titrations were performed to determine the midpoint potentials (E_m) of redox-active cytochrome in recombinant subunit ActE. The potential was controlled using a CH 620 C potentiostat (CH Instruments) and spectral changes of subunit ActE upon

reduction and oxidation were monitored at 552.0 nm by a Perkin Elmer Lambda 950 UV-Vis spectrophotometer[34]. The titration was carried out at room temperature in the presence of a mixture of the following redox mediators: Fe(III) EDTA ($E_{m,7}$ = +117 mV)[35], 1,2-napthoquinone-4-sulfonic acid ($E_{m,7}$ = +215 mV)[36], 2,3,5,6-tetramethyl-p-phenylenediamine (diaminodurene, DAD) ($E_{m,7}$ = +260 mV)[36], N, N-dimethyl-1,4-phenylenediamine dihydrochloride (DMPD) ($E_{m,7}$ = +371 mV)[37], potassium ferricyanide ($E_{m,7}$ = +435 mV)[38]. A stock solution of subunit ActE was diluted into 20 mM Tris buffer (pH 8.0) to a final concentration of 5 mg/ml, and each mediator was added to a final concentration of 50 µM.

2.2.3 ACIII isolation and purification from *C. aurantiacus*

C. aurantiacus strain J-10-fl was grown anaerobically under high-light conditions in modified medium D, under literature reported conditions with modifications[39]. The ACIII complex was purified according to procedures reported previously[10,11,24,40].

2.2.4 Subunit separation using the chaotropic agent KSCN

The purified ACIII complex was incubated with 1.5M potassium thiocyanate (KSCN) in buffer B (0.25% Triton X-100, 100 mM NaCl, 20mM Tris-HCl, pH 8.0) for 2 hrs at room temperature with gentle shaking. Afterwards, the sample was diluted 10-fold with the same buffer and concentrated through a centrifugal filter unit with a molecular weight cutoff of 100 kDa (Millipore). After twice repeating the dilution and concentration step, the residue was collected and loaded onto a Superdex-200 gel filtration column (16 mm x 60 cm) pre-equilibrated using buffer B. The eluted fractions were then analyzed by tricine SDS-PAGE

(12.5% T/3% C) [41] and BN-PAGE[42] using the method of Schägger and von Jagow. The filtrate was concentrated and analyzed by tricine SDS-PAGE and subsequent silver staining[43]. The KSCN-treated ACIII is designated ACIII'.

2.2.5 Reconstitution of ACIII' and ActE

Purified recombinant soluble ActE was loaded onto a 1mL gravity fed cobalt column. The column was washed with 200mM NaCl buffer A to remove any non-bound protein. ACIII' was then loaded onto the column with a concentration half of ActE to preserve the 2 ActE to 1 ACIII ratio. Protein concentration was determined by the BCA method. ACIII' was allowed to sit on the column for several minutes and then the column was washed with buffer A to remove any non-specific binding. The column was then washed with 3 column volumes of 10mM imidazole in buffer A. The imidazole was increased to 20mM and the washing continued. The reconstituted complex was eluted from the column during this step and fractions were collected. The visibly pink fraction was loaded onto a 2mL Superose-12 Gel Filtration column. Again, one pink species eluted from the column and was collected. A UV/vis spectrum was taken of this fraction to verify identity.

2.2.6 Enzyme activity of ACIII' and reconstituted ActE-ACIII'

The enzyme activity of ACIII' and freshly reconstituted ACIII'-ActE was monitored using excess reduced vitamin K2 as electron donor and oxidized horse heart cytochrome *c* as the electron acceptor according to the procedure reported previously[23,44]. The enzyme activity of ACIII' as menaquinol:cytochrome *c* oxidoreductase was measured at 25 °C by UV-Vis spectroscopy. The activity of the intact ACIII complex was also measured as a positive control.

The reaction was followed by the increase in absorption at 550 nm, due to the simultaneous menaquinol-4 (reduced vitamin K2) oxidation with horse heart cytochrome *c* reduction. The ACIII activity assays were performed in an anaerobic 1-ml cuvette at final concentrations of approximately 100 µM menaquinol-4, 100 µM cytochrome *c*, and *ca*. 5.0 nM ACIII. All the assays were carried out in 50 mM phosphate buffer (pH 7.3) in the presence of 0.2 mM EDTA, 1 mM NaN_3, 250 mM sucrose, 0.1% BSA and 0.02% n-dodecyl-β-D-maltoside. The reaction was started by the addition of menaquinol-4 to the mixture of the cytochrome *c* and the ACIII' (or ACIII) in buffer and then followed for 5 min at 550 nm. Additionally, the measurement of ACIII and ACIII' activity using auracyanin A as substrate utilized a similar protocol except that the reaction was followed by monitoring a decrease in absorption at 594 nm due to auracyanin A reduction. Auracyanin A was purified from *C. aurantiacus* and the final concentration was approximately 50 µM for the enzymatic assay.

2.3 Results

2.3.1 Expression and isolation of recombinant subunit ActE in E. coli

In order to obtain a finer analysis of the functional role that subunit ActE plays in the electron transfer pathway of the ACIII complex, heterologous expression of *C. aurantiacus* monoheme cytochrome *c* subunit (ActE) in *E. coli* was carried out. The ActE subunit is one of the two heme-containing subunits in the ACIII complex, which bind to the surface of the transmembrane subunit ActF at the periplasmic side of the membrane[24]. Like other typical *c*-type

cytochromes, it possesses a single *c*-type heme binding site (CXXCH) for the covalent attachment of heme and an N-terminal signal sequence (~27 amino acids), which is usually cleaved after translocation to the periplasm (with exceptions in a few bacterial species)[45]. The wild-type ACIII ActE subunit in *C. aurantiacus* has its own signal sequence cleaved off in the biogenesis process according to our previous ESI mass spectrometry analysis[24]. However, the attempt to directly express subunit ActE in *E. coli* without any assistance of a well-established helper signal sequence derived from *E. coli* proved to be unsuccessful. The ActE polypeptide was overexpressed in *E. coli*, which formed a large amount of inclusion bodies in the cytoplasm, and no heme attachment was observed by heme staining.

To solve this problem, we designed a plasmid pTEV5-ActE with an *E. coli* PelB signal sequence fused at the N-terminus of the *actE* gene and a 6xHis tag at the C-terminus, which was constructed in order to obtain the expression of a soluble subunit ActE, as described in Materials and Methods. Two parallel designs were attempted, using the whole gene sequence of ActE as well as using only the sequence coding the soluble portion of ActE. However, only *E. coli* harboring the former design of plasmid was able to survive under our experimental conditions. The pTEV5-ActE plasmid and a helper plasmid pSysI, encoding the complete CcmA-H protein complex, which is involved in the maturation of cytochrome *c*, were cotransformed to BL21 (DE3) cells for the expression of ActE.

An interesting phenomenon was observed during the purification of subunit ActE from *E. coli* cells. After separation of the membranes and the soluble fractions of host cells, a strong reactivity against 6xhis antibody and a peroxidase activity of heme around 20 to 25 kDa from the western blotting of SDS-PAGE were detected in both fractions. This indicated that both the membrane fraction and the periplasm fraction contained the folded subunit ActE with heme

attached. For that reason, similar parallel purification steps were applied on both fractions. Fig. 1 shows the electrophoresis results for purified subunit ActE in both membrane fractions and periplasm fractions. From the Coomassie blue-stained SDS-PAGE (Fig. 2.1C), the membrane-bound subunit ActE was around 23 kDa, larger than ActE purified from the periplasm fractions (20 kDa). The difference is consistent with the size of the signal peptide of ActE. The comparative yield of membrane-bound versus soluble versions of recombinant ActE is approximately 2:1 by using the BCA method. The membrane form of ActE is most likely due to the fact that the heme attachment machinery is located in the membrane. Recombinant membrane form ActE simply has not yet been transported out the periplasm where removal of the signal peptide takes place.

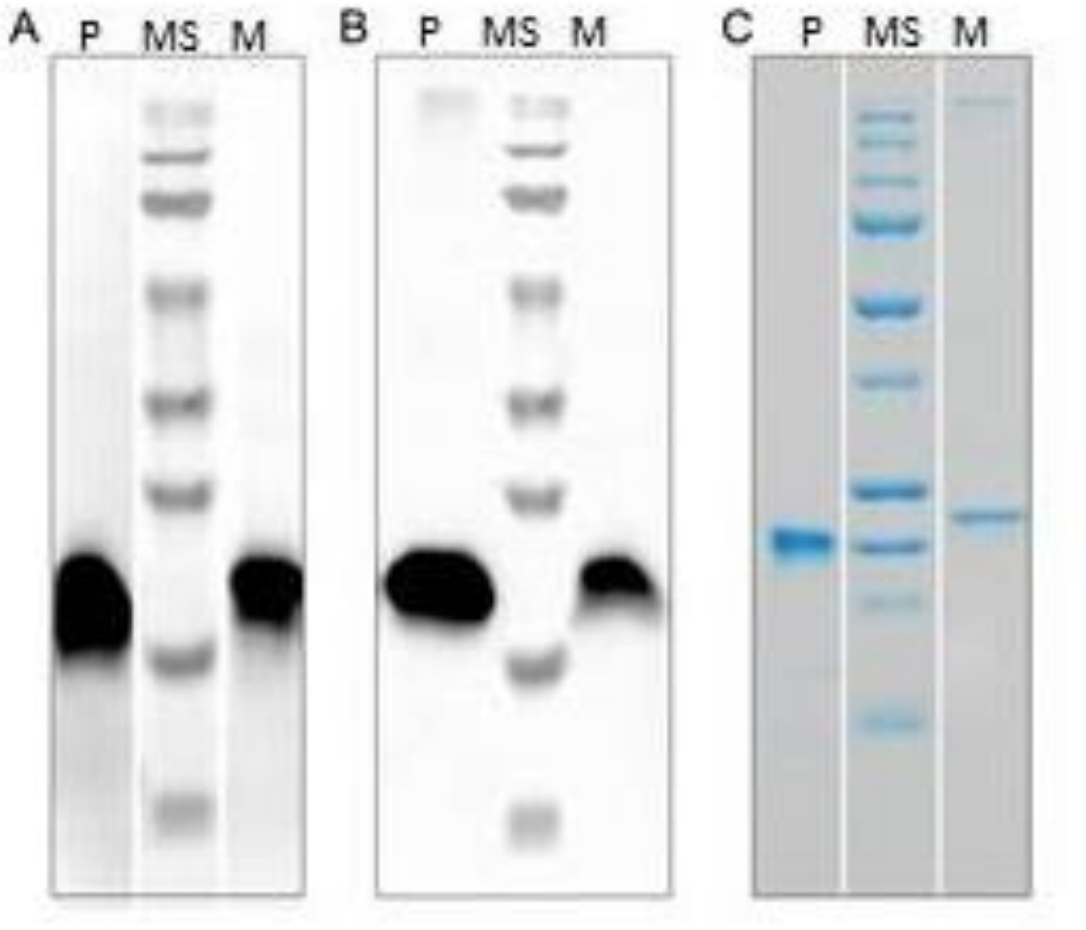

Figure 2.1 Overexpression of the mono-heme cytochrome subunit (ActE) of ACIII in *E. coli*. (A) Western blot of SDS-PAGE gel probed with anti-His-tag antibody. The left lane is the periplasmic fraction of subunit ActE without the signal peptide attached. The right lane is the membrane fraction of ActE with a signal peptide. The middle lane contains molecular mass standards (Bio-Rad), and the molecular masses of the standard proteins are 7, 20, 29, 37 and 53 kDa from the bottom. (B) Heme-stained SDS-PAGE with the periplasmic fraction of ActE on the left and the membrane fraction of ActE on the right. The middle lane contains the same molecular mass standards (Bio-Rad) as those in (A). (C) Coomassie stained SDS-PAGE of purified ActE with the soluble version on the left and the membrane version on the right. The right lane contains molecular mass standards (Bio-Rad), and the molecular masses of the standard proteins are 10, 15, 20, 25, 37, 50, 75, 100, 150, and 200 kDa from bottom to top.

Both bands observed *via* SDS-PAGE (Fig. 2.1C) were excised, digested with trypsin, and analyzed by peptide fingerprinting MALDI-TOF mass spectrometry. They were conclusively identified to be the monoheme-containing subunit ActE in *C. aurantiacus*. The search results are summarized in Table 2.1. Both the MASCOT score and the percent sequence coverage indicate

reliable correspondence with respect to the subunit ActE sequence of ACIII. It is also observed that a signal peptide fragment was present in the membrane-bound subunit ActE while there was no signal peptide fragment in the soluble subunit ActE (Fig. 2). This provides another piece of evidence that the difference between the two recombinant subunit ActE proteins is the presence or absence of the signal peptide. As stated above, native ActE has the signal sequence cleaved. While both membrane and soluble recombinant ActE are observed from the assembly process of this protein, the soluble purification of recombinant ActE is most like native ActE.

Table 2.1 Result of peptide mass fingerprinting for soluble recombinant ActE and membrane-bound recombinant ActE.

ActE	No. of fragments identified [b]	MASCOT score [b]	Percent sequence coverage [b]
soluble	9	68	48
membrane	8	61	49

[b] Provided by MASCOT Peptide Mass Fingerprint database search software (www.matrixscience.com)

Membrane:

M**QKPRLTSRM**IRFGWVGLLVLLLTACHQDMYDQQKYTTYEPSSFFADGRSSR
PNVPGTTPFEVVKTDEFLYTGLIDGQEVDAMPFPVTKDLLLRGQLKYNIYCA
VCHGEAGYGASMVAERGGIVPANFHQQRLREAPLSHFFVVITNGVYRGDPEN
GGYQSMYGYASRITPEDRWAIAAYIRALQLSQNATIDDVPPDQRAQLGN

Soluble:

MQKPRLTSRMIRFGWVGLLVLLLTACHQDMYDQQKYTTYEPSSFFADGRSSR
PNVPGTTPFEVVKTDEFLYTGLIDGQEVDAMPFPVTKDLLLRGQLKYNIYCA
VCHGEAGYGASMVAERGGIVPANFHQQRLREAPLSHFFVVITNGVYRGDPEN
GGYQSMYGYASRITPEDRWAIAAYIRALQLSQNATIDDVPPDQRAQLGN

Figure 2.2 Result of peptide mass fingerprinting for soluble recombinant ActE and membrane-bound recombinant ActE with matched peptides shown in red. One of the matched peptides (bold red) for membrane-bound recombinant subunit ActE indicates the existence of its signal sequence.

2.3.2 UV-Vis spectral analysis and Redox potentiometry

UV-Vis absorption spectroscopy at room temperature using both reduced and oxidized forms of soluble recombinant subunit ActE was conducted, and the results are shown in Fig. 2.3A. Both the membrane-bound ActE (data not shown) and soluble ActE gave identical absorbance over the measured range. The oxidized form exhibited a *c*-type cytochrome γ (Soret) band at 407 nm. Addition of dithionite resulted in reduction of the heme and gave rise to two absorption maxima at 523 nm (β band) and 552 nm (α band) and a red shift of the γ band to 416 nm. Compared with the absorption spectra of the intact ACIII complex[24], all three characteristic peaks (γ, β and α band) are blue shifted 2 to 3 nm in both oxidized and reduced conditions.

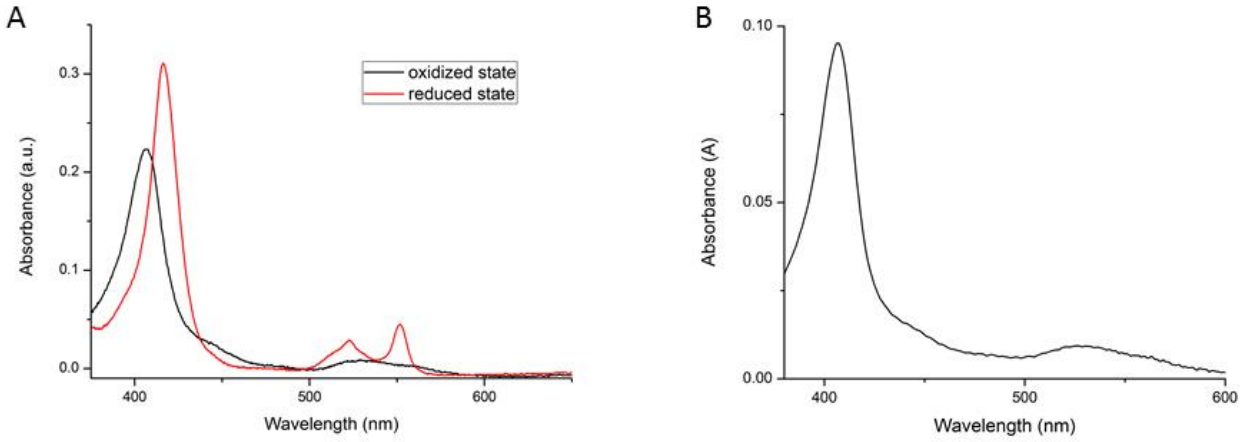

Figure 2.3 UV-vis absorption spectra at room temperature (A) of the monoheme subunit ActE overexpressed *E. coli.* The black line represents the air-oxidized form and the red line represents the dithioniteoreduced form. (B) Air-oxidized reconstitutued ACIII'-ActE.

Redox potentiometry gave a midpoint potential (E_m) of +385 mV versus NHE for both membrane-bound ActE (Fig. 2.4) and soluble recombinant ActE (data not shown). The standard error of the midpoint potential is ±1 mV obtained by fitting analysis (ORIGIN), but we estimate

the accuracy of the titration to be ±10 mV considering possible systematic errors. The redox titration plot showed a reversible Nernstian behavior corresponding to a one-electron oxidation/reduction reaction. This number corresponds well with the high potential heme of subunit ActE that was observed in the redox titration of the complete complex[24]. The potential of the recombinant subunit ActE (+385 mV) and the highest potential in the intact ACIII complex (+391 mV) strongly suggests that the highest potential hemes observed in the intact complex are due to ActE.

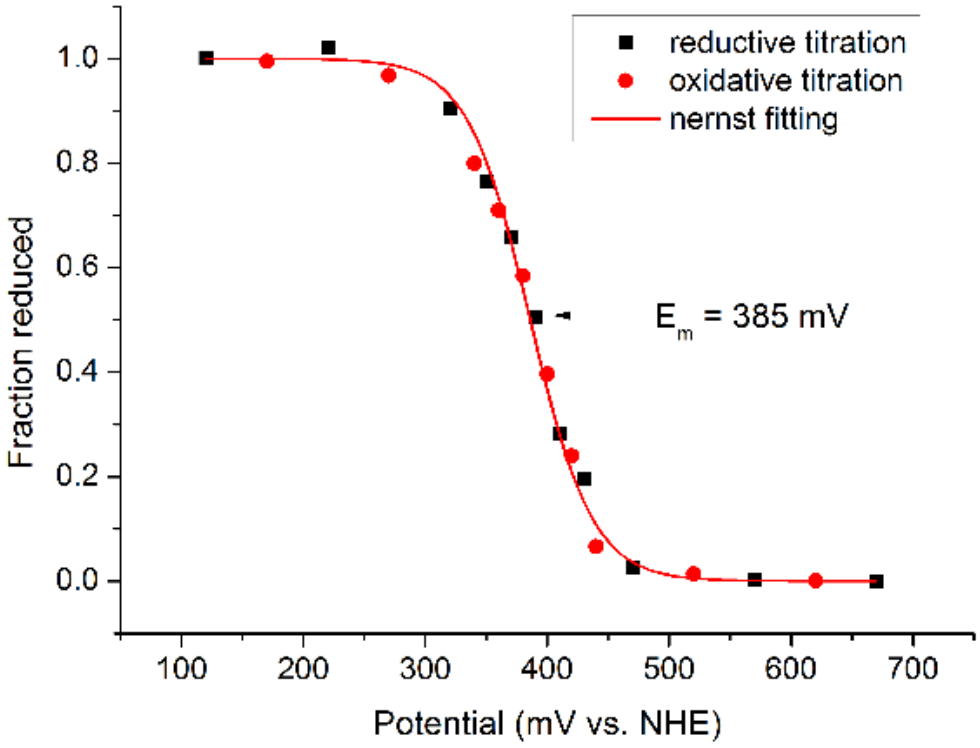

Figure 2.4 Potentiometric titration of recombinant subunit ActE (soluble) with grey circles representing the oxidative titration, black squares representing the reductive titration and solid line representing the Nernst fitting.

2.3.3 Subunit separation and Reconstitution

Detergents and chaotropic agents have been used for decades to resolve protein complexes[46-49]. By altering the concentrations of these additives, the weak interactions between adjacent subunits can be compromised, leading to separation of a subunit from the complex while keeping the rest of the complex in a near-native state. Various compounds were tested for their capability to isolate and solubilize individual subunits of purified ACIII complex (Table 2.2). The most effective was found to be the chaotropic agent potassium thiocyanate (KSCN). Treatment of ACIII with KSCN permitted the selective release of subunits ActE and ActG from the rest of the complex, as shown in Fig. 2.5.

Table 2.2 Dissociation of ACIII complex using different detergent and chaotropic agents.

Chemicals	Concentration	Separation of subunits[a]	Denaturation of protein[b]
Triton X-100	1%/3%/5%	-/-/-	-/-/-
DDM	1%/3%/5%	-/-/-	-/-/-
Deriphat-160	1%/3%/5%	-/+/+	-/-/-
NaI	1M/2M/3M	-/-/-	-/-/-
KI	1M/2M/3M	-/-/-	-/-/-
Urea	1M/2M/4M	-/-/-	-/-/-
KSCN	1M/1.5M/2M	-/+/+	-/-/-
Guanidinium chloride	1M	/	+
Lithium perchlorate	1M	/	+

[a] Separated and solubilized individual subunits but kept the rest of the protein complex undenatured. Reagents marked with "+" are competent in the separation of subunits as evaluated by blue native PAGE.

[b] Lead to protein aggregation or precipitation. Reagents marked with "+" are classified as destructive and causing protein precipitation.

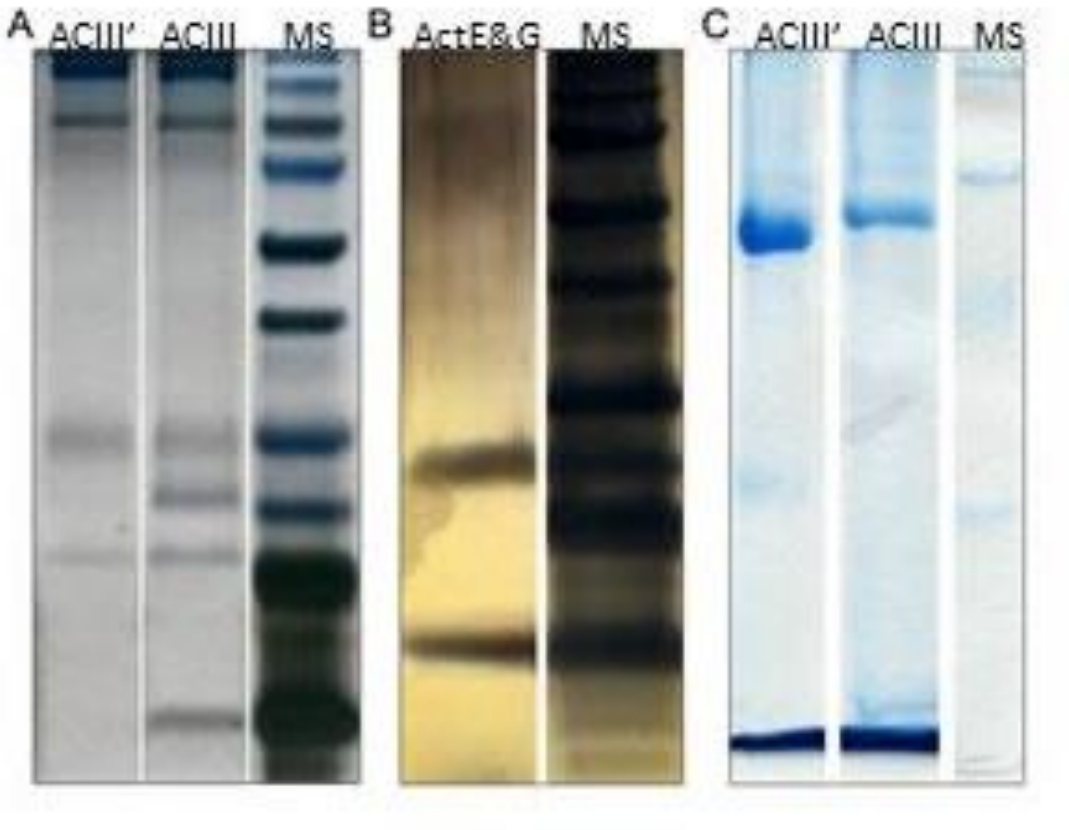

Figure 2.5 Electrophoresis analysis of subunit separation of ACIII by chaotropic agent KSCN. (A) Tricine SDS-PAGE of ACIII residue using a 12.5% T and 3% C gel system. The sample was incubated with 1.5M KSCN for 2 hours and then concentrated with a 100 kDa MWCO filter tube (left lane). The middle lane represents the isolated ACIII from *C. aurantiacus* as a control. The right lane contains molecular mass standards (Bio-Rad), and the molecular masses of the standard proteins are 10, 15, 20, 25, 37, 50, 75, 100, 150, and 200 kDa from bottom to top. (B) The left lane shows the smaller subunits of ACIII separated by KSCN which are found in the filtrate. The right lane contained the same molecular mass standards (Bio-Rad) as those in (A). (C) The blue native PAGE of KSCN treated ACIII (left) and pure ACIII control (middle). Molecular mass standards (GE) in the right lane are 140, 232, 440 and 669 kDa from bottom to top.

The separation of the subunits was achieved using filtration and size exclusion gel chromatography. Briefly, the ACIII-KSCN incubation mixture containing partially dissociated complex, small individual subunits and unaffected whole complex was filtered through a 100 kDa MWCO centrifugal filter unit. The residue in the filter that included all the complexes larger than 100 kDa was further isolated by a size exclusion gel filtration column, as described in Materials and Methods. Fig. 2.5A shows that subunits ActE and ActG are largely missing in the

KSCN-dissociated complexes (left lane), compared with the untreated whole ACIII complex (middle lane). The BN PAGE (Fig. 2.5C) of the two species (dissociated complex on the left and whole complex in the middle) gave a molecular weight difference of around 50-60 kDa, which is consistent with the loss of the two copies of subunit ActE (*ca.* 20 kDa each) and one copy of subunit ActG (*ca.* 10 kDa). Further confirmation came from the examination of the filtrate of the incubation mixture. The missing subunits ActE and ActG were recovered in the filtrate and identified by the SDS-PAGE followed by silver staining (Fig. 2.5B).

Reconstitution of the recombinant ActE with selectively denatured ACIII' was achieved using affinity and size exclusion gel chromatography. The His-tagged recombinant soluble ActE was allowed to bind a cobalt column. Soluble recombinant ActE was chosen because it is most like native ActE having the signal sequence cleaved. ACIII' was passed over the column and allowed to incubate. Pink fractions eluted by 20mM imidazole, the same concentration used to elute pure ActE, and were further purified with size exclusion chromatography, which yielded one pink fraction. The UV/vis absorption spectrum of the pink fraction matched the spectrum of ACIII, suggesting that reconstitution of the two proteins had been achieved (Fig 2.3B).

2.3.4. Enzymatic Activity Analysis

In order to determine the functional effect on ACIII after loss of subunits ActE and ActG, an enzymatic activity study was conducted on the partially dissociated ACIII (named ACIII') as well as the intact ACIII complex (see Materials and Methods section). The capability of ACIII' to perform as a menaquinol:cytochrome *c*/auracyanin oxidoreductase was monitored by the reduction reaction of cytochrome *c* or auracyanin using menaquinol as the reducing agent and ACIII' as the catalyst. The rate of the reduction reactions of both cytochrome *c* (Fig. 2.6) and

auracyanin (data not shown) showed a significant increase when intact ACIII was added, indicating enzymatic activity, at a similar rate as previously described[23]. However, the reaction rate after adding ACIII' showed a significantly smaller change compared to the non-catalytic reduction, indicating nearly complete loss of enzymatic activity (Fig. 2.6). The negligible absorption increase of cytochrome *c* at 550 nm and the absorption decrease of auracyanin at 594 nm are only from the non-catalytic reduction. This finding suggests that subunits ActE and/or ActG are indispensable to complete the electron transfer of ACIII.

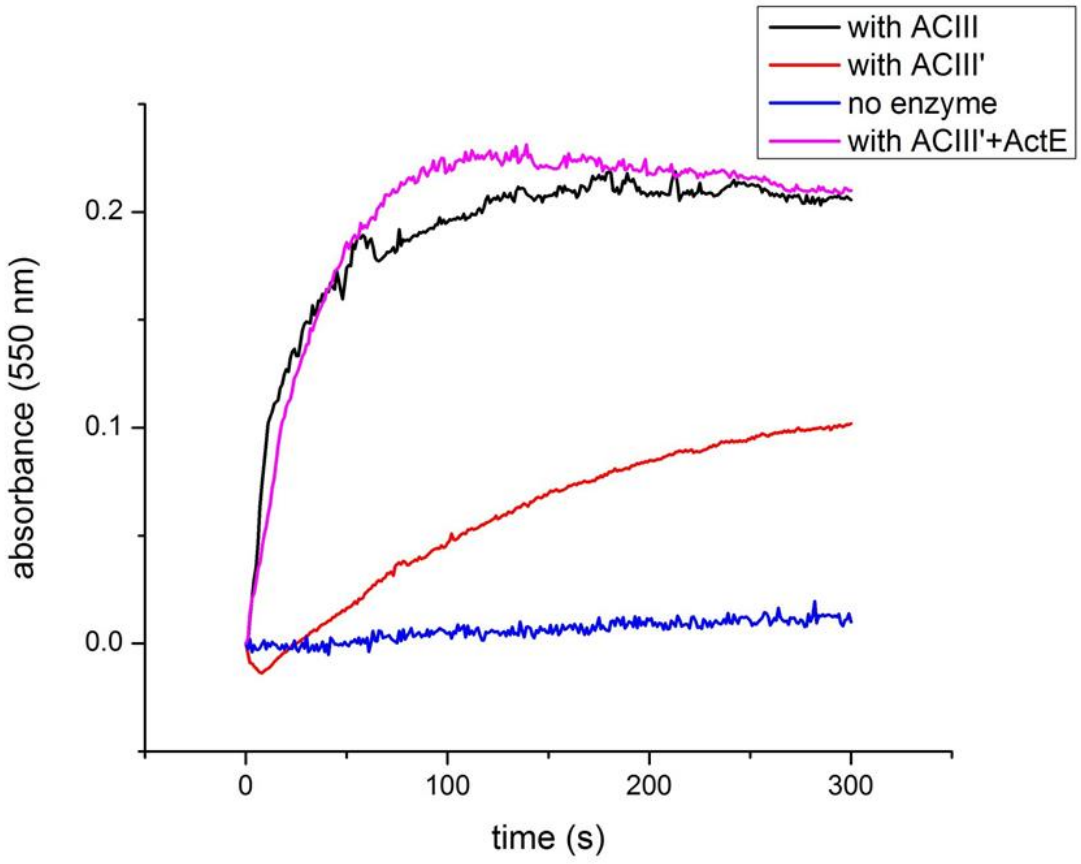

Figure 2.6 Quinol:cytochrome *c* oxidoreductase activity of the ACIII residue (ACIII') after incubation with KSCN and reconstituted ACIII'-ActE. The black line represents the absorption change at 550 nm when adding intact ACIII as an enzyme, the pink line represents the absorption change with reconstituted ACIII'-ActE, the red line represents the absorption change when adding the ACIII' as an enzyme and the blue line represents the absorption change without an enzyme.

To further analyze the role of ActE in ACIII electron transfer and donation to the soluble electron acceptor, ACIII' was reconstituted with recombinant ActE. Some free ActE may remain in the solution, but the amount would be very small. Reconsituted complex is run over a small gel filtration column before kinetic analysis. The weight difference between ActE and ACIII'-ActE is large enough for good separation. Immediately after preparation, the enzyme activity of the reconstituted complex was performed. The activity of the reconstituted ACIII'-ActE regained the full enzyme activity of native ACIII (Fig. 2.6). The initial rates for the four systems have been calculated and are presented in Table 2.3. These rates confirm that the reconstituted complex regained nearly the same activity as the native complex. The initial rate for ACIII' is a more than an order of magnitude lower than ACIII. The residual activity is likely due to some native ACIII remaining in solution, as the weights are so close, a small gel filtration column will not achieve optimum separation. This result demonstrates that ActE is critical for ACIII menaquinol:electron acceptor oxidoreductase activity and the ActG likely does not have a significant functional role. The high redox potential of ActE further suggests that ActE is the donor subunit to the electron acceptor. Like other cytochrome proteins, ActE appears to have an especially important role in the electron transfer and function of ACIII.

Table 2.3 Initial Enzyme Activity Rates

Activity Run	Initial Rate (ΔAU/s)*	Initial Rate (μg/s)[#]
No enzyme	.00001	.0005
ACIII'	.0008	.04
ACIII	.0074	.37
ACIII'+ActE	.0056	.28

*Calculated as slope of linear portion of kinetics plot
#Based on the extinction coefficient of horse heart cytochrome c of 20mM/cm

2.4 Discussion

The previous characterization of the unique integral membrane oxidoreductase complex ACIII indicates that this protein complex plays a critical role in the electron transfer chain of *C. aurantiacus*, replacing the cytochrome bc_1 or cytochrome b_6f complex. The challenge now is to determine the electron transfer function of ACIII related to the structure of the complex. In order to improve our understanding of the working mechanism of ACIII, it is necessary to investigate the functional roles of each individual subunit and how they participate in the electron transfer pathway. Herein, we report a study of the monoheme-containing subunit ActE, which was investigated by use of both biochemical strategies and molecular biology strategies. We provide some explanation of its role in the electron transfer of ACIII.

In order to further investigate the specific function of subunit ActE in this electron transfer machinery, molecular biology methods were employed to produce recombinant subunit ActE. We have succeeded in expressing subunit ActE in *E. coli* with the *c*-type heme attached. Two types of recombinant subunit ActE were obtained using our protocols for plasmid construction and protein expression. The soluble recombinant subunit ActE is located in the periplasm and without a signal peptide; the membrane-bound recombinant subunit ActE is attached to the membrane by a signal peptide. Both types showed indistinguishable UV-Vis absorption and redox properties. The redox titrations also showed that the recombinant subunit ActE has a redox potential of +385 mV, suggesting that it is indeed the high-potential heme in the intact complex. It also implies that subunit ActE serves as the final electron carrier in ACIII.

There is a redox potential mismatch between recombinant subunit ActE and auracyanin. One aspect of the thermodynamics of the ACIII:auracyanin system that is puzzling is that the

redox potential of auracyanin (+220 mV vs. NHE) [50] is significantly lower than one would expect to accept electrons from the high potential heme of subunit ActE (+385 mV vs. NHE). This makes the electron transfer substantially uphill. If not followed by a significantly downhill step or the potentials modified by complex formation, it could prove to be a barrier to electron flow. Dutton and coworkers have shown that surprisingly endergonic steps are permitted in electron transfer complexes as long as the overall process is exergonic[51]. This uphill electron transfer is well documented in the tetraheme cytochrome complex in the reaction center of *Blastochloris viridis*[52]. Another possible explanation for this situation is that the interaction between the heme subunit and auracyanin is such that potentials of one protein, or more likely, both proteins, are modified, perhaps bringing them closer together. These effects are also well documented, with perhaps the best example being with the blue copper protein amicyanin, which forms a ternary complex with methylamine dehydrogenase and cytochrome c_{551}[53,54]. In *Chloroflexus*, ACIII and auracyanin function with the Light Harvesting Reaction Center complex and menaquinone to perform cyclic electron transfer under photosynthetic growth. The ultimate electron sink in this system is the Reaction Center, at 360 mV has a redox potential approximately equal to ACIII[55]. Therefore, despite the mismatch, the cyclic electron transport system compensates overall of the redox potentials of individual members. Further work will be required to test these possibilities.

To study the role of ActE in ACIII function, we initially began with a "top-down" method and used the chaotropic agent KSCN to treat the purified ACIII complex, with the goal of releasing individual subunits from the whole complex while keeping them in their near-native states. KSCN selectively removes subunit ActE and subunit ActG from ACIII. By using filtration and size exclusion gel chromatography, we discovered that after treatment with KSCN

ACIII lost 3 peripheral subunits, including 2 copies of the *c* type mono-heme containing subunit ActE and the smallest subunit ActG. The blue native PAGE of partially dissociated ACIII showed an otherwise intact complex except for losing *ca*. 50 to 60 kDa mass. The KSCN-treated complex lost most of its activity as a quinol:auracyanin/cytochrome *c* oxidoreductase, which suggests that the subunit ActE and/or subunit ActG play a significant role in the electron transfer of ACIII. The residual activity seen for ACIII' in Figure 5 is attributed to some native ACIII remaining in solution. Although we cannot entirely rule out the possibility that the ActG subunit is critical for activity, previous studies found that subunit ActG is absent in the analogous protein complexes from several species by genome searching[25] and by ACIII purification in the related organism *Roseiflexus castenholzii* (data not shown), suggesting that it is not one of the key components to fulfill the function. Moreover, it lacks any common cofactor normally involved in electron transfer, such as a heme or an iron-sulfur cluster. Therefore, we have focused our effort on the other subunit, the monoheme-containing cytochrome subunit ActE.

To study further the role of ActE in ACIII, recombinant ActE was reconstituted with selectively denatured ACIII' and the enzyme activity was measured. Reconstituted ACIII'-ActE showed the same change in absorption and only slightly smaller initial rate of enzyme activity. This confirmed that ActE is essential for menquinone:electron acceptor oxidoreductase activity. Without ActE and ActG, ACIII' is inactive, but ACIII' is fully active when reconstituted with ActE. Therefore, the presence of ActE is mandatory for electron transfer function, but ActG is not. The finding for ActG is not surprising since it is not found in all ACIII gene clusters, as discussed above. The finding for ActE confirms the role of the monoheme subunit in electron transfer and argues against the possibility that electrons are only being transferred through the

iron-sulfur clusters of ActB or the pentaheme subunit of ActA. The electrons must pass through ActE, most likely as their final stop before being transferred to auracyanin.

We also propose a revised structural model of the ACIII complex, as shown in Fig. 2.7. Our previous structural model of the ACIII complex positioned subunit ActB, the iron-sulfur cluster-containing subunit, on the cytoplasmic side of the membrane because of the lack of a signal protein sequence and its multiple crosslinking products to subunit ActG, which also lacks a signal sequence[24]. However, additional analysis suggests that this assignment may be incorrect. ActB contains a Twin Arginine Translocation (TAT) motif. TAT motifs direct the translocation of folded proteins across membranes[56]. The crosslinking data also found a product containing ActB, ActA, ActE and ActG[24]. The cytochrome subunits ActA and ActE are clearly periplasmic in location, so this product suggests that all these subunits may be periplasmic. The only subunit that is anomalous in this revised view is subunit ActG, which is not predicted to have transmembrane helices and has neither a classic signal sequence nor a TAT motif. However, a "hitchhiker mechanism" was found and reported in bacterial periplasmic nickel-containing hydrogenases where a subunit lacking an export signal was co-translocated with an adjacent subunit containing a twin-arginine signal sequence[56]. In our case, ActG may "hitchhike" with the twin-arginine signal containing subunit ActB to translocate across the membrane.

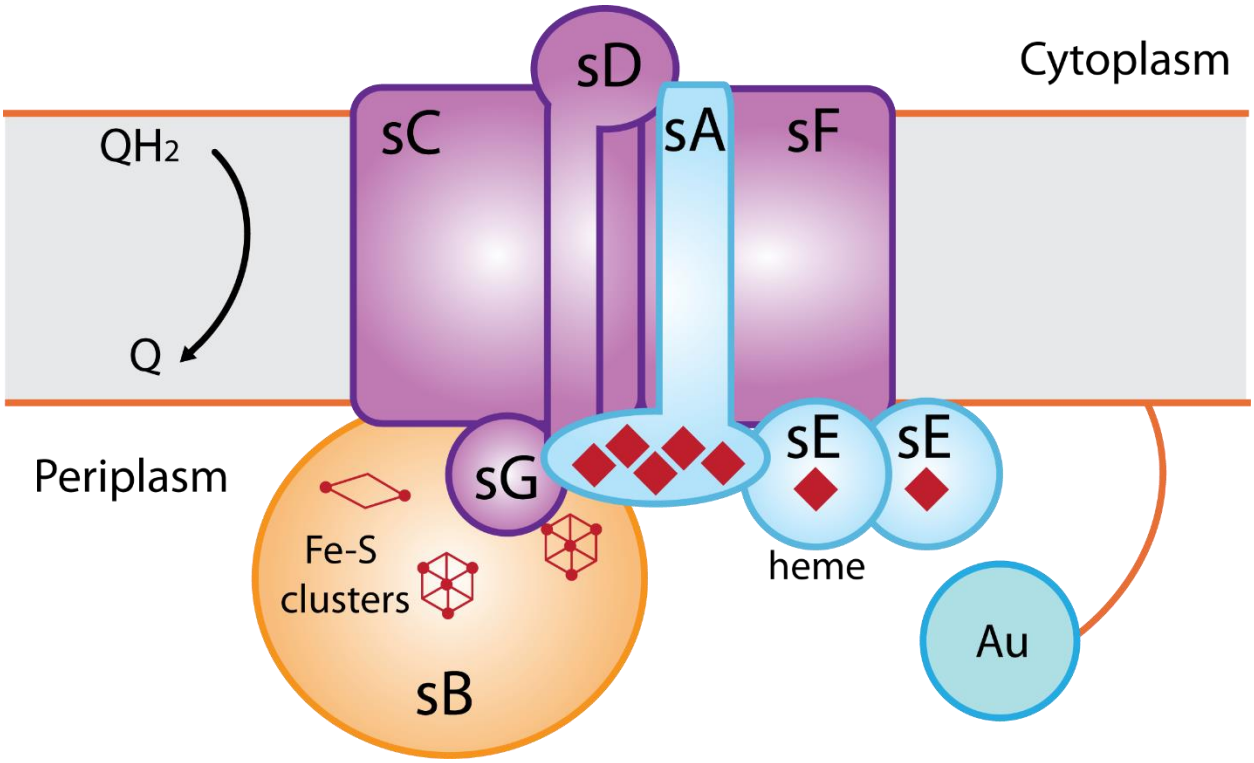

Figure 2.7 Revised structural model of ACIII subunit architecture from *C. aurantiacus* based on current understanding. The subunits arrangement of ACIII complex was obtained by transmembrane-helix analysis and membrane-translocation-mechanisms analysis, as well as the cofactors analysis and chemical cross-linking analysis described in previous work [24]. The positions of ActB and ActG were re-assigned according to the presence of the TAT mechanism. Similar models have been proposed for respiratory ACIII in *Rhodothermus marinus* [20].

In conclusion, we have produced recombinant subunit ActE in *E. coli*, and determined its midpoint redox potential. We have also used chaotropic agents to obtain partially dissociated ACIII complexes, and confirmed that the loss of subunits ActE and ActG caused this complex to lose its activity as a quinol:auracyanin oxidoreductase. Furthermore, we demonstrated that reconstituted ACIII'-ActE regained full native ACIII enzyme activity, indicating the critical role ActE plays in ACIII enzymatic electron transfer. Still, many intriguing questions remain to be answered in order to obtain a complete picture of ACIII in the electron transfer pathway in *C. aurantiacus* (see chapters 4-6). This work provides valuable information for establishing the manner in which the cofactors of ACIII are tuned to transfer electrons.

References

[1] R.E. Blankenship, Molecular Mechanisms of Photosynthesis, Blackwell Science, Oxford UK 2002.

[2] B.K. Pierson, R.W. Castenholz, A phototrophic gliding filamentous bacterium of hot springs, *Chloroflexus aurantiacus*, gen. and sp. nov., Arch. Microbiol. 100 (1974) 5-24.

[3] B.K. Pierson, Chloroflexaceae: Filamentous anoxygenic phototrophic bacteria. , in: D.R. Boone, R.W. Castenholz, G.M. Garrity (Eds.), Bergey's Manual of Systematic Bacteriology, 2nd ed., vol. 1, 2001, pp. 427-444.

[4] C.R. Woese, O. Kandler, M.L. Wheelis, Towards a natural system of organisms: proposal for the domains Archaea, Bacteria, and Eucarya, Proc. Natl. Acad. Sci. USA 87 (1990) 4576-4579.

[5] D.M. Kramer, W. Nitschke, J.W. Cooley, The cytochrome bc_1 and related *bc* complexes: The Rieske/cytochrome *b* complex as the functional core of a central electron/proton transfer complex., in: C.N. Hunter, F. Daldal, M.C. Thurnauer (Eds.), The purple phototrophic bacteria, Springer, Netherlands, 2008, pp. 451-173.

[6] B.L. Trumpower, Cytochrome bc_1 complexes of microorganisms., Microbiol. Rev. 54 (1990) 101-129.

[7] J.L. Cape, M.K. Bowman, D.M. Kramer, Understanding the cytochrome *bc* complexes by what they don't do. The Q-cycle at 30, Trends Plant Sci. 11 (2006) 46-55.

[8] A.R. Crofts, The cytochrome bc_1 complex: function in the context of structure., Ann. Rev. Physiol. 66 (2004) 689-733.

[9] A.R. Crofts, The bc1 complex: What is there left to argue about? , in: M.W. M (Ed.), Biophysical and Structural Aspects of Bioenergetics, Royal Society of Chemistry, Cambridge, 2005, pp. 123-155.

[10] M.F. Yanyushin, Fractionation of cytochromes of phototrophically grown *Chloroflexus aurantiacus*. Is there a cytochrome *bc* complex among them?, FEBS Lett. 512 (2002) 125-128.

[11] M.F. Yanyushin, M.C. del Rosario, D.C. Brune, R.E. Blankenship, New class of bacterial membrane oxidoreductases., Biochemistry 44 (2005) 10037-10045.

[12] C.S. Bond, R.E. Blankenship, H.C. Freeman, J.M. Guss, M.J. Maher, F.M. Selvaraj, M.C. Wilce, K.M. Willingham, Crystal structure of auracyanin, a "blue" copper protein from

the green thermophilic photosynthetic bacterium *Chloroflexus aurantiacus*., J Mol Biol. 306 (2001) 47-67.

[13] M. Lee, M.C. del Rosario, H.H. Harris, R.E. Blankenship, J.M. Guss, H.C. Freeman, The crystal structure of auracyanin A at 1.85 A resolution: the structures and functions of auracyanins A and B, two almost identical ‘‘blue’’ copper proteins, in the photosynthetic bacterium *Chloroflexus aurantiacus*, J Biol. Inorg. Chem. 14 (2009) 329-345.

[14] J.D. McManus, D.C. Brune, J. Han, J. Sanders-Loehr, T.E. Meyer, M.A. Cusanovich, G. Tollin, R.E. Blankenship, Isolation, characterization, and amino acid sequences of auracyanins, blue copper proteins from the green photosynthetic bacterium *Chloroflexus aurantiacus*., J. Biol. Chem. 267 (1992) 6531-6540.

[15] J.T. Trost, J.D. McManus, J.C. Freeman, B.L. Ramakrishna, R.E. Blankenship, Auracyanin: a blue copper protein from the green photosynthetic *Chloroflexus aurantiacus*. , Biochemistry 27 (1988) 7858-7863.

[16] G. Van Driessche, W. Hu, G. Van De Werken, F. Selvaraj, J.D. McManus, R.E. Blankenship, J.J. Van Beeumen, Auracyanin A from the green gliding photosynthetic bacterium *Chloroflexus aurantiacus* represents an unusual class of small blue copper proteins., Protein Sci. 8 (1999) 947-957.

[17] J.C. Freeman, R.E. Blankenship, Isolation and characterization of the membrane-bound cytochrome *c*-554 from the thermophilic green photosynthetic bacterium *Chloroflexus aurantiacus*, Photosynth. Res. 23 (1990) 29-38.

[18] M.M. Pereira, J.N. Carita, M. Teixeira, Membrane-bound electron transfer chain of the thermohalophilic bacterium *Rhodothermus marinus*: a novel multihemic cytochrome *bc*, a new complex III., Biochemistry 38 (1999) 1268-1275.

[19] M.M. Pereira, P.N. Refojo, G.O. Hreggvidsson, S. Hjorleifsdottir, M. Teixeira, The alternative complex III from *Rhodothermus marinus* – A prototype of a new family of quinol:electron acceptor oxidoreductases., FEBS Lett. 581 (2007) 4831-4835.

[20] P.N. Refojo, F.L. Sousa, M. Teixeira, M.M. Pereira, The alternative complex III: A different architecture using known building modules, Biochim. Biophys. Acta (In press) DOI: 10.1016/j.bbabio.2010.04.012 (2010).

[21] P.N. Refojo, M. Teixeira, M.M. Pereira, The alternative complex III of *Rhodothermus marinus* and its structural and functional association with caa_3 oxygen reductase Biochim. Biophys. Acta 1797 (2010) 1477-1482.

[22] E.L.W. Majumder, J.D. King, R.E. Blankenship, Alternative Complex III from phototrophic bacteria and its electron acceptor auracyanin. Biochim. Biophys. Acta (In press) (2013)

[23] X. Gao, Y. Xin, R.E. Blankenship, Enzymatic activity of the alternative complex III as a menaquinol:auracyanin oxidoreductase in the electron transfer chain of *Chloroflexus aurantiacus*, FEBS lett. 583 (2009) 3275-3279.

[24] X. Gao, Y. Xin, P.D. Bell, J. Wen, R.E. Blankenship, Structural analysis of alternative complex III in the photosynthetic electron transfer chain of *Chloroflexus aurantiacus*, Biochemistry 49 (2010) 6670-6679.

[25] K.-H. Tang, K. Barry, O. Chertkov, E. Dalin, C.S. Han, L.J. Hauser, B.M. Honchak, L.E. Karbach, M.L. Land, A. Lapidus, F.W. Larimer, N. Mikhailova, S. Pitluck, B.K. Pierson, R.E. Blankenship, Complete genome sequence of the filamentous anoxygenic phototrophic bacterium *Chloroflexus aurantiacus*, submitted (2011).

[26] J. Sambrook, E.F. Fritsch, T. Maniatis, Molecular cloning: a laboratory manual. 2. ed., Cold Spring Harbor Laboratory Press, New York, 1989.

[27] M.P. Weiner, C. Anderson, B. Jerpseth, S. Wells, B. Johnson-Browne, P. Vaillancourt, Studier pET system vectors and hosts., Strategies Mo. Bio. 7 (1994) 41-43.

[28] C.R. Rocco, K.L. Dennison, V.A. Klenchin, I. Rayment, J.C. Escalante-Semerena, Construction and use of new cloning vectors for the rapid isolation of recombinant proteins from *Escherichia coli.*, Plasmid 59 (2008) 231-237.

[29] F. Baneyx, Recombinant protein expression in *Escherichia coli.*, Curr. Opin. Biotech. 10 (1999) 411-421.

[30] M.Z. Li, S.J. Elledge, Harnessing homologous recombination *in vitro* to generate recombinant DNA via SLIC., Nature Methods 4 (2007) 251-256.

[31] R.E. Feissner, C.L. Richard-Fogal, E.R. Frawley, J.A. Loughman, K.W. Earley, R.G. Kranz, Recombinant cytochromes *c* biogenesis systems I and II and analysis of haem delivery pathways in *Escherichia coli*., Mol. Microbiol 60 (2006) 563-577.

[32] C.L. Richard-Fogal, E.R. Frawley, R.E. Feissner, R.G. Kranz, Heme concentration dependence and metalloporphyrin inhibition of the system I and II cytochrome *c* assembly pathways., J. Bacteriol. 189 (2007) 455-463.

[33] E.A. Berry, B.L. Trumpower, Simultaneous determination of hemes *a*, *b*, and *c* from pyridine hemochrome spectra, Anal. Biochem. 161 (1987) 1-15.

[34] P.D. Bell, Y. Xin, R.E. Blankenship, Purification and characterization of cytochrome c_6 from *Acaryochloris marina*, Photosynth. Res. 98 (2009) 131-140.

[35] M.J. Holden, D.G. Luster, R.L. Chaney, T.J. Buckhout, C. Robinson, Fe^{3+}-chelate reductase activity of plasma membranes isolated from tomato (Lycopersicon esculentum mill.) roots., Plant Physiol. 97 (1991) 537-544.

[36] B. Bolgiano, I. Salmon, W.J. Ingledew, R.K. Poole, Redox analysis of the cytochrome *o*-type quinol oxidase complex of *Escherichia coli* reveals three redox components, Biochem. J. 274 (1991) 723-730.

[37] N.B. Ugulava, A.R. Crofts, CD-monitored redox titration of the Rieske Fe-S protein of *Rhodobacter sphaeroides*: pH dependence of the midpoint potential in isolated bc_1 complex and in membranes., FEBS lett. 440 (1998) 409-413.

[38] H.-L. Kwong, Encyclopedia of Reagents for Organic Synthesis., J. Wiley & Sons, New York. DOI: 10.1002/047084289., 2004.

[39] B.K. Pierson, J.P. Thornber, Isolation and spectral characterization of photochemical reaction centers from the thermophilic green bacterium *Chloroflexus aurantiacus* strain J-10-fi., Proc. Natl. Acad. Sci. U.S.A. 80 (1983) 80-84.

[40] Y. Xin, Y.-K. Lu, P. Fromme, R.E. Blankenship, Purification, characterization and crystallization of menaquinol:fumarate oxidoreductase from the green filamentous photosynthetic bacterium *Chloroflexus aurantiacus*., Biochim. Biophys. Acta 1787 (2009) 86-96.

[41] H. Schägger, G. von Jagow, Tricine-sodium dodecyl sulfate-polyacrylamide gel electrophoresis for the separation of proteins in the range of 1 to 100 kDa, Anal. Biochem. 166 (1987) 368-379.

[42] H. Schägger, G. von Jagow, Blue native electrophoresis for isolation of membrane protein complexes in enzymatically active form, Anal. Biochem. 199 (1991) 223-231.

[43] J. Sambrook, E.F. Fritsch, T. Maniatis, Detection and analysis of proteins. In: Molecular Cloning. 2nd edition, Cold Spring Harbor Laboratory Press, New York, 1989, pp. 18.56-18.57.

[44] C.I. Ragan, M.T. Wilson, V.M. Darley-Usmar, P.N. Lowe, Sub-fractionation of mitochondria and isolation of the proteins of oxidative phosphorylation, in: V.M. Darley-Usmar, Rickwood, M.T. Wilson (Eds.), Mitochondria, A Practical Approach, IRL press, Oxford, 1987, pp. 96-101.

[45] L. Thony-Meyer, D. Ritz, H. Hennecke, Cytochrome c biogenesis in bacteria: a possible pathway begins to emerge, Molecular Mocrobiology 12 (1994) 1-9.

[46] Y. Hatefi, W.G. Hanstein, Solubilization of particulate proteins and nonelectrolytes by chaotropic agents., Proc. Natl. Acad. Sci. U. S. A. 62 (1969) 1129-1136.

[47] G. Salvi, P. De los Rios, M. Vendruscolo, Effective interactions between chaotropic agents and proteins., Proteins-Structure Function and Bioinformatics 61 (2005) 492-499.

[48] U. Boronowsky, S.-O. Wenk, D. Schneider, C. Jäger, M. Rögner, Isolation of membrane protein subunits in their native state: evidence for selective binding of chlorophyll and carotenoid to the b_6 subunit of the cytochrome b_6f complex., Biochim. Biophys. Acta 1506 (2001) 55-66.

[49] Q. Xu, T.S. Armbrust, J.A. Cuikema, P.R. Chitnis, Organization of photosystem I polypeptides., Plant Physiol. 106 (1994) 1057-1063.

[50] M.D. Rooney, M.J. Honeychurch, F.M. Selvaraj, R.E. Blankenship, B.A. and, F. HC, A thin-film electrochemical study of 'blue' copper proteins, auracyanin A and auracyanin B, from the photosynthetic bacterium *Chloroflexus aurantiacus*: The reduction potential as a function of pH., J. Biol. Inorg. Chem. 8 (2003) 306-317.

[51] C.C. Page, C.C. Moser, X. Chen, P.L. Dutton, Natural engineering principles of electron tunnelling in biological oxidation-reduction., Nature 402 (1999) 47-52.

[52] I.P. Chen, P. Mathis, J. Koepke and H. Michel, Uphill electron transfer in the tetraheme cytochrome subunit of the *Rhodopseudomonas viridis* photosynthetic reaction center: Evidence from site-directed mutagenesis. Biochemistry 39: (2000) 3592-3602.

[53] L.Y. Chen, R.C. Durley, F.S. Mathews, V.L. Davidson, Structure of an electron transfer complex: methylamine dehydrogenase, amicyanin, and cytochrome *c*551i, Science 264 (1994) 86-90.

[54] Z.Y. Zhu, L.M. Cunane, Z.W. Chen, R.C. Durley, F.S. Mathews, V.L. Davidson, Molecular basis for interprotein complex-dependent effects on the redox properties of amicyanin., Biochemistry 37 (1998) 17128-17136.

[55] B.D. Bruce, R.C. Fuller and R.E. Blankenship, Primary photochemistry in the facultatively aerobic green photosynthetic bacterium *Chloroflexus aurantiacus.* Proc. Natl. Acad. Sci. U.S.A. 79 (1982) 6532-6.

[55] B.C. Berks, F. Sargent, T. Palmer, The TAT protein export pathway., Mol. Microbiol 35 (2000) 260-274.

[56] A. Rodrigue, A. Chanal, K. Beck, M. Muller, L. Wu, Co-translocation of a periplasmic enzyme complex by a hitchhiker mechanism through the bacterial TAT pathway, J Biol Chem 274 (1999) 13223-13228.

Chapter 3: Structural analysis of diheme cytochrome *c* by hydrogen deuterium exchange mass spectrometry and homology modeling

Portions of this chapter have been previously published as: Zhang, Y., Majumder, E.L.W., Yue, H., Blankenship, R.E. & Gross, M.L. Analysis of diheme cytochrome *c* by hydrogen deuterium exchange mass spectrometry and homology modeling. *Biochemistry* **53,** 5619-5630 (2014). Used with permission of authors.

3.1 Introduction

Cytochrome *c*'s are electron-transport hemoproteins that are covalently bound through two thioether bonds between the vinyl groups of a heme macrocycle and the sulfhydryls of a CXXCH heme-binding motif[1]. Two heme propionate groups are exposed and can participate in hydrogen bonding. The main function is to mediate single-electron transfer reactions between protein electron donors and acceptors via reversible oxidation/reduction of Fe^{2+} and Fe^{3+}. The axial coordination of the heme iron and its effect on other parts of the larger protein environment play key roles in determining redox, electron transfer, and other properties of *c*-type cytochromes c[2, 3].

Prokaryotic diheme cytochrome *c*'s, as representatives of electron-transfer proteins with two iron centers, have been studied with various spectroscopic methods[4-6]. For example, cytochrome c_4 from *Pseudomonas stutzeri*, which shares the same origin and has a similar amino-acid sequence as DHCC[7], possesses a strong hydrogen bond involving the heme propionate groups, and the protein facilitates intramolecular, inter-heme electron transfer[8]. Both hemes contain hexa-coordinated iron involving histidine and methionine axial ligands. The hydrogen bond in *P. stutzeri* closes one edge of the heme, allowing it to act as the donor and the other as the acceptor.

DHCC from *Heliobacterium modesticaldum*, a gram-positive phototrophic anaerobic prokaryote, plays a role as the terminal electron acceptor in the high-potential electron-transfer chain of the cytochrome *bc* complex. This complex participates in the photosynthetic electron-transport cycle by oxidizing the quinone pool, sending electrons to the reaction center and pumping protons to establish an electrochemical gradient that drives ATP production. DHCC replaces the canonical monoheme cytochrome c_1 in the cytochrome bc_1 complex, or cytochrome *f* in the cytochrome b_6f complex[9, 10]. DHCC has two *c*-type hemes that are predicted to reside in

similar *c*-type cytochrome folds. The heme 1 domain is closer to the N-terminal helix, whereas the heme 2 domain begins approximately halfway through the sequence. The unusual diheme architecture is an interesting contrast with those of the more common mono-heme cytochromes.

In general, an electron transfer of one metal center induces conformational changes in the site of the other, and that usually enhances the rates of subsequent steps[11]. Studying the structure, function, and redox properties of this protein is crucial to the understanding of the function of the entire heliobacterial cytochrome *bc* complex. Furthermore, an understanding of the Heliobacterium electron transport chain (ETC), which is simpler and smaller than other phototrophic organisms, can provide clues to how life and photosynthesis evolved on Earth and possibly on other planets. Similarly, the simple nature of the ETC makes it an attractive target for biomimicry in solar energy production[12-15].

Redox-dependent conformations of cytochromes *c* have been studied extensively for decades by using various biochemical and biophysical approaches[16-23]. Although some comparative X-ray crystallographic studies of tuna-heart cytochromes *c* show little or no difference between the backbone structures[24], almost all solution-based studies show a clear conformational change between the two redox states[25-27]. Specifically in the case of horse heart cytochrome *c*, the radius of the oxidized state is significantly larger than that of the reduced one[25]. Despite the success of these approaches, there is a need for other methods. For example, many biophysical techniques usually require a large amount of sample[28-30], which is not always available, and their structural resolution is relatively low[28]. In contrast, mass-spectrometry (MS) approaches have high sensitivity and moderate structural resolution. For studying protein conformations, hydrogen deuterium exchange (HDX) coupled with MS is an effective and now commonly employed approach[31-35]. The exchange rates for HDX are good readouts for hydrogen bonding and solvent

accessibility at global, peptide and even amino acid levels[36]. It is also possible to use HDX data to adjudicate protein subunit docking and ligand-binding structural models[37-39].

In HDX studies, one often compares the exchange rate of the same protein regions for two different states that are produced by some protein perturbation (e.g., ligand binding, change in redox status, formation of a complex). Although each amino acid has different intrinsic deuterium exchange rate constants, this causes no problem because the experimental exchange rates between two states of the protein are compared. Previously, HDX coupled with infrared spectroscopy was used to study the conformations of reduced and oxidized horse heart cytochrome *c*[40]. Viala and co-workers[41] reported an HDX-MS study of the same system, indicating of a more open structure in the oxidized state. Thus far, however, there are no HDX-MS studies of the DHCC system. To test our proposed mechanism of the DHCC subunit of the heliobacterial cytochrome *bc* complex, which involves a more closed conformation upon reduction[42], we designed an HDX study of both the reduced and oxidized states of the heliobacterial DHCC in an effort to achieve peptide-level resolution of structural changes.

Homology Modeling (HM) is another common approach to protein structure and function especially when data from other structural approaches (e.g., X-ray crystallography and NMR) are not available. Although HM statistics for assigning model quality do not necessarily reflect the in vivo structure of the protein, the approach should be more accurate when coupled with experimental approaches. HDX-MS with HM was used previously to investigate docking and binding studies in combination with Electron Microscopy[43-46]. These semi-quantitative approaches rely on heavy computational techniques and assess quaternary structure of the protein. Here, we are using HDX-MS results to direct HM to obtain a low-resolution understanding of protein tertiary structure and to predict a reaction mechanism for the complex.

Our method relies on readily available applets for modeling and HDX for making qualitative structural distinction between a buried or exposed region to adjudicate the models, quite unlike the previous studies that use HDX to study the docking of ligands or subunits. Success will not only provide insight to DHCC but also to establish the utility of the combined approach for other protein systems.

3.2 Materials and methods

3.2.1 Protein Expression and Purification

The diheme cytochrome *c* subunit from *Heliobacterium modesticaldum bc* complex was expressed in *Escherichia coli* with the cytochrome *c* insertion plasmid and purified as previously described, yielding only the holo-protein[42]. The N-terminal transmembrane helix region was truncated to express only the fully soluble portion of the protein. Post-processing did not eliminate the hemes, both being covalently bound to the protein.

3.2.2 Hydrogen Deuterium exchange (HDX) of reduced and oxidized diheme cytochrome *c* samples

Differential, solution HDX experiments were performed at 4 °C. DHCC in 20 mM Tris-HCl buffer, pH 7.5 solution was incubated with either sodium dithionite (reductant), or potassium ferricyanide (oxidant) at a final concentration of 25 μM for both the protein and the reductant/oxidant. The samples were equilibrated for 1 h prior to initiating HDX. Continuous labeling was initiated by incubating 2 μL of the mixture with 18 μL of D_2O for seven predetermined times (0.17, 0.5, 1, 2, 15, 60, and 240 min). The exchange reaction was quenched by mixing the D_2O solution with 30 μL of 3 M urea, 1% trifluoroacetic acid (TFA) at 0 °C. The

quenched solution was then flash-frozen in liquid nitrogen and stored at -80 °C for less than 48 h prior to analysis.

The quenched sample was then digested by passing it through a custom-packed pepsin column (2 mm x 2 cm) at 200 μL/min; the peptides were captured on a C_8 trap column (2 mm x 1 cm, Agilent Inc., Santa Clara, CA, USA) and desalted with a 3 min flow. Peptides were then separated by using a C_{18} column (2.1 mm x 5 cm, 1.9 μm Hypersil Gold, Thermo Fisher Scientific, Waltham, MA, USA) with a 5 min linear gradient of 4% - 40% CH_3CN in 0.1% formic acid. Protein digestion and peptide separation were carried out in an ice-water bath to minimize back exchange. All analyses were with a hybrid LTQ Orbitrap (Thermo Fisher Scientific, San Jose, CA, USA) at an ESI capillary temperature of 225 °C. Each experiment was performed in duplicate.

3.2.3 Peptide identification and HDX data processing

MS/MS experiments were performed on the LTQ Orbitrap mass spectrometer. Product-ion spectra were acquired in a data-dependent mode, and the six most abundant ions were selected for product-ion analysis. The data files were converted using MassMatrix Mass Spectrometric Data File Conversion Tools (v 3.9) and then submitted to MassMatrix (v 2.4.2) for peptide identification[47]. Peptides used for HDX data analysis had a MassMatrix score of 10 or greater, and with peptide and MS/MS tolerances for *m/z* of 10 ppm and 0.8 Da, respectively. The MS/MS MassMatrix search was also performed against a decoy (reverse) sequence, and ambiguous identifications were ruled out. The product-ion spectra of all peptide ions from the MassMatrix search were manually inspected, and only those manually inspected were used in the following steps. The centroid masses of isotopic envelopes were calculated with HDX

WorkBench[48]: deuterium level (%) = ((m(P) – m(N))/(m(F) – m(N))) x 100%, where m(P), m(N), and m(F) are centroid masses of partially deuterated peptides, undeuterated peptides, and fully deuterated peptides, respectively. To accommodate the situation when a fully deuterated control was not available, m(F) was determined with m(F) = m(N) + (n - p - 2)/z, where n and p represent the total number of amino acids and prolines, respectively, and z represents the charge. The first two amino acids that do not retain deuterium were not taken into consideration (the value "2" in the equation). No correction was made for back exchange because all values are used in a relative way (used in a two-state comparison) and susceptible to the same back-exchange processes.

3.2.4 Homology Modeling and Model Refinement

Homology modeling of DHCC was carried out with three different modeling platforms. The first was with Modeller[49] v9.10 and v9.12 using alignment algorithms ClustalW2 and ClustalΩ, respectively, with both pdb files 1ETP[8] and 3MK7c[50] generating 100 models from each run. The best models from each run were selected based on the molpdf, GA341 and DOPE scores. The best model from each run was then tested by taking the experimental HDX data for each peptide as a measure of the secondary and tertiary structure of that portion of the protein. The amount of exchange in each section was compared to the secondary and tertiary structure predicted by the model. For regions that disagreed, the template to DHCC alignment was manually adjusted and another round of models with the new alignment was generated until the best match was obtained with the HDX data.

The second approach used models that were generated using the Phyre2[51] and I-TASSER[52] on-line modeling suites. The models generated from these two suites were compared to each

other because they do not allow for manual adjustment of the alignments or parameters or further analysis options. Disorder prediction was run on the best model in Phyre2. The top resulting model was compared to the HDX data and to the Modeller generated models.

The third approach was built on previous work[10] where a complete model of the cytochrome *bc* complex was built using the Phyre2 server to analyze the whole complex structure and predict mechanism for electron transfer within the complex.

3.2.5 Solvent Accessible Surface Area (SASA) assessment of homology models

Solvent Accessible Surface Area (SASA) was calculated for all four homology models using the program Get Area [1]. The SASA for the backbone only was chosen as the value to use in our assessment because HDX only exchanges the backbone hydrogens, not the entire residue. The backbone SASA is calculated for each residue and is reported in square Angstroms. To be able to compare to the HDX data, the SASA was averaged for all residues in each of the MS peptic peptides. The average SASA value for each model and peptide is reported in the table. The percent of deuterium uptake reported was calculated by taking the average of the initial and final percent of deuterium uptake (also known as extent of HDX exchange). The average of the initial and final HDX percent represents all four structure categories and HDX trends seen in Figure S1.

For comparison in the table, each structure category was color coded with warmer colors being more dynamic. The four categories were assigned by taking the range of HDX and SASA and dividing them into four equal ranges. The assigned ranges matched our previous categories in Table 2. The color coding allows for comparison of the trend in HDX extent and SASA. A higher percent of HDX corresponds to a larger SASA.

3.3 Results and Discussion

Prior to conducting HDX, we tested whether charge-state distributions of the intact protein could provide coarse structural data to distinguish the reduced and oxidized states of DHCC. Experiments revealed that the conditions of native ESI are sufficiently oxidative to preclude obtaining mass spectra for the pure reduced species. Expression of the protein with the covalently bound heme precluded any comparisons with the apo state. Thus, we turned to HDX footprinting to obtain structural data for the DHCC protein.

3.3.1 HDX shows the oxidized form of DHCC is more flexible

An on-line pepsin digestion of expressed and purified DHCC afforded hundreds of peptides, of which 69 detected with high signal/noise ratio and validated MS/MS information were chosen for the subsequent peptide mapping. The coverage is 95% (shown in Supplemental Figure 3.1), allowing us to assess nearly fully the protein in both of the redox states. *As mentioned before, no correction for back exchange of the protein was made because all data were used in two-state comparisons of the redox-state samples under identical conditions.* All samples are subjected to back exchange after quench and processing, and this converted any side chain deuteriums (e.g., on $-NH_2$) back to hydrogens. Thus, it is the back-bone deuteriums that remain on the polypeptide for the LC/MS analysis. Changes in protein dynamics, as reflected by HDX, reflect changes to the protein induced by reduction. The resulting perturbations alter the conformation of the protein backbone and its H bonding as reflected by changes in HDX. Therefore, all fluctuations in HDX rates reflect only reduction-induced changes. For example, we expect that less

constrained regions should exhibit relatively fast HDX, whereas structured and buried regions exchange slowly.

We plotted the HDX kinetic curves for each of the peptides from both the reduced (solid lines, Supplemental Figure 3.2 for a representative set) and oxidized (dashed lines, Supplemental Figure 3.2) states of the DHCC. When peptides of different charge cover the same region, we found that the results were nearly identical, indicating that the HDX results have good precision. More importantly, we conducted each experiment in duplicate and show the error bars (average deviations) in each plot. In summary, all the HDX experiments afforded a 0-3% relative average deviation for duplicate determinations.

The extents of HDX for most regions of the protein are different for the two states (oxidized and reduced), indicating that the structural conformation of DHCC is redox-state-dependent. For those regions that show differences, the oxidized state always shows greater deuterium uptake compared to the reduced state, indicating that the oxidized state is more flexible (less structurally constrained). This is consistent with other horse-heart-cytochrome *c* HDX studies that show that the oxidized state is more dynamic and flexible than the reduced[41].

The largest differences in HDX kinetics occur near the heme-binding CXXCH motif (i.e., for peptides 1-29 and 109-127) (Supplemental Figure 3.2). These differences indicate that conformational opening in the heme-binding region accompanies oxidation. This result suggests that redox-dependent conformational changes begin at the metal center. Comparing the changes in HDX for the oxidized and reduced states at the two heme binding pockets, we find similar outcomes. Specifically, the oxidized protein undergoes between 30 and 50% HDX at the two sites whereas the reduced protein undergoes between 20 and 40% exchange (Supplemental Figure 3.2). Our previous reported potentiometric titration of DHCC[42] shows a single observable

midpoint potential, which is consistent with the conclusion that the two heme binding pockets have similar chemical environments.

3.3.2 HDX reflects secondary structure

Although four regions display no changes upon reduction (e.g., 45-49, 130-138, 143-149, and 169-172, Supplemental Figure 3.2), they can be viewed as controls because they indicate that regions insensitive to oxidation do not show differences in HDX. Importantly, these regions also show no detectable HDX as a function of time, indicating that these regions are heavily H-bonded and/or buried in the protein. We assign these four regions to be involved in tertiary structural helix bundles (Category I). We take this result to indicate that the core structural components of DHCC do not change dramatically upon reduction, whereas flexible regions are more likely to be affected and participate in the conformational changes that accompany redox changes. In contrast, region 173-208 undergoes extensive exchange, even at short time (Supplemental Figure 3.2). We categorize regions of this type to be part of loops (Category II).

Regions that constitute a third category also show increasing HDX with time but at a more modest extent (none showed 90% or higher deuterium uptake). This lower HDX occurs in part because the peptides are long and likely cover regions containing both H-bonded helices and flexible loops, thus reporting an "average" of these structural elements. For example, the peptides for region 78-108 show deuterium uptake ranging from 20-50% for the reduced state and 30-60% for the oxidized state (Supplemental Figure 3.2). The helix region undergoes less HDX, whereas the peptide bonds in the flexible loop exchange more readily. Similarly, regions 78-91 and 92-108, also comprise helix and loop structures and, thus, show an intermediate level

of deuterium uptake (~ 60%). This intermediate exchange also pertains to region 109-127, and 150-168.

We also identified a fourth category where HDX at the shortest times in near zero but increases slowly with time (Supplemental Figure 3.2). We assigned these regions, including 38-44, 50-57, and 128-142, to be likely helices but not part of buried helix bundles.

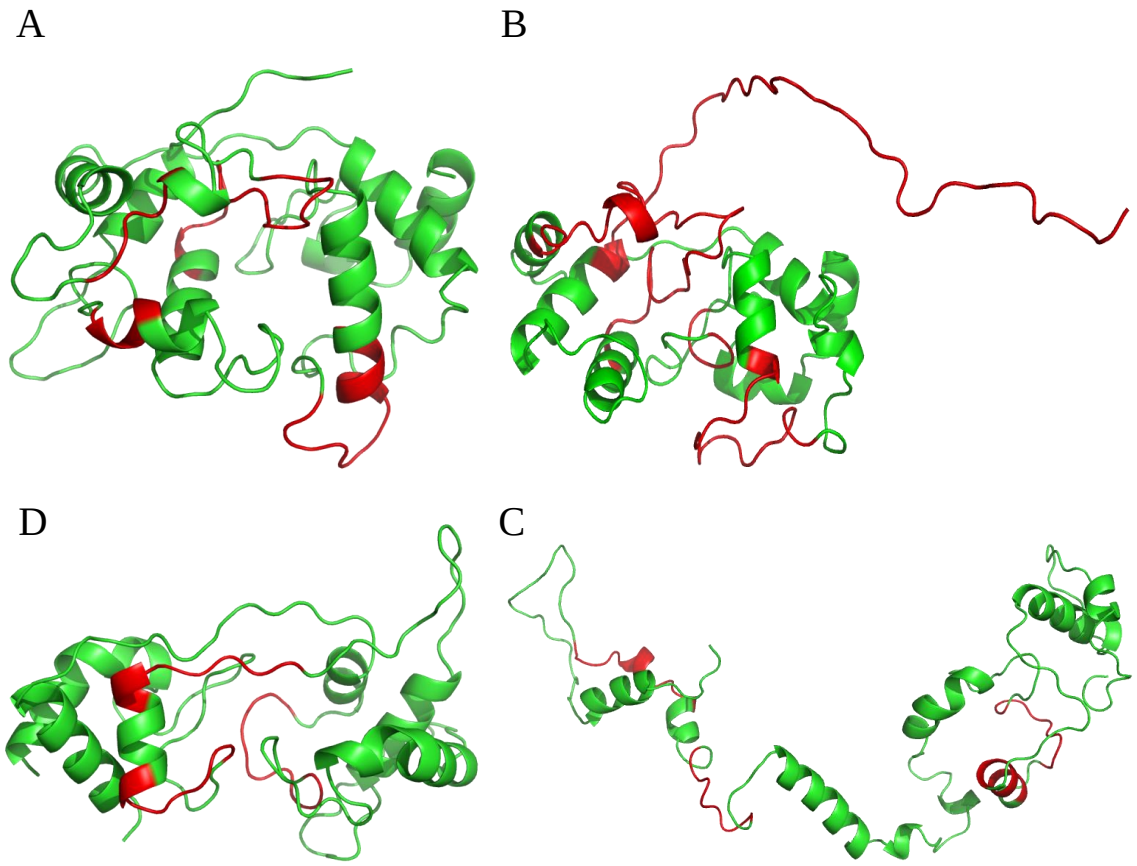

Figure 3.1 Homology models A to D. Regions that are highlighted in red do not agree with HDX results.

3.3.3 Homology Model building and Assessment

A series of homology models were generated with the software Modeller and PHYRE2 (Figure 3.1 and Table 3.1). To begin, we chose template 1ETP because it is a bacterial

cytochrome c_4 protein, and the evolutionary origin of DHCC may be the cytochrome c_4 protein family[42]. Likewise, 1ETP undergoes electron transfer from a donor to an acceptor protein[8]. We selected 3MK7c as the second template on the basis of bioinformatic analysis. A BLAST search of the Protein Data Bank (PDB) with DHCC's sequence returns 3MK7c as the most similar protein by alignment statistics. Functionally, 3MK7c is a soluble member of a protein complex, but it resides in the cytoplasm and accepts electrons from a cytoplasmic donor and shuttles them into the complex, the opposite direction from which DHCC should function[50]. Both 1ETP and 3MK7c have hemes with two different redox potentials. Although the generated homology models do not incorporate the cofactor heme by nature of the program, the templates we chose do include the cofactors within the protein. Even though we did not add the hemes in the HM modelling, the protein structure should still be representative. Functional considerations of the template are a way to assess model quality.

Table 3.1 Homology Modeling Data

Model	Template	Alignment Algorithm	Percent Similarity	Percent Identity	Modeling Software	Molpdf score
Model A	1ETP	ClustalW2	49% (100/205)	15% (32/205)	Modeller v9.10	0.24 (0.49-highest)
Model B	1ETP	Clustal Omega	45% (92/205)	16% (33/205)	Modeller v9.10, v9.12	0.12 (0.28-highest)
Model C	3MK7c	Clustal W2	57% (116/205)	28% (68/205)	Modeller v9.10	.46 (highest)
Model D	3MK7c	Phyre2	57% (116/205)	28% (58/205)	I-TASSER, PHYRE2	3.2Å Resolution N/A

Homology Modeling (HM) statistics assess model quality in a more quantitative way. The percent similarity and percent identity examine the alignment of the template and model sequences. Amino-acid residues that align are examined to see if they are identical or in the same category. The percent identity increases from Model A to Model B as a result of manual alignment changes implemented on the basis of the HDX data. Further increases in both percent similarity and percent identity occur for models C and D, which use 3MK7 as a template (Table 3.1). The higher these values, the more similar a model is to the template, and the more faithful is the homology model. The 28% identity achieved for Models C and D is just under that preferred for HM, but it is sufficient for further consideration. We also view it as acceptable because there are so few diheme cytochromes with solved structures in the PDB. After running HM in Modeller, score reports are generated for each model. The molpdf score can be used to compare models across runs. Model C has the highest molpdf score indicating it is the better homology model. Model B may be a better model functionally as discussed below, but it has a lower molpdf score because manual alignment changes were made (Table 3.1). Homology modeling data indicate that Models C and D are better models; therefore, 3MK7c is the better template. This result is only based on alignment and threading algorithms, however, and does not speak to function or biochemical properties of the models and templates. Thus, biochemical and/or biophysical data are needed to assess further these models.

3.3.4 HDX analysis of DHCC with its homology model

HDX data generated by MS can provide biophysical data that, when mapped onto the four homology models, should be able to test the correctness of secondary and tertiary structures generated by the models (Figure 3.1 and Table 3.2). For Model A, most of the regions that show discrepancies between the HDX results and the HM outcomes are the helical regions (Figure

3.1A and Table 3.2). For example, peptides in Category I show almost no deuterium uptake in either of the states (Supplemental Figure 3.2), suggesting they participate in forming tertiary structure, most likely a helix bundle. In Model A, however, only region 143-149 has the helix-bundle motif. Peptides 45-49 and 130-138 are modelled to be a loop or a singular helix structure. After manually adjusting the alignment based on this observation, Model B and C show better fits for 45-49, 143-149, and 169-172, as these regions are predicted to be helices in helix bundles. Furthermore, Model A HM did not identify the second heme binding motif and the alignment and subsequent modeling are poor in this region, 109-127.

Table 3.2 Comparison of HDX Data and Homology Models

Region[a]	Category[b]	Model A[c]	Model B	Model C	Model D	HDX agreement on the models[d]			
						A	B	C	D
1-29	III	**h/l**	**h/l**	**h/l**	**h/l**	**	**	**	**
33-37	III	**h/l**	**l**	**l**	**l**	**			*
38-44	IV	**h bundle**	**h/l**	**h/l**	**h/l**				*
45-49	I	**h**	**h bundle**	**h/l**	**h bundle**		**		**
50-57	IV	**l**	**l**	**h bundle**	**h/l**				*
58-65	II	**l**	**l**	**l**	**l**	**	**	**	**
78-91	III	**h/l**	**h/l**	**h/l**	**h/l**	**	**	**	**
92-108	III	**h/l**	**h/l**	**h/l**	**h/l**	**	**	**	**
109-127	III	**l**	**l**	**h/l**	**h/l**			**	**
128-142	IV	**h/l**	**l**	**l**	**l**	*			*
143-149	I	**h bundle**	**h bundle**	**h**	**h bundle**	**	**	*	**
150-168	III	**h/l**	**h/l**	**h/l**	**h/l**	**	**	**	**
169-172	I	**h**	**h bundle**	**h bundle**	**h bundle**		**	**	**
173-208	II	**h/l**	**l**	**h/l**	**h/l**	**	**	**	**

a. Regions that determined by HDX. Most of the regions are covered by multiple peptides, and they give similar results.
b. Different regions are signed in four categories based on their HDX behavior.
c. Secondary/tertiary structure elements in each model. “h” stands for helix, “l” stands for loop, “h/l” stands for mixture of helix and loop, and “h bundle” stands for helix bundle.

d. Measures of agreement degrees between HDX and modeling results. "**" stands for agreement, "*" stands for agreement with restrictions (information from order prediction by Phyre2), and blank cells represent lack of agreement.

To resolve regions for which there is a lack of agreement, we generated Model B (Figure 3.1B and Table 3.2) by manually adjusting the alignment based on the results of Model A as evaluated by HDX. Model B showed improved agreement between HDX and the HM structure. The helix bundle and 2nd heme regions predicted by Model B are consistent with the experimental results, but achieving these improvements sacrificed other regions that had agreed with Model A. For example, 33-37 shows as a loop, but it takes up only ~50% of possible deuterium. On the contrary, a mostly loop region, 173-208, does show ~70% HDX. In addition, residues 173-205 show the poorest agreement with HDX results compared to other models, as the sequence does not align with the template. 1ETP is a smaller protein, and in adjusting for the heme regions, residues at the end of DHCC were left without template residues. As a result, this region is unstructured according to Model B. Even though this region shows the highest HDX for the whole protein (~70%), it still should have some secondary structure. Despite these areas of disagreement, Model B is better than Model A because the active regions of the protein are consistent with the outcomes of both HDX and HM. Overall, the transition from Model A to Model B demonstrates that HDX data can inform the manual refinement and improve homology models.

Model C (Figure 3.1C and Table 3.2) was developed in the same manner as Models A and B, but used 3MK7c as a template. Model C gives better agreement for the second heme-binding region, 109-127, than do Models A and B (Table 3.2). It also decreased the number of regions of disagreement. The model points to a highly open structure, however, and it does not form the

expected two cytochrome *c*-type folds as seen in the other models. Thus, Model C, although affording better agreement in the second heme region, is not a good model overall for DHCC.

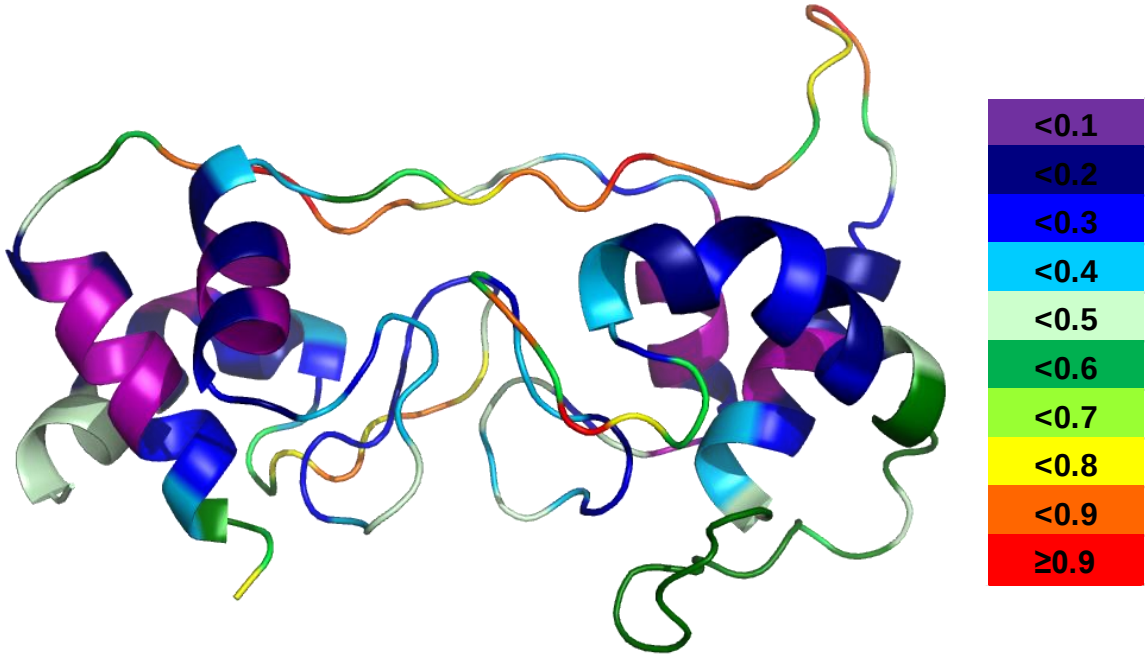

Figure 3.2 Model D with disorder prediction data. Warmer color and larger number indicates more disordered region. Color codes are shown on the right edge.

Model D (Figure 3.1D and Table 3.2) was generated from the online suites I-TASSER and Phyre2, and nearly identical results were obtained from running both I-TASSER and Phyre2. Both packages identified 3MK7c as the best template, gave highly similar alignments and consequently identical models. Model D is presented as that obtained by using Phyre2. It is consistent with the HDX results in all regions of the subunit except 38-44, 50-57, and 130-138 (Figure 3.1D and Table 3.2). These regions are loops in Model D; however, they undergo lower HDX, more typical of a rigid region. The Phyre2 software includes a disorder prediction, identifying secondary and tertiary structure (Figure 3.2), and a disorder prediction analysis was performed on Model D. More order is predicted for all three regions of disagreement, suggesting

that, although they are not alpha helices, there is more order in the region than can be explained by a loop. The order in these regions is likely caused by the interaction of the chains across the domains, as these regions are in the middle where the two domains interact. Thus, the regions of disagreement are actually areas of partial agreement. The region containing residues 130-138 is the only region that is inconsistent with all four models and across the three software packages, suggesting that the region is different than that seen in the templates. Taking all the evidence together, we conclude that Model D best agrees with the HDX data.

3.3.5 SASA calculation shows Model D correlates best with the HDX data

Table 3.3 Comparison of HDX Data and Solvent Accessible Surface Area for Homology Models

Region	deuterium uptake level	SASA-Backbone Only (Å^2)			
		A	B	C	D
1-29	44%	8	8	23	12
33-37	50%	6	1	16	15
38-44	25%	2	2	14	7
45-49	3%	0	1	11	0
50-57	27%	10	18	9	10
58-65	50%	13	10	15	17
78-91	32%	8	5	8	10
92-108	52%	5	10	19	13
109-127	44%	13	13	17	16
128-142	23%	8	3	16	12
143-149	1%	0	0	9	4
150-168	42%	12	13	17	14
169-172	3%	8	0	1	0
173-208	68%	10	26	16	21

Legend:

Category	Structure	HDX range	SASA range (Å^2)
I	h bundle	1 to 17	0 to 6.5
IV	h	17-34	6.5-13
III	h/l	34-51	13-19.5
II	l	51-68	19.5-26

A correlation of SASA at the peptide level (calculated as an average of the SASA for the individual amino acids comprising the region) and the average extents of HDX for the corresponding peptide regions confirmed our assignment of model D as the best homology model of DHCC (Figures 3.3 and Table 3.3). This model gave the best correlation coefficient in

comparison to correlations with Models A-C. In fact, the SASA analysis only disagreed in only one area with Model D. Model C has the most open structure, thus with larger SASA values. Overall, the SASA analysis is a more quantitative assessment to illustrate that Model D is the best model presented thus far.

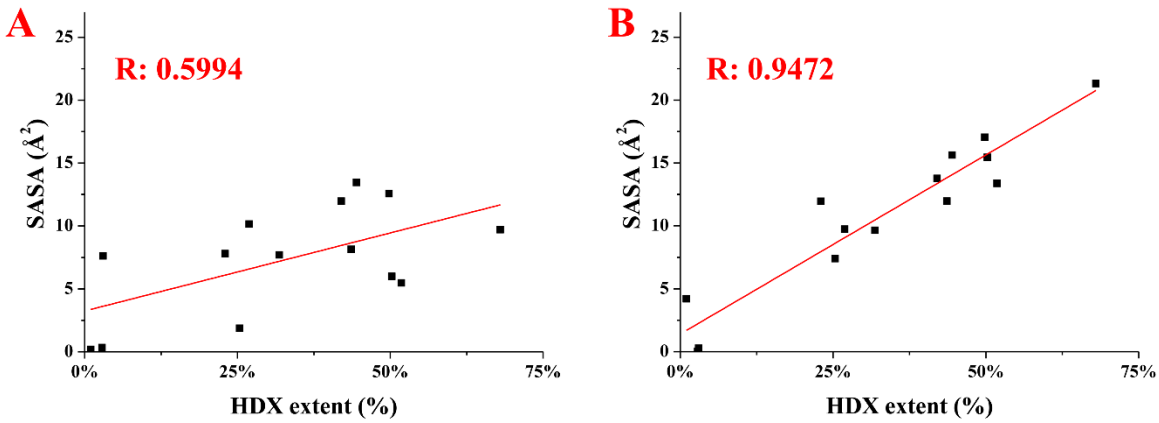

Figure 3.3 Correlation of HDX and SASA data for both Model A (A) and D (B). The Pearson correlation coefficients R's are shown in red. Similar plots for the other models are in the supplemental information.

3.3.6 HDX data mapping onto Model D

To view the two redox states at the protein level, we mapped the HDX differences between the two redox states of DHCC taken as an average of the differences for each time point onto homology Model D (Figure 3.4). The most prominent difference occurs for the short helix in the heme 2 domain (colored in blue in Figure 3.4). In agreement with the kinetic traces, most helical and loop regions around the heme sites have larger differences, indicating that structural changes accompany the redox chemistry. Adding credibility to this conclusion is that the cores of the two helix bundles show no significant changes.

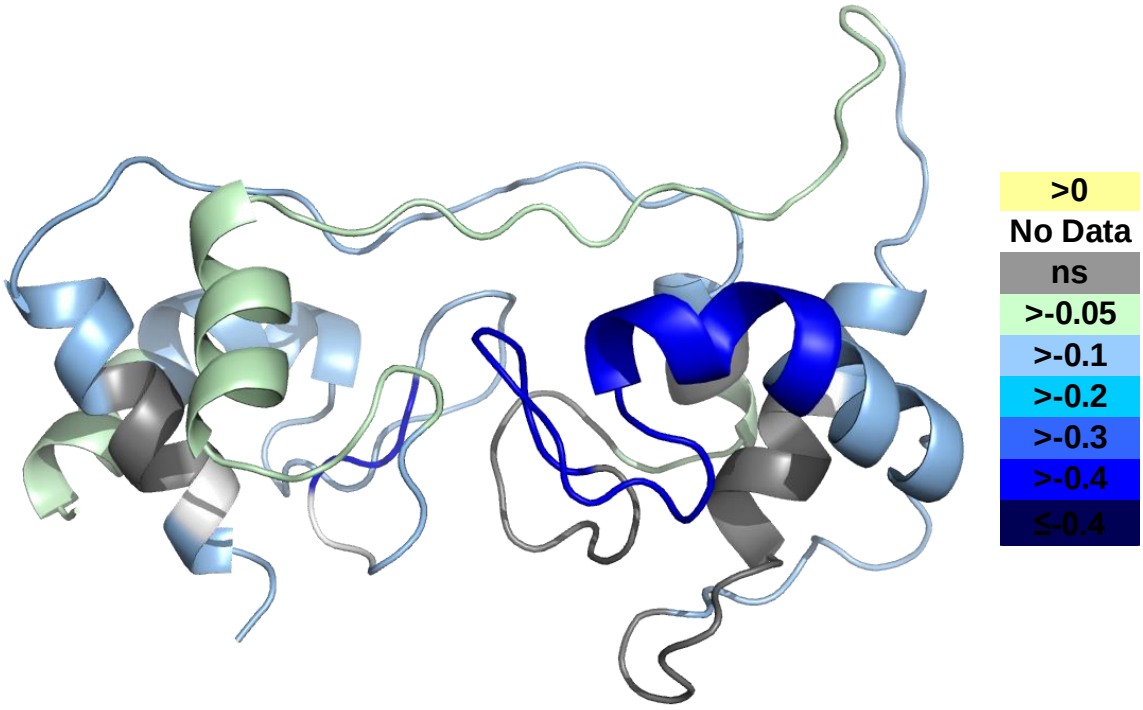

Figure 3.4 The deuterium uptake differences between the oxidized and reduced states of DHCC are mapped onto Model D. Color codes show the differences (reduced state subtracted by the oxidized state).

We also mapped the extent of HDX for all the peptide regions onto our best model, Model D, with a color scheme indicating the amount of exchange at each time point (Figure 3.5). Instead of an overall picture of kinetics information as in Figure 3.4, these maps show the dynamics of the protein at each time point. By comparing the same state at different times, we see most of the regions of oxidized state are dynamic, acquiring more deuterium (increasingly warmer colors).

General features of the protein's secondary structure are seen by the different HDX extents. Loop regions achieve either a higher level of HDX than helices or a similar level at an earlier time. Those loops undergoing less HDX are more ordered and constrained by interactions within the protein. The core regions within the helix bundle are always seen as cold colors, indicating they are so inflexible that HDX is small. The data reveal important trends about the impact of changing redox states as well as the secondary and tertiary structural and solvent accessibility changes of DHCC.

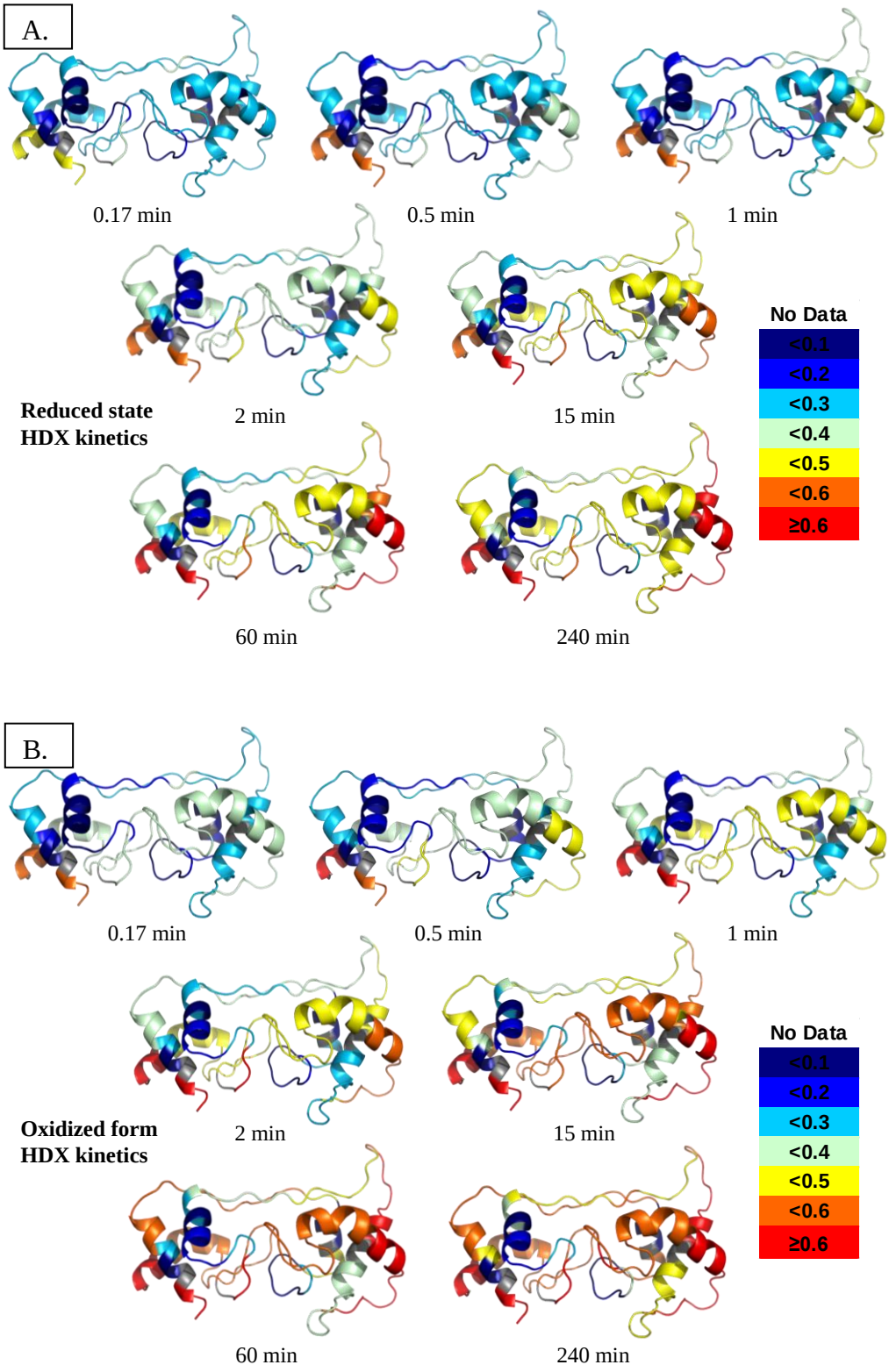

Figure 3.5 The deuterium uptake levels for all peptides are mapped with color for each exchange point onto Model D. The figures for oxidized state are in (A) and reduced in (B). Color codes are shown on the right edge.

3.3.7 Proposed function of DHCC

HDX provides kinetics and dynamics information on the peptide-level of DHCC in both reduced and oxidized states, whereas HM provides a potential protein structure even in the absence of a crystal structure. HM can only yield models that are as good as the information entered, and they cannot provide the high-resolution structural information of a crystal structure. The approach described here takes HM statistics and complements them with HDX results to assess model agreement. We used HDX data to refine Model A and correct areas of disagreement to generate Model B. Likewise, we used HDX to determine if Model B were more informative, and we found that it is in better agreement with HDX than Model A, demonstrating the utility of HDX data for testing and refining a homology model. Comparing all four models, we found that Model D had the highest HM statistics and the best agreement with HDX, including a good correlation with SASA. We subsequently selected it as the best model for the protein structure.

Functionally, the choice of templates will bias the model predicted. The DHCCs 1ETP and 3MK7c are the best templates for structural alignments and are both soluble proteins that contain two *c*-type hemes. Neither protein has been chemically oxidized or reduced; thus, the template structure is probably a mix of both forms. 1ETP, from *Pseudomonas stutzeri,* is a periplasmic diheme cytochrome c_4. It does not belong to a complex but instead shuttles electrons between complexes in an electron-transport chain. The two hemes are located in different protein environments, yielding two distinct redox potentials and allowing for inter-heme electron transfer. The protein 3MK7c, from *P. stutzeri,* is a subunit of the cbb_3 cytochrome oxidase. Like DHCC, 3MK7c is a soluble subunit with an N-terminal anchor. The cytochrome cbb_3 complex, however, moves electrons in the opposite direction of the cytochrome *bc* complex. As for 1ETP,

3MK7c has two distinct redox potentials, but they differ to a greater extent than do those of 1ETP. Inter-heme electron transfer is still observed. Based on their biological roles, 3MK7c is closer functionally to DHCC. This agrees with the observation that Model D accommodates better the HM parameters and the HDX data.

Numerous solution-based spectroscopic and computational studies have shown that there is a conformational change between the reduced and oxidized states of horse heart cytochrome *c*[40, 41]. These results are in apparent conflict with high-resolution crystallographic data that show the crystal structures of the two states are similar[54]. One explanation is that the solid-state X-ray structure does not reflect the solution structure, which is likely to be dynamic. It was proposed that the oxidized state undergoes lower-frequency and larger-amplitude motions than the reduced state[55]. Our HDX results for DHCC suggest that there are significant structural differences between the two different redox states. It is also possible that both X-ray structures represent the reduced form of the protein, produced by X-ray irradiation.

Just as the HDX kinetics suggest a redox-dependent conformational change for DHCC, they also indicate areas that are likely more solvent-accessible (less H-bonded). The heme 2 domain particularly exhibits faster exchange. It follows that the heme 2 domain interacts with the soluble electron acceptor cytochrome c_{553}. Similarly, *in vivo*, the heme 1 domain would have an N-terminal helix anchoring the protein to the *b* and IV subunits of the *bc* complex. Heme 1 would also then interact with the Rieske subunit. These subunit-subunit interactions would lower the HDX rates in the heme 1 region, as is observed.

For monoheme cytochromes, electron transfer is a two-step process. After the electron donor binds with and reduces the cytochrome, the cytochrome binds the electron acceptor and passes the electron to it. DHCC, as other diheme cytochrome *c*'s, adds one more step, the

intramolecular inter-heme electron transfer. In DHCCs from other species, the two hemes usually possess two distinct macroscopic redox potentials (e.g., 240 mV and 330 mV for cytochrome c_4 from *P. stutzeri*). The values are consistent with the negative and positive electrostatic charges of the two domains[11]. The direction of the electrostatic field within the protein gives rise to the distinct heme redox potentials and directs the flow of the electron from the lower to higher potential heme. The DHCC from *Heliobacterium* cytochrome *bc* complex, as studied here, however, has only one resolvable redox mid-potential[42], indicating similar chemical environments around the two heme-binding pockets. The HDX kinetics data are consistent with this observation. The significant conformational changes upon reduction, as revealed by HDX, may work to facilitate an inter-heme electron transfer despite the observation of a single mid-point potential *in vitro*. Our results point to formation of a closed structure upon reduction of the protein, providing a closer distance between the two hemes. In *P. stutzeri*, the inter-heme electron transfer occurs upon hydrogen-bond formation between the heme propionate groups and a surrounding hydrogen-bond network established by a conformational change to the reduced state, producing the closer heme-heme distance and an altered heme environment. Such alterations change the redox potential and facilitate inter-heme electron transfer. It is likely that only one redox potential is observed *in vitro* because the heme environments are sensitive to the truncated N-terminal helix and subunit interactions that are missing in the expressed DHCC. Thus, our prediction is consistent with the *in vitro* data.

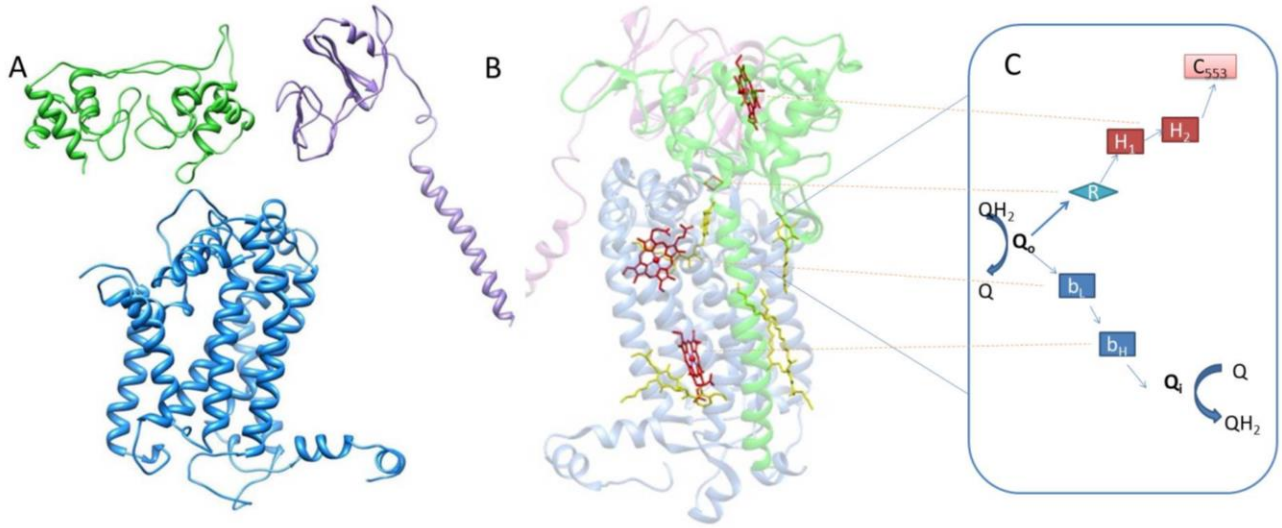

Figure 3.6 *bc* Complex Model (A) and (B) Assumed dimer of the *H. modesticaldum* cytochrome *bc* complex. Blue- cytochrome *b* subunit, Purple- Fe-S subunit, Green- cytochrome *f* subunit. A) Imagined left half of dimer shown as homology modelled subunits of the *H. modesticaldum* cytochrome *bc* complex. B) Right side of the dimer shown as the solved crystal structure of the cytochrome bc_1 complex from *R. sphaeroides* used as the template for 7A. Heme cofactors highlighted in red. (C) Proposed *H. modesticaldum* cytochrome *bc* complex bifurcated electron transfer steps and mechanism. Q- quinones, Q_o- quinone oxidation site, Q_i- quinone reduction site, R- Rieske Fe-S, $b_{L,H}$- *b*-type hemes, $H_{1,2}$- DHCC *c*-type hemes, c_{553}- electron acceptor soluble cytochrome c_{553}.

On the basis of the evidence discussed above, we can propose a potential complex mechanism for the *H. modelsicaldum bc* complex (Figure 3.6). As for other bc_1 or b_6f complexes, menaquinol enters at the Q_o site[56, 57]. Two electrons and two protons are removed, one at a time in a bifurcated electron transfer. The first electron is transferred quickly to the Rieske iron-sulfur cluster, reducing the Rieske cluster and causing it to move towards the periplasm, preventing rapid back transfer of the electron to Q_o. The Rieske cluster is then in position to transfer an electron to heme 1 of DHCC. Docking of the Rieske cluster is probably the first step in inducing the redox-based conformational changes of DHCC. Based on the mechanism of interheme electron transfer within other diheme cytochrome *c*'s, reducing heme 1 changes the conformation and causes formation of a hydrogen-bonding network that permits rapid inter-heme electron transfer. Heme 2 then donates the electron to soluble cytochrome c_{553}, which departs, allowing

the Rieske to return to Q_o. The second electron would then travel down the *b* heme pathway, reducing menaquinone at the Q_i site. Another menaquinol docks and the process repeats, completing one turnover of the *bc* complex and translocating a net of two protons to the periplasm.

Such a mechanism is efficient for many species with a monoheme but not with a diheme cytochrome. Dihemes often result from gene duplication that could be random[6]. However, multi-heme systems in nature serve to transport electrons rapidly or to store electrons[58]. In the mechanism proposed here, the diheme is fulfilling both of these functions. The interheme electron transfer has been observed to be very rapid compared to transfer to a donor and can be used to prevent back reaction with the Rieske cluster. Additionally, if cytochrome c_{553} is scarce or turning over at a slower rate than the *bc* complex, the diheme can store an electron and wait for cytochrome c_{553} without significantly hindering the turnover rate of the *bc* complex. Further study, particularly crystallographic information and inhibitor studies, will clarify these mechanistic proposals.

3.4 Conclusions

HDX data, when used in conjunction with HM and verified by SASA, improves protein structure models and allows mechanistic predictions. For DHCC, HDX kinetic analysis reveals that the oxidized state is more dynamic and open than the reduced one. This is seen in loop regions that generally undergo more extensive HDX at shorter times. The bundle core regions do not show significant differences between the redox states, suggesting that they are stable and undergo little conformational change during redox cycling. Redox-dependent conformational change facilitates the formation of potential hydrogen bonds, permitting inter-heme electron

transfer. The dynamics data reveal faster uptake on the heme 2 domain, suggesting that it is the site of electron donation to cytochrome c_{553}. This evidence is used to predict the mechanism for the *bc* complex of *H. modesticaldum*.

The chapter provides insight on the relation of conformational change to the binding of the electron donor Rieske subunit and soluble electron accepter, cytochrome c_{553}, and on the function of the DHCC subunit within the *bc* complex of *H. modesticaldum* photosynthetic electron-transfer chain. In addition, we believe that the combined approach of modeling and protein footprinting will be useful in other problems in structural biology where protein crystal or NMR structures are lacking. Information at the amino-acid level, such as that can be provided by HDX with electron-capture dissociation or electron-transfer dissociation or by OH radical footprinting (e.g., FPOP), will improve the ability to distinguish models. This method also paves the way to study many of the proteins discussed in this thesis that are examples of novel protein structure and lacking related structures in the literature. Many anoxygenic photosynthetic proteins remain poorly characterized because of the limited information available for comparison. Such a method as this will be a useful in such unique systems.

References

1. Margoliash, E. (1963) Primary Structure and Evolution of Cytochrome C, *Proceedings of the National Academy of Sciences of the United States of America 50*, 672-679.
2. Wallace, C. J., and Clark-Lewis, I. (1992) Functional role of heme ligation in cytochrome c. Effects of replacement of methionine 80 with natural and non-natural residues by semisynthesis, *The Journal of biological chemistry 267*, 3852-3861.
3. Wuttke, D. S., and Gray, H. B. (1993) Protein Engineering as a Tool for Understanding Electron-Transfer, *Curr Opin Struc Biol 3*, 555-563.
4. Van Beeumen, J. (1991) Primary structure diversity of prokaryotic diheme cytochromes c, *Biochimica et biophysica acta 1058*, 56-60.
5. Di Rocco, G., Battistuzzi, G., Bortolotti, C. A., Borsari, M., Ferrari, E., Monari, S., and Sola, M. (2011) Cloning, expression, and physicochemical characterization of a new

diheme cytochrome c from Shewanella baltica OS155, *Journal of biological inorganic chemistry : JBIC : a publication of the Society of Biological Inorganic Chemistry 16*, 461-471.
6. Gibson, H. R., Mowat, C. G., Miles, C. S., Li, B. R., Leys, D., Reid, G. A., and Chapman, S. K. (2006) Structural and functional studies on DHC, the diheme cytochrome c from Rhodobacter sphaeroides, and its interaction with SHP, the sphaeroides heme protein, *Biochemistry 45*, 6363-6371.
7. Baymann, F., and Nitschke, W. (2010) Heliobacterial Rieske/cytb complex, *Photosynthesis research 104*, 177-187.
8. Kadziola, A., and Larsen, S. (1997) Crystal structure of the dihaem cytochrome c4 from Pseudomonas stutzeri determined at 2.2A resolution, *Structure 5*, 203-216.
9. Xiong, J., Inoue, K., and Bauer, C. E. (1998) Tracking molecular evolution of photosynthesis by characterization of a major photosynthesis gene cluster from Heliobacillus mobilis, *Proceedings of the National Academy of Sciences of the United States of America 95*, 14851-14856.
10. Ducluzeau, A. L., Chenu, E., Capowiez, L., and Baymann, F. (2008) The Rieske/cytochrome b complex of Heliobacteria, *Biochimica et biophysica acta 1777*, 1140-1146.
11. Raffalt, A. C., Schmidt, L., Christensen, H. E., Chi, Q., and Ulstrup, J. (2009) Electron transfer patterns of the di-heme protein cytochrome c(4) from Pseudomonas stutzeri, *Journal of inorganic biochemistry 103*, 717-722.
12. Sattley, W. M., Madigan, M. T., Swingley, W. D., Cheung, P. C., Clocksin, K. M., Conrad, A. L., Dejesa, L. C., Honchak, B. M., Jung, D. O., Karbach, L. E., Kurdoglu, A., Lahiri, S., Mastrian, S. D., Page, L. E., Taylor, H. L., Wang, Z. T., Raymond, J., Chen, M., Blankenship, R. E., and Touchman, J. W. (2008) The genome of Heliobacterium modesticaldum, a phototrophic representative of the Firmicutes containing the simplest photosynthetic apparatus, *Journal of bacteriology 190*, 4687-4696.
13. Sattley, W. M., and Blankenship, R. E. (2010) Insights into heliobacterial photosynthesis and physiology from the genome of Heliobacterium modesticaldum, *Photosynthesis research 104*, 113-122.
14. Tang, K. H., Yue, H., and Blankenship, R. E. (2010) Energy metabolism of Heliobacterium modesticaldum during phototrophic and chemotrophic growth, *BMC microbiology 10*, 150.
15. Sarrou, I., Khan, Z., Cowgill, J., Lin, S., Brune, D., Romberger, S., Golbeck, J. H., and Redding, K. E. (2012) Purification of the photosynthetic reaction center from Heliobacterium modesticaldum, *Photosynthesis research 111*, 291-302.
16. Margoliash, E., and Schejter, A. (1966) Cytochrome c, *Advances in protein chemistry 21*, 113-286.
17. Salemme, F. R. (1977) Structure and function of cytochromes c, *Annual review of biochemistry 46*, 299-329.
18. Mines, G. A., Pascher, T., Lee, S. C., Winkler, J. R., and Gray, H. B. (1996) Cytochrome c folding triggered by electron transfer, *Chemistry & biology 3*, 491-497.
19. Pascher, T., Chesick, J. P., Winkler, J. R., and Gray, H. B. (1996) Protein folding triggered by electron transfer, *Science 271*, 1558-1560.
20. Feinberg, B. A., Liu, X., Ryan, M. D., Schejter, A., Zhang, C., and Margoliash, E. (1998) Direct voltammetric observation of redox driven changes in axial coordination and

intramolecular rearrangement of the phenylalanine-82-histidine variant of yeast iso-1-cytochrome c, *Biochemistry 37*, 13091-13101.
21. Baddam, S., and Bowler, B. E. (2006) Tuning the rate and pH accessibility of a conformational electron transfer gate, *Inorganic chemistry 45*, 6338-6346.
22. Bandi, S., Baddam, S., and Bowler, B. E. (2007) Alkaline conformational transition and gated electron transfer with a Lys 79 --> his variant of iso-1-cytochrome c, *Biochemistry 46*, 10643-10654.
23. Bandi, S., and Bowler, B. E. (2008) Probing the bottom of a folding funnel using conformationally gated electron transfer reactions, *Journal of the American Chemical Society 130*, 7540-7541.
24. Takano, T., and Dickerson, R. E. (1981) Conformation change of cytochrome c. II. Ferricytochrome c refinement at 1.8 A and comparison with the ferrocytochrome structure, *Journal of molecular biology 153*, 95-115.
25. Trewhella, J., Carlson, V. A., Curtis, E. H., and Heidorn, D. B. (1988) Differences in the solution structures of oxidized and reduced cytochrome c measured by small-angle X-ray scattering, *Biochemistry 27*, 1121-1125.
26. Calvert, J. F., Hill, J. L., and Dong, A. (1997) Redox-dependent conformational changes are common structural features of cytochrome c from various species, *Archives of biochemistry and biophysics 346*, 287-293.
27. Oellerich, S., Wackerbarth, H., and Hildebrandt, P. (2002) Spectroscopic characterization of nonnative conformational states of cytochrome c, *Journal of Physical Chemistry B 106*, 6566-6580.
28. Kelly, S. M., Jess, T. J., and Price, N. C. (2005) How to study proteins by circular dichroism, *Biochimica et biophysica acta 1751*, 119-139.
29. Storaska, A. J., and Neubig, R. R. (2013) NMR methods for detection of small molecule binding to RGS4, *Methods in enzymology 522*, 133-152.
30. Davis, A. M., Teague, S. J., and Kleywegt, G. J. (2003) Application and limitations of X-ray crystallographic data in structure-based ligand and drug design, *Angew Chem Int Ed Engl 42*, 2718-2736.
31. Chalmers, M. J., Busby, S. A., Pascal, B. D., West, G. M., and Griffin, P. R. (2011) Differential hydrogen/deuterium exchange mass spectrometry analysis of protein-ligand interactions, *Expert review of proteomics 8*, 43-59.
32. Kaltashov, I. A., Bobst, C. E., and Abzalimov, R. R. (2009) H/D exchange and mass spectrometry in the studies of protein conformation and dynamics: is there a need for a top-down approach?, *Analytical chemistry 81*, 7892-7899.
33. Roder, H., Elove, G. A., and Englander, S. W. (1988) Structural characterization of folding intermediates in cytochrome c by H-exchange labelling and proton NMR, *Nature 335*, 700-704.
34. Wales, T. E., and Engen, J. R. (2006) Hydrogen exchange mass spectrometry for the analysis of protein dynamics, *Mass spectrometry reviews 25*, 158-170.
35. Zhang, Z., and Smith, D. L. (1993) Determination of amide hydrogen exchange by mass spectrometry: a new tool for protein structure elucidation, *Protein Science 2*, 522-531.
36. Amon, S., Trelle, M. B., Jensen, O. N., and Jorgensen, T. J. (2012) Spatially resolved protein hydrogen exchange measured by subzero-cooled chip-based nanoelectrospray ionization tandem mass spectrometry, *Analytical chemistry 84*, 4467-4473.
37. Liu, T., Pantazatos, D., Li, S., Hamuro, Y., Hilser, V. J., and Woods, V. L., Jr. (2012)

Quantitative assessment of protein structural models by comparison of H/D exchange MS data with exchange behavior accurately predicted by DXCOREX, *Journal of the American Society for Mass Spectrometry 23*, 43-56.
38. Hamuro, Y., Burns, L., Canaves, J., Hoffman, R., Taylor, S., and Woods, V. (2002) Domain organization of D-AKAP2 revealed by enhanced deuterium exchange-mass spectrometry (DXMS), *Journal of molecular biology 321*, 703-714.
39. Hsu, Y. H., Burke, J. E., Li, S., Woods, V. L., Jr., and Dennis, E. A. (2009) Localizing the membrane binding region of Group VIA Ca2+-independent phospholipase A2 using peptide amide hydrogen/deuterium exchange mass spectrometry, *The Journal of biological chemistry 284*, 23652-23661.
40. Ulmer, D. D., and Kagi, J. H. (1968) Hydrogen-deuterium exchange of cytochrome c. I. Effect of oxidation state, *Biochemistry 7*, 2710-2717.
41. Nabedryk-Viala, E., Thiery, C., Calvet, P., and Thiery, J. M. (1976) Hydrogen-isotope exchange of oxidized and reduced cytochrome c. A comparison of mass spectrometry and infrared methods, *European journal of biochemistry / FEBS 61*, 253-258.
42. Yue, H., Kang, Y., Zhang, H., Gao, X., and Blankenship, R. E. (2012) Expression and characterization of the diheme cytochrome c subunit of the cytochrome bc complex in Heliobacterium modesticaldum, *Archives of biochemistry and biophysics 517*, 131-137.
43. Anand, G. S., Law, D., Mandell, J. G., Snead, A. N., Tsigelny, I., Taylor, S. S., Ten Eyck, L. F., and Komives, E. A. (2003) Identification of the protein kinase A regulatory RIalpha-catalytic subunit interface by amide H/2H exchange and protein docking, *Proceedings of the National Academy of Sciences of the United States of America 100*, 13264-13269.
44. Harms, M. J., Eick, G. N., Goswami, D., Colucci, J. K., Griffin, P. R., Ortlund, E. A., and Thornton, J. W. (2013) Biophysical mechanisms for large-effect mutations in the evolution of steroid hormone receptors, *Proceedings of the National Academy of Sciences of the United States of America 110*, 11475-11480.
45. Hsu, S., Kim, Y., Li, S., Durrant, E. S., Pace, R. M., Woods, V. L., Jr., and Gentry, M. S. (2009) Structural insights into glucan phosphatase dynamics using amide hydrogen-deuterium exchange mass spectrometry, *Biochemistry 48*, 9891-9902.
46. Noble, A. J., Zhang, Q., O'Donnell, J., Hariri, H., Bhattacharya, N., Marshall, A. G., and Stagg, S. M. (2013) A pseudoatomic model of the COPII cage obtained from cryo-electron microscopy and mass spectrometry, *Nature structural & molecular biology 20*, 167-173.
47. Xu, H., and Freitas, M. A. (2007) A mass accuracy sensitive probability based scoring algorithm for database searching of tandem mass spectrometry data, *BMC bioinformatics 8*, 133.
48. Pascal, B. D., Willis, S., Lauer, J. L., Landgraf, R. R., West, G. M., Marciano, D., Novick, S., Goswami, D., Chalmers, M. J., and Griffin, P. R. (2012) HDX workbench: software for the analysis of H/D exchange MS data, *Journal of the American Society for Mass Spectrometry 23*, 1512-1521.
49. Eswar, N., Webb, B., Marti-Renom, M. A., Madhusudhan, M. S., Eramian, D., Shen, M. Y., Pieper, U., and Sali, A. (2006) Comparative protein structure modeling using Modeller, *Current protocols in bioinformatics / editoral board, Andreas D. Baxevanis ... [et al.] Chapter 5*, Unit 5 6.
50. Buschmann, S., Warkentin, E., Xie, H., Langer, J. D., Ermler, U., and Michel, H. (2010)

The structure of cbb3 cytochrome oxidase provides insights into proton pumping, *Science 329*, 327-330.
51. Kelley, L. A., and Sternberg, M. J. (2009) Protein structure prediction on the Web: a case study using the Phyre server, *Nature protocols 4*, 363-371.
52. Roy, A., Kucukural, A., and Zhang, Y. (2010) I-TASSER: a unified platform for automated protein structure and function prediction, *Nature protocols 5*, 725-738.
53. Fraczkiewicz, R., and Braun, W. (1998) Exact and efficient analytical calculation of the accessible surface areas and their gradients for macromolecules, *Journal of Computational Chemistry 19*, 319-333.
54. Rackovsky, S., and Goldstein, D. A. (1984) On the redox conformational change in cytochrome c, *Proceedings of the National Academy of Sciences of the United States of America 81*, 5901-5905.
55. Eden, D., Matthew, J. B., Rosa, J. J., and Richards, F. M. (1982) Increase in apparent compressibility of cytochrome c upon oxidation, *Proceedings of the National Academy of Sciences of the United States of America 79*, 815-819.
56. Malnoe, A., Wollman, F. A., de Vitry, C., and Rappaport, F. (2011) Photosynthetic growth despite a broken Q-cycle, *Nature communications 2*, 301.
57. Hasan, S. S., Yamashita, E., Baniulis, D., and Cramer, W. A. (2013) Quinone-dependent proton transfer pathways in the photosynthetic cytochrome b6f complex, *Proceedings of the National Academy of Sciences of the United States of America 110*, 4297-4302.
58. Burggraf, F., and Koslowski, T. (2014) Charge transfer through a cytochrome multiheme chain: theory and simulation, *Biochimica et biophysica acta 1837*, 186-192.

Supplemental Figures for Chapter 3

Supplemental Figure 3.1 HDX peptide coverage map for DHCC showing 95% coverage. The same peptides with different charge states are also shown.

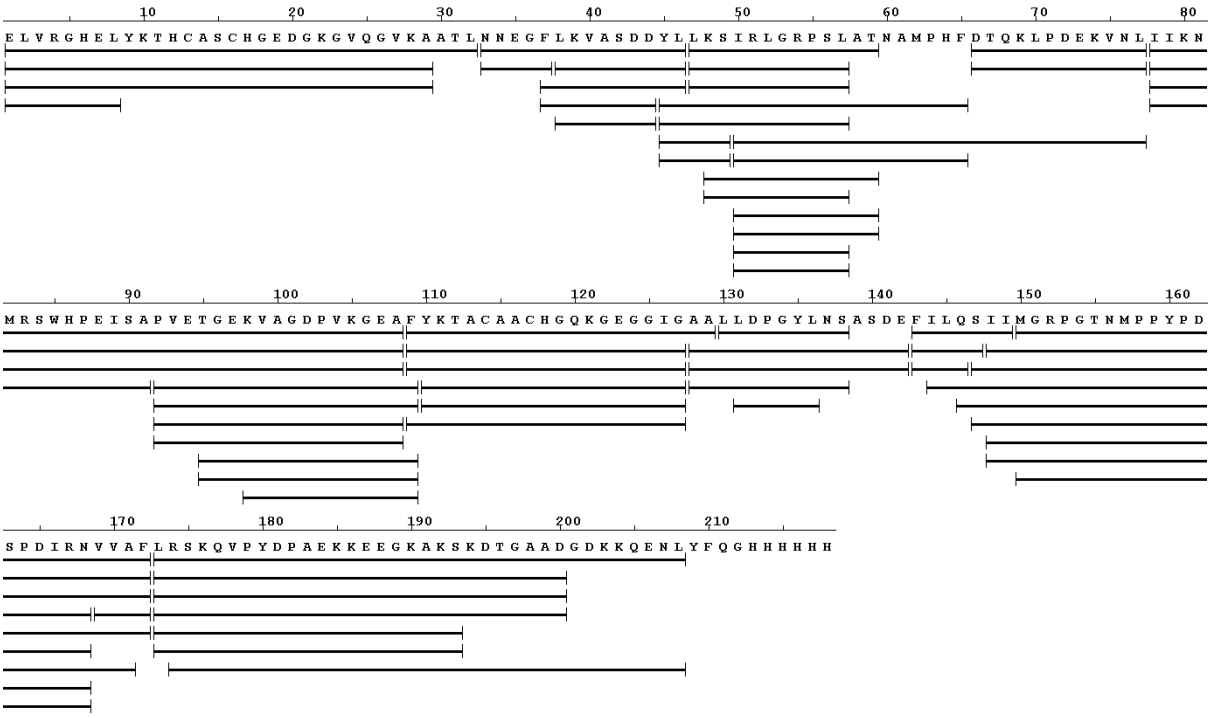

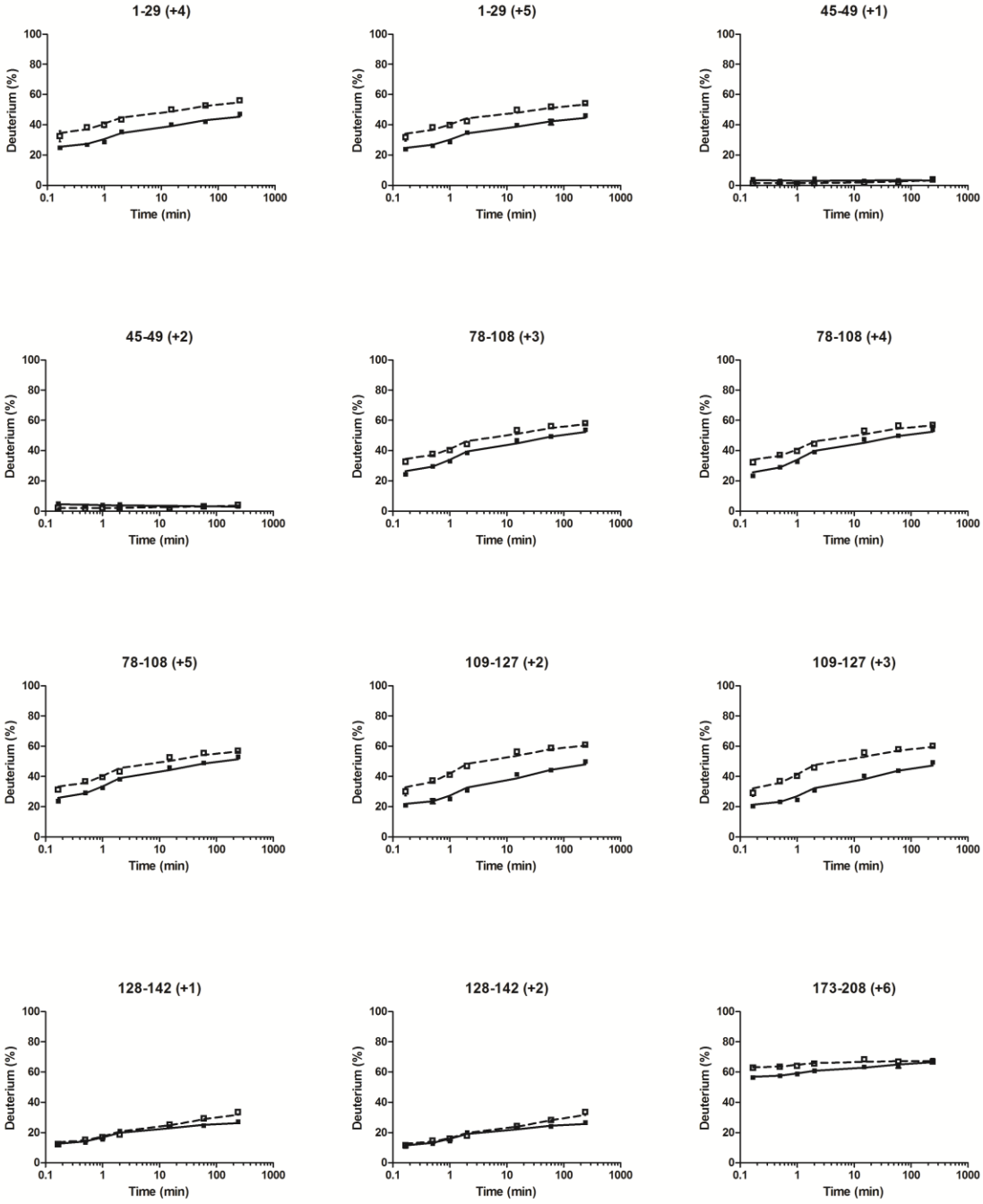

Supplemental Figure 3.2 Kinetic curves of selected peptides used for HDX mapping for reduced (solid line) and oxidized (dash line) states of the DHCC. Numbers in parentheses with "+" sign are the charge states of the peptides.

Chapter 4: Alternative Complex III from phototrophic bacteria and its electron acceptor auracyanin

Portions of this chapter has been previously published as: Majumder, E. L. W., King, J. D. & Blankenship, R. E. Alternative Complex III from phototrophic bacteria and its electron acceptor auracyanin. *Biochimica et Biophysica Acta* **11-12**, 1383-1391 (2013). Used with permission of authors.

4.1 Introduction

In order to survive, organisms need mechanisms to convert and store energy. For many organisms, this involves the establishment of a proton motive force (PMF) by coupling thermodynamically favorable electron transport to proton pumping. For anoxygenic phototrophs, this involves cyclic electron flow around a reaction center and a proton pump. In such systems, the reaction center uses light energy to reduce a quinone to a quinol. The quinol is subsequently oxidized by the proton pump to establish the PMF, and the electrons are donated back to reaction center via a periplasmic electron carrier[1]. Until very recently, it was thought that the cytochrome bc_1 or the related cytochrome b_6f complex were the only complexes able to oxidize quinol and reduce a periplasmic electron carrier in phototrophic organisms. A functional replacement for the cytochrome bc_1 has been recently characterized in the anoxygenic phototroph *Chloroflexus aurantiacus*. The complex has been named Alternative Complex III (ACIII). The complex itself is structurally and evolutionarily unrelated to the cytochrome bc_1 or cytochrome b_6f complexes. Instead, it is a new member of the complex iron-sulfur molybdoenzyme (CISM) superfamily.

The filamentous anoxygenic phototrophs (FAPs) are photosynthetic members of the *Chloroflexi* phylum. The founding member of this phylum, *C. aurantiacus,* was characterized in 1974 by Beverly Pierson and Richard Castenholz[2]. It was originally described as a thermophilic photoheterotroph similar in terms of photosynthetic metabolism to purple phototrophic bacteria. Subsequently, it has been shown to be capable of photoautotrophic growth using the hydroxypropionate cycle instead of the Calvin-Benson cycle[3]. The discovery of its type II reaction center prompted further comparisons with purple bacteria[4]. Despite the presence of very similar reaction center and integral membrane light-harvesting complexes to those found in the

purple bacteria, biochemical and spectroscopic techniques failed to identify a cytochrome bc_1 complex[5]. In the 1980's, a novel group of blue copper proteins were identified in *C. aurantiacus*[6]. The proteins were named auracyanins. Their similar nature to plastocyanin from oxygenic phototrophs and their ability to re-reduce the *C. aurantiacus* reaction center led to the conclusion that the auracyanins functioned as periplasmic electron carriers[7]. A more in-depth characterization of the heme-containing complexes in *C. aurantiacus* led to the discovery of ACIII[8]. Enzyme activity assays subsequently demonstrated ACIII's capacity to oxidize quinol and reduce auracyanins[9].

4.2 Discovery of ACIII

Evidence for ACIII came from two separate sources, a respiratory complex in the nonphototrophic thermophilic bacterium *Rhodothermus marinus* and a photosynthetic complex in *C. aurantiacus*[10,11]. Initially, the proteins were thought to be unrelated, but were later identified as related complexes. In both cases, the membranes of the bacteria were investigated for electron transfer chain components, but no typical complex III or cytochrome bc_1 complex was detected[12,13]. The activity usually held by complex III, menaquinone: electron acceptor oxidoreductase, was observed despite the lack of the traditional complex leading to the search for ACIII[9]. In *R. marinus*, the isolated complex was originally thought to contain *b* and *c* type hemes and donate to a soluble high-potential iron protein (HiPIP)[14]. Work in the *C. aurantiacus* system yielded a complex with only *c* type hemes and was recognized to have high homology with the CISM family[8]. The complex was originally named MFIcc, but after no molybdenum was found the name was changed to ACIII[15]. The respiratory and photosynthetic complexes were both then identified as ACIII when the electron transport activity was confirmed and the genomes

sequenced[9,16]. ACIII is widely distributed in a variety of bacteria phyla and represents a novel mechanism and structure for Complex III or cytochrome bc_1 activity since the ACIII is structurally and evolutionarily unrelated to either complex[17].

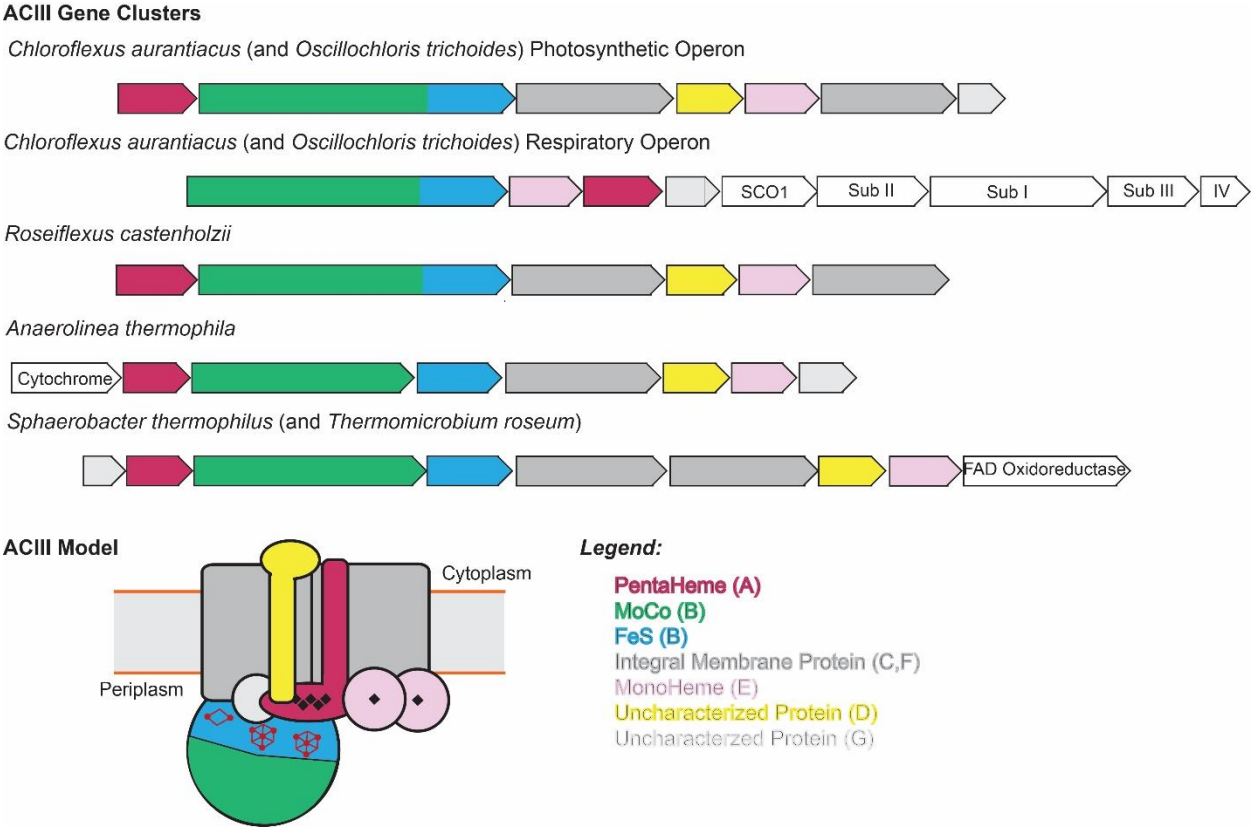

Figure 4.1 Current Model of ACIII. ACIII photosynthetic and respiratory operons from several bacteria. Schematic structure of ACIII as predicted by cross-linking data and topology and homology prediction.

4.3 Protein Subunits of ACIII

ACIII is a novel integral membrane protein with five to seven subunits coded for by genes on one putative operon. Several subunits of ACIII contain high homology to subunits of the energy converting Complex Iron-Sulfur Molybdoenzyme, CISM, protein family. Relations to this family provide clues to understand ACIII. ACIII is composed of 22 putative transmembrane helices, iron-sulfur clusters, *c*-type hemes and a putative quinol oxidation site. The subunits of

ACIII have been named ActA through ActG, with the genes that code for them named *actA* through *actF*. ActG is not found in all organisms that contain the ACIII complex, and in some cases the gene order is different than in *Chloroflexus aurantiacus* (Figure 4.1). Typically in ACIII ActA is a pentaheme subunit with one transmembrane helix and ActB contains iron-sulfur clusters. Act C & F are responsible for most of the transmembrane helices and quinone binding while ActD contributes one transmembrane helix. ActE is a monoheme periplasmic subunit and ActG is a periplasmic subunit of unknown function.

4.3.1 ActA

ActA is a 25 kDa pentaheme protein that is predicted to be oriented in the periplasm with an N-terminal transmembrane helix anchoring the subunit[15,18]. Biochemical prediction software labels the N-terminal region as both a transmembrane helix and a signal peptide[19,20]. For *C. aurantiacus*, mass spectrometry data has shown that the N-terminal region is not cleaved in the native protein indicating the presence of a transmembrane helix not a signal peptide (data not shown). This putative transmembrane helix is predicted to serve as a membrane anchor (Figure 4.1). Yet, in the related *E. coli* nitrite reductase second pentaheme subunit, NrfB, the N-terminal region is a signal peptide that is cleaved off after translocation to the periplasm[21]. Homology modeling of this subunit has been performed using the pentaheme subunit from *E. coli* nitrite reductase, NrfB, as a template (Figure 4.2A)[22-25]. The overall alignment, with the N-terminal signal peptide region truncated, is useful for modeling with 40% similarity, and presents a first look at a potential structure for ActA. NrfB contains hemes with both parallel and perpendicular alignments; however, the sequence in ActA does not contain the residues that typically indicate a parallel heme alignment[21]. The full protein has also been modeled with the N-terminal and C-terminal ends of the dodecaheme protein, cytochrome *c* GSU1996, from *Geobacter*

sulfurreducens (data not shown) revealing that ActA has similarity to other multiheme proteins[26]. Despite having an additional heme and not being related to ACIII, the *Geobacter* protein has higher similarity and identity (Table 4.1).

The homology model in Figure 4.2 is a first guess of the structure of this complicated enzyme. Homology modeling was carried out using Modeller v9.10 to generate the models and Chimera to visualize the results. Modeller takes a template known structure and maps the sequence with unknown structure onto the known structure. Template searching was done by BLAST as well as in Modeller. Sequence alignments were done in BLAST, Mega or Modeller using the ClustalW algorithm. At least 100 models were generated per sequence. The best model was chosen based on three evaluation scores provided in Modeller: DOPE, GA341 and molpdf, rather than a RMSD value. The scores are only sensible relative to the other models generated on the same run so are not seen as comparison across runs or sequences and not presented here. As a general base-line 20% identity is the minimum to construct a good homology model. While some of the identities here are slightly below that benchmark, the alignments are refined more in Modeller than in the simple alignment step, so the results are still meaningful. Also, for some protein families, like NrfD, only one crystal structure is known (2VPW) which limits the template options to one structure.

Table 4.1 Alignment Scores Summary (for global alignment by ClustalW)

ACIII Sequences: Template (PDB Code)	Percent Similarity	Percent Identity
ActA: NrfB (2OZY)	(73/185) 39.5%	(22/185) 11.9%
ActA: GsuN (3OUQ)	(83/185) 44.86%	(34/185) 18.4%
ActA: GsuC (3OUE)	(87/185) 47.0%	(32/185) 17.3%
ActB1: PsrA (2VPW_A)	(365/840) 43.5%	(120/840) 14.3%
ActB2: PsrB (2VPW_B)	(127/259) 49.0%	(64/259) 24.7%
ActC: PsrC (2VPW_C)	(135/331) 40.8%	(53/331) 16.0%
ActF: PsrG (2VPW_G)	(124/285) 43.5%	(39/285) 13.7%
ActC: ActF	(241/486) 49.6%	(88/486) 18.1%
PsrC: PsrG (2VPW)	(191/191) 100%	(191/191) 100%

Multiheme proteins are involved in electron transport where the hemes form a nanowire for efficient electron transfer[26]. The heme redox potentials in ActA for *C. aurantiacus* were determined as -228mV, -110mV and +94mV with a ratio of 3:1:1 respectively. The two remaining redox potentials were +391mV and belong to a dimeric monoheme subunit, ActE[15]. Redox titration measurement of the whole complex in *R. marinus* showed a redox potential range of -45 to +235mV[12]. There is a large difference in the measurement of the redox potentials for the complexes, which may result from having different electron acceptors or being part of different cycles. ActA does not seem to house another cofactor or active site, so the subunit theoretically donates its electrons to the monoheme subunit, ActE[27]. Many enzymes in nature extend their heme nanowires by donating to an additional adjacent heme subunit, as would the case in ACIII if ActA donated to ActE. The electron donor to the pentaheme subunit is still a mystery. A plausible electron source is the Fe-S clusters from ActB, which will be discussed in the next section.

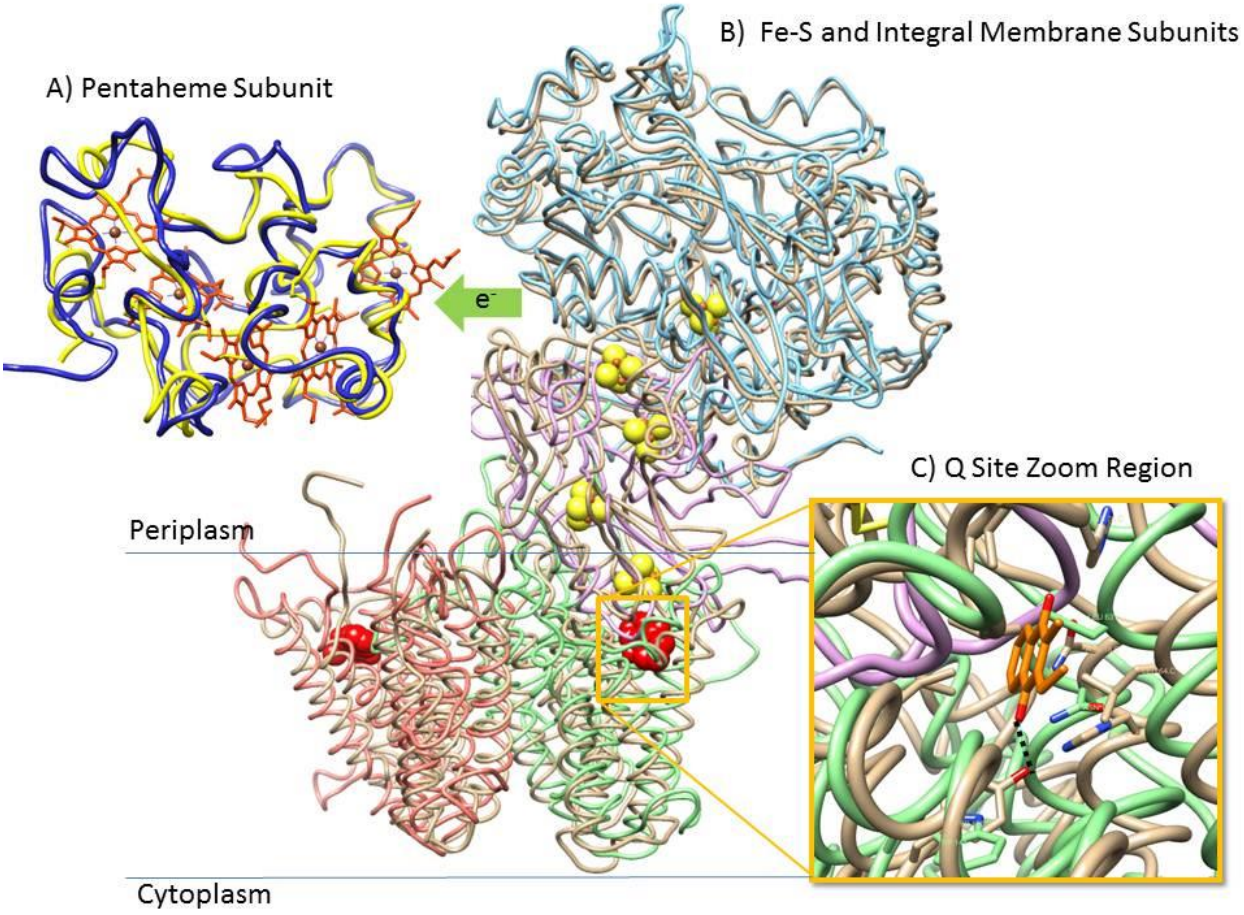

Figure 4.2 Homology Model of Selected Subunits of ACIII. A. ActA (blue) modeled onto NrfB 2OZY (yellow). C type hemes (brown dot with orange-red ligands) are from NrfB. Green arrow denotes putative flow of electrons. **B.** ActB1 (blue), ActB2 (purple), ActC (green) and ActF (pink) independently modeled onto corresponding 2VPW PsrABCG subunits (tan). Iron-Sulfur clusters (yellow), menaquinone-7 (red) and the Molybdopterin cofactor (magenta) are from PSR. **C.** Zoom in of the quinone binding site with MK-7(orange) bound. Subunits making up the pocket are ActC (green), ActB2 (purple) and PsrBC (tan). Side chains of potential hydrogen bonding or other important residues are shown. The known H-bond from PSR is shown (black dashed line).

4.3.2 ActB

ActB is the largest subunit of the ACIII complex with a mass of ca. 113 kDa and is a putative gene fusion product of two smaller genes[8]. The domain referred to as B1 has high homology to subunits that contain a molybdopterin cofactor. Atomic Absorption determination of ACIII has not detected molybdenum, manganese, or tungsten[15]. Mo-cofactor binding residues in ActB are not conserved[27]. Similar mutations occur in other complexes from the CISM family

that also lack molybdenum[28]. Other members of the CISM family have replaced the Mo-cofactor with W, Ni or a lone Fe-S cluster[29]. Thus far, there is no evidence for a cofactor in the B1 domain of ActB from ACIII. B1 comes first in the gene and is putatively located on top of B2 further away from the membrane (Figure 4.1). B1 aligns well with many members of the CISM family and homology modeling has been performed with Polysulfide reductase, PSR, from *Thermus thermophilus* (Figure 4.2B)[30]. Despite the presumed lack of a cofactor or iron sulfur clusters in B1, the model provides a general sense of the structure but does not provide new clues as to the function on the B1 domain. The B1 domain does contain the Twin Arginine Translocase sequence (TAT) sequence that is reported to promote the translocation of the subunit to the periplasm[31]. However, new debate has arisen over the orientation of the B subunit and this issue will be discussed in more detail below.

The B2 domain is the iron-sulfur cluster-containing domain of the ActB subunit. It is the smaller portion of ActB, being the last ca. 251 of 1029 residues in *C. aurantiacus*. Despite high sequence similarity among ACIII's from different families, 57% identity between *C. aurantiacus* and *R. marinus*, the number and type of predicted iron-sulfur clusters has varied in the literature. Biochemical evidence in *C. aurantiacus* yields 17 iron atoms per complex, with seven belonging to hemes and the remaining ten to iron-sulfur clusters, which were assigned as [2Fe-2S] and two [4Fe-4S]based on sequence and number of irons detected[15]. In contrast, biochemical and sequence evidence in *R. marinus* ascribes 21 irons per complex with 15 belonging to one [3Fe-4S] and three [4Fe-4S][16]. EPR work elucidated the [3Fe-4S] cluster in *R. marinus* with a reduction potential of +140mV[12]. Examination of the sequences using known Fe-S binding motifs predict one [3Fe-4S] and two to three [4Fe-4S]. The third [4Fe-4S] cluster has an atypical motif conserved in all ACIIIs. Typical [4Fe-4S] binding motifs have two residues in between the

middle cysteines[32]. Other CISM family Fe-S proteins have more than two residues in the middle with 11-12. ACIII's have 26-33. With the extended spacing, the physiological presence of the third [4Fe-4S] cluster is uncertain. B2 has also been modeled with PsrB (Figure 4.2B). PsrB has four [4 Fe-4S] clusters in a ferredoxin-like fold, but with the same [Fe-S] binding motifs as ACIII. In the model, the Fe-S motifs are intact, but with extra loops from ACIII[30]. The exact content for the Fe-S clusters of ACIII remains to be determined.

The orientation of the ActB subunit with respect to the membrane has been a topic of debate. Cross-linking data from *C. aurantiacus* placed ActB in cytoplasm[15]. However, a TAT sequence is present on the N-terminus of the protein, which suggests a periplasmic location[8,27]. Recent sequence investigation proposed that for the TAT translocation to be active, additional motifs later on in the sequence are necessary, but these motifs are not present in ACIII, again suggesting a cytoplasmic orientation[27]. Homology modeling presented here aligns ActB in a periplasmic orientation based modeling with the periplasmically located PsrAB as a template (Figure 4.2B). Also, the quinone site in PsrC is on the periplasmic face of the membrane and capped by PsrB, so the iron-sulfur clusters of PsrB are within electron transfer distance. The quinone site of ActC is also modeled in the same manner, with topology prediction also putting the quinone on the periplasmic face (Figure 4.2B & 4.2C)[33,34]. Cross-linking data shows that ActB and ActC interact[15]. ActB would then be located in the periplasm to accommodate electron transfer from a periplasmic faced quinone site, as is seen in the homology modeling (Figure 4.2B). Additionally, the predicted topology of the NrfD domain of ACIII matches the predicted and known topology of the NrfD domain in PsrC (Figure 4.4). Finally, a verification calculation of the predicted topologies was performed using the extrinsic loop similarity method of Weiner[35]. The simple calculation method yielded small agreement with a periplasmic orientation

with a value of 0.222 over the loop similarity average for the CISM NrfD family, but the empirical calculation showed moderate agreement with cytoplasmic orientation (Figure 4.3 and Table 4.2 & 4.3). A similar debate has existed in the case of DMSO reductase from *E. coli* for over twenty years, as biochemical and sequence based evidence continues to accrue[36-38]. DmsABC was the only family presented by Weiner where the calculation did not agree with the experimental data[35]. The answer has not as yet been resolved in DmsABC or ACIII and is not likely to be resolved until more structural data is obtained.

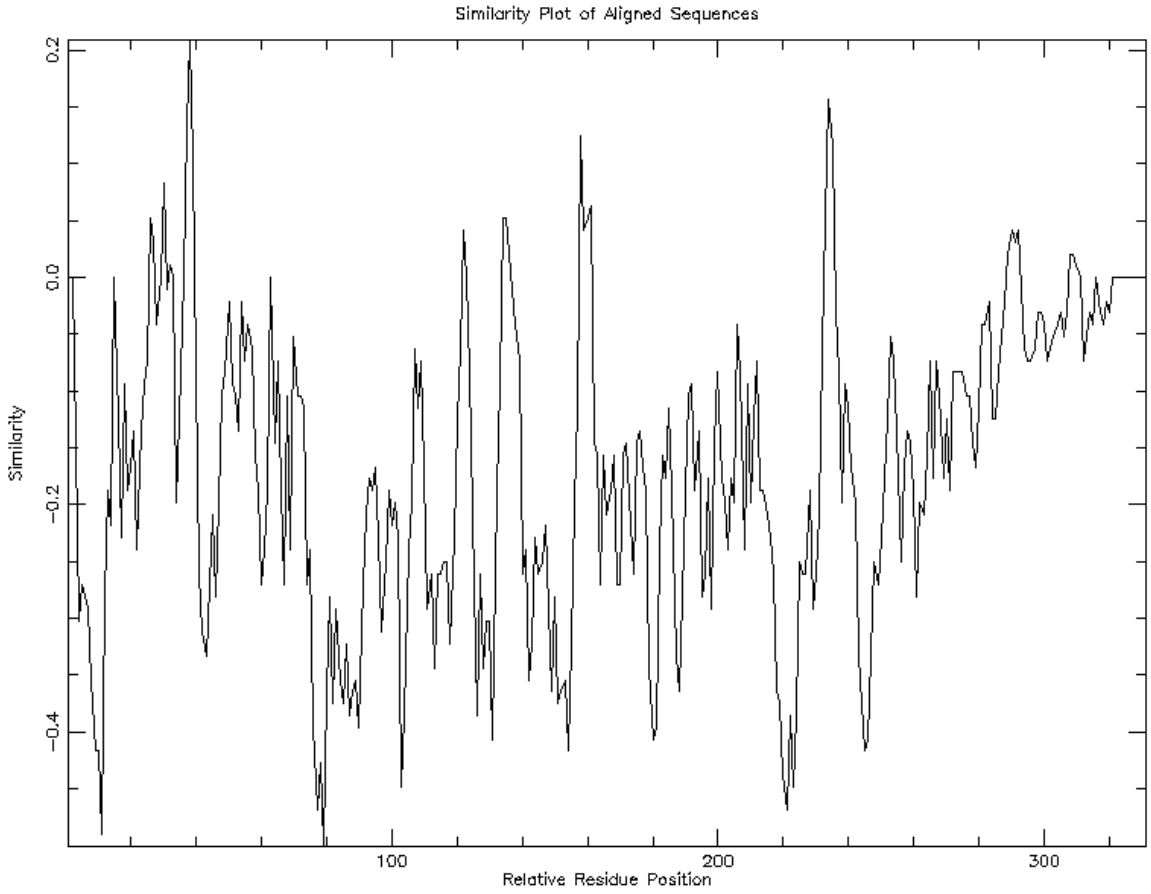

Figure 4.3 Similarity Plot of aligned amino acid sequences from ActCtr, PsrC, NrfD, DmsC by Plotcon for Weiner Method Calculations

Table 4.2 Data from similarity plot

ActC Feature	Residue Number	Average Score (from plot in Figure 4.3)	
N-term P	1 17	-0.25	
TM 1	18-38	-0.075	
Loop 1 C	39-49	-0.125	
TM 2	50-70	-0.11111	
Loop 2 P	71-98	-0.215	
TM 3	99-119	-0.25	
Loop 3 C	120-155	-0.2	
TM 4	156-176	-0.125	
Loop 4 P	177-195	-0.215	
TM 5	196-216	-0.15	
Loop 5 C	217-236	-0.2	
TM 6	237-257	-0.15	
Loop 6 P	258-271	-0.15	
TM 7	272-292	-0.075	
Loop 7 C	293-300	-0.025	
TM 8	301-321	-0.025	
C-term P	322-331	0	
		loop avg	-0.15333
	ActCtr	TM avg	-0.12014

Table 4.3 Weiner Method Calculations

Simple Method	Average score from Table 2				S score		Empirical Method			
	v= -.15333	v is <,>, = loop score			1, 0, -1		Empirical loop value			
N-term P	-0.25	greater			1		-0.0967	P		
Loop 1 C	-0.125	less			1		0.0283	C		
Loop 2 P	-0.215	greater			1		-0.0617	P		
Loop 3 C	-0.2	greater			-1		-0.0467	C		
Loop 4 P	-0.215	greater			1		-0.0617	P		
Loop 5 C	-0.2	greater			-1		-0.0467	C		
Loop 6 P	-0.15	equal			0		0.0033	P		
Loop 7 C	-0.025	less			1		0.1283	C	ap	-0.0635
C term P	0	less			-1		0.1533	P	ac	0.0632
Agreement					**0.2222**				**ac-ap**	**0.1267**
		1= complete agreement, -1= complete disagreement							ac-ap>0 = cytoplasmic subunit	

ap= average of periplasmic loops ac= average

4.3.3 ActC & ActF

ActC and ActF represent the major integral membrane subunits of ACIII. They are highly similar to each other, containing ten transmembrane helices (Supplemental Table 1). ActF is slightly smaller than ActC, with a mass of 46 kDa and 55 kDa respectively, and is likely to have resulted from a gene duplication event[8]. While most ACIII's have both ActC and ActF, some species only have ActC (Figure1). The middle eight helices of both ActC and ActF have high homology of over 40% to the NrfD protein family (Supplemental Table 1). The NrfD family consists of integral membrane proteins that house quinone binding sites[29]. In NrfD proteins with known structures, these eight helices are arranged in two four-helix bundles[30]. The N-terminal bundle hosts the quinone binding site and the C-terminal bundle is involved in proton translocation and uptake from the cytoplasm. The only crystallized NrfD protein PSR also has two identical integral membrane subunits, PsrC and PsrG, which interact via the C-terminal bundles. This interaction suggests a conformationally linked mechanism of proton pumping[30].

The NrfD domain regions of ActC and ActF have been homology modeled onto PsrC and PsrG respectively (Figure 4.2B). Since PsrC and PsrG are identical, the modeling could have been switched. However, since PsrA and PsrB were used for ActB and ActB has been shown to interact with ActC by crosslinking, the model was constructed to match the known interactions by crosslinking. A view of the quinone binding site for the model is also shown with MK-7 bound (Figure 4.2C). Based on modeling, the hydrophobic residues are in place as well as potential ligand binding residues. Previous fluorescence quenching titration work with known quinone oxidation site inhibitor 4-hydroxy-2-heptylquinoline-N-oxide on ACIII has only revealed one quinone oxidation binding site[18]. Although the possibility of more quinone sites cannot be excluded, the presence of one quinone oxidation site that responds to a known

inhibitor suggests a similar mechanism for ACIII and PSR in terms of the integral membrane subunits, quinone site and electron transfer to iron-sulfur clusters. However, isolated ACIII is monomeric, according to blue-native gel analysis and has only one Fe-S containing subunit[15]. Both sides of the dimer in PSR are active with a total of two quinone oxidation sites, so the exact same mechanism is not possible in ACIII. However, we suggest that the conformationally linked motion for proton pumping and the interaction at the one identified quinone site with its iron-sulfur subunit would be conserved. Only the NrfD domains of ACIII ActC & F are used in the homology model, which leaves two α-helices per subunit unaccounted for. The additional helices must have a role in the structure and function of the complex, so the PSR-based model is not a complete picture. However, the high similarity of sequences and similar functions suggest some likely possibilities for ACIII.

Topology Prediction has also been carried out for ActC (Figure 4.4A)[33,34]. The ten transmembrane helices are labeled definitively by software prediction with the N and C-terminals predicted to be cytoplasmic. This puts the eight middle helices in agreement with the NrfD family, which has the N and C-terminals in the periplasm (stars, Figure 4.4A). Homology modeling and extrinsic loop sequence similarity call for the inclusion of the two horizontal periplasmic helices as are found in PSR (H1 & H2, Figure 4.4A). Important residues for quinone binding as well as proton pumping have been identified by sequence alignments, homology modeling and topology prediction (green hexagons Figure 4.4A, colored residues Figure 4.4B). In polysulfide reductase, the quinone binding site is located very close to the periplasmic surface of the membrane and has residues from PsrB putting the cap on the channel. The pocket is formed by hydrophobic residues from the integral membrane subunit. In polysulfide reductase, an asparagine and histidine near the top of helix 1 are potential hydrogen bonding residues while

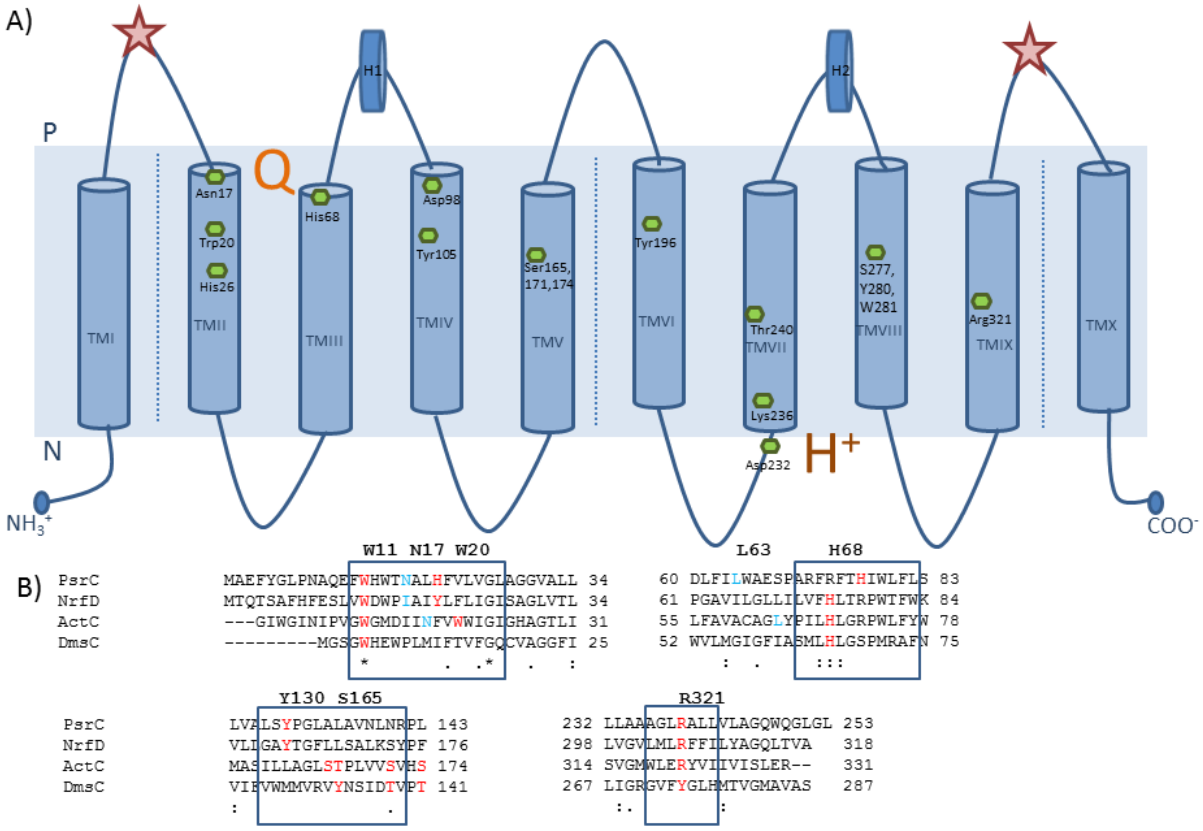

Figure 4.4 ActC Predicted Topology and Alignments. **A.** Predicted topology of ActC. Stars indicate start and end of NrfD domain. Dashed lines indicate predicted regions for four helix bundles. Green Hexagons denote approximate location of conserved or biologically relevant amino acid residues. Orange Q and H^+ show possible location of Quinone binding site and site of proton uptake respectively. H1 and H2 represent putative periplasmic horizontal helices. **B.** Alignment of similar integral membrane subunits from the CISM family. Red and blue letters denote conserved or interesting residues and alternate for visual clarity. PsrC is the integral membrane subunit from polysulfide reductase in *Thermus thermophilus*. NrfD is the integral membrane subunit from nitrite reductase in *E. coli*. ActC is the integral membrane subunit from Alternative Complex III in *C. aurantiacus*. DmsC is the integral membrane subunit from DMSO reductase in *E. coli*.

the tyrosine on helix 5 acts as the primary H-bonding ligand to MK-7[30]. In ACIII ActC there is a corresponding asparagine, Asn17, in the same location at the start of helix II, TMII (green hexagons, Figure 4.4A). A histidine, His26, is found later in TMII but a tryptophan, Trp20, is in

a better location to serve as a Hydrogen bonding site. Although the tyrosine, Tyr130, is conserved in many NrfD proteins, a tyrosine is not predicted in that location for ACIII (Figure 4.4B). The shorter alcohol-containing residue serine in found in approximately the same location with three possible serines within 10 residues on the same helix: Ser165, 171, 174. A tyrosine, Tyr105, on the previous helix may also be a suitable replacement (Figure 4.4A and 4.4B). Other conserved residues on the N-terminal helix bundle of ACIII include His68 and Asp98, which may contribute to the quinone oxidation cycle[30,37]. Based on the similarity and conservation of residues, a periplasmic facing quinone binding site is predicted for ACIII.

Based on the crystal structure for polysulfide reductase, a putative proton-pumping pathway was proposed[30]. Many of the same residues or types of residues are predicted in similar positions within the NrfD domain of ActC. These include: Asp232 for proton uptake from the cytoplasm, other charged residues such as Lys236 and Arg321, of which Arg321 is highly conserved, and polar residues with alcohol functional groups like Thr240, Tyr196, Ser277, Tyr280 or Trp281 (Figure 4.4A&B). The proton channel passes from uptake in the cytoplasm in the C-terminal bundle through the residues listed above, to water molecules that may assist between helix bundles and finally near the Q-site and into the periplasm[30]. Important residues for the primary functions of ACIII, quinone oxidation and proton translocation, are conserved as with other members of the CISM and NrfD families.

4.3.4 ActD and ActG

ActD and ActG are the least characterized subunits of ACIII. ActD at 20 kDa, is predicted to contain one transmembrane helix and was found to be associated with subunit ActB by a long range crosslinker and ActF by a shorter crosslinking agent[15]. ActD is fused to the

pentaheme subunit ActE in genomes belonging to the *Planctomycetes* phylum (data not shown). ActG is a small, 12 kDa, membrane associated subunit with unknown function[9]. As demonstrated in *C. aurantiacus*, it can be selectively removed from the complex by chaotropic agents (Chapter 3). ActG is not found in all ACIII operons. For instance, even though *C. aurantiacus* and *Roseiflexus castenholzii* are closely related photosynthetic bacteria, *R. castenholzii* does not appear to have ActG, as determined from both biochemical and genetic data (Figure 4.1). The contribution of these two subunits should become clearer when more is understood about the structure of the protein.

4.3.5 ActE

ActE is a 23 kDa monoheme soluble periplasmic subunit[8]. Despite the abundance of monoheme cytochrome proteins now known, ActE does not have strong similarity to any of them as determined by protein BLAST[39]. It is putatively the final member of the electron transfer system in ACIII, accepting electrons from ActA and donating electrons to the soluble electron acceptor and carrier auracyanin or soluble cytochromes. ActE would extend the heme network nanowire that sends electrons over a longer distance efficiently and compensates for apparent disagreement in reduction potentials[26]. Recent work has shown ActE to be present in two copies in *C. aurantiacus* despite a singular copy of *actE* in the operon. For *C. aurantiacus*, the reduction potential of the monoheme cytochrome is +391mV in the intact complex and +385mV in the recombinant system, showing agreement between the two systems (Chapter 3). The two copies of ActE could explain the difference in heme-bound iron content between *R. marinus* and *C. aurantiacus*. *R. marinus* sequence based analysis places six irons bound in heme, whereas biochemical work in *C. aurantiacus* indicates seven heme-bound irons in the complex[15,17]. The

exact role of ActE in ACIII electron transfer remains to be determined as well as its ability to interact with soluble electron carriers.

4.4 Putative Electron Transfer Mechanism for ACIII

How all of the subunits fit together in ACIII and exactly what function the enzyme is performing in the cell remain unclear. However, the structural clues from its relation to the CISM family and a lack of other proteins in the genome that could replace its activity allow us to make some predictions as to a potential mechanism. From biochemical data like cross-linking and subunit identification, certain subunits are known to be in close proximity or interacting with others[15]. Based on known heme reduction potentials and the preliminary data on Fe-S clusters, we can predict a flow of electrons through the complex[15,27]. It is also believed that this complex pumps protons across the membrane but no empirical evidence has been generated yet.

Figure 4.5 illustrates three possible mechanisms for ACIII, taking inspiration from a known counterpart in the CISM protein family. Since the mechanism is ACIII is not known, predictions are made from enzymes in the same protein family that have similar functions and components. Recent work by Refojo has proposed similar mechanisms for ACIII suggesting some consensus on likely options for the complex[27]. Taking after DMSO reductase with the iron sulfur clusters subunit located in the cytoplasm, we suggest a scheme of bifurcated electron transfer from the quinone site. In DMSO reductase, it is known that the electrons flow from the quinone site to the iron-sulfur clusters to the Mo-cofactor and finally to DMSO to make DMS (Figure 4.5A). If ActB were cytoplasmically located, one electron from quinol oxidation could flow through the iron sulfur clusters into the cytoplasm to an unidentified electron acceptor or

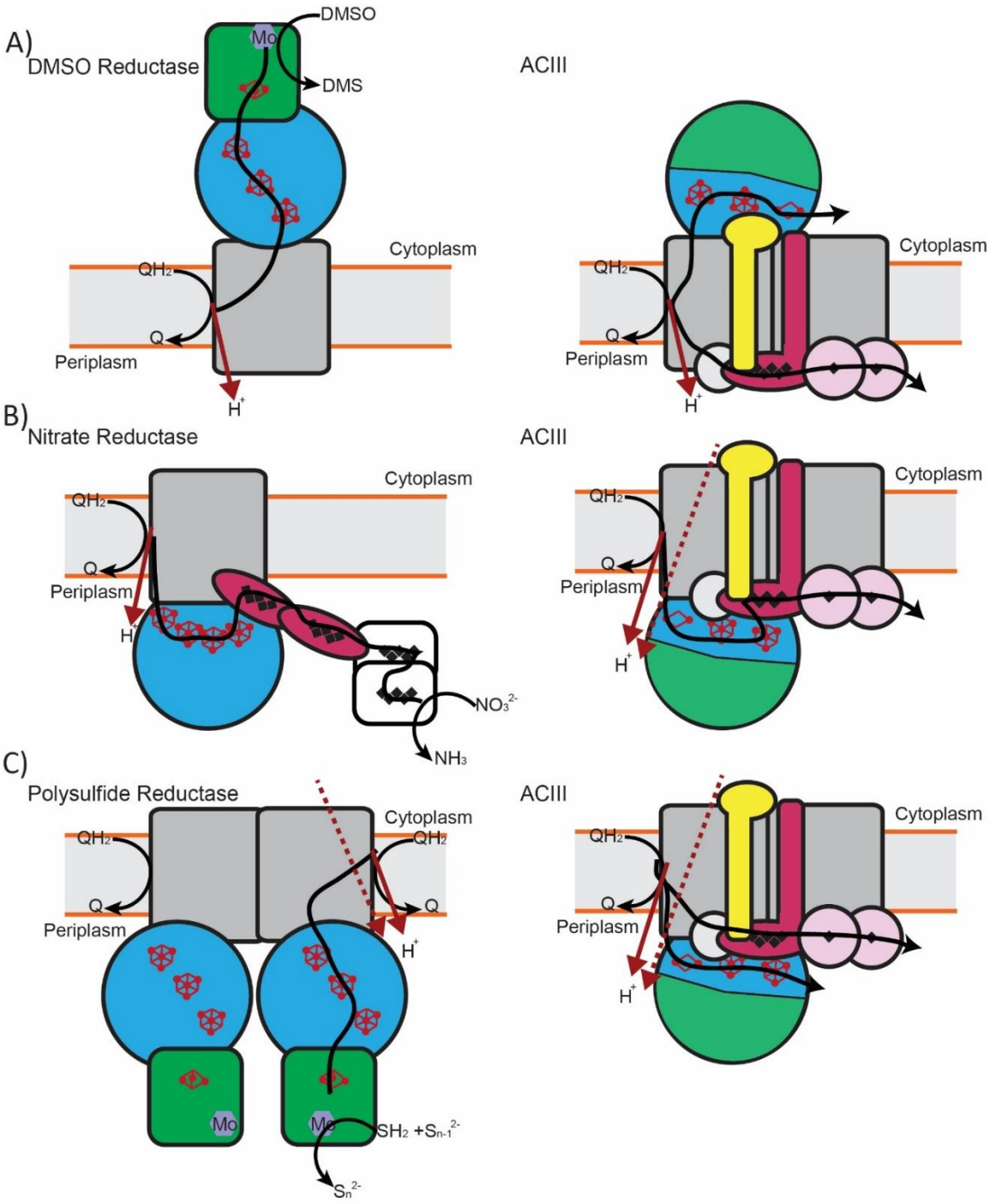

Figure 4.5 Possible Electron Transfer Pathways in ACIII. Left Column: Known Electron Flow in CISM member. Right Column: Possible electron flow in ACIII based on CISM family member **A.** DMSO Reductase. **B.** Nitrite Reductase **C.** Polysulfide Reductase. Black arrows designate electron flow. Red arrows show proton flow from the quinone site. Red dashed arrows represent proton translocation across the membrane. QH_2 is quinol and Q is quinone. Grey boxes are integral membrane subunits. Blue circles with red structures are iron-sulfur cluster containing subunits. Green boxes are Molybdenum co-factor subunits. Black diamonds are hemes. ACIII subunit color-coding corresponds to Figure 4.1.

cofactor. The second electron would then take advantage of the heme network and pass through the periplasmically located hemes to auracyanin to complete the known ACIII complex activity. (Figure 4.5A)[36]. Two protons would be translocated from the quinol oxidation. Another proton translocation from the cytoplasm is unlikely given this mechanism.

A second possible electron transfer scheme is proposed based on the flow of electrons in nitrite reductase (NIR). NIR has straightforward linear electron transfer from quinone to iron-sulfur clusters to hemes to nitrite (Figure 4.5B). If ACIII performed similarly to NIR, electrons would be transferred from quinone to Fe-S clusters and then directly to the pentaheme subunit without a cofactor in subunit ActB. The pentaheme subunit then gives the electrons to the monoheme subunit and finally from there to auracyanin. Proton pumping is seen from the quinone site and across the membrane yielding a net movement of three protons (Figure 4.5B)[22]. The periplasmic linear electron flow seems the most reasonable based on known electron acceptors, known reduction potentials, enzyme activity data and homology modeling.

A third possibility comes from comparisons with PSR. Since polysulfide reductase is a dimer with both sides active, the same flow happens on both sides[30]. The corresponding mechanism in ACIII would be much like that of the one predicted by DMSO reductase in Figure 4.5A, but having both possible pathways in the periplasm. In PSR, electrons flow from quinone to iron-sulfur clusters to a Mo-cofactor to polysulfide (Figure 4.5C). The proton pumping is generated mechanically by the interaction of the two integral membrane subunits. Then in ACIII, a similar flow for one electron will go down the iron-sulfur clusters to an additional unidentified periplasmic electron acceptor. If this were the only pathway, then all the hemes would not be utilized and the known complex activity is not happening. So, the second electron would flow down the heme nanowire to auracyanin. The heme subunits are more likely to donate to

auracyanin than the iron-sulfur clusters. Two protons would be pumped from the quinol site as well two more protons from the cytoplasm (Figure 4.5C). So for DMSO reductase and PSR, one pathway of the bifurcation takes inspiration from the known complex mechanism and the second pathway is predicted to complete complex activity and make use of the hemes. The exact mechanism in ACIII remains unclear, but it is clear that ACIII should be contributing to cyclic electron transfer and to the establishment of the electrochemical gradient.

4.5 Electron Transport Chains Involving ACIII

Biochemical and genomic evidence suggests that ACIII can function in photosynthetic and aerobic electron transport chains. Examples of ACIII operons containing a traditional caa3-type oxidases and cbb3 oxygen reductase are known. The fact that ACIII has become associated with multiple cytochrome *c* oxidases implies a strong relationship between ACIII and aerobic electron transfer. Additionally, most aerobic ACIII containing organisms lack a cytochrome bc_1 complex.

In the *Chloroflexi* phylum, most members encode an ACIII, although there are several exceptions. The *Dehalococcoides* class and *Herpetosiphon aurantiacus* lack ACIII. *Oscillochloris trichoides* encodes two ACIII copies and a cytochrome bc_1 complex. *C. aurantiacus* also encodes two copies of ACIII. One operon includes a caa_3-type oxidase and is expressed under aerobic growth. The other operon is expressed under photosynthetic growth (Figure 4.1). The existence of two copies in *O. trichoides* and *C. aurantiacus* probably functions to separate the aerobic and photosynthetic electron transport chains (Figure 4.6). ACIII participates in cyclic electron transfer both in photosynthetic and respiratory electron transport chains. In *C. aurantiacus*, light is harvested in the chlorosome and the energy passed into the

reaction center[53]. The reaction center reduces quinone to quinol which passes through the membrane to ACIII. ACIII oxidizes quinol to quinone, transporting the protons across the membrane and donating the electrons to the small blue copper protein, auracyanin. Auracyanin acts as the soluble electron transporter and brings the electrons back to the reaction center (Figure 4.6A). The respiratory chain has different members but ACIII still serves as the quinol oxidizer and donates electrons to auracyanin (Figure 4.6B). Auracyanin will be discussed in the next section.

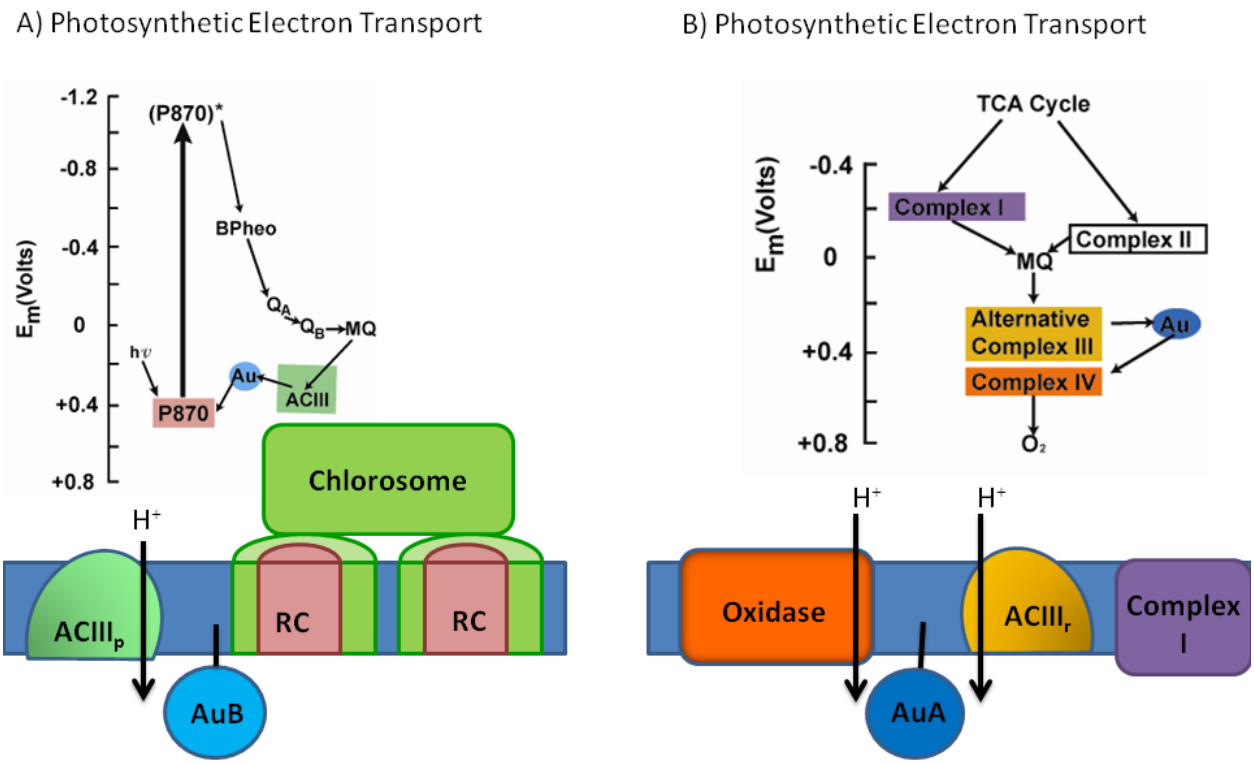

Figure 4.6 Photosynthetic and Respiratory Electron Transport Chains in *C. aurantiacus*. A. Photosynthetic Electron Transport Chain **B.** Respiratory Electron Transport Chain Z-scheme shows energy level throughout cyclic electron transport. RC is the reaction center which holds the P870 pigment, bacteriopheophytin pigment, QA and QB sites. MQ is menaquinone. Au is auracyanin. TCA is the tricarboxylic acid cycle. Oxidase is cytochrome c oxidase or Complex IV.

4.6 Auracyanins

In order for ACIII to pass electrons to an oxidized reaction center or a terminal oxidase, it is expected to require a periplasmic electron transfer. The blue copper proteins, auracyanins, are hypothesized to fulfill this role in the *Chloroflexi* bacteria. *C. aurantiacus* encodes four auracyanin genes, labeled A-D [40]. Auracyanins A and B have been purified from *C. aurantiacus*[41]. Initial expression studies of auracyanins A and B suggested that auracyanin A was expressed under photosynthetic growth and auracyanin B was constitutively expressed[42]. However, recent mass spectrometry data comparing photosynthetic and aerobic growth showed the opposite trend with auracyanin A being expressed under aerobic growth and auracyanin B being expressed under photosynthetic growth[43]. Unpublished western blot data from the authors confirmed the mass spectrometry result (King, Majumder, and Blankenship). Auracyanins C and D have never been detected biochemically, but are known from genomic evidence[40]. All four proteins have been expressed in *E. coli.* The *E. coli* expressed auracyanins A and B lack the glycosylation and lipidation normally present in those derived from *C. aurantiacus.* However, the redox potential and spectra are identical[42]. Recombinant auracyanins C and D are currently being characterized. An additional auracyanin has been characterized from the related *R. castenholzii;* this auracyanin will be referred to as auracyanin RC. Studies on the native and recombinant forms of auracyanins have led to a good understanding of their structures and some predictions of their functions.

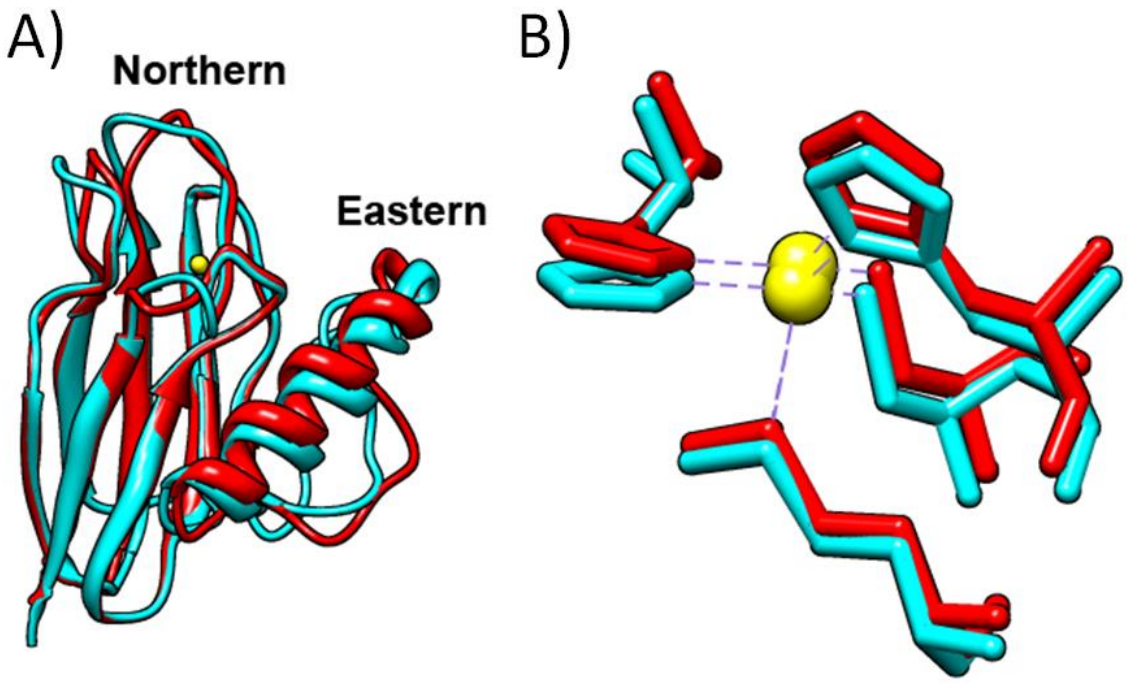

Figure 4.7 Structure of Auracyanin. A. Overall Structural Comparison of auracyanins A and B. **B.** Comparison of Ligand Geometry of auracyanins A and B. In B, the overlay of auracyanins A and B has been displaced slightly for clarity. Auracyanin A is shown in red and auracyanin B is shown in cyan. Copper atom is shown in gold.

4.6.1 Structure of Auracyanins

Auracyanins A and B both have solved crystal structures (Figure 4.7)[42,46]. Like other Type 1 blue copper proteins, the auracyanins have eight beta strands arranged in two sheets. The arrangement of the beta strands forms a Greek-key fold (Figure 4.7A). The copper ion is sandwiched between the two sheets and is coordinated by a cysteine thiolate, two histidine imidazoles, and a methionine thioether. The cysteine, one of the histidines, and the methionine can all be found in the loop between beta strand 7 and 8. The axial methionine ligand is weakly bonded, resulting in a geometry that can be described as a distorted trigonal-pyramidal[42]. The

ligand geometry is essentially identical between auracyanins A and B (Figure 4.7B). This is surprising as UV-vis, circular dichroism, resonance Raman, and electron paramagnetic resonance predicted highly different copper sites[41]. However, the ligand distances and geometries calculated from the crystals were confirmed by XAS on solutions of auracyanins A and B[42].

Blue copper proteins interact with their redox partners near the copper site[44,45]. This is unsurprising as electron transfer efficiency falls off with distance. The regions labeled "north" and "east" in Figure 4.7A are primarily responsible for the docking in other blue copper proteins. Electron transfer is thought to proceed from the copper site through the top of the "northern" face. The distance from the northern face of the auracyanins to the surface is 6 Å. Auracyanins A and B have hydrophobic patches on their "northern" face[42]. However, auracyanin B has many polar residues not present in auracyanin A in this region[46]. Auracyanin B also has evidence of glycoslation[41]. The poorly conserved "variable region" between beta strands 4 and 5 of blue copper proteins is fairly similar between auracyanins A and B. This region is thought to be important for redox interactions in other blue copper proteins[46]. The surface similarities with minor differences suggest that auracyanins A and B might have similar, but distinct redox partners.

Sequence alignment leads to several interesting predictions about auracyanins C and D. First, the first coordinating histidine is followed by a glutamic acid in auracyanin C and a serine in auracyanin D. This residue is normally conserved as an asparagine in all other blue copper proteins. Changing this asparagine to a serine led to an increase of +130 mV in the redox potential of the blue copper protein azurin[47]. Second, sequence alignment suggests that auracyanin D has a glutamine axial ligand. Glutamine is occasionally seen as an axial ligand in blue copper proteins. Replacing the typical methionine with glutamine in azurin resulted in 263

mV decrease in potential[47,48]. Finally, it is worth noting that the variable region is poorly conserved between auracyanins C and D in *C. aurantiacus,* yet fairly conserved in other auracyanins. This suggests that auracyanins C and D may have novel functions.

4.6.2 Localization of Auracyanins

Auracyanins A and B are both membrane anchored, and hypothesized to be periplasmic based on putative signal peptides. Auracyanin A appears to be a lipoprotein. Mass spectrometry suggests that auracyanin A contains an acetyl-N-cysteine-S-glycerol modification at its amino terminus. This group is attached to the protein at a cysteine residue following the signal peptide[49]. This cysteine residue is conserved in all auracyanins except for auracyanin B and the auracyanin B homologue from *O. trichoides* DG6. The cysteine is flanked by conserved alanine and glycine. The +2 rule for bacterial lipoproteins predicts that auracyanin A with a glycine in the +2 position would be mostly chaperoned to the outer membrane[50]. However, recent arguments have suggested that *Chloroflexi* bacteria are monoderm (i.e. lacking an outer membrane)[51]. Additionally, the LolAB chaperones which function in gram-negative bacteria as the chaperones responsible for moving lipoproteins to the outer membrane appear to be lacking in the *Chloroflexi* genomes. As a result, we place auracyanin attached to the cytoplasmic membrane but facing into the periplasmic or equivalent space. However, it is unresolved if *Chloroflexi* are truly monoderm, and *Chloroflexi* bacteria could use different lipoprotein processing machinery as they are very distant from bacteria whose lipoprotein pathway has been characterized. Thus, it is possible that auracyanin A is transported to an outer membrane via an unknown mechanism.

Auracyanin B and the auracyanin B-like protein from *O. trichoides* DG6 are unique amongst the auracyanins in that they lack the conserved lipid signal. Instead, both proteins have an extended N-terminal region containing a putative transmembrane domain[49]. Interestingly, *C. aurantiacus* and *O. trichoides* are examples of photosynthetic *Chloroflexi* bacteria that use a chlorosome antenna for light harvesting[52]. This antenna is found attached to the cytoplasmic side of the inner cell membrane. It is assumed that the reaction center and photosynthetic electron transport chains are also restricted to certain domains[53]. Expression data suggests that auracyanin B is expressed during photosynthetic growth[43]. Thus, the replacement of the lipid signal with a transmembrane domain may limit auracyanin B to regions of membrane associated with photosynthetic electron transport.

4.6.3 Evidence Supporting Auracyanins as a Mobile Electron Carrier

There exists a debate as to whether the auracyanins in fact perform the periplasmic respiratory and photosynthetic electron transfers. Initially, auracyanin seemed like the ideal candidate as both auracyanin A and B could reduce purified reaction centers in *C. aurantiacus*[41]. This was further supported by the ability of auracyanin A to oxidize purified ACIII from *C. aurantiacus*[9]. However, spectroscopic studies on membrane from the related FAP *R. castenholzii* showed no photoreduction in the presence of auracyanin RC. The authors of this paper suggest that the protocol used, which was optimized for purple bacteria, may not work in *R. castenholzii*. Alternatively, *R. castenholzii* may use a different electron carrier[54].

A second major argument against auracyanin as the mobile carrier is the redox mismatch between the auracyanins and ACIII. Auracyanin A ($E_{m,\,7}$ = 205±7 mV) and B ($E_{m,\,7}$ = 215±7 mV) have redox potentials well below their proposed ACIII redox partner ActE ($E_{m,\,7}$ = +391mV)[15,55].

Such an uphill reaction seems is thermodynamically unfavorable. Despite this difference, reduced ACIII is able to reduce oxidized auracyanin A in solution. It is possible that ActE is not the auracyanin redox partner, as proposed. Alternatively, it is well documented that the blue copper protein amicyanin's potential changes upon binding to its redox partners, allowing an otherwise uphill reaction to occur[56]. Another possibility is that an uphill reaction between ActE and auracyanin occurs, but the driving force from menaquinol to auracyanin is enough to overcome this. Such a process is known to happen in the tetraheme subunit of the reaction center of purple bacteria[57].

Compared with other photosynthetic systems, *C. aurantiacus* could use a cytochrome *c* or blue copper protein to reduce the reaction center[58]. The auracyanins are a favorable option due to their high abundance in the cell. In purple bacteria, electrons are carried from the cytochrome bc_1 complex to the reaction center by the soluble proteins cytochrome c_2 or HiPIP[58]. The *C. aurantiacus* J-10-fl genome lacks any genes encoding a HiPIP using the PFAM definition (PFAM01355). However, the genome has genes for two possible cytochrome *c* proteins (Caur_0845 and Caur_0980). Caur_0980 is on an operon with bilirubin oxidase, and likely functions in the heme degradation pathway. Caur_0845 appears to be monocistronic, and could function in electron transport. However, both cytochrome *c*'s have not been detected by heme staining[5] or mass spectrometry[59]. It is entirely possible that one of the cytochrome *c* proteins functions in electron transport, but is below traditional detection limits. It is also possible that *C. aurantiacus* could use a novel mechanism to carry electrons from ACIII to the reaction center that does not involve a blue copper protein, a HiPIP, or a cyt *c*. With these possibilities in mind, auracyanins still seem like the most likely mobile electron carriers. Additional experiments on ACIII's redox pathway and enzyme activity assays should clarify this issue.

4.7 Concluding Thoughts

The electron transport chains in many phototrophic bacteria still remain to be characterized and understood. ACIII and its soluble electron acceptor auracyanin are among the more unusual members of those electron transport chains. Homology to related enzymes has provided significant clues to structure and mechanism, especially when coupled with existing biochemical data. Understanding of auracyanin is developing and revealing new limits for blue copper proteins. A complete understanding of the ACIII- auracyanin system will enhance our knowledge of the photosynthetic mechanisms of bacteria, particularly *Chloroflexii*.

References

[1] R.E. Blankenship, Molecular Mechanisms of Photosynthesis, Blackwell Science, Oxford, 2014.

[2] B.K. Pierson, R.W. Castenholz, A phototrophic gliding filamentous bacterium of hot springs, *Chloroflexus aurantiacus*;, gen. and sp. nov, Archives of Microbiology, 100 (1974) 5-24.

[3] G. Strauss, G. Fuchs, Enzymes of a novel autotrophic CO2 fixation pathway in the phototrophic bacterium *Chloroflexus aurantiacus*, the 3-hydroxypropionate cycle, European Journal of Biochemistry, 215 (1993) 633-643.

[4] R.E. Blankenship, R. Feick, B.D. Bruce, C. Kirmaier, D. Holten, R.C. Fuller, Primary photochemistry in the facultative green photosynthetic bacterium *Chloroflexus aurantiacus*, Journal of Cellular Biochemistry, 22 (1983) 251-261.

[5] B. Pierson, Cytochromes in *Chloroflexus aurantiacus* grown with and without oxygen, Arch Microbiol, 143 (1985) 260 - 265.

[6] J. Trost, J. Mcmanus, J. Freeman, B. Ramakrishna, R. Blankenship, Auracyanin, a blue copper protein from the green photosynthetic bacterium *Chloroflexus aurantiacus*, Biochemistry, 27 (1988) 7858 - 7863.

[7] J.D. McManus, D.C. Brune, J. Han, J. Sanders-Loehr, T.E. Meyer, M.A. Cusanovich, G. Tollin, R.E. Blankenship, Isolation, characterization, and amino acid sequences of auracyanins, blue copper proteins from the green photosynthetic bacterium *Chloroflexus aurantiacus*, Journal of Biological Chemistry, 267 (1992) 6531-6540.

[8] M. Yanyushin, M. del Rosario, D. Brune, R. Blankenship, New class of bacterial membrane oxidoreductases, Biochemistry, 44 (2005) 10037 - 10045.

[9] X. Gao, Y. Xin, R. Blankenship, Enzymatic activity of the alternative complex III as a menaquinol:auracyanin oxidoreductase in the electron transfer chain of *Chloroflexus aurantiacus*, FEBS Lett, 583 (2009) 3275 - 3279.

[10] M.M. Pereira, A.M. Antunes, O.C. Nunes, M.S. Dacosta, M. Teixeira, A Membrane-Bound Hipip Type Center in the Thermohalophile-*Rhodothermus Marinus*, FEBS Letters, 352 (1994) 327-330.

[11] R.M. Wynn, T.E. Redlinger, J.M. Foster, R.E. Blankenship, R.C. Fuller, R.W. Shaw, D.B. Knaff, Electron-transport chains of phototrophically and chemotrophically grown *Chloroflexus aurantiacus*, Biochimica et Biophysica Acta (BBA) - Bioenergetics, 891 (1987) 216-226.

[12] M.M. Pereira, J. N. Carita, M. Teixeira, Membrane-bound electron transfer chain of the thermohalophilic bacterium *Rhodothermus marinus*: A novel multihemic cytochrome bc, a new complex III, Biochemistry (Easton), 38 (1999) 1268-1275.

[13] M.F. Yanyushin, Fractionation of cytochromes of phototrophically grown *Chloroflexus aurantiacus*. Is there a cytochrome bc complex among them?, FEBS Letters, 512 (2002) 125-128.

[14] M.M. Pereira, J. N. Carita, M. Teixeira, Membrane-bound electron transfer chain of the thermohalophilic bacterium *Rhodothermus marinus*: Characterization of the iron-sulfur centers from the dehydrogenases and investigation of the high-potential iron-sulfur protein function by in vitro reconstitut, Biochemistry (Easton), 38 (1999) 1276-1283.

[15] X. Gao, Y. Xin, P.D. Bell, J. Wen, R.E. Blankenship, Structural Analysis of Alternative Complex III in the Photosynthetic Electron Transfer Chain of *Chloroflexus aurantiacus*, Biochemistry, 49 (2010) 6670-6679.

[16] M.M. Pereira, P.N. Refojo, G.O. Hreggvidsson, S. Hjorlelfsdottir, M. Teixeira, The alternative complex III from *Rhodothermus marinus* - A prototype of a new family of quinol : electron acceptor oxidoreductases, FEBS Letters, 581 (2007) 4831-4835.

[17] P.N. Refojo, F.L. Sousa, M. Teixeira, M.M. Pereira, The alternative complex III: A different architecture using known building modules, Quinone Binding and Catalysis, 1797 (2010) 1869-1876.

[18] P.N. Refojo, M. Teixeira, M.M. Pereira, The alternative complex III of *Rhodothermus marinus* and its structural and functional association with caa(3) oxygen reductase, BIOCHIMICA ET BIOPHYSICA ACTA-BIOENERGETICS, 1797 (2010) 1477-1482.

[19] T. Hirokawa, S. Boon-Chieng, S. Mitaku, SOSUI: classification and secondary structure prediction system for membrane proteins, Bioinformatics, 14 (1998) 378-379.

[20] J. Schultz, F. Milpetz, P. Bork, C.P. Ponting, SMART, a simple modular architecture research tool: Identification of signaling domains, Proceedings of the National Academy of Sciences, 95 (1998) 5857-5864.

[21] T.A. Clarke, V. Dennison, H.E. Seward, B. Burlat, J.A. Cole, A.M. Hemmings, D.J. Richardson, Purification and spectropotentiometric characterization of *Escherichia coli* NrfB, a decaheme homodimer that transfers electrons to the decaheme periplasmic nitrite reductase complex., The Journal of biological chemistry, 279 (2004) 41333-41339.

[22] T.A. Clarke, J. A. Cole, D. J. Richardson, A. M. Hemmings, The crystal structure of the pentahaem c-type cytochrome NrfB and characterization of its solution-state interaction with the pentahaem nitrite reductase NrfA, (2007).

[23] M.A. Larkin, G. Blackshields, N.P. Brown, R. Chenna, P.A. McGettigan, H. McWilliam, F. Valentin, I.M. Wallace, A. Wilm, R. Lopez, J.D. Thompson, T.J. Gibson, D.G. Higgins, Clustal W and Clustal X version 2.0, Bioinformatics, 23 (2007) 2947-2948.

[24] N. Eswar, B. Webb, M.A. Marti-Renom, M.S. Madhusudhan, D. Eramian, M.-y. Shen, U. Pieper, A. Sali, Comparative Protein Structure Modeling Using Modeller, in: Current Protocols in Bioinformatics, John Wiley & Sons, Inc., 2002.

[25] E.F. Pettersen, T.D. Goddard, C.C. Huang, G.S. Couch, D.M. Greenblatt, E.C. Meng, T.E. Ferrin, UCSF Chimera—A visualization system for exploratory research and analysis, Journal of Computational Chemistry, 25 (2004) 1605-1612.

[26] P.R. Pokkuluri, Y.Y. Londer, N.E.C. Duke, M. Pessanha, X. Yang, V. Orshonsky, L. Orshonsky, J. Erickson, Y. Zagyanskiy, C.A. Salgueiro, M. Schiffer, Structure of a novel dodecaheme cytochrome c from *Geobacter sulfurreducens* reveals an extended 12 nm protein with interacting hemes., Journal of structural biology, 174 (2011) 223-233.

[27] P.N. Refojo, M. Teixeira, M.M. Pereira, The Alternative complex III: Properties and possible mechanisms for electron transfer and energy conservation, Biochimica et Biophysica Acta (BBA) - Bioenergetics, (2012) In Press.

[28] L.A. Sazanov, P. Hinchliffe, Structure of the hydrophilic domain of respiratory complex I from Thermus thermophilus., Science (New York, N.Y.), 311 (2006) 1430-1436.

[29] R.A. Rothery, G.J. Workun, J.H. Weiner, The prokaryotic complex iron-sulfur molybdoenzyme family., Biochimica et biophysica acta, 1778 (2008) 1897-1929.

[30] M. Jormakka, K. Yokoyama, T. Yano, M. Tamakoshi, S. Akimoto, T. Shimamura, P. Curmi, S. Iwata, Molecular mechanism of energy conservation in polysulfide respiration., Nature structural & molecular biology, 15 (2008) 730-737.

[31] B.C. Berks, F. Sargent, T. Palmer, The Tat protein export pathway, Molecular Microbiology, 35 (2000) 260-274.

[32] I. Bertini, H. B. Gray, E. I. Steifel, J. S. Valentine, Biological inorganic chemistry: structure and reactivity, University Science Books, Sausalito, (2007).

[33] D.T. Jones, Protein secondary structure prediction based on position-specific scoring matrices, Journal of Molecular Biology, 292 (1999) 195-202.

[34] G. von Heijne, Membrane protein structure prediction: Hydrophobicity analysis and the positive-inside rule, Journal of Molecular Biology, 225 (1992) 487-494.

[35] R.A. Rothery, N. Kalra, R.J. Turner, J.H. Weiner, Sequence similarity as a predictor of the transmembrane topology of membrane-intrinsic subunits of bacterial respiratory chain enzymes., Journal of molecular microbiology and biotechnology, 4 (2002) 133-150.

[36] P.T. Bilous, J.H. Weiner, Proton translocation coupled to dimethyl sulfoxide reduction in anaerobically grown *Escherichia coli* HB101., J. Bacteriol., 163 (1985) 369-375.

[37] P. Geijer, J. H. Weiner, Glutamate 87 is important for menaquinol binding in DmsC of the DMSO reductase (DmsABC) from *Escherichia coli*, Biochimica et Biophysica Acta (BBA) - Biomembranes, 1660 (2004) 66-74.

[38] F. Schneider, J. Löwe, R. Huber, H. Schindelin, C. Kisker, J. Knäblein, Crystal structure of dimethyl sulfoxide reductase from *Rhodobacter capsulatus* at 1.88 A resolution., Journal of Molecular Biology, 263 (1996) 53-69.

[39] S.F. Altschul, W. Gish, W. Miller, E.W. Myers, D.J. Lipman, Basic local alignment search tool, Journal of Molecular Biology, 215 (1990) 403-410.

[40] K.-H. Tang, K. Barry, O. Chertkov, E. Dalin, C. Han, L. Hauser, B. Honchak, L. Karbach, M. Land, A. Lapidus, F. Larimer, N. Mikhailova, S. Pitluck, B. Pierson, R. Blankenship, Complete genome sequence of the filamentous anoxygenic phototrophic bacterium *Chloroflexus aurantiacus*, BMC Genomics, 12 (2011) 334.

[41] J. McManus, D. Brune, J. Han, J. Sanders-Loehr, T. Meyer, M. Cusanovich, G. Tollin, R. Blankenship, Isolation, characterization, and amino acid sequences of auracyanins, blue copper proteins from the green photosynthetic bacterium *Chloroflexus aurantiacus*, J Biol Chem, 267 (1992) 6531 - 6540.

[42] M. Lee, M. del Rosario, H. Harris, R. Blankenship, J. Guss, H. Freeman, The crystal structure of auracyanin A at 1.85 Å resolution: the structures and functions of auracyanins A and B, two almost identical “blue” copper proteins, in the photosynthetic bacterium *Chloroflexus aurantiacus*, Journal of Biological Inorganic Chemistry, 14 (2009) 329-345.

[43] L. Cao, D. A. Bryant, Schepmoes, K. Vogl, R. Smith, M. Lipton, S. Callister, Comparison of *Chloroflexus aurantiacus* strain J-10-fl proteomes of cells grown chemoheterotrophically and photoheterotrophically, Photosynthesis research, 110 (2012) 153-168.

[44] I. Díaz-Moreno, A. Díaz-Quintana, M.A. De la Rosa, M. Ubbink, Structure of the Complex between Plastocyanin and Cytochrome f from the Cyanobacterium *Nostoc* sp. PCC 7119 as Determined by Paramagnetic NMR, Journal of Biological Chemistry, 280 (2005) 18908-18915.

[45] F. Meschi, F. Wiertz, L. Klauss, C. Cavalieri, A. Blok, B. Ludwig, H.A. Heering, A. Merli, G.L. Rossi, M. Ubbink, Amicyanin Transfers Electrons from Methylamine Dehydrogenase to

Cytochrome c-551i via a Ping-Pong Mechanism, not a Ternary Complex, Journal of the American Chemical Society, 132 (2010) 14537-14545.

[46] C.S. Bond, R.E. Blankenship, H.C. Freeman, J.M. Guss, M.J. Maher, F.M. Selvaraj, M.C.J. Wilce, K.M. Willingham, Crystal structure of auracyanin, a "blue" copper protein from the green thermophilic photosynthetic bacterium *Chloroflexus aurantiacus*, Journal of Molecular Biology, 306 (2001) 47-67.

[47] N.M. Marshall, D.K. Garner, T.D. Wilson, Y.-G. Gao, H. Robinson, M.J. Nilges, Y. Lu, Rationally tuning the reduction potential of a single cupredoxin beyond the natural range, Nature, 462 (2009) 113-116.

[48] A. Romero, C.W.G. Hoitink, H. Nar, R. Huber, A. Messerschmidt, G.W. Canters, X-ray Analysis and Spectroscopic Characterization of M121Q Azurin: A Copper Site Model for Stellacyanin, Journal of Molecular Biology, 229 (1993) 1007-1021.

[49] G.V. Driessche, W. Hu, G.V.D. Werken, F. Selvaraj, J.D. McManus, R.E. Blankenship, J.J. Van Beeumen, Auracyanin a from the thermophilic green gliding photosynthetic bacterium *Chloroflexus aurantiacus* represents an unusual class of small blue copper proteins, Protein Science, 8 (1999) 947-957.

[50] A. Seydel, P. Gounon, A.P. Pugsley, Testing the '+2 rule' for lipoprotein sorting in the *Escherichia coli* cell envelope with a new genetic selection, Molecular Microbiology, 34 (1999) 810-821.

[51] I.C. Sutcliffe, Cell envelope architecture in the *Chloroflexi*: a shifting frontline in a phylogenetic turf war, Environmental Microbiology, 13 (2011) 279-282.

[52] S. Hanada, B. Pierson, The Family Chloroflexaceae. In: The Prokaryotes, M. Dworkin, S. Falkow, E. Rosenberg, K.-H. Schleifer, E. Stackebrandt (Eds.), Springer New York, 2006, pp. 815-842.

[53] R. Blankenship, K. Matsuura, Antenna complexes from green photosynthetic bacteria, Anoxygenic Photosynthetic Bacteria, (2003) 195 - 217.

[54] Y. Tsukatani, N. Nakayama, K. Shimada, H. Mino, S. Itoh, K. Matsuura, S. Hanada, K.V.P. Nagashima, Characterization of a blue-copper protein, auracyanin, of the filamentous anoxygenic phototrophic bacterium *Roseiflexus castenholzii*, Archives of Biochemistry and Biophysics, 490 (2009) 57-62.

[55] M. Rooney, M. Honeychurch, F. Selvaraj, R. Blankenship, A. Bond, H. Freeman, A thin-film electrochemical study of the "blue" copper proteins, auracyanin A and auracyanin B, from the photosynthetic bacterium *Chloroflexus aurantiacus* the reduction potential as a function of pH, Journal of Biological Inorganic Chemistry, 8 (2003) 306-317.

[56] Z. Zhu, L.M. Cunane, Z.-w. Chen, R.C.E. Durley, F.S. Mathews, V.L. Davidson, Molecular Basis for Interprotein Complex-Dependent Effects on the Redox Properties of Amicyanin†, Biochemistry, 37 (1998) 17128-17136.

[57] I.P. Chen, P. Mathis, J. Koepke, H. Michel, Uphill Electron Transfer in the Tetraheme Cytochrome Subunit of the *Rhodopseudomonas viridis* Photosynthetic Reaction Center: Evidence from Site-Directed Mutagenesis†, Biochemistry, 39 (2000) 3592-3602.

[58] T. Meyer, M. Cusanovich, Discovery and characterization of electron transfer proteins in the photosynthetic bacteria, Photosynthesis Research, 76 (2003) 111-126.

[59] L. Cao, D.A. Bryant, A.A. Schepmoes, K. Vogl, R.D. Smith, M.S. Lipton, S.J. Callister, Comparison of *Chloroflexus aurantiacus* strain J-10-fl proteomes of cells grown chemoheterotrophically and photoheterotrophically., Photosynthesis research, 110 (2012) 153-168.

Chapter 5: Supramolecular organization of the photosynthetic complexes in the membranes of *Roseiflexus castenholzii*

This chapter has been submitted for publication to a special issue of *Photosynthesis Research*. Erica L.-W. Majumder, John D. Olsen, Pu Qian, Aaron M. Collins, C. Neil Hunter and Robert E. Blankenship. Supramolecular organization of the photosynthetic complexes in the membranes of *Roseiflexus castenholzii*. *Photosynthesis Research*. Submitted (2015). Used with permission of authors.

5.1 Introduction

Optimal function of the photosynthetic apparatus relies on the proteins present and how they are proteins arranged in the membrane. Mega-complexes in cyanobacteria, supercomplexes in purple bacteria and other kinds of higher order structure or supramolecular organization have been shown to enhance solar energy capture and conversion efficiency[1,2]. Purple Bacteria (PB) such as *Rhodobacter sphaeroides* have tightly packed arrays of light harvesting antenna LH2[3], that encircle RC-LH1 core complexes, which can form S-shaped dimers in complexes or exist as standalone rings[4–6]. These organized arrays permit the rapid diffusion of excitation energy between complexes and to the reaction center, where this energy is conserved in the form of a reduced quinone acceptor[7,8]. Here we investigate the structure of individual photosynthetic Light Harvesting Reaction Center (LHRC) protein complexes and the supramolecular organization of the photosynthetic membranes of the phototrophic bacterium *Roseiflexus castenholzii*.

Roseiflexus castenholzii (RFX) is a photosynthetic bacterium belonging to the Filamentous Anoxygenic Phototrophs (FAPs)[9]. The FAPs are generally thermophiles, exist in niche environments and have a unique set of photosynthetic proteins that may have been acquired through horizontal gene transfer events[10,11]. The large light harvesting antenna structure called the chlorosome is also found in the Green Sulfur Bacteria (GSB) and the type II reaction center and its associated core antenna, RC-LH1 is similar to that found in Purple Bacteria (PB)[12–14]. Finally, FAPs have a novel replacement for the cytochrome bc_1 complex called the Alternative Complex III and a small blue copper protein, auracyanin, as the soluble electron carrier[15,16].

RFX was isolated from middle layers of hot spring microbial mats, first in Japan and later in Yellowstone National Park[17,18]. It is closely related to the founding organism of the FAP's,

Chloroflexus aurantiacus (CFX)[14]. The major difference between CFXs and RFX is that RFX does not have the large accessory light harvesting antenna, the chlorosome[9]. The photosynthetic core complex of RFX has been isolated and biochemically characterized revealing several unique features[19]. First, this bacterium only has a combined light harvesting reaction center complex to absorb light, much like a RC-LH1 system, but does not have an LH2 type antenna or any other accessory antenna[20]. Secondly, this LHRC complex absorbs further into the red than most organisms at 880nm, which allows it to survive in the filtered light environments of the microbial mats. Also, it can still use this lower energy light to drive photosynthesis[21]. Third, the RFX LHRC has been shown to have the ring-like structure of an RC-LH1, but behaves spectroscopically more like an LH2 complex[22]. Fourth, the LHRC is lacking the RC-H and PufX or W subunits typically found in the related purple bacteria type II reaction centers and core complexes[23]. Additionally, the complex contains a firmly attached tetraheme cytochrome *c*, as first observed in the *Blastochloris viridis* system, but not ubiquitously found in other purple bacteria or type II RCs[24,25].

The other major component of the *Roseiflexus* membranes is a functional replacement for the cytochrome bc_1 complex called the Alternative Complex III (ACIII). ACIII has been shown to be an oxidoreductase oxidizing menaquinone from the RC and returning electrons to the RC special pair via the small blue copper protein auracyanin[26,27]. ACIII has no structural or evolutionary relationship to the cytochrome bc_1 complex but is related to enzymes from the Complex Iron-Sulfur Molybdopterin family, and is therefore a novel protein in photosynthetic membranes[28]. Auracyanin replaces the typical soluble cytochrome electron carrier. Auracyanin has been previously characterized and crystallized in the CFX system[29]. RFX auracyanin has a

sequence similar to a mixture of auracyanins A & B, but there is only one copy in the genome and the C-terminal membrane tether tail is predicted to be slightly shorter[16].

The basic biochemical characterization of the major protein players of the FAP photosynthetic cyclic electron transport chain revealed novel complexes with distinct features. Despite the studies of the LHRC, ACIII and auracyanin, the FAP ETC remains poorly understood. No crystal structure has been solved of the LHRC or the ACIII from any FAP. Likewise, the mechanism and cofactor content and arrangement within each complex remains unknown. The full cyclic electron transport chain cycle has also not been demonstrated biochemically, specifically the interaction between auracyanin and the membrane protein complexes. It is also not known how these complexes are organized in the membrane or exactly how they function as a unit. However, based on the similarity of the FAP LHRC to the PB RC-LH1 systems, we predict the FAP supramolecular organization to mirror the PB patterns.

In this work, we made further efforts to determine the structure of the LHRC and to visualize the components of the photosynthetic system in the membrane. The RFX photosynthetic unit has been studied with both Transmission Electron Microscopy (EM) and Atomic Force Microscopy (AFM), as well as biochemical and *in silico* techniques. We found the RFX LHRC to be structurally similar to PB RC-LH1 complexes, but did not find a highly ordered pattern as seen in the supramolecular organization of the membrane of *Bl. viridis*[30]. We propose a model for LHRC, ACIII and auracyanin in the photosynthetic membranes of RFX.

5.2 Materials and Methods

5.2.1 Purification of LHRC and LH-only complexes

Isolation and purification of the LHRC and LH-only complexes of photosynthetically grown *Roseiflexus castenholzii* HL08 was carried out by the method described in Collins et al 2010[22]. Briefly, whole membranes were isolated from the cells by sonication and ultracentrifugation and then solubilized in 2% LDAO. The solubilized membranes were centrifuged and filtered to remove debris and loaded onto a QSHP ion exchange column and eluted with a NaCl gradient. For LH only complexes, the column was washed in 1% LDAO for at least one column volume before applying the salt gradient. Collected colored fractions were analyzed by UV/Vis spectrophotometry. Those containing the desired complex were concentrated using 100 kDa MWCO Spin Filters and run over a S200 gel filtration column. Fractions were checked again and the pure complexes were concentrated and verified by SDS-PAGE.

5.2.2 Electron Microscopy

Concentration of the purified samples, LHRC and LH-only complexes from RFX, were adjusted to 0.1 mg/ml protein. Five μL of the protein solution was loaded on the surface of freshly glow-discharged EM copper grid coated with 16 nm thickness carbon film. After 30 seconds, the excess protein solution was blotted by the use of filter paper. The grid was washed with distilled water twice, and then stained with 0.75% (w/v) uranyl formate for 30 seconds. The stain solution was blotted and the grid was dried in air. The grids were examined using a Philips CM100 electron microscopy under 100 kV accelerating voltage. Micrographs were recorded with a 1K x 1K Gatan Multiscan 794 CCD camera at a normal magnification of 52,000 X with variation of underfocus values from 0.5 to 1.5 μm, resulting in a pixel size of 3.93 Å at specimen level.

Particles were picked from selected images. All micrographs that showed drifting, bad staining or unsuitable under-focus were discarded. In total, 18945 LHRC and 6086 LH-only particles were collected for data processing initially by the use of EMAN2[31]. After CTF correction, two data sets were compiled, and subsets containing 5837 particles for LHRC and 3242 LH-only complexes were used to produce reference free 2D class averages. Selected 2D averaged classes were used to establish the initial 3D model, which was used for primarily 3D reconstruction with the corresponding subset data. The full-set data were applied at the second refinement stage. Iteration of the refinement continued until a stable model was obtained. During each iteration, 10% bad particles were rejected.

The resolution of the final model was estimated by calculating the Fourier shell correlation (FSC) between two 3D reconstruction models that were built up separately from two halves of the 2D classes.

5.2.3 Preparation of intracytoplasmic membranes

Membranes were isolated from whole cells of photosynthetically grown RFX. Whole wet cells were suspended in 20 mM Tris buffer pH 8 with 2% Triton X-100 and 500 mM EDTA and 0.1 M NaCl at 2 mL per every gram of cells to remove the glycosylated layer around the cells. The cell suspension was placed in a 37°C water bath for at least 15 min. The cells were pelleted at 12,000 RPM in 5 minutes. The supernatant was discarded, and the reddish colored pellets were resuspended in 20 mM Tris buffer pH 8 with 100 mM EDTA and 0.1 M NaCl. Egg white lysozyme was added from a stock solution to a final concentration of 0.8 mg/mL. The suspension was again incubated at 37°C for 30 min and then pelleted by the same method. If the pellet was colorless/white and the supernatant was red/orange/ brown, then patches had been obtained. If

the pellet was still colored, the cells were subjected to one round on the French Press at 20,000 PSI.

Membrane patches were prepared from the total membrane preparation using 5 ODU at 882 nm of these membranes layered onto a 30/34/37/40/50% w/w sucrose, 20 mM HEPES pH 7.5, 1 mM EDTA discontinuous gradient and centrifuged in a Beckman SW41 rotor for 2 hours at 40,000 rpm, 4^{o}C and the resultant bands collected. These detergent-free membranes were stored at -20^{o}C until used for imaging.

The membranes were diluted by between 5- and 10-fold with 20 mM HEPES pH 7.5 and 5µl of this diluted suspension pipette into 35 µl of absorption buffer, 20 mM HEPES pH 7.5, 150 mM KCl, 25 mM MgCl2, on a freshly cleaved 6 mm diameter mica disc and mixed by gentle pipetting. The membranes were allowed to adsorb to the mica for a minimum of 1 hour at RT in a closed Petri dish with a piece of moist tissue to minimize evaporation. The disc was washed twice with imaging buffer, 20 mM HEPES pH 7.5, 100 mM KCl, immediately prior to imaging in the AFM.

5.2.4 Atomic force microscopy (AFM)

Peak Force tapping mode imaging was conducted using SNL probes, 0.24 N/m spring constant, 2 KHz operating frequency mounted in a standard liquid cell in a Nanoscope V Multimode 8 with E scanner. The images were recorded at scan frequencies of 0.5-1.0 Hz and subsequently analyzed as described below.

Topographs were flattened and three-dimensional (3-D) representations generated using Bruker Nanoscope Analysis software (v1.4). Statistical analysis of high resolution topographs was performed using the same software to measure peak to peak of height profiles across

individual molecules in line with the scan and overall height with respect to the mica substrate or surrounding lipid bilayer surface. Only clearly defined complexes were examined to produce the most accurate analysis.

5.2.5 Heme protein quantitation

Whole Membranes (WM) were isolated as in section 5.2.1, but were collected before the detergent addition of the solubilization step. The whole membranes were diluted 1:1 with 20 mM Tris pH 8 buffer. The WM samples were prepared for SDS-PAGE by the 1:1 mixing of membrane with reductant free SDS-PAGE sample buffer, 30% glucose, 0.05% Commassie Blue 250, 4% Sodium Dodecyl Sulfate in 150 mM Tris pH 7. The samples were vortexed and allowed to incubate at 65°C for at least 30 min. Samples were loaded onto an 8 M urea 12% SDS-PAGE gel with a linearly increasing amount of sample added per well. Two identical gels were run at 30 V for one hour and 100 V for at least 2 hours until the blue dye began to leak from the bottom of the gel.

Gels were stained in the following manner. One was stained with CBR-250 in methanol and water for four hours and then destained in 10% acetic acid overnight. The second gel was stained, photographed and destained with the TMBZ heme staining procedure as described in Goodhew et al 1986[32]. The quantity of TMBZ staining was measured with the gel analysis function in FIJI-ImageJ.

5.3 Results

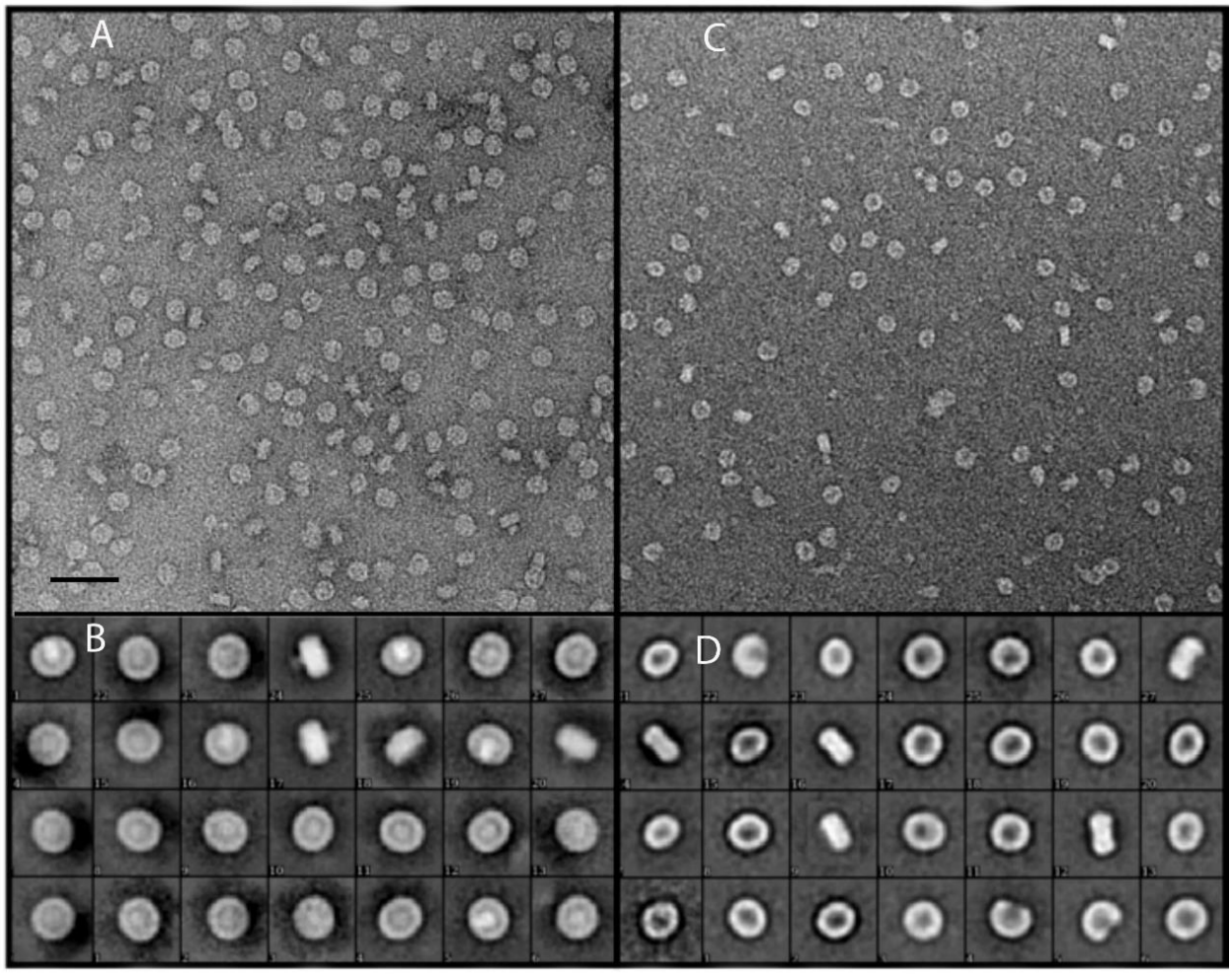

Figure 5.1 Single particles of purified LHRC and LH-only complexes. (A) Electron micrograph of the LHRC complex. Scalebar = 50 nm. (B) Selected 2D averaged classes from single particles of the LHRC complex. (C) LH-only electron micrograph and (D) Selected 2D averaged classes of LH-only particles. Box size = 28.3 x 28.3 nm.

5.3.1 EM single particle analysis and 3D reconstruction

RFX LHRC and LH-only complexes were isolated and purified as described above. The complexes were placed on EM grids, negatively stained and imaged. Under negative stain conditions, the single protein molecules can be seen clearly under the magnification of 60015 X. A total of 18945 RCLHC and 6086 LHC-only particles were selected from negative stained EM micrographs and 28 representative classes identified, most showing face-on orientations (Fig 5.1). Different orientations of the LHRC particles on the EM grid can be distinguished. The

molecules facing-up or down with respect to the membrane, were an elliptical circle with a clear central density attributed to the RC. (Fig 5.1A). The molecules lying on their sides showed a protruding density on one side of the LH ring, assigned as the cytochrome *c* subunit (Fig 5.1B). In the EM grid of LH-only (Fig 5.1C&D), LH complexes were empty elliptical circles, indicating that the RC was removed successfully from the purified LHRC. After 2D classification, discrete orientations of the LHRC and LH-only proteins on the EM grid were revealed as seen in Fig 5.1B&D.

From the 28 classes of EM images of the LHRC and the LH-only complexes, it was possible to conduct a 3D reconstructions to ≤ 20 Å resolution. The resulting structures are shown in three orientations in Figure 5.2. Panels A & B from figure 5.2 are in the plane of the membrane with the periplasmic face up. Panels C & D are rotated 90^{o} to A & B to show the periplasmic face, and panels E & F are rotated a further 180^{o} to show the cytoplasmic face. The 3D reconstructions show the ring structure of the LH-only complex like that of a LH1 complex from purple bacteria, and the central density of the RC in the LHRC with the tetraheme cytochrome *c* subunit protruding into the periplasm. On the cytoplasmic face, there is less density than observed in RC's with an H subunit. The reconstructions were generated on the same scale allowing a size comparison. We observe that the LH-only is smaller than the LHRC by about 10%. This can be seen more clearly in Figure 5.3A, where we have overlaid the LHRC, mesh, on the LH-only, solid surface. This also shows that the cytoplasmic and periplasmic faces of the LH-only complex are less protuberant when the RC is removed.

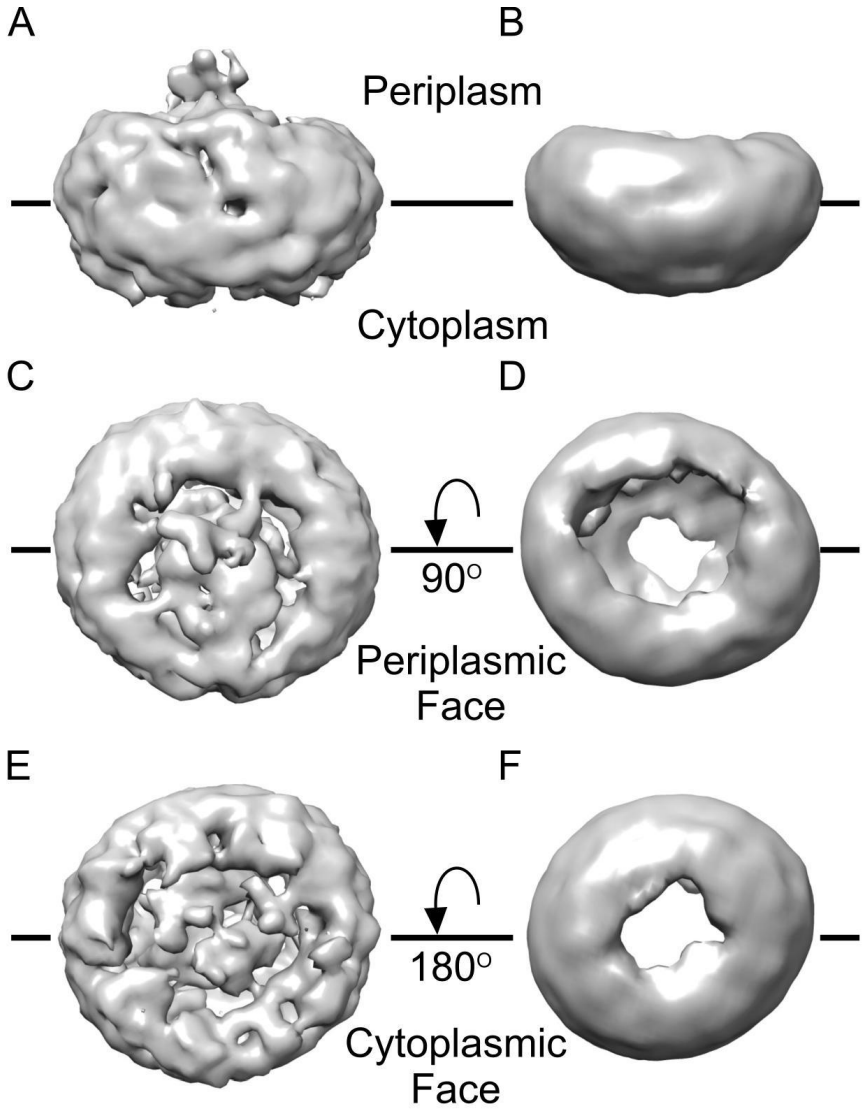

Fig 5.2 3D models of LHRC (left) and LH-only (right) complex from RFX. (A), (B) side view with the periplasmic side uppermost; (C), (D) top view from the periplasmic side; (E) and (F) bottom view from the cytoplasmic side. Images were produced using UCFS Chimera[33]

In addition to the overall shape and conformation, the 3D reconstruction EM models can be used to calculate the resolution limits and dimensions of the complexes. Resolution calculations were carried out based on 0.5 Fourier shell correlation criteria and show that the LHRC and LH-only models were determined to 14.6 Å and 19.4 Å resolution respectively (Fig 5.4 A&B). Although these resolutions are still not high enough to resolve individual

transmembrane helices, the 3D reconstruction models of LHRC and LH-only complexes reveal interesting structural features. The LH complex embraces the RC to form a complete elliptical ring with a long axis of 15.3 nm and a short axis of 14.1 nm. Removing the RC changes the dimension of the LH ring; it is still a complete elliptical ring, but shrinks to have a long axis of 14.1 nm and a short axis of 12.6 nm, losing over a nanometer in both directions. The C-subunit of the LHRC protrudes from the periplasmic side. The total height measured from the cytoplasmic side of the LHRC complex to the top of the C-subunit is 10.7 nm, while the height of LH ring in the LHRC complex is about 7.5 nm. The height of the LH-only complex is 7.1 nm. There is a depressed area on the cytoplasmic side of the LHRC complex, which in most of the core complexes from PB is occupied by the RC-H subunit that protrudes from the cytoplasmic side of the LH1 ring[34–36]. The lack of protusion on the cytoplasmic face confirms the lack of RC-H subunit or any type of replacement density in the core complex from RFX.

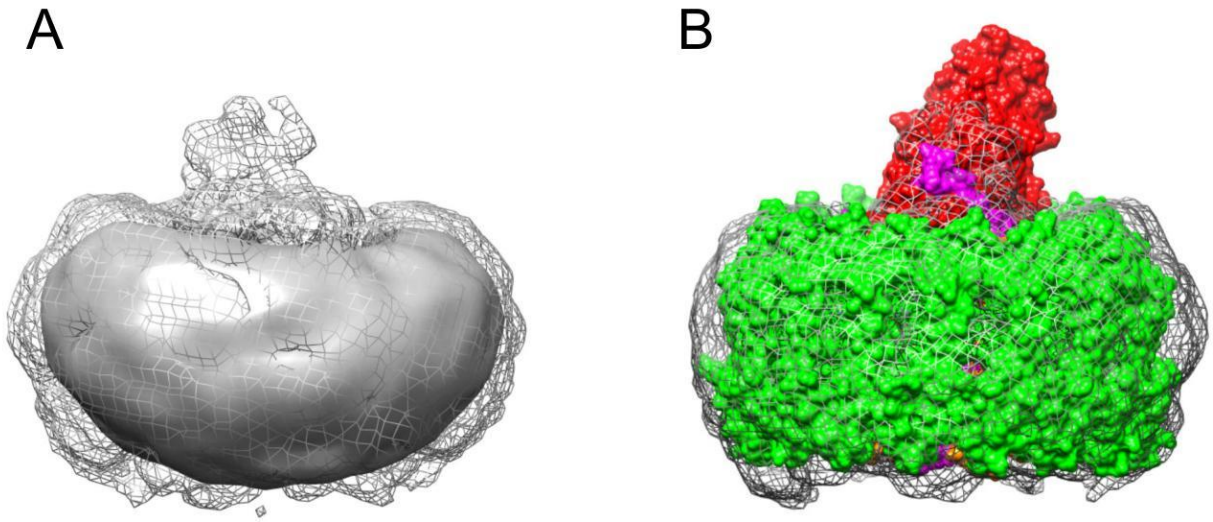

Figure 5.3 Comparison of the LHRC and LH-only with the RC-LH1 *T. tepidum* crystal structure. A) Overlaid 3D EM reconstruction models of the LRHC (mesh) and LH-only (solid) complexes. B) LHRC of the RFX(mesh) and RC-LH1 of the *T. tepidum* (solid) with a spacefill representation, LH1 is in green, RC in purple and the cytochrome is in red. The EM model of LHRC of the RFX was condensed to match the overall shape of the RC-LH1 complex from *T. tepidum.* The threshold level of the 3D EM model was adjusted such that total volume matches its predicted molecular weight[22]. This method was applied to EM 3D model of LH as well in panel A.

Fig 5.3 compares the 3D reconstruction of the RFX LHRC with the crystal structure of RC-LH1 from *T. tepidum*[35]. The overall size and shape of the RFX LHRC model and the *T. tepidum* crystal structure are a close match with the exception of the bound cytochrome (Fig 5.3B). On the basis of the similar diameters, we propose that the LH surrounding the RC in *R. castenholzii* is composed of 16 $\alpha_1\beta_1$bchl$_3$ units in agreement with the number of LH α/β dimer pairs observed in *T. tepidum* structure and biochemically determined in RFX. The disparity in the cytochrome *c* subunit is that the RFX model EM density is a couple of nanometers shorter and almost appears folded over compared to the *T. tepidum* C subunit. This is likely to be due to the negative stain used and the imposition of rotational symmetry on the reconstruction. Despite the size discrepancy in the cytochrome subunit, we believe our 20 Å EM 3D reconstruction model is a good approximation of the size and shape of the RFX LHRC.

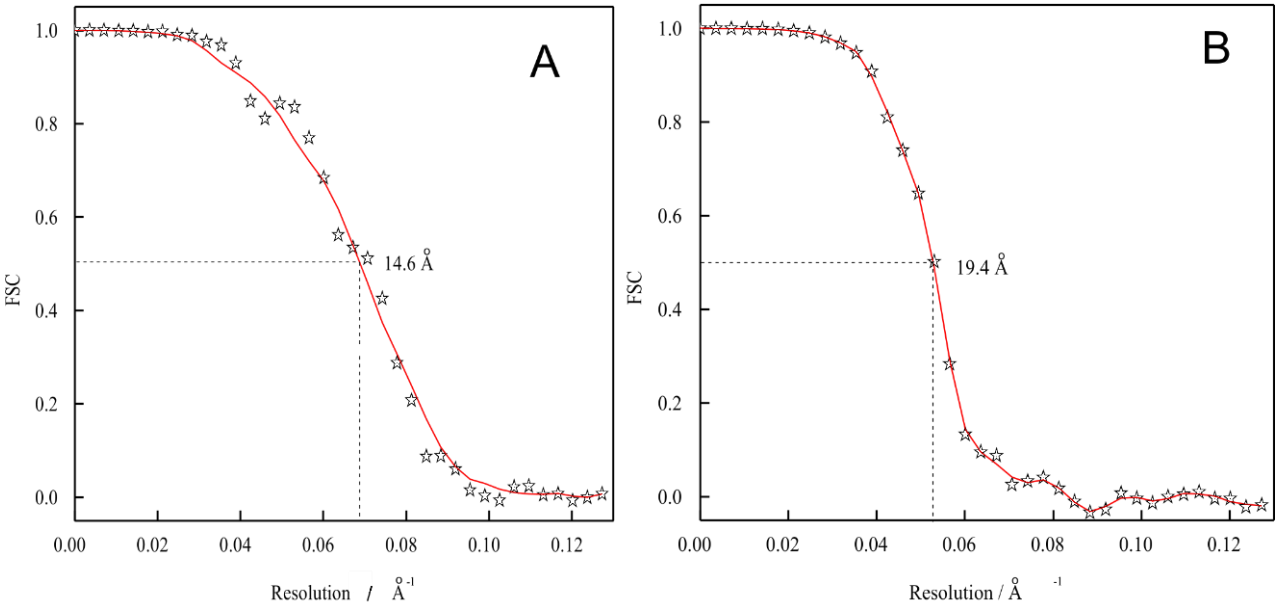

Figure 5.4 0.5 Fourier shell correlation criteria for resolution determination of 3D models. (A) LHRC and (B) LH-only from RFX.

5.3.2 Membrane isolation and AFM of membrane patches

Photosynthetic RFX membranes from lysed cells were fractionated on a discontinuous sucrose density gradient. The red colored band from the gradient yielded a variety of membrane patches, and AFM of several such patches showed the presence of loosely packed proteins of distinct heights (Fig. 5.5A). Their separation, as measured from the highest point to the highest point of the adjacent protein, and overall height as measured from the mica substrate (Fig 5.5B) showed that there were at least two types of protein complexes present, the most numerous being 11.1 ± 0.7 nm (SD), n = 106, and the second 13.7 ± 0.4 nm (SD), n = 13. The height of the small proteins is consistent with the height derived from single particle analysis of purified LHRC of 11.0 – 11.5 nm[22] and from the EM 3D reconstruction model of 10.7 nm, where the C-subunit is known to be compressed. Moreover, the height of the protrusion relative to the surrounding membrane was measured by AFM to be 3.9 ± 0.5 nm (SD), n = 20, which is compatible with the 4 nm height of the C subunit protrusion measured in Collins et al. (2010)[22] and the 3.2 nm height difference in the 3D EM model. On the basis of these dimensions and the fact that this membrane patch came from a colored band having the absorbance spectrum of the LHRC complex including the cytochrome, we assign these features as arising from the periplasmic face of the LHRC complex *in situ* in the membrane.

There is an elevated section of the membrane which has similar proteins within it, which is likely to be due to an underlying piece of empty lipid membrane (Fig. 5.5A, yellow area). The overall height of these proteins was not measured, however the height of the protrusions with respect to the surrounding membrane was measured as 3.9 ± 0.5 nm (SD), n = 12, thus it seems very likely that these are also LHRC complexes.

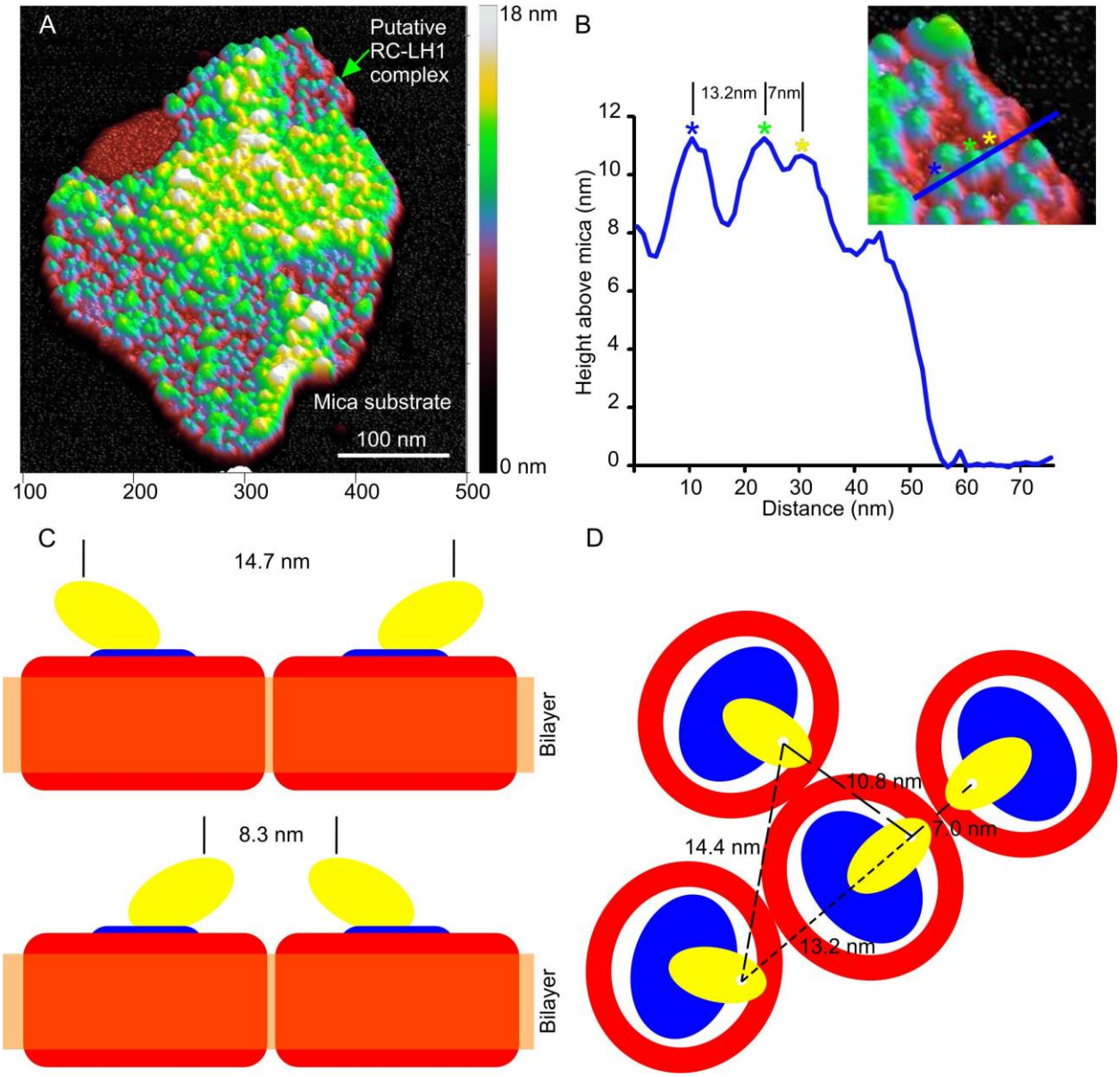

Figure 5.5 Organization of the *RFX* putative photosynthetic membrane A) 3D representation of medium resolution AFM height data in false color where black is the mica substrate, full z = 18 nm. The patch has numerous protrusions in blue, average height above the mica 11.1 ± 0.7 nm SD, n = 106, assigned as putative LHRCs. Similar sized protrusions in yellow may also be LHRCs that are raised off the mica by an underlying piece of membrane, however these were not included in our assessment. B) A scan line across three putative LHRCs in the membrane, shown in blue on the inset, and their separations, highest point to highest point of 13.2 and 7 nm. C) A cartoon highlighting the highly asymmetric position of the cytochrome subunit of *R. castenholzii* with vertical lines denoting the highest point of the complex. Depending upon the orientation of the complexes the resulting separation would be as large as 14.7 nm or as small as 8.3 nm based on *T. tepidum* X-ray structure. D) A cartoon representation of the organization of 4 LHRCs based upon their measured separation, highest point to highest point, demonstrating that the complexes do not appear to be closely packed but do have an aligned orientation.

The identity of the larger proteins is more difficult to assign with confidence as the most likely candidate, ACIII, which functionally replaces the cytochrome bc_1 complex in *Chloroflexi*, has no 3D structure available; this is addressed in the Discussion.

Analysis of the spacing and packing patterns was done using a line scan and measuring the distances between the putative LHRCs (smaller proteins) and the putative ACIIIs (larger proteins). A scan line across three putative LHRCs in the membrane (Fig 5.5B, blue line on the inset) reveals their separations, highest point to highest point of 13.2 and 7 nm (Fig. 5.5B). The average separation distance of 11.5 ± 2.4 nm (SD), n = 72, was determined for the clearly defined examples in the patches. The large fluctuation in average spacing distance is attributed to the tilted and off-center position of the periplasmic cytochrome subunit as it protrudes above the membrane. This notion is explored in Figure 5.5C with a cartoon highlighting the highly asymmetric position of the C-subunit in the LHRC complex. Two complexes are paired to show the maximum distance, 14.7 nm, if the C-subunits were as far apart as possible and the minimum distance, 8.3 nm, if the C-subunits were as close as possible. If the C-subunits were vertically perpendicular to the membrane, we would expect a more consistent separation distance.

After the separation distance was measured, the patches were analyzed for any overall pattern in the arrangement of the smaller and larger proteins within the membrane. The smaller proteins are intermixed with the larger in a loosely packed and chaotic manner with no clear pattern discernible, but the smaller proteins did appear to cluster together. This apparent clustering, which is explored in the cartoon in figure 5.5D and is based upon their measured separation, highest point to highest point. This model demonstrates that the complexes do not appear to be closely packed, as in PB membranes, but do have an aligned orientation. It appears that the LHRCs are clustered such that their cytochrome subunits are aligned, supported by

analysis of the measured average separation of the putative LHRC complexes, which is 11.5 ± 2.4 nm SD, n = 72. This distance is too small for the known dimensions of the complex, average diameter 13.1 nm, but is compatible with an orientation where the cytochromes are proximal in any 'pair' of complexes, as explored in Figure 5.5C. It also appears that these clusters of putative LHRCs are congregated near the larger proteins, putative ACIIIs, which would promote efficiency of the electron transport function within the membrane. While no higher order definitive membrane packing patterns were observed, the number of complexes, putative identities, separation distances and clustering pattern were determined.

5.3.3 Heme Quantitation and Membrane Protein Ratio Determination

The ratio of LHRC to ACIII in the photosynthetic membranes of RFX was determined using SDS-PAGE and TMBZ heme staining. This method was chosen because TMBZ selectively stains *c*-type hemes and the dominant three *c*-type heme containing proteins in the membranes of RFX are the tetraheme cytochrome *c* subunit of the RC, the ActA pentaheme and ActE monoheme subunits of the ACIII. Therefore, the amount of LHRC is represented by the cyt *c* band and the amount of ACIII is shown in the ActA and ActE bands. Based on the molecular weights and previous gels with protein identity confirmation by mass spectrometry[15,22], we can confidently identify proteins from the gel bands. RC cyt *c* runs at around 36 kDa, ActA about 25 kDa and ActE at 20 kDa (Fig. 5.6A). It was evident from the TMBZ stained gel that the three subunits we knew to contain *c*-type hemes, are the only subunits with *c*-type hemes in the membrane at detectable amounts. The image of the TMBZ stained gel was analyzed in the Fiji-ImageJ Gel Analysis program yielding intensity plots of each lane. The area under the intensity profile peaks was measured, which corresponds to the amount of protein in each band, and then plotted and found to increase linearly corresponding to the gel loading (Fig. 5.6B). Then the ratio

of the areas was calculated, however the ratio is approximate since TMBZ signal strength varies with peroxidase activity and each cytochrome has different levels of peroxidase activity (personal communication Robert Kranz). Since the gel was loaded with an increasing linear amount of sample, the calculated area of the intensity from all lanes should also linearly increase. Lanes that were not in the linear region due to overloading were not included in the ratio calculation. The ratio from all linear lanes was calculated and found to range from approximately 3 LHRC to 1 ACIII for overloaded samples, consistent with the RC-LH1 to cyt bc_1 ratio found in purple bacteria[37] up to 10 LHRC to 1 ACIII for not overloaded samples.

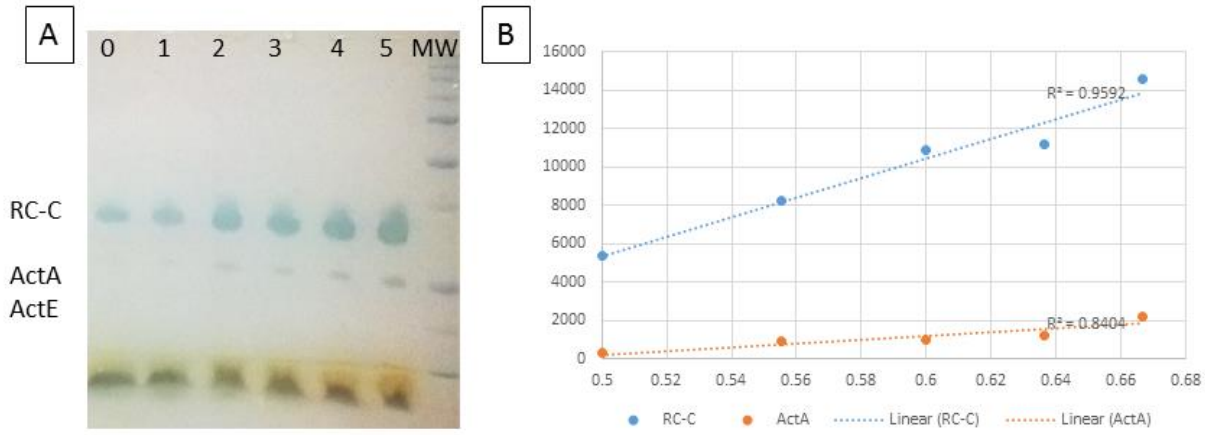

Figure 5.6 Membrane Ratio determined by Heme Staining A) TMBZ stained 8M urea SDS-PAGE gel of whole membrane. MW, molecular weight markers, numbers, volume of OD 10 whole membrane in sample. B) Plot of area under the intensity profile for RC-C and ActA.

5.4 Discussion

5.4.1 EM- LHRC Size, Shape and Structure

We characterized the LHRC and the detergent derived LH complex by negative stain EM and single particle analysis, which clearly showed the periplasmically exposed bound cytochrome subunit (Fig 5.1). The distinct protruding shape of this subunit allows for the determination of the orientation of the complex, namely the periplasmic and cytoplasmic faces as indicated in Figure 5.2. The 3D reconstruction of both complexes, at ~20 Å resolution, allows us to superimpose the LH on the LHRC to better appreciate this size difference, but it must be borne in mind that this is a symmetrized structure which averages out the slightly ovoid shape of the LHRC and centers the asymmetrically positioned bound cytochrome (Figure 5.3).

We have aligned the images in Figure 5.2 making an assumption about the orientation of the LH complex based upon our ability to fit the LH 3D reconstruction within the bounds of the LHRC reconstruction (Fig. 5.3A). In all three orientations shown in figure 5.2, the LH is smaller than the LHRC for which there are two probable explanations. One, the loss of the RC mediates shrinking of the LH-only or damages the ring upon removal. A feature of the LH-only data is the presence of partial rings (Fig. 5.1B), which are likely caused by the detergent removal of the RC during solubilization of the LHRC. There are three classes of LH in the EM data that have clearly open, incomplete, rings. We consider these open rings to be due to partial solubilization of the LH during RC extraction, where 2 or more $\alpha_1\beta_1$bchl$_3$ subunits have been removed preventing a closed ring from reforming. The smaller closed rings of the LH could be the result of the loss of a single $\alpha_1\beta_1$bchl$_3$, which does not prevent a closed ring reforming. The alternative is that there is a compaction of the LH after RC removal without the loss of an α/β pair simply

because the RC is not there to force a certain shape or size as a physical mold but also from a loss of intermolecular interactions.

A second explanation of the LH appearing smaller in the LH-only complex is the variability of inter-subunit spacings, as observed in the RC-LH1 crystal structures of related PB. Niwa et al. noted substantive variations in the inter-subunit spacings with a maximum difference of 1.9 Å between the α polypeptides on the periplasmic face and 3.5 Å on the cytoplasmic face. If these distances were to minimize upon the removal of the RC, then the LH would indeed have a smaller diameter than the LHRC and would 'shrink' on RC removal. On this basis, the bowl shape of the LH-only reconstruction also validates our orientation of the LH in figure 5.2. The partial rings observed in EM cannot be explained by this inter-subunit spacing loss mechanism so it seems likely that the smaller observed size is the result of a combination of the two proposals, damage during solubilization and compaction.

A comparison of the LHRC 3D reconstruction and the crystal structure of *T. tepidum* shows a close match in overall physical dimensions (Fig. 5.3B), which makes it likely that the LH ring is composed of 16 $\alpha_1\beta_1$bchl$_3$ subunits, in agreement with Collins et al. (2010) who derived a figure of 15±1. The final volume of the EM 3D model of the LHRC has been adjusted based on the comparison with the X-ray model of the RCLH1 from *T. tepidum*, from which the H subunit was removed for ease of comparison with the RFX complex. The density threshold levels of the EM 3D models of the LHRC and LH-only complexes from RFX were adjusted based on their molecular masses[22]. The RC cytochrome *c* subunit of RFX was observed by EM to be smaller than the corresponding subunit of *T. tepidum;* this difference could arise from the larger size of the *T. tepidum* subunit, which is about 80 amino acid residues linger than its RFX counterpart (Fig. 5.7C). Additionally, detergent and stain effects can increase the apparent size

of 3D EM models [38–40]; a high-resolution method is needed for precise measurement of size and structure of this complex.

A

```
T_Tep_LH_alpha      MFTMNANLYKIWLILDPRRV----LVSIVAFQIVLGLLIHMIVLS-TDLNWLDDNIPVSY
RFX_LH_alpha        -------------MKDRPFEFRTSVVVSTLLGLVMALLIHFVVLSSGAFNWLRAP-----
CFX_LH_alpha        --------------MQPRSPVRTNIVIFTILGFVVALLIHFIVLSSPEYNWLSNAEGGAL
                                  :        :*  . : :*:.***::***    **
T_Tep_LH_alpha      QALGKK-----
RFX_LH_alpha        -----------
CFX_LH_alpha        LLSAARALFGI
```

B

```
T_Tep_LH_beta       --MAEQK-----SLTGLTDDEAKEFHAIFMQSMYAWFGLVVIAHLLAWLYRPWL-
RFX_LH_beta         MTDKPQNDLVPDQWKPLFNNAQWLVHDIVVKTIYGGLIIAVIAHVLCWAWTPWIR
CFX_LH_beta         --MRDDDDLVPPKWRPLFNNQDWLLHDIVVKSFYGFGVIAAIAHLLVYLWKPWLP
                         :.     .   * ::    .* *.::::*.   :..**:* : : **:
```

C

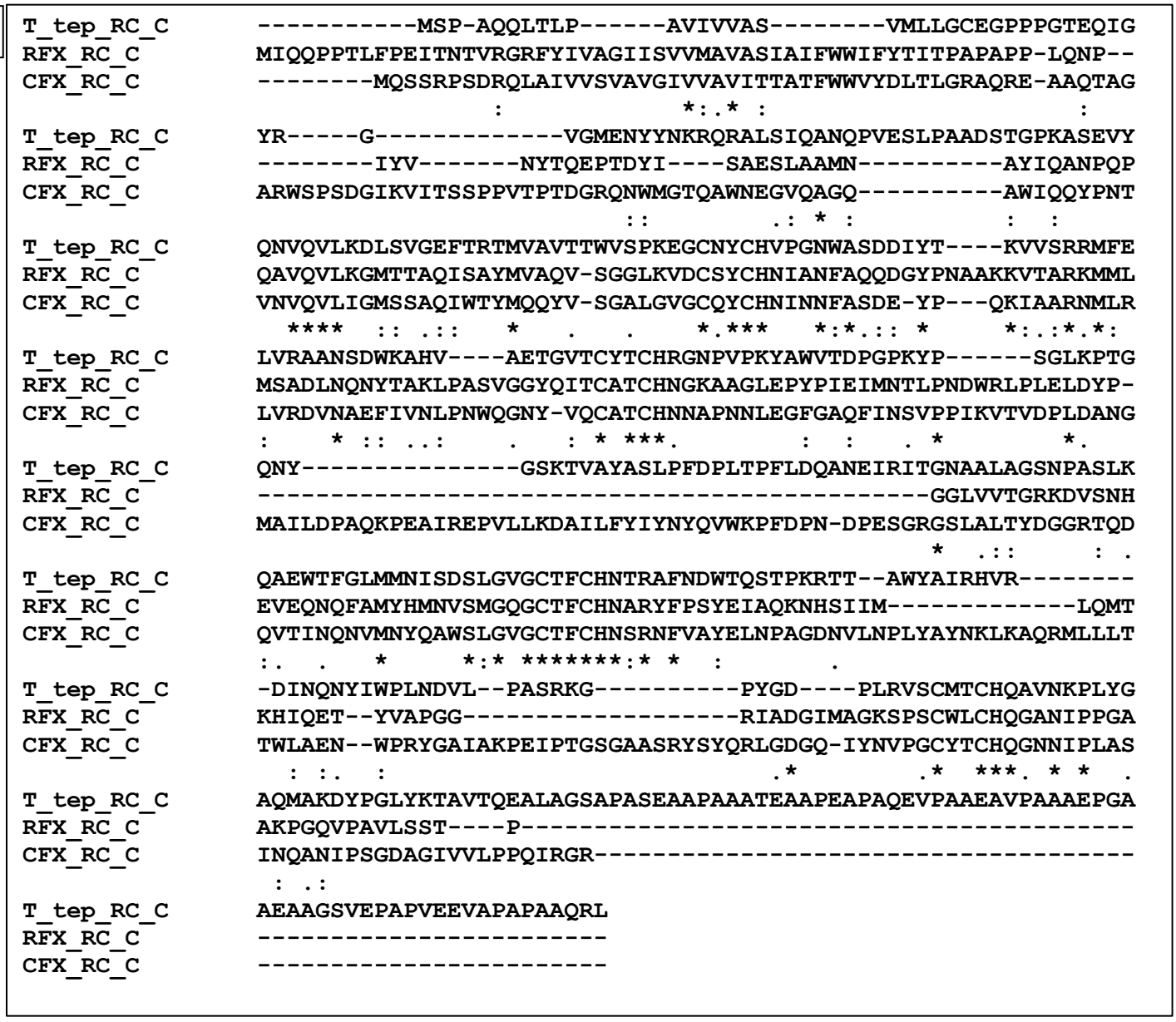
T_tep_RC_C ----------MSP-AQQLTLP------AVIVVAS--------VMLLGCEGPPPGTEQIG
RFX_RC_C MIQQPPTLFPEITNTVRGRFYIVAGIISVVMAVASIAIFWWIFYTITPAPAPP-LQNP--
CFX_RC_C --------MQSSRPSDRQLAIVVSVAVGIVVAVITTATFWWVYDLTLGRAQRE-AAQTAG
T_tep_RC_C YR-----G------------VGMENYYNKRQRALSIQANQPVESLPAADSTGPKASEVY
RFX_RC_C --------IYV-------NYTQEPTDYI----SAESLAAMN----------AYIQANPQP
CFX_RC_C ARWSPSDGIKVITSSPPVTPTDGRQNWMGTQAWNEGVQAGQ----------AWIQQYPNT
T_tep_RC_C QNVQVLKDLSVGEFTRTMVAVTTWVSPKEGCNYCHVPGNWASDDIYT----KVVSRRMFE
RFX_RC_C QAVQVLKGMTTAQISAYMVAQV-SGGLKVDCSYCHNIANFAQQDGYPNAAKKVTARKMML
CFX_RC_C VNVQVLIGMSSAQIWTYMQQYV-SGALGVGCQYCHNINNFASDE-YP---QKIAARNMLR
T_tep_RC_C LVRAANSDWKAHV----AETGVTCYTCHRGNPVPKYAWVTDPGPKYP------SGLKPTG
RFX_RC_C MSADLNQNYTAKLPASVGGYQITCATCHNGKAAGLEPYPIEIMNTLPNDWRLPLELDYP-
CFX_RC_C LVRDVNAEFIVNLPNWQGNY-VQCATCHNNAPNNLEGFGAQFINSVPPIKVTVDPLDANG
T_tep_RC_C QNY--------------GSKTVAYASLPFDPLTPFLDQANEIRITGNAALAGSNPASLK
RFX_RC_C --GGLVVTGRKDVSNH
CFX_RC_C MAILDPAQKPEAIREPVLLKDAILFYIYNYQVWKPFDPN-DPESGRGSLALTYDGGRTQD
T_tep_RC_C QAEWTFGLMMNISDSLGVGCTFCHNTRAFNDWTQSTPKRTT--AWYAIRHVR--------
RFX_RC_C EVEQNQFAMYHMNVSMGQGCTFCHNARYFPSYEIAQKNHSIIM----------LQMT
CFX_RC_C QVTINQNVMNYQAWSLGVGCTFCHNSRNFVAYELNPAGDNVLNPLYAYNKLKAQRMLLLT
T_tep_RC_C -DINQNYIWPLNDVL--PASRKG----------PYGD----PLRVSCMTCHQAVNKPLYG
RFX_RC_C KHIQET--YVAPGG-----------------RIADGIMAGKSPSCWLCHQGANIPPGA
CFX_RC_C TWLAEN--WPRYGAIAKPEIPTGSGAASRYSYQRLGDGQ-IYNVPGCYTCHQGNNIPLAS
T_tep_RC_C AQMAKDYPGLYKTAVTQEALAGSAPASEAAPAAATEAAPEAPAQEVPAAEAVPAAAEPGA
RFX_RC_C AKPGQVPAVLSST----P--
CFX_RC_C INQANIPSGDAGIVVLPPQIRGR-----------------------------------
T_tep_RC_C AEAAGSVEPAPVEEVAPAPAAQRL
RFX_RC_C ------------------------
CFX_RC_C ------------------------

D

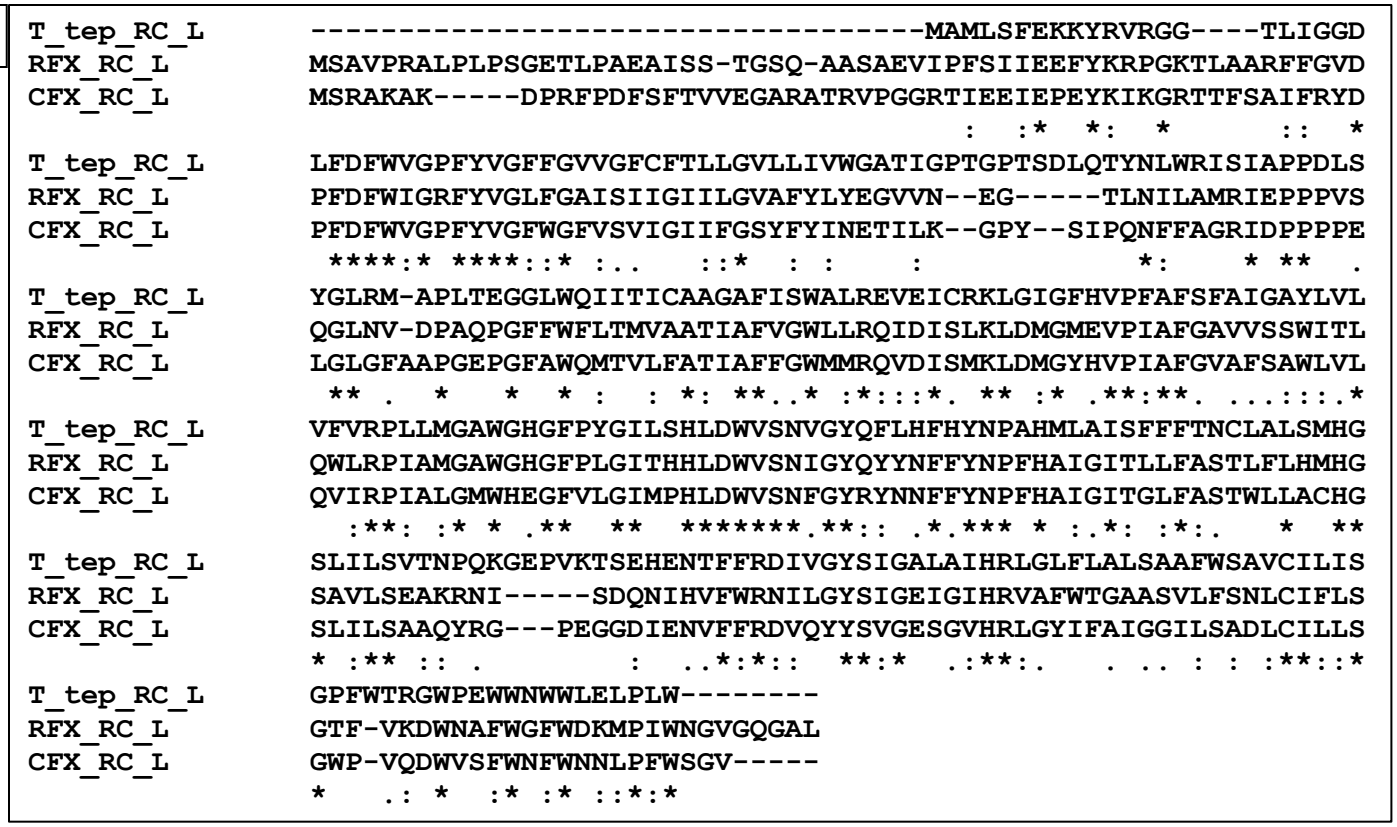
T_tep_RC_L ----------MAMLSFEKKYRVRGG----TLIGGD
RFX_RC_L MSAVPRALPLPSGETLPAEAISS-TGSQ-AASAEVIPFSIIEEFYKRPGKTLAARFFGVD
CFX_RC_L MSRAKAK-----DPRFPDFSFTVVEGARATRVPGGRTIEEIEPEYKIKGRTTFSAIFRYD
T_tep_RC_L LFDFWVGPFYVGFFGVVGFCFTLLGVLLIVWGATIGPTGPTSDLQTYNLWRISIAPPDLS
RFX_RC_L PFDFWIGRFYVGLFGAISIIGIILGVAFYLYEGVVN--EG-----TLNILAMRIEPPPVS
CFX_RC_L PFDFWVGPFYVGFWGFVSVIGIIFGSYFYINETILK--GPY--SIPQNFFAGRIDPPPPE
T_tep_RC_L YGLRM-APLTEGGLWQIITICAAGAFISWALREVEICRKLGIGFHVPFAFSFAIGAYLVL
RFX_RC_L QGLNV-DPAQPGFFWFLTMVAATIAFVGWLLRQIDISLKLDMGMEVPIAFGAVVSSWITL
CFX_RC_L LGLGFAAPGEPGFAWQMTVLFATIAFFGWMMRQVDISMKLDMGYHVPIAFGVAFSAWLVL
T_tep_RC_L VFVRPLLMGAWGHGFPYGILSHLDWVSNVGYQFLHFHYNPAHMLAISFFFTNCLALSMHG
RFX_RC_L QWLRPIAMGAWGHGFPLGITHHLDWVSNIGYQYYNFFYNPFHAIGITLLFASTLFLHMHG
CFX_RC_L QVIRPIALGMWHEGFVLGIMPHLDWVSNFGYRYNNFFYNPFHAIGITGLFASTWLLACHG
T_tep_RC_L SLILSVTNPQKGEPVKTSEHENTFFRDIVGYSIGALAIHRLGLFLALSAAFWSAVCILIS
RFX_RC_L SAVLSEAKRNI-----SDQNIHVFWRNILGYSIGEIGIHRVAFWTGAASVLFSNLCIFLS
CFX_RC_L SLILSAAQYRG---PEGGDIENVFFRDVQYYSVGESGVHRLGYIFAIGGILSADLCILLS
T_tep_RC_L GPFWTRGWPEWWNWWLELPLW--------
RFX_RC_L GTF-VKDWNAFWGFWDKMPIWNGVGQGAL
CFX_RC_L GWP-VQDWVSFWNFWNNLPFWSGV-----

E

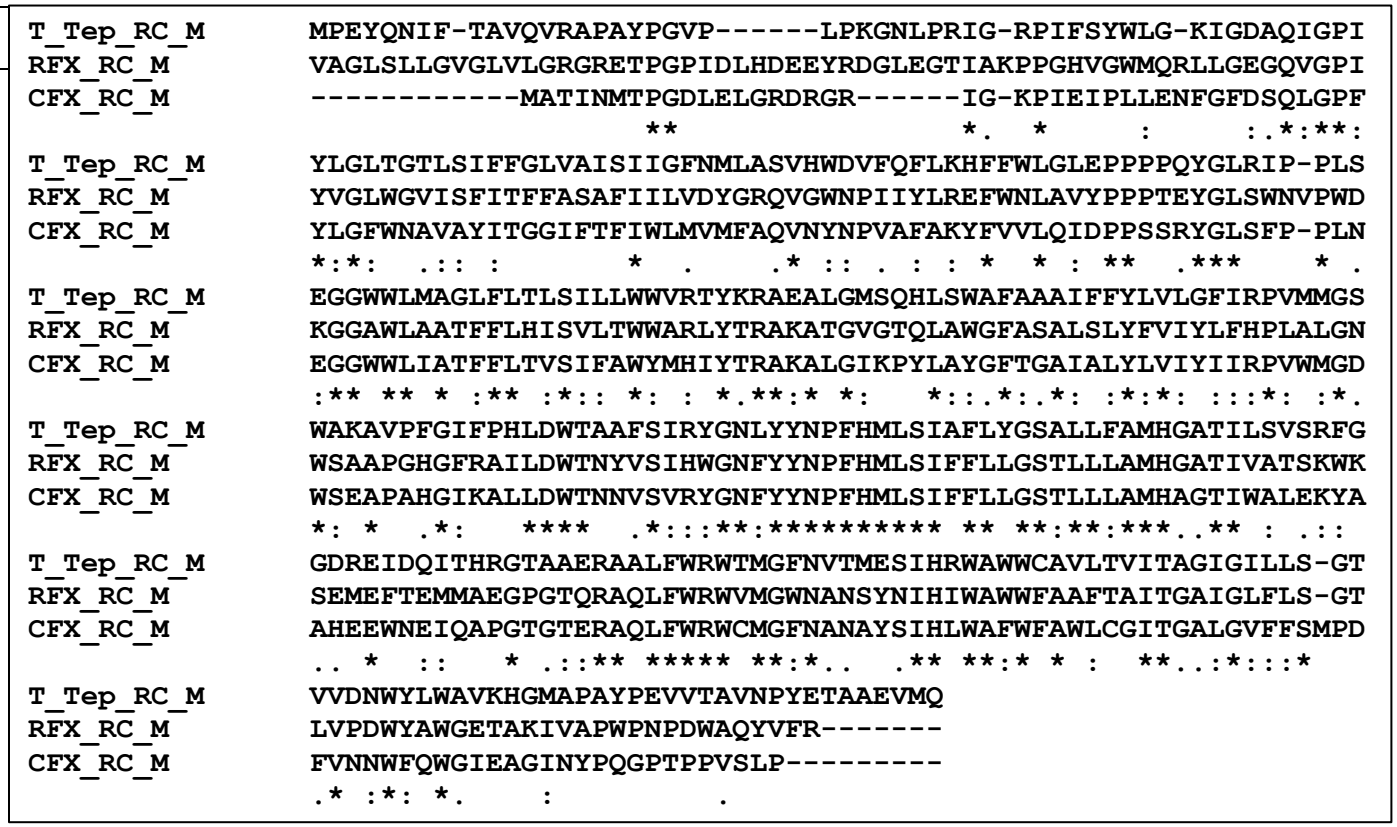
T_Tep_RC_M MPEYQNIF-TAVQVRAPAYPGVP------LPKGNLPRIG-RPIFSYWLG-KIGDAQIGPI
RFX_RC_M VAGLSLLGVGLVLGRGRETPGPIDLHDEEYRDGLEGTIAKPPGHVGWMQRLLGEGQVGPI
CFX_RC_M ------------MATINMTPGDLELGRDRGR------IG-KPIEIPLLENFGFDSQLGPF
T_Tep_RC_M YLGLTGTLSIFFGLVAISIIGFNMLASVHWDVFQFLKHFFWLGLEPPPPQYGLRIP-PLS
RFX_RC_M YVGLWGVISFITFFASAFIILVDYGRQVGWNPIIYLREFWNLAVYPPPTEYGLSWNVPWD
CFX_RC_M YLGFWNAVAYITGGIFTFIWLMVMFAQVNYNPVAFAKYFVVLQIDPPSSRYGLSFP-PLN
T_Tep_RC_M EGGWWLMAGLFLTLSILLWWVRTYKRAEALGMSQHLSWAFAAAIFFYLVLGFIRPVMMGS
RFX_RC_M KGGAWLAATFFLHISVLTWWARLYTRAKATGVGTQLAWGFASALSLYFVIYLFHPLALGN
CFX_RC_M EGGWWLIATFFLTVSIFAWYMHIYTRAKALGIKPYLAYGFTGAIALYLVIYIIRPVWMGD
T_Tep_RC_M WAKAVPFGIFPHLDWTAAFSIRYGNLYYNPFHMLSIAFLYGSALLFAMHGATILSVSRFG
RFX_RC_M WSAAPGHGFRAILDWTNYVSIHWGNFYYNPFHMLSIFFLLGSTLLLAMHGATIVATSKWK
CFX_RC_M WSEAPAHGIKALLDWTNNVSVRYGNFYYNPFHMLSIFFLLGSTLLLAMHAGTIWALEKYA
T_Tep_RC_M GDREIDQITHRGTAAERAALFWRWTMGFNVTMESIHRWAWWCAVLTVITAGIGILLS-GT
RFX_RC_M SEMEFTEMMAEGPGTQRAQLFWRWVMGWNANSYNIHIWAWWFAAFTAITGAIGLFLS-GT
CFX_RC_M AHEEWNEIQAPGTGTERAQLFWRWCMGFNANAYSIHLWAFWFAWLCGITGALGVFFSMPD
T_Tep_RC_M VVDNWYLWAVKHGMAPAYPEVVTAVNPYETAAEVMQ
RFX_RC_M LVPDWYAWGETAKIVAPWPNPDWAQYVFR-------
CFX_RC_M FVNNWFQWGIEAGINYPQGPTPPVSLP---------

Figure 5.7 Amino acid alignment of LHRC proteins Alignment of RFX with the *T. tepidum* and *Chloroflexus aurantiacus* subunits by ClustalΩ. Pigment binding histidines are shown in red. A) Light harvesting alpha subunit B) Light harvesting beta subunit C) Reaction Center cytochrome c subunit D) Reaction Center L subunit E) Reaction Center M subunit

The amino acid alignment and structural dimensions of RFX LHRC with the solved purple bacteria RC-LH1s allow us to make predictions about the arrangement of the pigments. FAPs and purple bacteria share type II reaction centers with the symmetrical pigment arrangements. Crystal structures of purple bacteria have indicated which amino acid residues are responsible for the type II pigment arrangements[35,36]. Based on amino acid sequence alignments, we predict the pigments of RFX to look like much like those of the PB systems within the RC (Fig. 5.7 D & E). In PB, the RC pigments are four bacteriochlorophyll *a* (bchl a) and two bacteriopheophytins (bphe)[41]. RFX replaces one bchl *a* with an additional bphe[19], a substitution that is likely to direct electron flow due to the asymmetry introduced into the system. The other key difference in the RC of RFX versus that of PB is the lack of the H subunit. In our models, the H subunit has been removed from the PB to compare. The H subunit does not bind any pigments, but adds protein volume on the cytoplasmic face of the complex, which is absent in RFX. This will likely affect the complex in some manner, but not in the core pigment structure.

Encircling the RC, is the LH system which we expect the RFX LH to diverge more from the PB model than the RC. The main difference in the RC was one pigment substitution and lack of the H subunit. The RFX LH portion is more distinct because it has been described as a LH1/LH2 hybrid. The *T. tepidum* PB LH1 system contains two bchls *a* and one carotenoid per alpha beta pair, although the ratio is 2 bchls a and 2 carotenoids per alpha beta pair in bacteria such as *Rhodobacter sphaeroides*[34]. The RFX complex has three bchl *a* and one carotenoid per alpha beta pair, similar to the ratio found in some PB LH2 complexes and compatible with the

view that the RFX complex is a LH1/LH2 hybrid. In alignments with the PB LH systems, two conserved histidine residues in the beta subunit and one histidine in the alpha subunit likely bind the Mg of the bacteriochlorophyll *a* molecules (Fig. 5.7 A&B). Since the pigment binding residues are conserved and there are three bchl a's in the RFX LH system, we predict the pigments in the RFX LH system should have a ring of bchl a parallel to the transmembrane helices with 2 bchl a per apha beta pair as in PB LH1. A second ring perpendicular to the transmembrane helices with 1 bchl a per alpha beta pair in the manner of PB LH2 should account for the final bchl a. The idea of the parallel and perpendicular bchl a rings in bolstered by the UV/vis absorbance spectrum of the complex which has peaks at 880 and 800 nm for the LH and 850 for the RC. The typical PB LH2 complex provides the 800 and 850 signal and the 880 is typical of the 30nm red shift found in LH1 complexes. Additional evidence from sequence also pints to the LH1/LH2 hybrid nature of the RFX LH complex. When analyzed using BLAST, the RFX LH alpha and beta sequences aligned with sequences from PB LH1, LH2, and LH3 complexes. Therefore in one core complex, RFX has the elements of PB LH2, LH1 and RC.

Table 5.1 Kinetics of reaction center core complexes

Species	bc_1/ACIII enzyme activity		LH1 to RC (trapping time-equilibration of P+I- with excited antenna)	Tertaheme re-reduction of SP (P* lifetime)	Bleaching of SP ($P+H_A^-$ lifetime)	Charge Separation Yield
	$k(s^{-1})$	K_m (uM)				
FAPS *RFX and CFX*	51.7[26]*	4.3*	60 ps (open) 210 ps (closed)[23]	480 ns[25]	200 ps[25]	≥90%[25]
	70.3[26]^	2.6^				
Rhodobacter capsulatus	65.5[42]*	3.75*				~100%
	68.9[42#]	3.17[#]				
Blastochloris viridis	43.4[42]*	7.25*	60 (open) 200 (closed)[43]	460 ns[44]	~ 200 ps[45]	~100%
	28.7[42#]	4.62[#]				
Rhodospirillum rubrum			35 ps[46]			~100%
Rhodobacter sphaeroides					229 ±25 ps[47]	~100%

* measured with Horse Heart cytochrome *c* as soluble acceptor
^ measured with auracyanin A as soluble acceptor
[#] measured with cytochrome c_2 as soluble acceptor

The notion of the LH1/LH2 hybrid idea can also be examined in terms of kinetics of energy and electron transfer within the complexes. The similarity in predicted pigment arrangement within the RC and LH portions of the RFX and PB systems could account for the observed similarities in kinetic rates and conversion efficiencies measured in previous studies (Table 5.1). A notable feature of the PB RC is that it has nearly 100% yield of charge separation. This implies that nearly every time the RC special pair receives excitation energy, charge separation yielding electron movement is achieved. The yield of charge separation was about 10% less in RFX than in PB, which could result from the pigment substitution in the RC or any of the other differences between the systems[25]. Even though it is less than in PB, the RC conversion efficiency in RFX is high.

The kinetics within the RC of RFX are also comparable to those of PB. The measured trapping time representing LH1 donating excitation energy to the special pair of the RC in both RFX and several PB species was 60 ps for open RCs and ~200 ps for closed RCs. This indicates the hybrid RFX LH complex is able to donate to the RC at the same rate as a LH1 complex[23,43,46]. Bleaching of the special pair, lifetime of the $P^{+}H_{A}^{-}$ state, was also measured to be approximately 200 ps in RFX and PB[25,45,47]. Despite the substitution of the bchl for a bphe, the internal kinetics of the RCs are comparable. Similarly, the tetraheme subunit high potential heme could donate to the special pair on a very similar timescale, 480 ns lifetime of the excited special pair in RFX vs 460 ns in *Blc. viridis*[25,44]. The LHRC kinetics indicate that the one antenna core complex of the RFX system is able to keep up with a multi complex LH2-LH1-RC system.

After charge separation in the RC, the electron is transferred to a second membrane protein complex that completes the cyclic electron transport chain. The second protein is the cytochrome bc_1 complex in PB and the Alternative Complex III, ACIII, in FAPs. Both bc_1 and ACIII take electrons from quinol and give them to the soluble acceptor protein that shuttles electrons back to the RC. They also pump protons across the membrane to establish the electrochemical gradient. In order for the RC and whole electron transport chain to operate smoothly, the proton pump/quinol oxidizing enzyme needs to turn over at a rate in line with the RC. PB bc_1 complexes measured as rate constant, k, range from 30 to 70 s^{-1}(Table 5.1). The turnover rate of the ACIII was in the middle of the rates measured for two PB cytochrome bc_1 complexes indicating that this side of the electron transport chain turns over at nearly equal rates[26,42].

Another important consideration in the efficiency of these LHRC and ACIII systems is the ability of quinone to access the RC through the LH ring. Quinone channels have been

observed in PB in three motifs: PufX, W, and closed. In some systems with PufX, the complexes are arranged as a dimeric S shape with an opening, like drawing back a curtain, for quinone diffusion between each RC in the dimer[34,48,49]. However, PufX does not always promote dimer formation, such as the monomeric *Rha. capsultaus* system[50]. The W motif may create an opening in monomeric systems, but has not yet been shown[51]. The closed motif has been observed most recently. Niwa et al. (2014) noted the presence of holes within the LH1 complex, which they proposed were the quinone diffusion channels, that had variable dimensions around the ring[35]. The size of the RFX LH complex is closest to *T. tepidum* and also lacks the pufX or W subunits. Although our EM model is at a lower resolution, we believe the quinone channels would probably follow the same mold as the *T. tepidum* structure. The EM models have allowed us to investigate the structure, energy, electron, and quinone flow of the RFX LHRC.

5.4.2 AFM Supramolecular organization

We used AFM and heme quantification to look at the supramolecular organization and electron flow of the major photosynthetic complexes in the membranes of RFX. While it is known that *R. castenholzii* does not have chlorosomes, there is an LHRC complex that has many similarities to the well-studied purple bacterial RC-LH1 core complex, but it lacks a H subunit on the cytoplasmic face of the complex and has pigment substitutions as discussed above. The LHRC complex alone would be sufficient to support photosynthetic growth in a manner similar to the PB such as *Rhodospirillum rubrum* and *Blc. viridis*. In AFM images of the latter photosynthetic membranes large arrays of circular complexes with a protruding C subunit can be seen, however these are much better resolved than the proteins in membrane pieces derived from RFX and it is clear that the *Blc. viridis* RC-LH1-Cyt complexes have little space between them[52,53]. The RFX membrane shows a looser packing of LHRC complexes, with an apparently

empty lipid bilayer between some of them (Fig. 5.5). This loose packing has also been observed in the EM images of the related *Chloroflexus aurantiacus* membranes, which differs from RFX by the presence of a large membrane associated antenna, the chlorosome. The EM of CFX membranes showed an average RC center-to-center separation distance of 18 nm, larger than observed by AFM in RFX. In the CFX EM, some samples did not remove the chlorosomes and areas under the chlorosomes had tighter packing with 11 LHRCs per chlorosome[54]. The absence of the chlorosome or any other type of accessory antenna, either integral membrane or periplasmic may account for the looser and random packing in the membranes of RFX. However, the resolution is not high enough to exclude the possibility of small proteins with little exposed topology interspersed among the LHRC's, which would also account for the loose packing observed, but cannot be imaged by AFM. We would expect many copies of the tethered electron carrier auracyanin, which has been proposed to be the equivalent of cyt c_2 in purple bacteria to be present in this membrane. The highly flexible nature of the tether of auracyanin, estimated to be ~8.7 nm long, also promotes loose packing amongst the membrane complexes.

The average separation of the putative LHRC complexes, 11.5 ± 2.4 nm, is too small when compared to the known diameter of the complex of 13.0 ± 1 nm[22]. We believe that this disparity, where complexes appear too close or too far apart, is due to the fact that we are measuring separations on the basis of the highest point of the proteins, i.e. the C subunit, which we observed to be substantially off center within the LH ring. Two C subunits 'leaning' towards each other would lead to a substantially shorter measured separation than a true center to center separation, and similarly, the C subunits 'leaning' directly away from each other would lead to a much greater perceived distance (Fig. 5.5C). Allowing for the unconstrained rotation of the largely circular complexes within the membrane could explain all the measured separations, two

extremes of which are illustrated in the single scan line data of 13.2 nm vs 7 nm (Fig. 5.5B). We have tested this hypothesis by modeling the separation, as measured by the highest point to the highest point, in a model made by placing two *T. tepidum* RC-LH1-Cyt 3D structures side by side in two configurations that place the off center C subunits proximal and distal to each other for measurement purposes. The separations of 8.4 nm and 14.7 nm are indicative of the large variation that could be expected for *in situ* complexes of *R. castenholzii* and are illustrated in the cartoon in figure 5.5C. It should also be borne in mind that the downwards force exerted by the AFM is likely to influence the 'lean' of the C subunit by making it more horizontal and this will be reflected in the subsequent separations measured. The model was extended to illustrate how the orientation of four C subunits, seen in figure 5.5D, could match with their measured separations.

With knowledge from the EM model and related X-ray structures, the assignment of the smaller proteins in the membrane patch measured by AFM were assigned as the LHRC complexes. The assignment of the larger protein is much more speculative, but we suggest that it is the ACIII complex, a functional analogue of the cytochrome bc_1 or b_6f complex in other photosynthetic organisms (for a review see Majumder et al. 2013). Although there is no atomic structure for any ACIII complex Majumder et al. (2014) have proposed a homology based model that uses the polysulfide reductase (PSR) of *Thermus thermophilus,* another member of the complex iron-sulphur molybdoenzyme (CISM) family[55]. Taking a measurement of the height of the PSR complex from its PDB file (2VPW) yields a figure of 13.5 nm, which is within the measured height range of the larger proteins within the membrane patch of 13.7 ± 0.4 nm. The orientation of the ACIII complex within the membrane is currently debated but if it was as modelled in Majumder et al. (2013) then the ActB1 and ActB2 subunits would protrude into the

periplasm and thus be imaged by the AFM[28]. Thus, at this time we tentatively assign these taller proteins as ACIII complexes. We have therefore tentatively assigned the major integral membrane proteins player of the cyclic electron transport chain in RFX.

To explore the validity of the ACIII assignment the ratio of the LHRC to the ACIII was determined. In the membrane patch illustrated in Figure 5.5A the ratio of putative LHRC complexes to the taller putative ACIII complexes is 5.7:1. Heme staining data on whole membrane from RFX estimates the ratio of LHRC to ACIII from the whole membranes closer to 10:1, but as low as 3:1 (Fig. 5.6). The 5.7 LHRC to 1ACIII value from AFM is in the middle of the heme staining determined ratios suggesting that the numbers are in range of each other. In *Rba. sphaeroides* the ratio of RC-LH1-PufX complexes to cyt bc_1 complexes for a low-light chromatophore has been estimated as 3:1[37]. The larger ratio in RFX than that for PB may reflect the limited light gathering capacity of the LHRC complexes in comparison with that of *Rba. sphaeroides* photosystem which is augmented by large numbers of LH2 complexes. The ratio in PB LH2:RC is 2.7: 1, in a low light chromatophore[37]. However, the number of LH2 and RC-LH1 from PB added together is similar to the number LHRCs in RFX. Since the overall number of light harvesting complexes in the membranes of PB and RFX are about the same, this may point the LH1/LH2 hybrid nature of the RFX LHRC complex rather than a limited light gathering capacity.

The enzyme kinetics observed for the ACIII and the cytochrome bc_1 complex are very similar to each other, as well as the kinetics within the LHRC system[26,56] (Table 5.1). Similar kinetic rates of electron transfer are consistent with having a similar ratio of LHRC/RC-LH1 and ACIII/bc_1 protein complexes. We have used our data to make a simple limited model for the photosynthetic membranes of RFX (Fig. 5.8)

5.5 Conclusion

A 3D EM reconstruction model of the RFX was generated, which is similar to the X-ray structure of the *T. tepidum* RC-LH1 complex with the H subunit removed. Superposition of the X-ray structure on the EM model and amino acid sequence alignment yielded clues about pigment arrangement. It also provided size dimensions, particularly heights, which allowed us to assign the LHRC complex to topographic features in the AFM images of RFX membrane patches. We were also putatively able to assign ACIII complexes from previous homology modeling and LHRC to ACIII protein ratio was measured. Taken together, the measured membrane packing distances taken from AFM, shape from EM and system kinetics from previous work indicate how the photosynthetic cyclic electron transport chain operates within the membranes of *Roseiflexus castenholzii*. We therefore propose a model for how the LHRC, ACIII and auracyanin may arrange themselves in the membrane, as viewed from the periplasm (Figure 5.8) and for the operation of this photosynthetic apparatus.

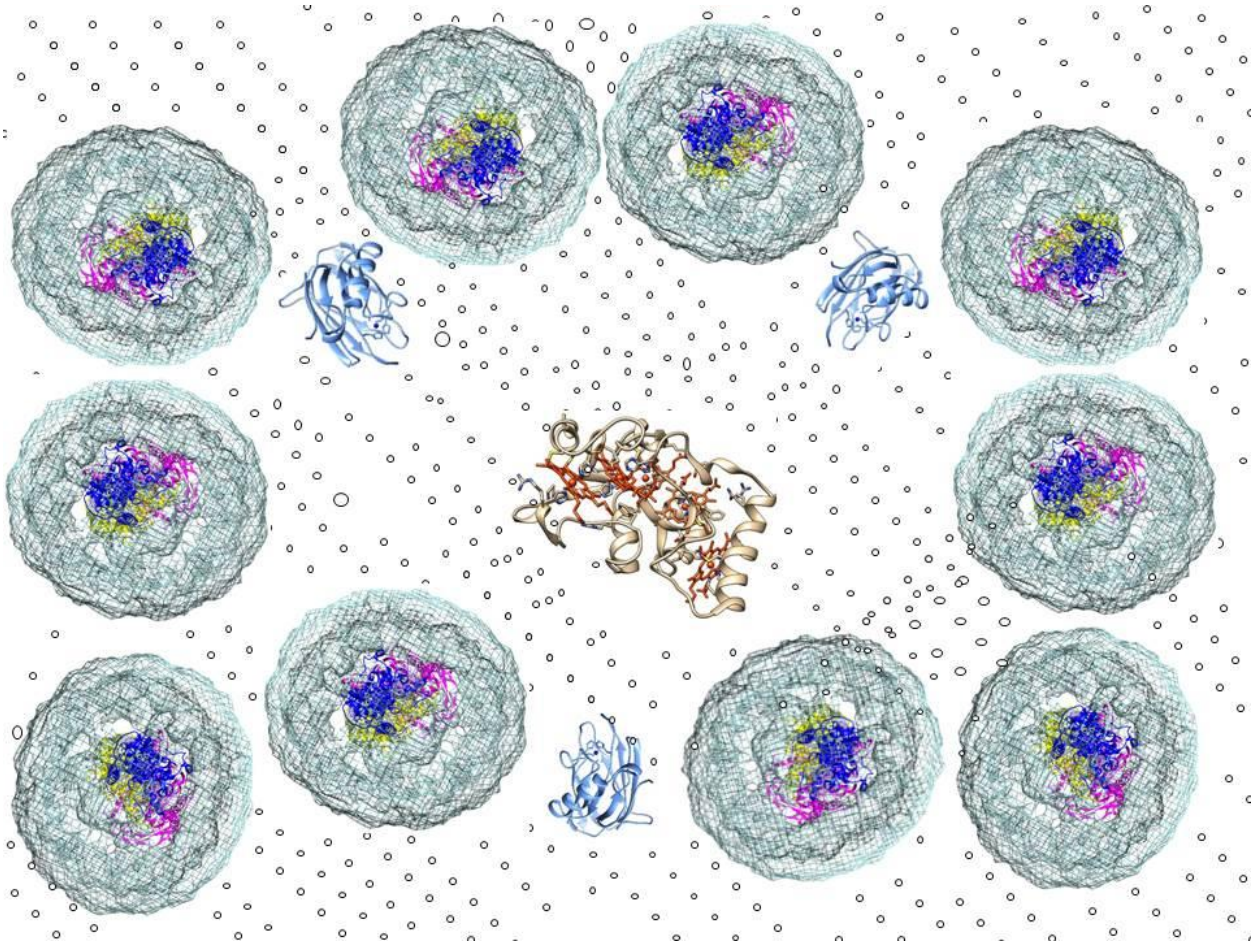

Figure 5.8 Full Model of RFX photosynthetic membrane system View is looking down onto the top of the periplasmic face of the membrane. Teal and grey rings are the LH complex. Dark blue is the cytochrome subunit. Yellow is the M subunit and pink is the M subunit. Blue proteins are auracyanin. Tan is the homology model of ACIII based on Polysulfide reductase.

References

(1) Liu, H., Zhang, H., Niedzwiedzki, D. M., Prado, M., He, G., Gross, M. L., and Blankenship, R. E. (2013) Phycobilisomes supply excitations to both photosystems in a megacomplex in cyanobacteria. *Science 342*, 1104–7.

(2) Sturgis, J. N. J., and Niederman, R. R. A. (2008) Atomic force microscopy reveals multiple patterns of antenna organization in purple bacteria: implications for energy transduction mechanisms and membrane modeling. *Photosynth. Res. 95*, 269–78.

(3) Jungas, C., Ranck, J. L., Rigaud, J. L., Joliot, P., and Verméglio, A. (1999) Supramolecular organization of the photosynthetic apparatus of Rhodobacter sphaeroides. *EMBO J. 18*, 534–542.

(4) Qian, P., Bullough, P., and Hunter, C. (2008) Three-dimensional Reconstruction of a Membrane-bending Complex THE RC-LH1-PufX CORE DIMER OF RHODOBACTER SPHAEROIDES. *J. Biol. Chem.* 14002–14011.

(5) Olsen, J., Adams, P., Jackson, P., Dickman, M. J., Pu, Q., and Hunter, C. N. (2014) Aberrant Assembly Complexes of the Reaction Center Light-harvesting 1 PufX (RC-LH1-PufX) Core Complex of Rhodobacter sphaeroides Imaged by Atomic Force. *J. Biol. Chem.* 29927–29936.

(6) Sener, M. K., Olsen, J. D., Hunter, C. N., and Schulten, K. (2007) Atomic-level structural and functional model of a bacterial photosynthetic membrane vesicle. *Proc. Natl. Acad. Sci. U. S. A. 104*, 15723–8.

(7) Hu, X., and Ritz, T. (2002) Photosynthetic apparatus of purple bacteria. *Q. Rev. Biophys. 35*, 1–62.

(8) Robert, B., Cogdell, R., and Grondelle, R. van. (2003) The light-harvesting system of purple bacteria, in *Light-Harvesting Antennas in Photosynthesis*, pp 169–194.

(9) Hanada, S., Takaichi, S., Matsuura, K., and Nakamura, K. (2002) Roseiflexus castenholzii gen. nov., sp nov., a thermophilic, filamentous, photosynthetic bacterium that lacks chlorosomes. *Int. J. Syst. Evol. Microbiol. 52*, 187–193.

(10) Van der Meer, M. T. J., Klatt, C. G., Wood, J., Bryant, D. A., Bateson, M. M., Lammerts, L., Schouten, S., Damsté, J. S. S., Madigan, M. T., Ward, D. M., and Sinninghe Damste, J. S. (2010) Cultivation and genomic, nutritional, and lipid biomarker characterization of Roseiflexus strains closely related to predominant in situ populations inhabiting Yellowstone hot spring microbial mats. *J. Bacteriol. 192*, 3033–42.

(11) Cao, L., Bryant, D. A., Schepmoes, A. A., Vogl, K., Smith, R. D., Lipton, M. S., and Callister, S. J. (2012) Comparison of Chloroflexus aurantiacus strain J-10-fl proteomes of cells grown chemoheterotrophically and photoheterotrophically. *Photosynth. Res. 110*, 153–68.

(12) Hohmann-Marriott, M. F., and Blankenship, R. E. (2011) Evolution of photosynthesis. *Annu. Rev. Plant Biol. 62*, 515–48.

(13) Blankenship, R. E. (2010) Early Evolution of Photosynthesis. *Plant Physiol. 154*, 434–438.

(14) Tang, K.-H., Barry, K., Chertkov, O., Dalin, E., Han, C. S., Hauser, L. J., Honchak, B. M., Karbach, L. E., Land, M. L., Lapidus, A., Larimer, F. W., Mikhailova, N., Pitluck, S., Pierson, B. K., and Blankenship, R. E. (2011) Complete Genome Sequence of the Filamentous Anoxygenic Phototrophic Bacterium Chloroflexus aurantiacus. *BMC Genomics 12*, 334.

(15) Gao, X., Xin, Y., Bell, P. D., Wen, J., and Blankenship, R. E. (2010) Structural Analysis of Alternative Complex III in the Photosynthetic Electron Transfer Chain of Chloroflexus aurantiacus. *Biochemistry 49*, 6670–6679.

(16) Tsukatani, Y., Nakayama, N., Shimada, K., Mino, H., Itoh, S., Matsuura, K., Hanada, S., and Nagashima, K. V. P. (2009) Characterization of a blue-copper protein, auracyanin, of the filamentous anoxygenic phototrophic bacterium Roseiflexus castenholzii. *Arch. Biochem. Biophys. 490*, 57–62.

(17) Takaichi, S., Maoka, T., Yamada, M., Matsuura, K., Haikawa, Y., and Hanada, S. (2001) Absence of carotenes and presence of a tertiary methoxy group in a carotenoid from a thermophilic filamentous photosynthetic bacterium Roseiflexus castenholzii. *Plant Cell Physiol. 42*, 1355–62.

(18) Van ver Meer, M. T. J., Schouten, S., Hanada, S., Hopmans, E. C., Damsté, J. S. S., and Ward, D. M. (2002) Alkane-1,2-diol-based glycosides and fatty glycosides and wax esters in Roseiflexus castenholzii and hot spring microbial mats. *Arch. Microbiol. 178*, 229–37.

(19) Collins, A. M., Xin, Y., and Blankenship, R. E. (2009) Pigment organization in the photosynthetic apparatus of Roseiflexus castenholzii. *Biochim. Biophys. Acta 1787*, 1050–6.

(20) Yamada, M., Zhang, H., Hanada, S., Nagashima, K. V. P., Shimada, K., and Matsuura, K. (2005) Structural and spectroscopic properties of a reaction center complex from the chlorosome-lacking filamentous anoxygenic phototrophic bacterium Roseiflexus castenholzii. *J. Bacteriol. 187*, 1702–9.

(21) Niedzwiedzki, D. M., Collins, A. M., LaFountain, A. M., Enriquez, M. M., Frank, H. A., and Blankenship, R. E. (2010) Spectroscopic studies of carotenoid-to-bacteriochlorophyll energy transfer in LHRC photosynthetic complex from Roseiflexus castenholzii. *J. Phys. Chem. B 114*, 8723–34.

(22) Collins, A., Qian, P., Tang, Q., and Bocian, D. (2010) Light-harvesting antenna system from the phototrophic bacterium Roseiflexus castenholzii. *Biochemistry 49*, 7524–7531.

(23) Xin, Y., Pan, J., Collins, A., Lin, S., and Blankenship, R. E. (2012) Excitation energy transfer and trapping dynamics in the core complex of the filamentous photosynthetic bacterium Roseiflexus castenholzii. *Photosynth. Res. 111*, 149–156.

(24) Deisenhofer, J., Epp, O., Miki, K., Huber, R., and Michel, H. (1985) Structure of the protein subunits in the photosynthetic reaction centre of Rhodopseudomonas viridis at 3Å resolution. *Nature 318*, 618–624.

(25) Collins, A., Kirmaier, C., Holten, D., and Blankenship, R. E. (2011) Kinetics and energetics of electron transfer in reaction centers of the photosynthetic bacterium Roseiflexus castenholzii. *Biochim. Biophys. … 1807*, 262–269.

(26) Gao, X., Xin, Y., and Blankenship, R. E. (2009) Enzymatic activity of the alternative complex III as a menaquinol:auracyanin oxidoreductase in the electron transfer chain of Chloroflexus aurantiacus. *FEBS Lett. 583*, 3275–9.

(27) Gao, X., Majumder, E. W., Kang, Y., Yue, H., and Blankenship, R. E. (2013) Functional analysis and expression of the mono-heme containing cytochrome c subunit of alternative complex III in Chloroflexus aurantiacus. *Arch. Biochem. Biophys. 535*, 197–204.

(28) Majumder, E. L. W., King, J. D., and Blankenship, R. E. (2013) Alternative Complex III from phototrophic bacteria and its electron acceptor auracyanin. *Biochim. Biophys. Acta*.

(29) Bond, C. S., Blankenship, R. E., Freeman, H. C., Guss, J. M., Maher, M. J., Selvaraj, F. M., Wilce, M. C., and Willingham, K. M. (2001) Crystal structure of auracyanin, a “blue” copper protein from the green thermophilic photosynthetic bacterium Chloroflexus aurantiacus. *J. Mol. Biol. 306*, 47–67.

(30) Scheuring, S., and Sturgis, J. N. (2009) Atomic force microscopy of the bacterial photosynthetic apparatus: plain pictures of an elaborate machinery. *Photosynth. Res. 102*, 197–211.

(31) Tang, G., Peng, L., Baldwin, P. R., Mann, D. S., Jiang, W., Rees, I., and Ludtke, S. J. (2007) EMAN2: an extensible image processing suite for electron microscopy. *J. Struct. Biol. 157*, 38–46.

(32) Goodhew, C. F., Brown, K. R., and Pettigrew, G. W. (1986) Haem staining in gels, a useful tool in the study of bacterial c-type cytochromes. *Biochim. Biophys. Acta - Bioenerg. 852*, 288–294.

(33) Pettersen, E. F., Goddard, T. D., Huang, C. C., Couch, G. S., Greenblatt, D. M., Meng, E. C., and Ferrin, T. E. (2004) UCSF Chimera--a visualization system for exploratory research and analysis. *J. Comput. Chem. 25*, 1605–12.

(34) Qian, P., Papiz, M. Z., Jackson, P. J., Brindley, A. A., Ng, I. W., Olsen, J. D., Dickman, M. J., Bullough, P. A., and Hunter, C. N. (2013) Three-Dimensional Structure of the Rhodobacter

sphaeroides RC-LH1-PufX Complex: Dimerization and Quinone Channels Promoted by PufX. *Biochemistry*.

(35) Niwa, S., Yu, L., Takeda, K., Hirano, Y., Kawakami, T., Wang-Otomo, Z.-Y., and Miki, K. (2014) Structure of the LH1-RC complex from Thermochromatium tepidum at 3.0 A. *Nature* 228–232.

(36) Roszak, A. W., Howard, T. D., Southall, J., Gardiner, A. T., Law, C. J., Isaacs, N. W., and Cogdell, R. J. (2003) Crystal structure of the RC-LH1 core complex from Rhodopseudomonas palustris. *Science 302*, 1969–72.

(37) Cartron, M. L., Olsen, J. D., Sener, M., Jackson, P. J., Brindley, A. A., Qian, P., Dickman, M. J., Leggett, G. J., Schulten, K., and Neil Hunter, C. (2014) Integration of energy and electron transfer processes in the photosynthetic membrane of Rhodobacter sphaeroides. *Biochim. Biophys. Acta*.

(38) Boonstra, A. F., Germeroth, L., and Boekema, E. J. (1994) Structure of the light harvesting antenna from Rhodospirillum molischianum studied by electron microscopy. *Biochim. Biophys. Acta - Bioenerg. 1184*, 227–234.

(39) Boonstra, A. F., Visschers, R. W., Calkoen, F., van Grondelle, R., van Bruggen, E. F. J., and Boekema, E. J. (1993) Structural characterization of the B800–850 and B875 light-harvesting antenna complexes from Rhodobacter sphaeroides by electron microscopy. *Biochim. Biophys. Acta - Bioenerg. 1142*, 181–188.

(40) Timmins, P. A., Leonhard, M., Weltzien, H. U., Wacker, T., and Welte, W. (1988) A physical characterization of some detergents of potential use for membrane protein crystallization. *FEBS Lett. 238*, 361–368.

(41) Sundström, V., and Grondelle, R. van. (1995) Kinetics of excitation transfer and trapping in purple bacteria. *Anoxygenic Photosynth. Bact. 2*, 349–372.

(42) Guner, S., Willie, A., Millett, F., Caffrey, M. S., Cusanovich, M. A., Robertson, D. E., and Knaff, D. B. (1993) The interaction between cytochrome c2 and the cytochrome bc1 complex in the photosynthetic purple bacteria Rhodobacter capsulatus and Rhodopseudomonas viridis. *Biochemistry 32*, 4793–4800.

(43) Pullerits, T., Visscher, K. J., Hess, S., Sundström, V., Freiberg, A., Timpmann, K., and van Grondelle, R. (1994) Energy transfer in the inhomogeneously broadened core antenna of purple bacteria: a simultaneous fit of low-intensity picosecond absorption and fluorescence kinetics. *Biophys. J. 66*, 236–48.

(44) Ortega, J. M., and Mathis, P. (1993) Electron transfer from the tetraheme cytochrome to the special pair in isolated reaction centers of Rhodopseudomonas viridis. *Biochemistry 32*, 1141–1151.

(45) Kirmaier, C., and Holten, D. (1987) Primary photochemistry of reaction centers from the photosynthetic purple bacteria. *Photosynth. Res. 13*, 225–60.

(46) Pullerits, T., and Sundström, V. (1996) Photosynthetic light-harvesting pigment-protein complexes: toward understanding how and why. *Acc. Chem. Res.*

(47) Kirmaier, C., Holten, D., and Parson, W. W. (1985) Temperature and detection-wavelength dependence of the picosecond electron-transfer kinetics measured in Rhodopseudomonas sphaeroides reaction centers. Resolution of new spectral and kinetic components in the primary charge-separation process. *Biochim. Biophys. Acta - Bioenerg. 810*, 33–48.

(48) Qian, P., Hunter, C., and Bullough, P. (2005) The 8.5 Å projection structure of the core RC–LH1–PufX dimer of Rhodobacter sphaeroides. *J. Mol. Biol. 349*, 948–960.

(49) Comayras, F., Jungas, C., and Lavergne, J. (2005) Functional consequences of the organization of the photosynthetic apparatus in Rhodobacter sphaeroides. I. Quinone domains and excitation transfer in chromatophores and reaction center.antenna complexes. *J. Biol. Chem. 280*, 11203–13.

(50) Crouch, L., and Jones, M. (2012) Cross-species investigation of the functions of the Rhodobacter PufX polypeptide and the composition of the RC–LH1 core complex. *Biochim. Biophys. Acta (BBA)-Bioenergetics*.

(51) Cogdell, R., and Roszak, A. (2014) Structural biology: The purple heart of photosynthesis. *Nature* 196–197.

(52) Scheuring, S., Lévy, D., and Rigaud, J.-L. (2005) Watching the components of photosynthetic bacterial membranes and their in situ organisation by atomic force microscopy. *Biochim. Biophys. Acta 1712*, 109–27.

(53) Scheuring, S., Boudier, T., and Sturgis, J. (2007) From high-resolution AFM topographs to atomic models of supramolecular assemblies. *J. Struct. Biol. 159*, 268–276.

(54) Bína, D., Gardian, Z., Vácha, F., and Litvín, R. (2014) Supramolecular organization of photosynthetic membrane proteins in the chlorosome-containing bacterium Chloroflexus aurantiacus. *Photosynth. Res.*

(55) Jormakka, M., Yokoyama, K., Yano, T., Tamakoshi, M., Akimoto, S., Shimamura, T., Curmi, P., and Iwata, S. (2008) Molecular mechanism of energy conservation in polysulfide respiration. *Nat. Struct. Mol. Biol. 15*, 730–7.

(56) Hall, J., Zha, X., Durham, B., O'Brien, P., Vieira, B., Davis, D., Okamura, M., and Millett, F. (1987) Reaction of cytochrome c and c2 with the Rhodobacter sphaeroides reaction center involves the heme crevice domain. *Biochemistry 26*, 4494–4500.

Chapter 6: Purification and Characterization of the Alternative Complex III from *Roseiflexus castenholzii*

6.1 Introduction

The Alternative Complex III is a novel integral membrane protein found in some anoxygenic bacterial phyla, such as the Filamentous Anoxygenic Phototrophs (FAPs), and in δ-proteobacteria[1]. ACIII is purported to be a functional replacement for the cytochrome bc_1 or b_6f complex, completing the quinone:soluble electron carrier oxdioreductase function[2]. Some bacterial taxa have genes for both the bc_1 and ACIII, while some families just have ACIII[3]. The ACIII complex has no structural homology or evolutionary relationship to cytochrome bc_1 and thus represents novel protein structure and mechanism to achieve the same function[4]. For an in-depth review of ACIII please see Chapters 2 and 4.

ACIII has been previously isolated, purified and characterized in two species, the FAP *Chloroflexus aurantiacus* (CFX) and the non-photosynthetic anaerobe *Rhodothermus marinus*[4–7]. The two isolations revealed generally similar proteins and complementary information about the cofactor and subunit composition of the enzyme[4,8]. One distinct difference is that in CFX two slightly different ACIII complexes function in both the photosynthetic and respiratory electron transport chain, whereas the *Rh. marinus* contains a single enzyme that functions in the respiratory chain. It then follows and has been shown that the two enzymes from the two strains use two different electron acceptors: CFX a small blue copper protein called auracyanin and *Rh. marinus* a more canonical cytochrome *c* protein[9,10].

To continue to explore this novel enzyme, in this chapter, we present the first isolation, purification and characterization of the ACIII from *Roseiflexus castenholzii*. We chose to study the *Roseiflexus* ACIII because of the relationship between CFX and RFX, as two highly related FAPs. The primary difference between CFX and RFX is the presence and lack, respectively, of the large accessory light harvesting antenna the chlorosome[11]. The chlorosome enables CFX to

capture more incoming light[12]. Another difference in addition to the chlorosome, CFX has two slightly different copies of ACIII in the genome, presumably one for photosynthetic growth and one for respiratory growth, whereas RFX just has one that likely functions in both systems[1]. Likewise, the operon for CFX ACIII has seven subunits but the RFX operon only has six. Here we explore the functional implications of these differences by first isolating the RFX ACIII.

6.2 Materials and Methods

6.2.1 Bacteria Strain Growth

Roseiflexus castenholzii HL08 was grown anaerobically in screw cap bottles with gentle stirring near one 60W incandescent light bulb at 50°C in a growth incubator. 02YE media was used. Every seven days the cultures were scaled up with a 10% inoculum. To grow the weight of cells necessary for protein purification, RFX was cultured in a 14L bioreactor, again on 02YE media with stirring, three 60W incandescent light bulbs, and 50°C for one week.

6.2.2 Culture Harvest and Membrane Isolation

After one week, cells were removed from the bioreactor by pumping in nitrogen gas. The culture solution was loaded into 1 liter centrifuge bottles. Cells were pelleted at 8000 RPM for 20min and 4°C. Supernatant was decanted off and wet cell pellets were transferred to one container. Cells were either frozen at -20°C for later use or membrane isolation was immediately started.

RFX cells were first thawed, if using freezer stock, and then resuspended in 20mM Tris HCl pH8, buffer A, at 4mL of buffer per one gram of wet cells. The cells were then placed in an ice bath and disrupted by tip sonication for three sessions of four minutes sessions at 60% output and 80% duty. Cells were allowed to rest for 15 min in between each sonication session. The broken cells were again centrifuged at 8000 RPM for 15 minutes to remove debris and unbroken

cells. The supernatant was collected and poured into 70mL ultracentrifugation tubes. To isolate the membranes, the tubes were spun down on the ultracentrifuge at 41,000 RPM at 4°C for two hours. The membrane pellet has a reddish color and typically a jam-like consistency. Isolated membranes were either stored at -80°C or immediately solubilized.

6.2.3 Membrane Solubilization

Thawed isolated membranes were resuspended in 20mM Tris HCl pH8 at 4mL per gram of membranes. Gentle stirring or a paint brush was used to resuspend the membranes without disrupting them. The final solution was adjusted to OD_{880} =10. Resuspended membranes were placed in an ice bath on a stir plate in the dark. Detergent was slowly added dropwise to a final concentration of 1% Triton X-100 reduced and 1% Lauryldimethylamine-oxide (LDAO). The detergent and membrane solution was allowed to stir for 90min.

After the 90min incubation, the solution was again loaded into ultracentrifuge tubes. The solubilized membranes were spun at 41,000 RPM for 90min at 4°C. The supernatant was collected and the white pellet discarded. If the pellet was colored reddish-brown, the solubilization was not successful and solubilzation procedure was repeated with a second addition of detergent, incubation and ultracentrifugation.

Solubilized membranes were filtered on a 0.22μM pore sized vacuum filter to remove any remaining debris and were diluted 2:1 with 20mM Tris HCl pH8 and 0.1% Triton X-100 reduced and 0.1% LDAO, buffer B. The solubilized membranes were then ready to begin protein purification.

6.2.4 Protein Isolation & Purification

Solubilized and diluted membranes were loaded onto a 200mL QSFF ion exchange column. The column was washed with 50mL of buffer B after loading to ensure complete binding. A NaCl step gradient from 0.05M to 0.5M NaCl in buffer B was applied to the column with steps increasing of 0.05M NaCl. Salt concentration was only increased when each species was fully eluted. Fractions containing a reddish brown color were collected and analyzed by Uv/Vis spectroscopy. Fractions containing peaks associated with *c*-type cytochromes were then collected and concentrated and de-salted on a 100 kDa MWCO spin filter at 3500 RPM for 5-10 minutes or until the total volume was less than 5mL or became too concentrated.

Concentrated sample was loaded onto a 180mL S200 gel filtration column at 0.75mL/min. an isocratic wash of Buffer B with 0.1M NaCl, buffer C, was applied at the same rate until the reddish brown fraction eluted off the column. Fractions were once again collected, analyzed and de-salted in the same manner.

The red sample was then loaded onto a 5mL QHP ion exchange column in buffer B. The column was washed to remove any residue. Then a linear salt gradient from 0M NaCl to 0.5M NaCl was applied at 2.5mL/min for 50mL. Red fractions were again collected and verified by UV/Vis. At this step, the sample was also run over a SDS-PAGE gel to confirm the presence of ACIII by the subunits and not just the spectral signature.

Concentrated fractions with ACIII spectral signatures and corresponding protein bands were loaded onto a superpose-12 column in buffer C as a final clean up step to achieve a high purity protein. An isocratic flow at 0.5mL/min of buffer C was applied until the red fraction eluted. If necessary, fractions were concentrated using the 100 kDa MWCO spin filter or by repeating the 5mL QHP column procedure.

6.2.5 UV/Vis spectroscopy

Pure isolated ACIII was analyzed by UV/vis spectroscopy. Spectra of the isolated complex were taken from 900nm-200nm at room temperature. First, the spectrum of an air oxidized sample without modification was taken. Then, spectra of the fully oxidized and fully reduced sampels were taken. To achieve the fully oxidized condition, two granules of potassium ferricyanide was added to the solution and stirred and the spectrum was taken immediately. Fully reduced spectra were taken by adding a couple granules of sodium dithionite to the cuvette, stirring and then putting a cap on the cuvette to prevent re-oxidation from the air.

6.2.6 Gel Analysis

The purified complex was analyzed by acrylamide gels. 8M Urea SDS-PAGE gels were made and then complex was loaded onto the gels after incubating in SDS-PAGE sample buffer to denature the complex. The SDS-PAGE gels were stained either by Commassie Blue 250 to view the subunits or by TMBZ heme staining to identity the cytochrome c containing subunits. Pure sample was also run over a BN-PAGE gel to confirm purity and weight of the native complex.

6.2.7 Mass Spectrometry

Both the native complex and cut gel bands of ACIII were analyzed by mass spectrometry to confirm identity and mass of the complex. Gel bands were excised from the gel and digested with Trypsin following the protocol used in Chapter 3. Digested samples were analyzed by LC/MS and the subunits identified using MassAssign software. The whole complex was precipitated using amino acetate and then analyzed with LC/MS and the Peaks software.

6.3 Results and Discussion

The ACIII from *Roseiflexus castenholzii* has been isolated, purified and characterized from the membranes of photosynthetically grown cells. The purification was completed with detergent solubilization and a column chromatography series including gel filtration and ion exchange columns yielding a pure red colored complex (Figure 6.1). The color of the complex resembles that of the CFX ACIII system.

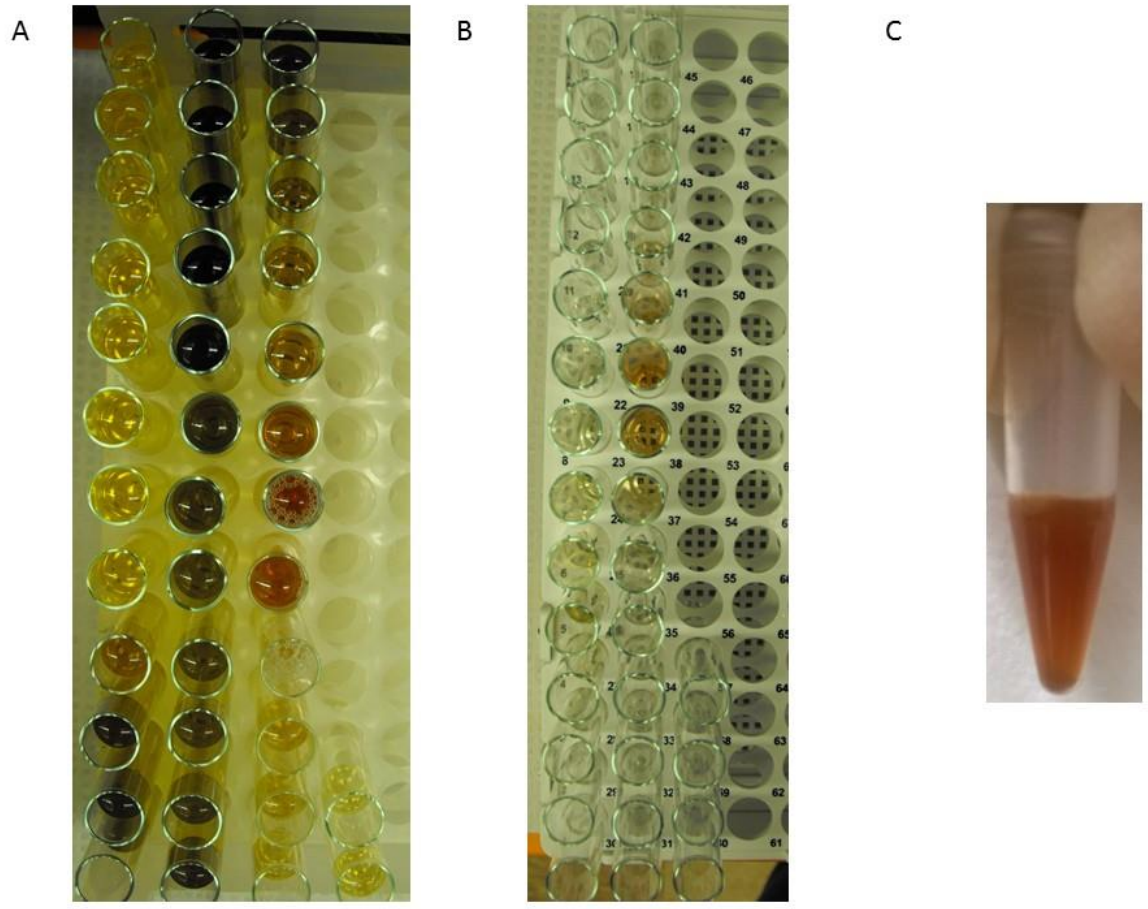

Figure 6.1 Column or picture of isolated complex
A) Fractions from QSFF ion exchange column B) Fractions from S200 Gel Filtration Column C) Final Purified Complex

The UV/vis spectra of the complex revealed features that are characteristic of *c*-type heme containing proteins and in line with what was observed in the CFX and *Rh. marinus* complexes. Only *c*-type hemes and no photosynthetic pigments were found in the complex. The reduced spectrum more clearly shows the heme peaks and is diagnostic of *c*-type hemes with 413, 525 and 554nm as the main peaks (Fig. 6.2). The reduced-oxidized spectrum also resolves the unique heme peaks, indicating hemes at 553, 554 and 555nm (data not shown). The spectra do show a very small amount of contamination from the RFX LHRC complex (peaks at 880 and 800). This is due to the differences between the CFX and RFX LHRC and the resulting biochemical purification challenges. The CFX LHRC cytochrome subunit is easily disassociated from the complex and reduces the mass to under 300 kDa of the whole complex[13]. The corresponding C-subunit in the RFX LHRC does not disassociate easily, therefore the LHRC and the ACIII both weigh approximately 330 kDa and are membrane proteins with almost identical predicted isoelectric points[14]. Therefore it is difficult to separate the RFX ACIII from the RFX LHRC because they are almost identical in the biochemical properties that our purification techniques target for separation. Repeated column chromatography and being highly selective in choosing which fractions to keep increases the purity of ACIII against LHRC, but there is a significant drop in protein yield. The decision to end with a small amount of very pure complex or larger amount of less pure protein was determined by the requirements of subsequent biochemical assays.

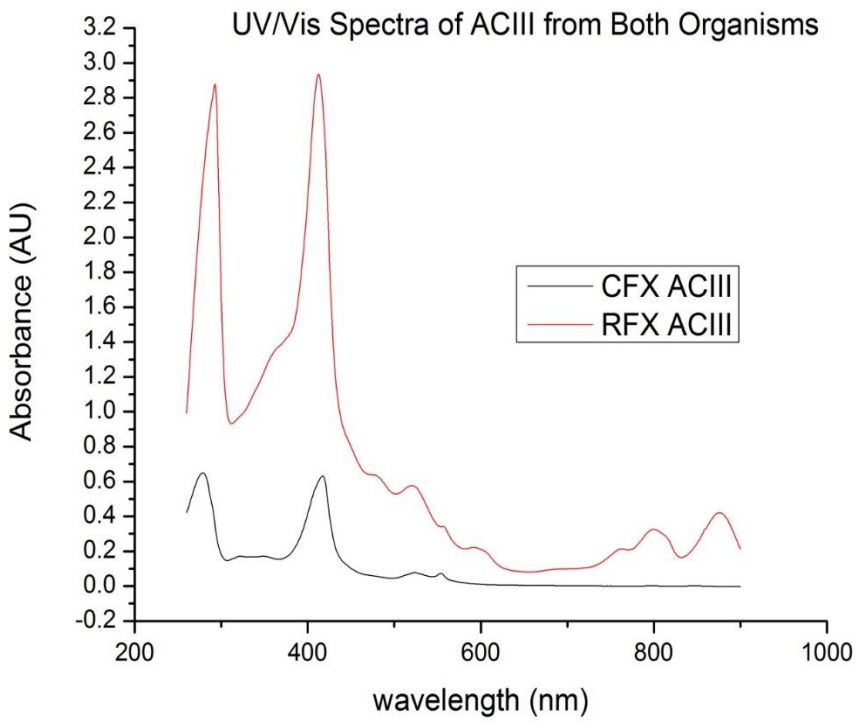

Figure 6.2 UV/Vis Spectra of *Chloroflexus* and *Roseiflxus*

The BN-PAGE and SDS-PAGE gels showed the apparent weight of the whole complex and the subunit composition. The apparent weight is ~330kDa, in line with the CFX system and predictions from sequence based calculations[4] (Fig. 6.3A). The SDS-PAGE gel showed six subunits, as predicted from the genome sequence. These six subunits are, in order of weight, ActB, ActC, ActF, ActA, ActE, and ActD (Fig. 6.3B). Compared to the CFX system, RFX ACIII is smaller by one subunit. RFX ACIII is missing ActG, the smallest membrane associated subunit of unknown function. The missing ActG is a distinct difference between the RFX and CFX systems. In Chapter 2 we saw that ActG was not required for menaquinone:cytochrome c oxido reductase activity of the enzyme[15]. It is therefore probably not necessary for function of the enzyme. Since the RFX ACIII lacks the ActG subunit and the CFX subunit is not necessary,

the absence probably does not affect the RFX ACIII in any significant way. The heme staining of the SDS-PAGE gel was carried out both by TMBZ heme staining and by the chemiluminescent method using the horseradish peroxidiase activity assay[16,17]. Both methods confirmed two c-type heme containing subunits, ActA and ActE (Fig. 6.3C). The signal is stronger for ActA consistent with ActA having five hemes and ActE only having one heme per subunit.

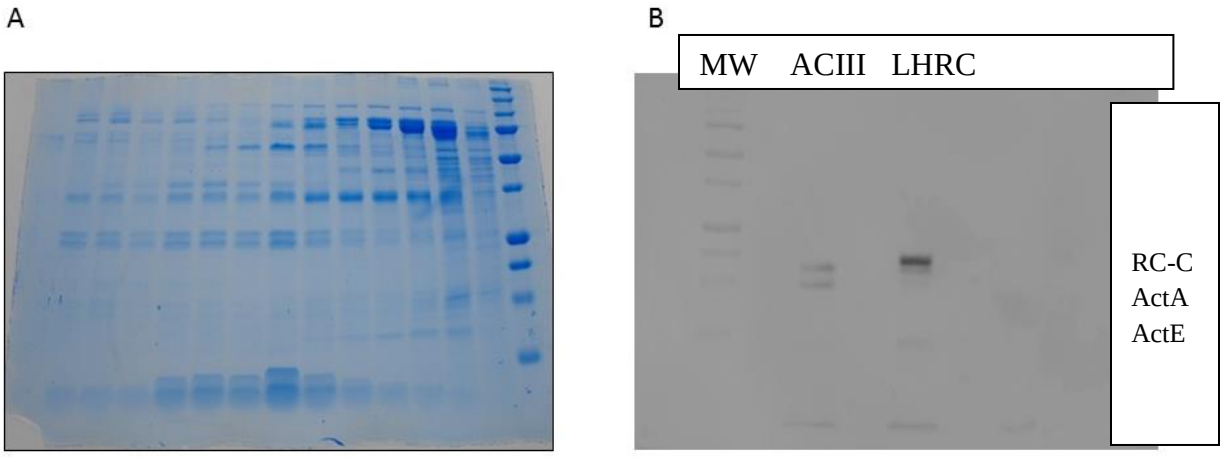

Figure 6.3 SDS and BN-PAGE gels (A) CBB 250 Stained SDS-PAGE gel of the purification procedure (B) Chemiluminescent heme stained gel

The identity of the complex was confirmed by trypsin digestion and mass spectrometry analysis, which identifies the subunits by the sequences detected in the mass spectrometer compared to a genomic and protein sequence database. The whole complex as well as each individual subunit were positively identified. As in the gel analysis, only ActA-ActE subunits were found, as ActF and ActG were not present. ActG is not seen on the gels and operon and is not expected to be a part of the RFX ACIII complex. ActF is highly similar to ActC, and based on eh area of sequence idenitified in ActC, it is possible ActC and ActF were labeled as the same peptide. Additionally, ActC and ActF are the only completely inetgeral membrane subunits of the complex and due to their hydrophobic nature do not fly well in the mass spectrometer, which

also accounts for the small number of peptides measured. From gel evidence, genomic data and whole complex mass, we expect ActF to be part of the RFX ACIII complex Therefore, the RFX ACIII has been purified and identified.

Table 6.1 Mass Spectrometry Protein Identification

Subunit	10lgP	Coverage (%)	#Peptides	#Unique	Avg. Mass	Description
ActA	316.59	38	11	11	26042	Uncharacterized protein OS=Roseiflexus castenholzii (strain DSM 13941 / HLO8) GN=Rcas_1462 PE=4 SV=1
ActB	652.88	64	124	124	110976	FeSclustercontaining hydrogenase components 1like protein OS=Roseiflexus c astenholzii (strain DSM 13941 / HLO8) GN=Rcas_1463 PE=4 SV=1
ActC	33.68	2	1	1	53895	Polysulphide reductase NrfD OS=Roseiflexus castenholzii (strain DSM 13941 / HLO 8) GN=Rcas_1464 PE=4 SV=1
ActD	169.44	14	2	2	21051	Uncharacterized protein OS=Roseiflexus castenholzii (strain DSM 13941 / HLO8) GN=Rcas_1465 PE=4 SV=1
ActE	428.27	57	27	27	21834	Uncharacterized protein OS=Roseiflexus castenholzii (strain DSM 13941 / HLO8) GN=Rcas_1466 PE=4 SV=1
ActF						* Identified with ActC, very similar

6.4 Conclusion

The Alternative Complex III from *Roseiflexus castenholzii* has been isolated, purified and characterized. This is the third species and second photosynthetic species from which this novel

enzyme has been isolated. The RFX ACIII adds to the understanding of ACIII by presenting a case that is likely to function in both the photosynthetic and respiratory chain, as well as existing on a smaller set of subunits, lacking ActG. Future work will review the structure and mechanism of this unique enzyme.

References

(1) Majumder, E. L. W., King, J. D., and Blankenship, R. E. (2013) Alternative Complex III from phototrophic bacteria and its electron acceptor auracyanin. *Biochim. Biophys. Acta - Bioenerg. 1827*, 1383–1391.

(2) Gao, X., Xin, Y., and Blankenship, R. E. (2009) Enzymatic activity of the alternative complex III as a menaquinol: auracyanin oxidoreductase in the electron transfer chain of Chloroflexus aurantiacus. *FEBS Lett. 583*, 3275–3279.

(3) Pereira, M. M., Refojo, P. N., Hreggvidsson, G. O., Hjorlelfsdottir, S., and Teixeira, M. (2007) The alternative complex III from Rhodothermus marinus - A prototype of a new family of quinol : electron acceptor oxidoreductases. *FEBS Lett. 581*, 4831–4835.

(4) Gao, X., Xin, Y., Bell, P. D., Wen, J., and Blankenship, R. E. (2010) Structural Analysis of Alternative Complex III in the Photosynthetic Electron Transfer Chain of Chloroflexus aurantiacus. *Biochemistry 49*, 6670–6679.

(5) Refojo, P. N., Sousa, F. L., Teixeira, M., and Pereira, M. M. (2010) The alternative complex III: A different architecture using known building modules. *Quinone Bind. Catal. 1797*, 1869–1876.

(6) Yanyushin, M. F., del Rosario, M. C., Bruno, D. C., and Blankenship, R. E. (2005) New class of bacterial membrane oxidoreductases. *Biochemistry 44*, 10037–10045.

(7) Yanyushin, M. F. (2002) Fractionation of cytochromes of phototrophically grown Chloroflexus aurantiacus. Is there a cytochrome bc complex among them? *FEBS Lett. 512*, 125–8.

(8) Refojo, P. N., Teixeira, M., and Pereira, M. M. (2012) The Alternative complex III: Properties and possible mechanisms for electron transfer and energy conservation. *Biochim. Biophys. Acta - Bioenerg.*

(9) Refojo, P. N., Ribeiro, M. A., Calisto, F., Teixeira, M., and Pereira, M. M. (2013) Structural composition of alternative complex III: Variations on the same theme. *Biochim. Biophys. Acta - Bioenerg. 1827*, 1378–1382.

(10) Tsukatani, Y., Nakayama, N., Shimada, K., Mino, H., Itoh, S., Matsuura, K., Hanada, S., and Nagashima, K. V. P. (2009) Characterization of a blue-copper protein, auracyanin, of the filamentous anoxygenic phototrophic bacterium Roseiflexus castenholzii. *Arch. Biochem. Biophys. 490*, 57–62.

(11) Hanada, S., Takaichi, S., Matsuura, K., and Nakamura, K. (2002) Roseiflexus castenholzii gen. nov., sp. nov., a thermophilic, filamentous, photosynthetic bacterium that lacks chlorosomes. *Int. J. Syst. Evol. Microbiol. 52*, 187–93.

(12) Bína, D., Gardian, Z., Vácha, F., and Litvín, R. (2014) Supramolecular organization of photosynthetic membrane proteins in the chlorosome-containing bacterium Chloroflexus aurantiacus. *Photosynth. Res. 122*, 13–21.

(13) Meyer, T. E., Tollin, G., Cusanovich, M. A., Freeman, J. C., and Blankenship, R. E. (1989) In vitro kinetics of reduction of cytochrome c554 isolated from the reaction center of the green phototrophic bacterium, Chloroflexus aurantiacus. *Arch. Biochem. Biophys. 272*, 254–61.

(14) Collins, A. M., Qian, P., Tang, Q., Bocian, D. F., Hunter, C. N., and Blankenship, R. E. (2010) Light-harvesting antenna system from the phototrophic bacterium Roseiflexus castenholzii. *Biochemistry 49*, 7524–31.

(15) Gao, X., Majumder, E. W., Kang, Y., Yue, H., and Blankenship, R. E. (2013) Functional analysis and expression of the mono-heme containing cytochrome c subunit of alternative complex III in Chloroflexus aurantiacus. *Arch. Biochem. Biophys. 535*, 197–204.

(16) Goodhew, C. F., Brown, K. R., and Pettigrew, G. W. (1986) Haem staining in gels, a useful tool in the study of bacterial c-type cytochromes. *Biochim. Biophys. Acta - Bioenerg. 852*, 288–294.

(17) Alegria-Schaffer, A. (2014) Western blotting using chemiluminescent substrates. *Methods Enzymol. 541*, 251–9.

Chapter 7: Conclusions and Future Directions

7.1 Conclusions

In this dissertation, the structure and function of cytochrome proteins from anoxygenic photosynthetic bacteria have been explored. We first examined the variety of cytochromes employed by prokaryotic phototrophic organisms. The range of functional moieties enable the bacteria to grow in diverse and sometimes adverse conditions to life by using redox potentials that span the scale of measured potentials and atypical electron donors and acceptors. In some cases, two or more cytochromes are expressed in the bacterium that carry out the same function, which adds flexibility to adapt to their environment. Cytochromes are critical to every process that drives energy production in the cell, making their structure, function and mechanism important targets for photosynthesis research.

After exploring the range of cytochromes in anoxygenic photosynthesis processes, we began studying individual cytochrome proteins in more detail. In Chapter 2, the monoheme subunit ActE from the Alternative Complex III (ACIII) protein in *Chloroflexus aurantiacus* was studied. The subunit was heterologously expressed in *E. coli* and characterized apart from the complex. The UV/vis spectra arose from the c-type heme cofactor and redox potential was measured to be ~+390 mV. The function of ActE within ACIII was examined using enzyme activity. ACIII was selectively denatured losing ActE and ActG, and the denatured ACIII lost menaquinone:cytochrome oxidoreductase activity. The denatured ACIII was reconstituted with expressed ActE and the complex regained fully enzyme activity. This indicates that ActE is necessary for enzyme activity and based on the redox potential is likely the last point of electron transfer within the complex. This finding sheds light on the mechanism of ACIII and contributed to our understanding of ActE.

The second cytochrome protein investigated in detail was the diheme cytochrome *c* (DHCC) from the *bc* complex of *Heliobacteria modesticaldum,* Chapter 3. In the absence of a purified *bc* complex, DHCC was expressed in *E. coli*. The subunit was biochemically characterized and then studied using Hydrogen-Deuterium exchange mass spectrometry (HDX). Since there is no solved crystal structure, homology modelling was used to envision the protein. In a method developed by the co-authors, kinetics and dynamics from HDX were used as a physical test to adjudicate the validity and the homology models. Models were refined and the best selected based on these principles. The refined model, biochemical data and HDX data were used in conjunction to propose a mechanism for the cytochrome *bc* complex and in particular suggest the functional role of having a diheme subunit where other complexes use a monoheme subunit. Our data suggest a need for rapid electron transport, achieved by the diheme, to prevent the electron recombining with the donor.

Building in complexity from individual subunits, we then probed the structure, function and mechanism of whole protein complexes as well as their supramolecular organization in the membrane. Chapter 4 looked at the properties of ACIII and its electron acceptor auracyanin. The role of the proteins in the electron transport chain was explored as well as their individual attributes. For ACIII, sequences alignment and topology predictions were carried out with known members of the Complex Iron-Sulfur Molybdopterin Complex family. These procedures predicted potential quinone oxidation sites and possible proton uptake pathways from the cytoplasm to the periplasm. They also informed structural homology models that were built for the majority of subunits of ACIII. The alignments, topology and homology models pointed to prediction of mechanism and electron flow within ACIII. Current evidence points to a linear

electron flow, but bifurcation and the possibility of the complex carrying out a second chemistry cannot be excluded.

In Chapter 5, we expanded out from the ACIII and investigated the supramolecular organization of the major photosynthetic proteins in the membranes of *Roseiflexus castenholzii* (RFX). To begin, single particle analysis with transmission electron microscopy was performed on the Light Harvesting Reaction Center (LHRC) complex. This yielded size and shape information including dimensions and the 3D reconstruction of the complex which aligned with recently solved RC-LH1 structures from purple bacteria. Then the whole membranes were studied with Atomic Force Microscopy. The proteins seen in the AFM images were putatively assigned as the LHRC, from the EM data, and the ACIII from the homology modelling data in Chapter 4. The ratio LHRC:ACIII was determined biochemically and agreed with the AFM data. The membrane did not show the higher order structure patterns as conserved in purple bacteria systems, but this is likely because RFX lacks an accessory antenna proteins that drive the tight packing arrangement. The packing in RFX is loose, but the LHRC and ACIII are still within the tether distance of the auracyanin membrane linker tail and the LHRCs appear to orient themselves so that the cytochrome subunits are aligned. Thus, this arrangement would still permit efficient energy transfer in the system. The membranes of RFX were modelled using this data.

Finally, in Chapter 6, the first isolation of the RFX ACIII was reported. The RFX ACIII was found to be similar to the CFX ACIII but lacked the ActG subunit. This purification was challenging given the similarity in biochemical properties of the LHRC and ACIII in RFX. With purification of the RFX ACIII, three ACIIIs have now been isolated. Despite their close

relationship, the isolated ACIIIs function in the photosynthetic, respiratory or both electron transport chains. Again, we find nature using cytochromes in unique ways.

7.2 Future Directions

Moving forward, there are many interesting questions yet to be answered about the cytochrome proteins explored here and in other anoxygenic systems. The origin and evolution of cytochrome *f* will be an interesting problem to untangle as more and more organisms have the genomes sequenced. The cytochrome *bc* complex from *Heliobacteria* is yet to be isolated in intact form and is an interesting target because of its early place in evolution and simpler construction. It would also add greatly to the knowledge to compare the kinetics of the *Heliobacteria bc* complex with other such complexes to measure the functional implications of the DHCC and overall efficiency of the enzyme.

Within the FAP systems, much is yet known in these poorly characterized organisms and the proteins of their photosynthetic machinery, namely the LHRC and the ACIII. Determining the X-ray crystal structure of both LHRC and ACIII would add considerable information to the field. Both proteins have unique features that can only be revealed with high resolution structural information. The crystal structure will also resolve a number of issues and outstanding questions. First, the pigment arrangement in the LHRC. For the LH component, what exactly do the pigments in a LH1/LH2 hybrid look like? How are all 3 bacteriochlorophylls and carotenoids engaged by the α/β dimer pair? In the RC, we have only speculated as to the location of the third bacteriopheophytin, does it indeed substitute for H_A as predicted? How much asymmetry does

that introduce to this type II RC? Is there a free metal such as manganese in between MQ_A and MQ_B? How in quinone getting in and out of the complex? Secondly, in ACIII there are many questions. What exactly are the cofactors, particularly the iron-sulfur clusters, and how are they arranged. Perhaps the biggest question is: which side of the membrane is ActB on? Many of the subunits do not have a homologous protein yet in the PDB, like ActD&E- what do these proteins look like? Is there a quinol oxidation site and a quinone reduction site? Are there two pathways for electron transfer or one? Are there proton channels across the membrane as we predicted? High resolution structures of both complexes will answer many questions and suggest many more.

In addition to structure, there are major functional questions about each protein and the FAP ETC as a whole. For the RFX LHRC, the large functional questions would be the complete path of excitation energy transfer through the complex and if the residual chlorosome acceptor pigment is used by the system even though there is not a chlorosome antenna in this species. It has also not been definitively shown that auracyanin donates electrons to the tetraheme subunit of the RFX LHRC. For ACIII, the most pertinent question regarding this complex is if it is a proton pump or not. To truly be a functional replacement for the cytochrome bc_1 complex, it must also pump protons across the membrane to establish the electrochemical gradient. It has not been demonstrated biochemically if this occurs nor has the proton to electron stoichiometry been measured. Additionally, the enzyme activity with auracyanin has not been directly demonstrated using biochemistry. The interaction of ACIII with auracyanin should be measured; as well as in the CFX system, ACIII should be screened with all four genomic auracyanins to determine with auracyanin functions in which capacity. This dissertation has started to create a model for the system, but much remains to be learned about LHRC, ACIII and auracyanin.

Curriculum Vitae

Erica L-Wunderlich Majumder

1206 Moorlands Drive
Apartment 1N
Saint Louis, MO 63117

Office Phone: (314) 935-9162
Home Phone: (314) 307-0527
Email: ewunderlich@wustl.edu

Professional Profile

Ph.D. candidate in bioinorganic chemistry with research emphasis on structure and function of integral membrane energy-conserving photosynthetic proteins using biochemistry, mass spectrometry, low and high resolution structural methods and spectroscopy. Additional experience in teaching, mentoring, consulting and non-profit management. Interested in a post-doctoral appointment focusing on protein chemistry research.

Education

Ph.D. Chemistry, Washington University in St. Louis May 2015
B.A. Chemistry with honors, *summa cum laude***,** Drury University, Springfield, MO 2010
Minors in Global Studies, Spanish, Math and Physics

Academic and Research Highlights

- Recipient of the Mr. & Mrs. Spencer T. Olin Fellowship and the P.E.O. Scholar Award
- Recipient of Department Teaching Award and University Teaching Citation
- Development of combined homology modelling and hydrogen deuterium exchange mass spectrometry technique for protein structure and mechanism prediction
- Best graduate student poster at Midwest/Southeast Photosynthesis Meeting for reconstituting recombinant subunit with denatured native protein complex

Leadership Highlights

- Developer of renewable energy science outreach program and green labs initiative
- Program Coordinator and supervisor of ten person team at youth development camp
- Taught masters level research-to-classroom program for high school biology teachers
- Lead team of undergraduate mentors who facilitate chemistry help sessions
- Vice-President of biotech consulting firm for start-up companies in St. Louis
- Founding member and director of science policy advocacy graduate student group

Research Experience

Graduate Research Assistant, Washington University, Blankenship Lab 2010-present
Structure and Function of Photosynthetic Cyclic Electron Transport Chain Membrane Proteins

- Reconstitution and mechanistic studies of the Alternative Complex III
- Purification and crystallization of the Light Harvesting Reaction Center complex
- Developed technique to refine protein homology models with Hydrogen Deuterium Exchange mass spectrometry yielding mechanistic insights of Di-Heme Cytochrome *c*
- Photosynthetic organism adaption to stress growth conditions of far red light

Undergraduate Research, Drury University, Independent 2009-2010
Designed experiments attempting to create a greener synthesis of the mosquito repellent DEET.

- Applied Green Chemistry techniques toward a novel synthetic approach

Undergraduate Research, Drury University, Roy Lab 2006-2008
Analytical chemistry to determine the physiological properties of standard buffer solutions

- Measured and standardized buffer constants of zwitterionic systems

Summer Student Research, Saint Louis University, Zonosko Lab summer 2005
Determined the thermodynamic parameters of naturally occurring secondary structures in RNA.

- Purified and measured the melting temperatures of 1x2 internal loops in RNA
- Cataloged complete list of naturally occurring 1x2 internal loops

Business and Leadership Experience

Consulting, The BALSA Group 2012-present
Vice President, Project Manager, Consultant
Business management and technology development consulting for start-up companies

- Worked on eleven consulting projects (3 consultant, 1 project manager, 7 adviser)
- Currently serving as Vice President recruiting clients and advising projects
- Served one year as Director of Human Resources: recruited & managed 80 consultants

Science Policy, Promoting Science Policy, Education, Research 2012-present
Founding member, Member Education Director
Science policy and science literacy outreach and advocacy graduate student group

- Served as the Director of Member Education
- Organized Science Policy 101 Summer Series for three years
- Participated in AAAS Congressional Visit Day

Youth Development, American Youth Foundation Camp Miniwanca summers 2007- 2009
Program Coordinator, Girls Camp Cabin Leader
Youth leadership development camp and program

- Coordinated daily activities and supervised team leading the activities
- Lead and lived with cabin of six middle school girls

Teaching Experience

Certifications

Teaching Citation, Washington University 2013

- Completed future faculty preparation program by teaching 5 semesters of STEM classes

Mentoring Experience

Undergraduate Research Mentor 2012-2014

Carotenoid variation under native-like growth conditions in *Roseiflexus castenholzii*

- Mentored undergraduate student in research for two years, guiding senior research project
- Found variability of pigment expression and energy transfer efficiency with different growth conditions in an early-evolving photosynthetic bacterium

Residential Peer Mentor Coordinator, Washington University 2013- present

- Instruct undergraduate chemistry peer mentors on teaching review sessions
- Organize program logistics and coordinate across departments

Science Outreach Experience

Catalysts for Change, Facilitator & Lab Coordinator 2012-2014

Program to encourage high school freshman girls to pursue careers in science

- Plan and organize hands-on chemistry labs, coordinate volunteers, invite speakers

Discovering Renewable Energy at Camp, Developer & Facilitator 2011-2012

Program engaging summer campers in renewable energy science without classroom pressure

- Developed and taught hands-on inquiry activities on solar and biomass energy

Teaching Assistantships

Matter and Energy Transformations, TA & content expert, University College at WUSTL 2014

- Taught masters of biology class to high school biology teachers
- Emphasis on connecting teaching content to current research and real-world applications

January Intensive Program in General Chemistry, Instructor, Washington University 2014

- Week long intensive program for underprepared students in general chemistry

Practical Applications of Academic Mentoring, Coordinator, Washington University 2013-2015

- Organize and mentor undergraduates serving as chemistry peer mentors

General Chemistry Lecture, T.A., Washington University 2011-2012

- Taught three recitation sections each semester for large lecture general chemistry course
- Facilitated elective POGIL recitation sections of the course
- Graded quizzes and exams

General Chemistry Laboratory, T.A., Washington University 2010-2011

- Taught two laboratory sections each semester for large general chemistry course
- Graded pre-labs, reports and exams

Organic Chemistry Laboratory, Lab T.A., Drury University 2007-2009

- Assisted lab instructor teach the lab sections, help students with experiments
- Prepped solutions for organic and analytical laboratory classes

General and Organic Chemistry Tutoring 2007-2011, 2014

Fellowships and Scholarships

P.E.O. Scholar Award, P.E.O. International Sisterhood 2014-2015

- Won national merit based dissertation fellowship for women from the P.E.O.

Mr. and Mrs. Spencer T. Olin Fellow, Washington University 2010-2015

- Awarded four-year merit based fellowship for women in higher education

Dr. Bruce R. and Jean E. Erdal Scholar, Washington University 2011-2012

- Awarded one year tuition based on departmental nomination

Trustee Scholar, Drury University 2006- 2010

- Awarded four year full-ride academic merit, leadership and service based scholarship

Publications

1. Majumder, E.L.W., Liu, H.J., Timlin, J.A., Berg, R.H. & Blankenship, R.E. Whole cell responses to far red light acclimation in chlorophyll *f* containing cyanobacteria. Manuscript in preparation. (2015).
2. Majumder, E.L.W., King, J. D. & Blankenship, R. E. Characterization and enzyme activity of the Alternative Complex III from *Roseiflexus castenholzii* and *Chloroflexus aurantiacus*. Manuscript in preparation. (2015).
3. Majumder, E.L.W., Olsen, J.D., Qian, P., Hunter, C.N. & Blankenship, R.E. Supramolecular organization of the photosynthetic complexes in the membranes of *Roseiflexus castenholzii*. Submitted. *Photosynthesis Research* (2015).
4. Zhang, Y., Majumder, E.L.W., Yue, H., Blankenship, R.E. & Gross, M.L. Analysis of diheme cytochrome *c* by hydrogen deuterium exchange mass spectrometry and homology modeling. *Biochemistry* **53,** 5619-5630 (2014).
5. Majumder, E.L.W. & Blankenship, R.E. Diversity of Photosynthetic Cytochrome Proteins. *Cytochrome Proteins in Photosynthesis and Respiration*. Eds. Cramer, W. & Kallas, T. Advances in Photosynthesis and Respiration. Accepted, (2014). (Book Chapter)
6. Gao, X., Majumder, E.L.W., Kang, Y., Yue, H. & Blankenship, R. E. Functional analysis and expression of the mono-heme containing cytochrome c subunit of alternative complex III in Chloroflexus aurantiacus. *Archives of Biochemistry and Biophysics* **535,** 197–204 (2013).
7. Majumder, E. L. W., King, J. D. & Blankenship, R. E. Alternative Complex III from phototrophic bacteria and its electron acceptor auracyanin. *Biochimica et Biophysica Acta* **11-12**, 1383-1391 (2013).
8. Badhwar, J., Karri, S., Cass, C. K., Wunderlich, E. L. & Znosko, B. M. Thermodynamic characterization of RNA duplexes containing naturally occurring 1 x 2 nucleotide internal loops. *Biochemistry* **46,** 14715–14724 (2007).

Honors and Awards

Elevator Pitch Contest Winner, PARC All-Hands Meeting 2013

- Won contest for best two minute explanation of my research to the general public

Best Graduate Student Poster, Midwest/Southeast Regional Photosynthesis Meeting 2012

- Received the award for research poster presentation of ACIII reconstitution studies

Chemistry Department Teaching Assistant Award, Washington University 2011-2012

- Awarded annually to outstanding TA based on faculty and student evaluation

Grants

ACS International Office Travel Award 2014

- Grant from American Chemical Society to attend Latin American Chemistry Congress and present outreach activities in Spanish at the Festival de Quimica

Photosynthetic Antenna Research Center (PARC) Scientific Exchange Grant 2013

- Grant from DOE-EFRC PARC to learn crystallography with collaborating labs in UK

PARC Educational Outreach Mini-Grant 2011, renewed 2012

- Grant from research center to develop and conduct renewable energy outreach program at summer camp, focused on hands-on experiential learning using outdoors as resource

Abstracts and Presentations

Latin American Chemistry Congress, Lima, Peru, speaker October 2014
The Protein Society Meeting, San Diego, CA, poster July 2014
Christmas Bioenergetics Meeting, London, UK, speaker December 2013
Midwest/Southeast Regional Photosynthesis Meeting, speaker November 2011-2014
ACS Midwest Regional Meeting, Springfield, MO, speaker October 2013
ASBMB Science Outreach and Communication Career Symposium, poster September 2013
International Congress on Photosynthesis Research, speaker and poster August 2013
Light Harvesting Satellite Meeting, poster August 2013
Photosynthetic Antenna Research Center Mini All-Hands Meeting, speaker January 2013
Photosynthesis Gordon Conference, poster presentation July 2012
ACS Midwest/Great Lakes Regional Meeting, poster presentation October 2011
ACS National Meeting Chicago, IL and Salt Lake City, UT March 2007 and March 2010

Community Service

WUSTL Chemistry Peer Mentors, Mentor & Group Co-leader 2011-2013

- Led group and organized events to welcome and transition new graduate students

University City Symphony Orchestra, Cellist 2011-present

- UCSO provides five free concerts to the community annually

American Youth Foundation, Alumni Advisory Team 2010-present

- Plan scholarship fundraising events and volunteer support for such events

Memberships

The Protein Society 2014-present
Photosynthetic Antenna Research Center (PARC) 2012-present
American Chemical Society (ACS) 2007-present

Languages

English (Native Proficiency)
Spanish (Minimum Professional Proficiency)

References

Robert E. Blankenship, Professor of Chemistry and Biology, Washington University in St. Louis
Primary Investigator and Research Mentor
314-935-7971, blankenship@wustl.edu

Brett Maricque, President, The BALSA Group
Supervisor
Brett.maricque@thebalsagroup.org

Nancy Pope, Associate Dean of the Graduate School of Arts & Sciences, Washington University
Director of the Olin Fellowship Program
314-935-6848, n.p.pope@wustl.edu

Regina Frey, Moog Professor of STEM Education and Chemistry, Washington University
Director of the Teaching Center
314-935-7474, gfrey@wustl.edu